Heidelberg University

Department of Physics and Astronomy

Book in Progress

An Introduction to Computational Physics

Leonard Storcks

January 29, 2024

Abstract

Computation - quickly crunching billions of numbers - can give us a new perspective and understanding of physical systems. This book aims to equip the reader with fundamental knowledge of numerics, computation and statistics as well as tools to tackle problems from physics (and many other disciplines).

Contents

1 Introduction **1**

I Basics of Numerical Computation 2

2 Digital Representation of Numbers **3**

2.1 Integer Arithmetic . . . 3
2.1.1 Unsigned integers . . . 3
2.1.2 Two's complement for negative numbers . . . 6
2.1.3 Integer types in C . . . 7
2.1.4 Byte Ordering in Storage: Big and Little Endian . . . 7
2.1.5 Properties and Caveats of Integer Arithmetic . . . 8
2.1.6 Can there be integer-overflow in python? . . . 9
2.2 Floating Point Arithmetic . . . 9
2.2.1 IEEE 754 Floating Point Standard . . . 10
2.2.2 Only a finite set of floating point numbers can be represented exactly 12
2.2.3 Machine Precision is finite . . . 13
2.2.4 Rounding and Pitfalls of Floating Point Arithmetic . . . 13
2.2.5 Rewriting Expressions to Avoid Cancellation I . . . 14
2.2.6 Rewriting Expressions to Avoid Cancellation II . . . 16
2.2.7 Accumulation of Round-off Errors . . . 16
2.2.8 Higher Precision . . . 16
2.3 A more general view on sources of numerical error . . . 17
2.4 Backward error, forward error and condition number . . . 17
2.4.1 Conditioning . . . 17

II Simulation Methods 19

3 Integration of ordinary differential equations **19**

3.1 Notes on ODEs . . . 19
3.1.1 Converting to a first order system . . . 19
3.1.2 Existence and uniqueness of an ODE solution for an initial value problem - Picard-Lindelöf and Lipschitz condition . . . 20
3.2 Introduction of Numerical Integration at the hand of the two-body problem . 20
3.2.1 The two-body problem . . . 21
3.2.2 Integrals of Motion . . . 21

3.2.3 Kepler Orbits are Conic Sections . . . 22
3.2.4 Connection of the Runge-Lenz vector to the eccentricity of a conic section . . . 25
3.2.5 Rescaling to Dimensionless variables . . . 25
3.2.6 Solving the two-body problem using explicit (aka forward) Euler . . . 25
3.2.7 Probing the accuracy of an integration scheme - energy error of explicit Euler . . . 26
3.3 Explicit Euler and it's shortcomings . . . 27
3.3.1 Explicit Euler is only first order accurate | truncation error . . . 27
3.3.2 Explicit Euler has stability issues . . . 27
3.4 Introduction of the Problem of Stiffness and Implicit Euler to the help . . . 29
3.4.1 Introducing stiffness at the hand of a simple example . . . 29
3.4.2 A *definition* of stiffness . . . 31
3.4.3 Implicit Euler to the help . . . 31
3.5 Construction of higher-order methods . . . 36
3.5.1 Meaning of going to higher order . . . 36
3.5.2 Approaches to constructing a higher order method . . . 37
3.5.3 Construction by Taylor expansion . . . 37
3.5.4 Runge-Kutta (RK) Integration schemes I: General Idea . . . 38
3.5.5 Runge-Kutta (RK) Integration schemes II: Derivation of the general RK scheme . . . 39
3.5.6 Runge-Kutta (RK) Integration schemes III: General m-substep RK method . . . 41
3.5.6.1 Butcher-Tableau for visualizing the RK coefficients . . . 41
3.5.7 Runge-Kutta (RK) Integration schemes IV: Taylor expansion to identify RK parameters for 2nd order schemes . . . 43
3.5.7.1 Comparison of coefficients . . . 43
3.5.7.2 Resulting integration formula with free parameter q . . . 44
3.5.7.3 Different integration schemes based on the choice of q . . . 44
3.5.8 Runge-Kutta (RK) Integration schemes V: Classical 4th order RK scheme (RK-4) . . . 45
3.6 Adaptive Step Sizes . . . 46
3.6.1 Step halving and doubling method . . . 47
3.6.2 Note on the Local accuracy . . . 48
3.6.3 When does doubling make sense? . . . 48
3.6.4 Adaptively choosing ϵ_0 . . . 49
3.6.5 Continuous time step adjustment . . . 49
3.6.5.1 Continuous adaptive time step control scheme . . . 49

3.6.5.2 Embedded Runge-Kutta schemes for cheaper error estimates 50
3.7 The problem of conserved quantities | Symplectic Integrators 50
3.7.1 Hamiltonian Systems and Symplecticity 50
3.7.1.1 Poisson brackets and constants of motion (first integrals) . . 51
3.7.1.2 Canonical transformations 51
3.7.1.3 Definition of symplectic transformations 52
3.7.2 Runge-Kutta methods do not conserve energy and are not symplectic 52
3.7.3 Symplectic integrators to the help 55
3.7.4 Verlet Scheme 56
3.7.4.1 Velocity Verlet algorithm 57
3.7.5 The Leapfrog Method 58
3.7.5.1 Connection between Leapfrog and Velocity Verlet 59
3.7.5.2 Kick-drift-kick and Drift-kick-drift Leapfrog formulations to have velocity and position information at the same time . . 59
3.7.5.3 Advantages of the Leapfrog scheme 61
3.7.5.4 Leapfrog is symmetric (time reversible) 61
3.7.5.5 Symplecticity of the leapfrog scheme I: Intuition and Meaning 62
3.7.5.6 Symplecticity of the leapfrog scheme II: Proof 62
3.8 Extrapolation method: Bulirsch-Stoer algorithm 65
3.8.1 Basic integration method | second order method with $\mathcal{O}(h^2)$; midpoint rule $\rightarrow$ modified midpoint rule 67
3.8.1.1 Modified midpoint rule 68
3.8.1.2 Combining modified midpoint calculations with different h; advantage of modified midpoint 68
3.8.1.3 What extrapolation nodes to choose? - how to inrease n (or rather decrease h) 69
3.8.1.4 How to extrapolate from multiple $F(h_n)$ to the limit $h \rightarrow 0$? 69
3.9 Predictor-corrector methods 70
3.9.1 One-step predictor-corrector method: RK2 and $P(EC)^k$ 71
3.9.2 4th order Adams-Bashforth-Moulton 71
3.10 Shooting | adapting parameters until boundary conditions are fulfilled 72
3.10.1 Remark on ODE solutions in phase space 72
3.10.2 Examplary Shooting Problem 72
3.10.3 Shooting 73

4 Simulation of Physical Systems - from Quantum Mechanics to Fluid Dynamics 74
4.1 Different levels of modelling from Quantum Mechanics to Kinetic Gas theory 74

4.2 From a classical particle description to the Boltzmann equation 75
4.3 Emergence of irreversibility in the Boltzmann equation 76

5 Basic Fluid Dynamics **78**
5.1 Basic notes on fluid description - the fluid from the view of a parcel 78
5.1.1 When is a fluid description valid? 78
5.1.1.1 Connection between temperature and random movement . . 78
5.1.1.2 Continuum Hypothesis 78
5.1.2 Example: the plasma in the intercluster medium can be considered a fluid* 79
5.1.2.1 Mean free path in a model of colliding spheres 79
5.1.2.2 Collisional cross-section of an electron in a plasma and first approximation of λ_{mfp} 80
5.1.2.3 A better approximation to the mean free path in an ionized plasma 80
5.1.3 Fluid description based on fluid parcels 81
5.1.3.1 Eulerian and Lagrangian fluid dynamics 81
5.1.3.2 Continuity equation 82
5.1.3.3 Incompressible fluids 82
5.1.3.4 Equation of motion of a fluid parcel, general path towards Navier-Stokes 83
5.2 Basic Gas Dynamics 84
5.2.1 Distribution function and Boltzmann equation 84
5.2.2 Retrieving information from the Boltzmann equation 85
5.2.3 Mass conservation | continuity equation (1st moment) 85
5.2.3.1 Derivation of the continuity equation* 86
5.2.4 Momentum conservation | Navier Stokes equation (2nd moment) . . . 86
5.2.4.1 Notes on the derivation of the Navier-Stokes equation 87
5.2.4.2 Interpretation and viscous stress tensor for a Newtonian fluid 87
5.2.5 Energy conservation (3rd moment) 88
5.2.5.1 Notes on the conductive heat flux 89
5.2.5.2 Evolution equation for the total specific energy $e = e_{th} + \underline{v}^2/2$ 89
5.2.6 Entropy conservation 90
5.3 Euler Equation and Navier-Stokes equation 90
5.3.1 Euler Equations 90
5.3.2 Navier-Stokes equation 91
5.3.2.1 Simplification of the Navier-Stokes equations for incompressible fluids ($\underline{\nabla} \cdot \underline{v} = 0$) 92

5.3.2.2 Characterizing flow | Reynolds number . . . 93
5.4 Shocks . . . 94
5.4.1 Propagation of disturbances 1: Speed of sound . . . 94
5.4.2 Characteristics of Perturbations . . . 95
5.4.3 Formation of a shock . . . 97
5.4.3.1 Formation as a pressure driven compressive disturbance . . . 97
5.4.3.2 Causes for shocks . . . 97
5.4.4 Collisional and collisionless shocks | shock front . . . 97
5.4.5 Properties at fluid discontinuities . . . 98
5.4.5.1 (Rankine-Hugoniot) Jump conditions I: Assumptions . . . 98
5.4.5.2 (Rankine-Hugoniot) Jump conditions II: Jump condition from the continuity equation . . . 98
5.4.5.3 (Rankine-Hugoniot) Jump conditions III: Jump condition from the momentum equation . . . 99
5.4.5.4 (Rankine-Hugoniot) Jump conditions IV: Jump condition from the energy equation . . . 100
5.4.5.5 Types of dicontinuities: contact discontinuity vs. shock . . . 100
5.4.6 Characterizing the Shock strength - Mach number . . . 100
5.4.6.1 Occurence of the Mach number in the continuity equation . 101
5.4.6.2 Rewriting the Rankine-Hugoniot jump conditions in terms of $\mathcal{M}_1$ - relating pre- and post-shock quantities . . . 101
5.4.6.3 Conversion of kinetic to thermal energy in the shock . . . 102
5.4.6.4 Conservation of energy in the shock . . . 102
5.4.6.5 Connection between pre- and post-shock Mach number . . . 104
5.4.6.6 Shock adiabatic curve* . . . 104
5.4.6.7 Oblique shocks . . . 105
5.5 Fluid instabilities . . . 106
5.5.1 Stability of a shear flow . . . 106
5.5.2 Rayleigh-Taylor instability . . . 106
5.5.3 Kelvin-Helmholtz instability . . . 107
5.5.4 Further instabilities . . . 107
5.6 Turbulence . . . 107
5.6.1 Subsonic (incompressible) turbulence, low Mach numbers | rotational modes . . . 108
5.6.2 How to quantify turbulence? - Reynolds number . . . 109
5.6.2.1 Reynolds number as the ratio between advection and dissipation timescale . . . 109

5.6.3 Supersonic turbulence, shocks $\mathcal{M} \gg 1$ | rotational and compressive modes . . . 109
5.6.4 Schematic concept of turbulence . . . 110
5.6.5 Kolmogorov scales of turbulence . . . 110
5.6.5.1 Dissipation scale - smallest scale to be resolved in a simulation 110
5.6.6 Scaling of the eddy velocity and vorticity in the inertial range . . . 110
5.6.7 Power spectrum of Kolmogorov turbulence . . . 111
5.6.7.1 Derivation of the energy spectrum of Kolmogorov turbulence 111

6 Eulerian Hydrodynamics | Solving PDEs 112
6.1 Introductory notes on PDEs . . . 112
6.2 Types of PDEs . . . 113
6.2.1 Classification of linear 2nd order PDEs in analogy with conic sections 113
6.2.1.1 Derivation | homogeneous solutions are conic section in k-space 113
6.2.1.2 Classification into elliptic, parabolic, hyperbolic . . . 114
6.2.1.3 Qualitative differences on the types of PDEs . . . 114
6.2.2 Typical examples and classification of homogeneous 2nd order PDEs . 115
6.2.3 Classification of linear 2nd order PDEs with more unknowns . . . 115
6.2.4 Linear systems of 1st order homogeneous PDEs . . . 116
6.2.4.1 Extension to conservation laws . . . 116
6.3 Solution schemes for PDEs . . . 116
6.4 Advection - Keep information flow in the physical system in mind . . . 118
6.4.0.1 Analytic solution to the advection equation . . . 118
6.4.0.2 Simple but wrong approach | we need to consider the flow of information . . . 119
6.4.0.3 Directional splitting / upwind scheme to the rescue . . . 120
6.4.0.4 Where does the smoothing in the upwind scheme come from? 120
6.4.0.5 What is the maximum timestep we can take? | Courant-Friedrichs-Lewy (CFL) criterion . . . 122
6.4.0.6 Hyperbolic conservation laws | changing upwind direction . . 123
6.4.0.7 What if identifying the local characteristics is very difficult? 123
6.5 Intermezzo: CFL like criterion and connection to stiffness in a reaction diffusion system . . . 123
6.6 Riemann problem | Riemann solvers . . . 126
6.6.1 Structure of the solution of the Euler-Riemann-Problem . . . 127
6.6.1.1 Characteristics of the three waves . . . 127
6.6.1.2 Example Riemann-Problem situation . . . 127
6.6.1.3 Properties of shock, contact discontinuity and rarefaction wave 128

6.7 Finite volume discretization | Reducing a hyperbolic conservation law to a Riemann problem | Godunov scheme . . . 130
6.7.1 Problem | solve a hyperbolic conservation law PDE . . . 130
6.7.2 Deriving a finite volume scheme where only Riemann problems are left to solve . . . 130
6.7.2.1 Caveats of the Godunov scheme . . . 132
6.7.3 Godunov's method and Riemann solver | reconstruct - evolve - average (REA) . . . 132
6.8 Approximate Riemann solvers | HLL solver . . . 133
6.8.1 1D Riemann problem to solve . . . 133
6.8.2 Basic HLL assumptions and problem statement . . . 133
6.8.3 Deriving the solution of the Riemann problem in the HLL scheme . . . 134
6.8.3.1 Derivation of the middle state u^{HLL} at $t = T$ . . . 134
6.8.3.2 Deriving the intercell flux $f^{HLL} = f^*$ . . . 135
6.8.4 Final HLL solution . . . 135
6.8.5 Mind that the extreme velocities can point into the same direction . . . 136
6.8.6 Godunov scheme with HLL solver . . . 136
6.8.7 Pointers to extensions of the HLL scheme . . . 137
6.8.8 Ansätze for the maximum wave velocities S_L and S_R . . . 138
6.9 Extension of Eulerian hydrodynamics to multiple dimensions . . . 138
6.9.1 Dimensional splitting Ansatz . . . 139
6.9.1.1 1st order ansatz . . . 140
6.9.1.2 2nd order accurate in 2D examples . . . 140
6.9.2 2nd order accurate in 3D example . . . 140
6.9.3 Unsplit schemes . . . 141
6.10 Extensions for high-oder accuracy . . . 142
6.10.1 What even is a schemes order? . . . 142
6.10.2 2nd order extension to Godunov's scheme by changing the reconstruction step from piecewise-constant to linear . . . 142
6.10.2.1 How to estimate the time derivatives $(\partial_t \underline{U})_i$? | MUSCL-Hancock scheme . . . 144
6.10.3 Idea and discussion of even higher order methods . . . 144
6.10.3.1 Discussion of higher order methods . . . 144
6.11 Flux / slope limiters | adaptively switching between a high and low order method . . . 147
6.11.1 Possibly advantageous properties of the flux limiter . . . 148

7 Smoothed Particle Hydrodynamics - Lagrangian Particle Method 149

7.1 Lagrangian fluid equations (i.e. as material derivatives) . . . 150
7.1.1 Continuity equation . . . 150
7.1.2 Navier-Stokes equation | Conservation law of Linear Momentum . . . 150
7.1.3 Energy equation . . . 150
7.2 A simple SPH fluid simulator* . . . 151
7.3 Smooth then discretize - smoothing kernels and their usage . . . 152
7.3.1 Properties of the smoothing | approach for calculating derivatives of the smoothed fluid quantities . . . 152
7.3.2 Discrete formulation of the smoothing . . . 153
7.3.3 Why a kernel with compact support is preferred? . . . 153
7.3.4 How to make the smoothing length h variable in space to account for variations in the density? | sampling procedure in SPH - scatter and gather approach . . . 156
7.3.4.1 How to choose h_i? . . . 157
7.4 SPH continuity equation and equations of motion . . . 159
7.4.1 SPH continuity equation . . . 159
7.4.2 Gradients in SPH . . . 160
7.4.3 SPH Euler equation | The central ingredient to making our simple fluid simulator work . . . 161
7.4.4 Including further accelerations . . . 161
7.5 Artificial Viscosity . . . 162
7.5.1 Viscous Pressure . . . 162
7.5.2 Adding the artificial viscosity to the equation of motion . . . 162
7.5.3 Shear-Flow-Balsara correction . . . 163
7.5.4 Further viscosity switches . . . 163
7.6 SPH energy equation with artificial viscosity . . . 164
7.7 SPH Entropy equation . . . 164
7.8 Maximum timestep - CFL criterion . . . 165
7.9 Notes on boundary modeling* . . . 165
7.10 Reversibility in the context of viscosity-free, weakly-compressible SPH* . . . 165
7.11 Notes on the conservative formulation using Lagrange multipliers . . . 168
7.12 Further improvements . . . 168
7.13 Advantages and Disadvantages of SPH . . . 168

8 Finite Element Methods 169
8.1 Finite element methods for linear PDEs . . . 170
8.1.1 The solution is represented by weighted base functions on nodes within finite elements . . . 170

8.1.1.1 Example 1D linear reconstruction . . . 171
8.1.2 From the PDE to an algebraic equation for the expansion coefficients $\phi_1, \ldots, \phi_n$ . . . 171
8.1.2.1 Inserting the finite element approximation into the PDE yields a residuum . . . 172
8.1.2.2 Finding the expansion coefficients by minimizing the residual in some sense . . . 172
8.1.2.3 A linear system for $\phi_1, \ldots, \phi_{\mathcal{N}}$ in the Galerkin scheme . . . 173
8.1.2.4 Example Application of Galerkin FEM . . . 174
8.2 Discontinuous Galerkin Method . . . 175
8.2.1 Problem we want to tackle | Euler equations . . . 176
8.2.2 Steps in formulating the Dicontinuous Galerkin (DG) scheme . . . 176
8.2.3 Subdivision and Representation | modal vs nodal . . . 177
8.2.3.1 Example for an orthogonal polynomial basis: Legendre polynomials . . . 178
8.2.4 Solving for the weights . . . 179
8.2.4.1 What even is Gauss-Legendre quadrature?* . . . 180
8.2.5 Finding initial weights - just apply the determination of weights to the initial state . . . 181
8.2.6 Evolution equation for the weights . . . 181
8.2.7 Efficiency of DG and refinement schemes . . . 182

References **184**

1 Introduction

Add / refer to example applications

Computational physics encompasses

- simulation as a new paradigm to approach physical problems and validate theories by comparing simulated results to experiments
- statistics and data analysis to make sense of experimental or simulated data
- scientific machine learning to incorporate physical knowledge into Machine Learning and Machine Learning into simulations

This books aim is to give an introduction to Computational Physics with the presented concepts often also being of great use in other fields (e.g. solving partial differential equations computationally in not only greatly important for physics but for instance also for solving the Black-Scholes equation in finance).

Content included mainly encompasses the lectures

- Fundamentals of Simulation Methods (Ralf Klessen and Philip Girichidis, 2023)
- Computational Statistics and Data Analysis (Daniel Durstewitz, 2023)

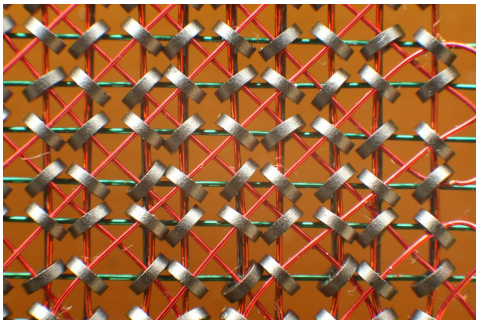

(a) Historic Magnetic Core Storage. Bits are stored as the direction of magnetic flux.

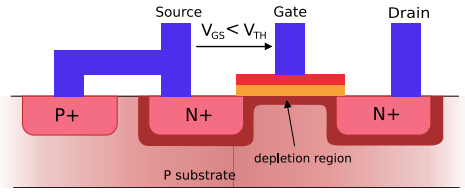

(b) Field-effect transistor (more specifically MOSFET schematic). Power-efficiently switching currents is at the heart of modern computing. Based on a Floating-Gate or Charge-Trapping mechanism and the tunnel effect, storage can be realized via stored charges.

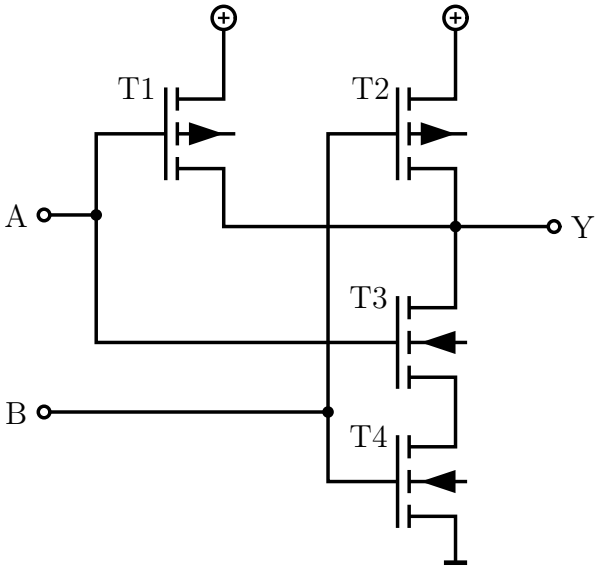

(c) NAND-Gate. Bit operations lie at the core of computations.

Figure 1: Basics of Computation.

Part I

Basics of Numerical Computation

How we write what algorithms is informed by how we represent data. While there exist exotic approaches like analog computers that can e.g. handle integration elegantly (Ulmann, 2020) or quantum computing which might e.g. at some point accelerate machine learning (Biamonte et al., 2017), standard binary data representation is vastly prevailing.

Binary data can be very efficiently and reliably stored and operated on (see figure 1), but the respective chosen representations might come with caveats.

2 Digital Representation of Numbers

In C, `int x = 100 * 200 * 300 * 400;` will surprisingly yield -1894967296 (for a 32-bit integer representation) (*overflow*), `float f1 = (2.3 + 1e20) - 1e20;` yields 0.0 (*round-off-error*) but `float f2 = 2.3 + (1e20 - 1e20);` correctly gives 2.3.

We want to understand and mitigate such caveats of arithmetic on computers, where we want quick calculations while also using as little storage as possible - simulations can quickly become big in storage (e.g. lots of particles).

Further details can be found in Higham, 2002 and Bryant and O'Hallaron, 2011.

2.1 Integer Arithmetic

In C, integers ($\in \mathbb{Z}$) are stored as fixed-size bit-sequences. The respective size dictates a range. C provides both unsigned and signed integer types, with negative numbers in the signed case represented using *two's-complements*.

2.1.1 Unsigned integers

For a bit-vector $\underline{x} = [x_{\omega-1}, x_{\omega-2}, \ldots, x_0]$ the unsigned conversion is

$$B2U_\omega := \sum_{i=0}^{\omega-1} x_i 2^i \tag{1}$$

(illustrated in figure 2) and the range is $0, \ldots, 2^\omega - 1$. In case of overflow in operations, the overflow is truncated in the most significant bits (see figure 3). As $B2U_\omega[x_{\omega-1}, x_{\omega-2}, \ldots, x_0] \mod 2^k = B2U_\omega[x_{k-1}, x_{k-2}, \ldots, x_0]$ we effectively store arithmetic result $\mod 2^\omega$.

$x_{\omega-1}$ is called most significant bit (MSB) and x_0 least significant bit (LSB).

Problem: When the result of an arithmetic operation exceeds the range of an integer type, unexpected results occur (overflow) (and also underflow in the signed case)

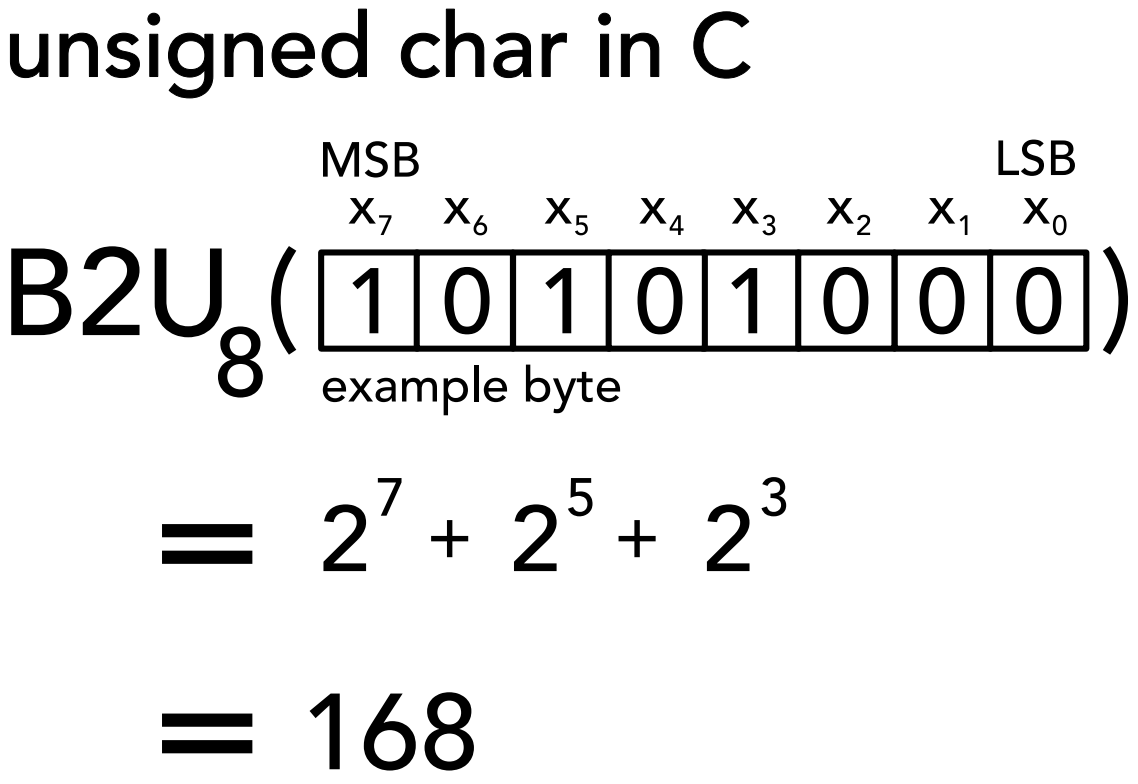

Figure 2: Example of an unsigned char in C.

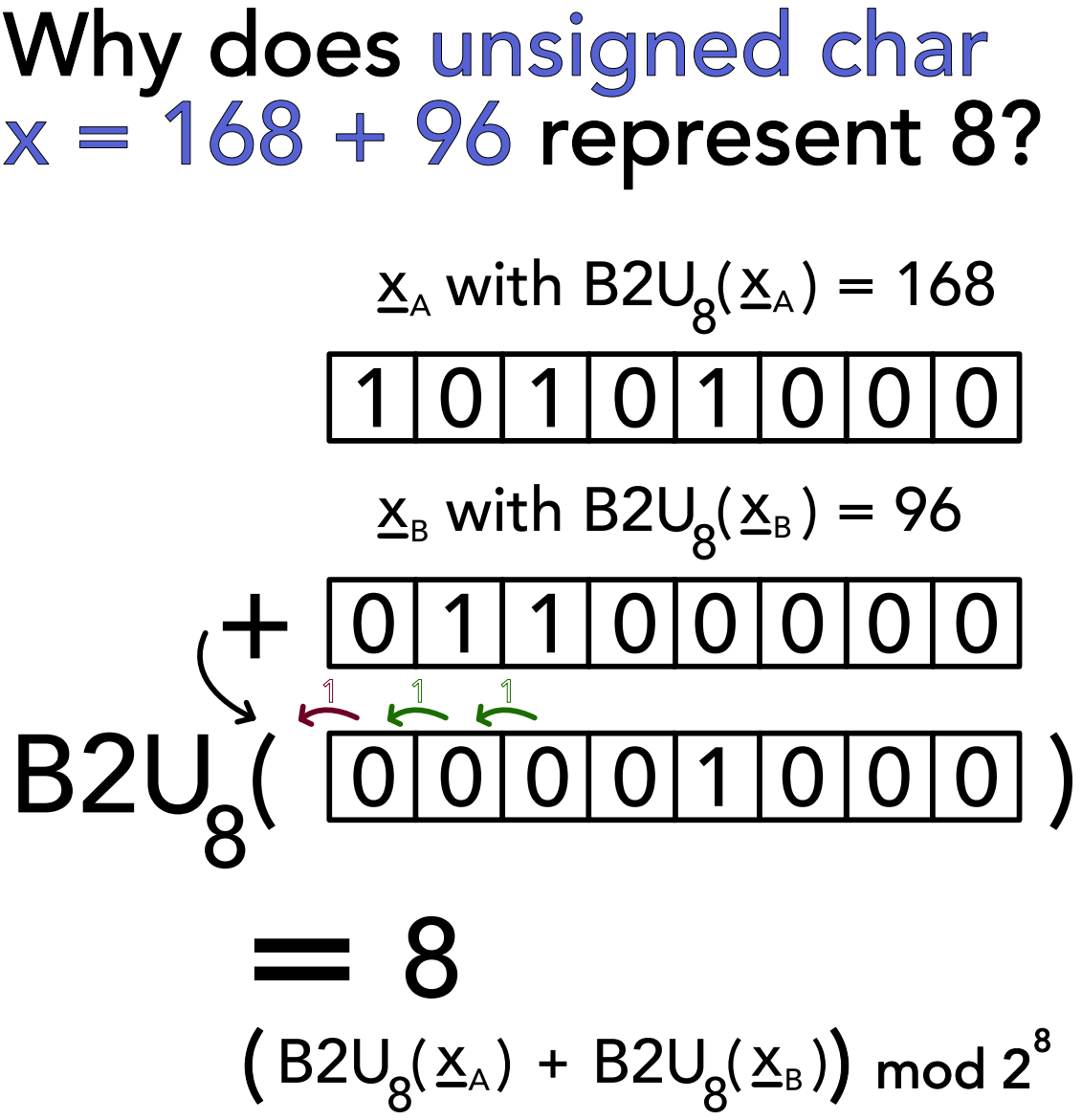

Figure 3: Example of unsigned char overflow.

2.1.2 Two's complement for negative numbers

Note that addition of integers by bitwise addition with carry-on is very fast.

Why can't we just let the MSB encode the sign?: A representation of the form

$$B2S_\omega(\underline{x}) := (-1)^{x_{\omega-1}} \cdot \sum_{i=0}^{\omega-2} x_i 2^i \tag{2}$$

(sign magnitude) has the disadvantage, that normal bitwise addition with carry-on does not work. Also, zero is encoded twice, as ± 0.

Idea of the two's-complement: The MSB flags the sign in $\underline{x} = [x_{\omega-1}, x_{\omega-2}, \ldots, x_0]$ by having a weighting factor $-2^{\omega-1}$

$$B2T_\omega(\underline{x}) := -x_{\omega-1} 2^{\omega-1} + \sum_{i=0}^{\omega-2} x_i 2^i \tag{3}$$

Carry-on to the ω-th bit in addition is again ignored. As we really just have to add positive numbers in bits x_0 to $x_{\omega-2}$ with correct sign-switch by carry-on, no special handling is necessary (see figure 4). The range is $-2^{\omega-1} \ldots 2^{\omega-1} - 1$.

From an unsigned int to the two's complement and vice versa we can get by

1. invert all bits
2. add +1 to the result[1]

If we want $\underline{x}$ with $B2T_\omega(\underline{x}) = -u$ then the bits following the MSB must encode k with $-u = -2^{\omega-1} + k$, so the encoded unsigned number must be $B2T_\omega(\underline{x}) = \underbrace{2^{\omega-1}}_{\text{sign bit}} + k = 2^\omega - u$ - a *two's complement.*

[1] These rules intuitively follow from the constraint, that bitwise addition with carry-on of $-u$ and u should result in an all-zero bitvector. Adding a bitvector to its inverted self results in an all-1 bitvector, adding one more then results in all zeros, as the last carry-on is discarded.

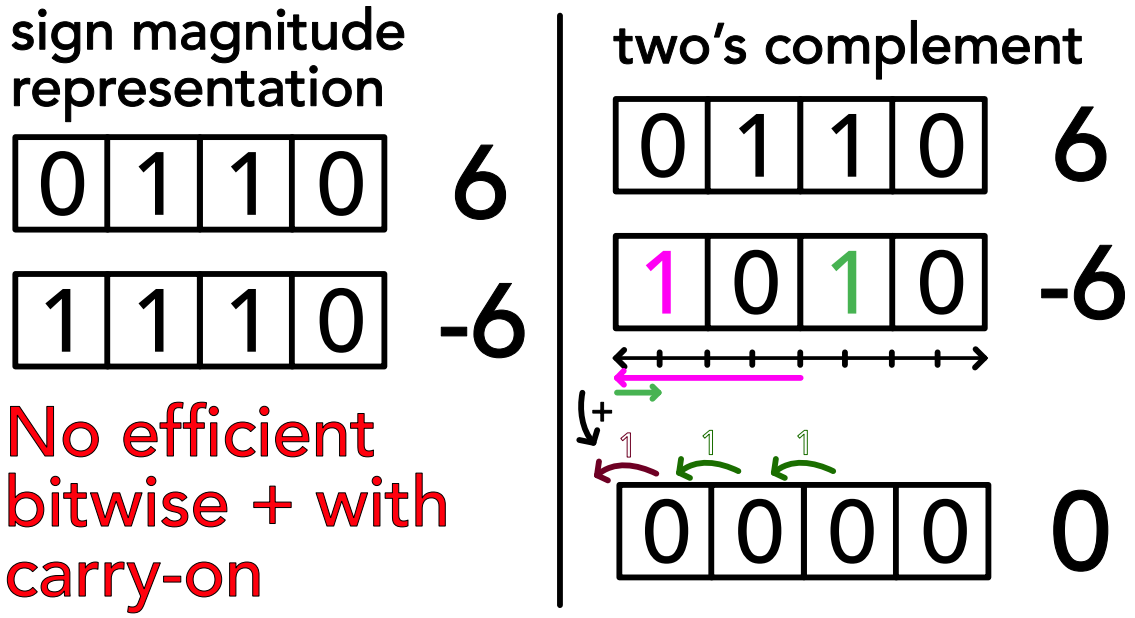

Figure 4: Illustration of the defining feature of the two's complement - addition is simple.

2.1.3 Integer types in C

Some common integer types with respective minimum sizes are given in table 1.

Type	Minimum Size ω
`char`	8 bits
`short`	16 bits
`int`	16 bits
`long`	32 bits
`long long`	64 bits

Table 1: Common integer types in C, signed ranges are $-2^{\omega-1} \dots 2^{\omega-1}-1$, unsigned ranges are $0 \dots 2^{\omega}-1$.

Problem: Using unsigned can come with unexpected results, when being cast from a negative number. E.g. `unsigned int x = -1;` will result in $2^{32}-1$ in a 32-bit system (the two's complement is read as if an unsigned representation). More deviously, $-1 < 0U$ will evaluate to false, as all integers in a comparison are cast to unsigned, when one of them is unsigned.

2.1.4 Byte Ordering in Storage: Big and Little Endian

Bytes of e.g. a multi-byte integer can be stored from most significant byte to least significant byte (big endian) or vice versa (little endian), see figure 5.

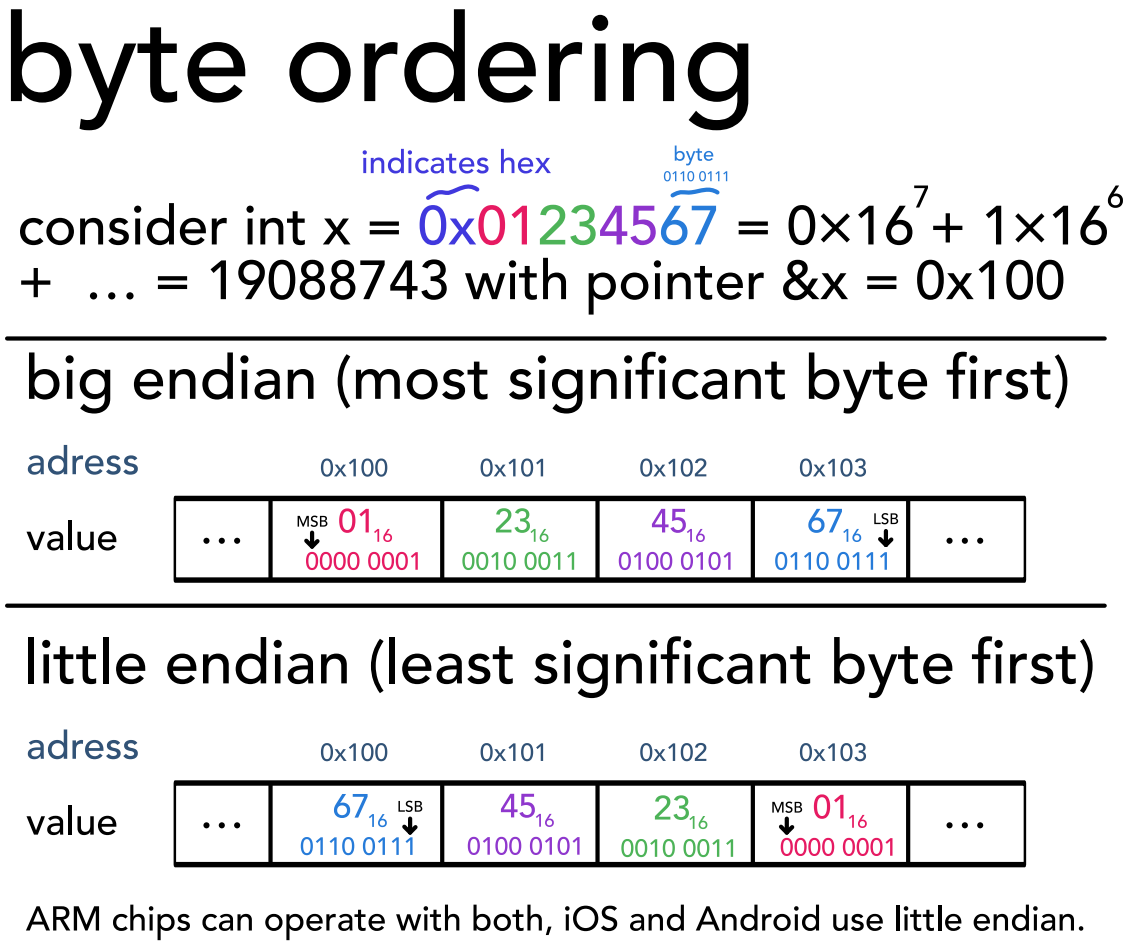

Figure 5: Big and Little Endian.

2.1.5 Properties and Caveats of Integer Arithmetic

Typical problems in integer arithmetic are overflow, integer division, the modulo operation and implicit type conversion.

Overflow: The respective integer ranges have finite ranges, overflow in arithmetic operations is cut-off. We must choose a type with sufficient range - mind that choosing types with too large of a footprint (e.g. always long) wastes storage and compute.

Example I: In `char c = 100 * 4; // range -128 to 127` the result is -112 as 400 in bits is 000110010000 where a cut-off to one byte means 10010000 so $-2^7+2^4 = -128+16 = -112$.

Example II: For `int a = -1 * pow(2,31); int b = 10;` we have $a < b$ but not $a - b < 0$ (for char the behavior is a bit different as up to int there is implicit type conversion.)

Integer division: All decimal places are truncated, so

$$5/3 = 1; -5/3 = -1; 5/-3 = -1$$

Modulo operation: The modulus in C is defined as $n\%m = n - (n/m)m$ so

$$5\%3 = 2; -5\%3 = -2; 5\% - 3 = -2$$

Implicit type conversion: In C, the type can implicitly be converted up to unsigned int, which can avoid overflow, as illustrated in table 2.

implicit type conversion up to int can be helpful

```
char a,b;
a = 100;
b = 4;
int c = a * b; //
  ↪ 400
```

mind its only up to int

```
int a = 2e9;
int b = 3;
long long c = a *
  ↪ b;
printf("%llu\n",
  ↪ c); //
  ↪ 1705032704
```

As $2^{32} - 1 \approx 4 \cdot 10^9 < 6 \cdot 10^9 < 2^{33} - 1$ (unsigned ranges) we overflow to the 33rd-bit, which is cut-off, giving the unsigned result of $6 \cdot 10^9 - 2^{32} = 1705032704$.

explicit type consversion

```
int a = 2e9;
int b = 3;
long long c =
  ↪ ((long long) a)
  ↪ * ((long long)
  ↪ b);
printf("%llu\n",
  ↪ c); //
  ↪ 6000000000
```

Table 2: Type conversion and its caveats

2.1.6 Can there be integer-overflow in python?

Note that in python3, integers are implemented as "long" integer objects of arbitrary size, overflows are impossible (at the cost of speed; mind that e.g. numpy is based on C code).

2.2 Floating Point Arithmetic

In the following, we will encode rational numbers in the form $V = x \cdot 2^y$, with $x, y \in \mathbb{Z}$. Similar to the decimal notation

$$d_m d_{m-1} \dots d_0 . d_{-1} d_{-2} \dots d_{-n} = \sum_{i=-n}^{m} d_i 10^i \tag{4}$$

we can write in binary notation

$$b_m b_{m-1} \dots b_0 . b_{-1} b_{-2} \dots b_{-n} = \sum_{i=-n}^{m} b_i 2^i, \quad 0.01_2 = 0.25_{10} \tag{5}$$

or generally in base β in scientific notation

$$\begin{gathered}(-1)^s \cdot \underbrace{b_0 . b_{-1} b_{-2} \dots b_{-n}}_{\text{mantissa M}} \cdot \beta^e = \beta^e \cdot \sum_{i=-n}^{0} b_i 2^i, \quad \text{exponent } e, \\ \text{precision (number of digits) } p = n+1, \quad \text{sign-bit } s \in \{0,1\}\end{gathered} \tag{6}$$

Note that in this notation (in the form $V = x \cdot 2^y$) we cannot exactly represent e.g. 0.1 or 0.2.

$$0.1_{10} = 1.10011[0011] \dots_2 \cdot 2^{-4} \tag{7}$$

Disastrous historic example: In the first Gulf War (more specifically on 25th February 1991), a Patriot missile defense battery failed to intercept an incoming Iraqi Scud missile, because it used an internal clock counting up in tenths of a second represented by a 23-bit sequence. Future missile positions are predicted by extrapolating from past position with constant velocity. The Patriot system mixed both this inaccurate internal clock and a more accurate one, leading to the failed interception and 28 deaths among soldiers.

2.2.1 IEEE 754 Floating Point Standard

Based on the representation in scientific notation, we can store a floating point number in a bit-vector with

- a sign bit s
- an exponent e stored as an unsigned integer $E = e + b$ with bias b
- a mantissa M

where for single precision (32-bit)

- the exponent is stored in 8 bits, $b = 127$, $e_{min} = -126$, $e_{max} = 127$ with $E = 255$ and $E = 0$ reserved for special cases
- the mantissa is stored in 23 bits, with the first bit being implicitly 1 (**normalization**), which can always be assumed by appropriately choosing the exponent (floating point representations are not unique), so we have $p = 23(+1)$ bits of precision encoding an integer M but need a special representation for 0

where based on the exponent we differentiate between

- **normalized values for** $1 \leq E \leq 254$ with value of the floating point number

$$V = (-1)^s \cdot \left(1 + \frac{M}{2^p}\right) \cdot 2^{E-b}, \quad \text{sign bit } s$$
$$\text{biased exponent } E = e + b, \quad \text{integer representation of mantissa } M \tag{8}$$
$$\text{precision } p = \#\text{mantissa bits} + 1 \text{ implicit bit}$$

- **denormalized values for** $E = 0$ with value of the floating point number

$$V = (-1)^s \cdot \frac{M}{2^p} \cdot 2^{-b+1}, \quad \text{for } M = 0, V = \pm 0 \text{ depending on } s \tag{9}$$

  The denormalized numbers start just below the normalized ones (by the factor 2^{-b+1} with $+1$ as we do not have the implicit leading 1 here) and now no normalization (implicit starting 1-bit) is assumed. This allows to approach zero with gradually decreasing precision (and even spacing) (smaller numbers occupy fewer digits as of the leading zeros) and ensures that for $x \neq y$, $x - y$ is non-zero, so $\frac{1}{x-y}$ is safe for $x \neq y$.

- $\pm\infty$ **for** $E = 255$ **and** $M = 0$
- **NaN (Not a Number) for** $E = 255$ **and** $M \neq 0$

Why is the exponent stored in a biased way, not two's complement?: In a two's complement representation of the exponent to compare two numbers, we have to compare the exponents and mantissas separately and the exponent-comparison is a bit more complicated than comparing biased representations. In the biased exponent representation we can just compare the bitvectors of exponent followed by mantissa interpreted as integers (also mind the sign).

The cases are illustrated in figure 6, with a specific example in figure 7.

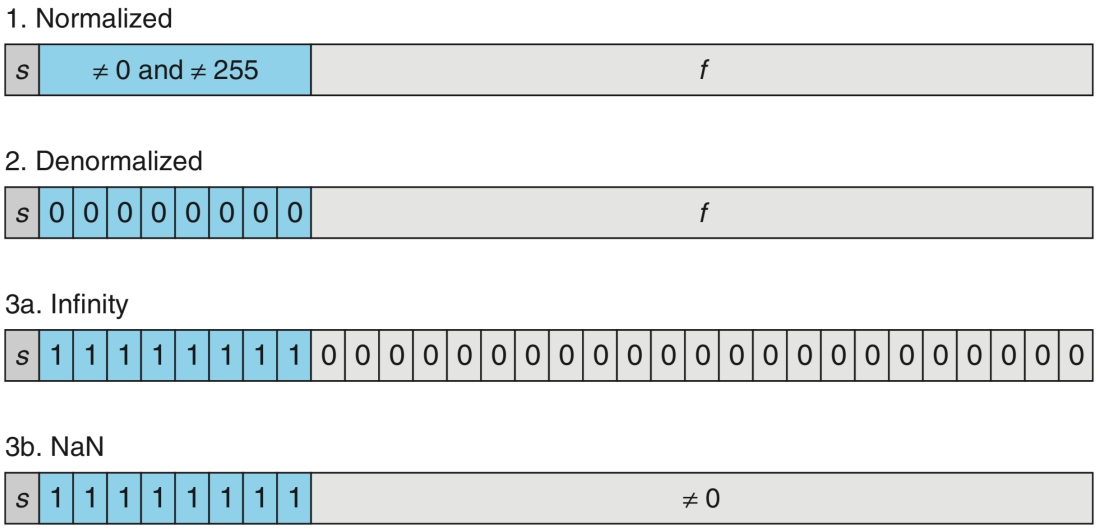

Figure 6: Cases of the IEEE 754 Floating Point Standard.

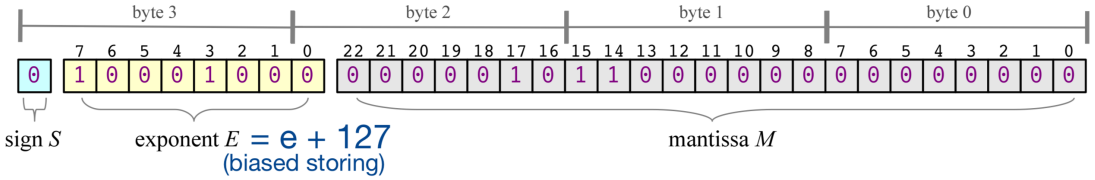

Figure 7: 523 can be written as $1.000001011_2 \cdot 2^9$ so $e = 9, E = e + 127 = 136$. As of the normalization, the leading 1 in the mantissa is implicit. The number is given as a single precision float in big endian.

2.2.2 Only a finite set of floating point numbers can be represented exactly

With 32 bits, 2^{32} states can be encoded (and mind that here e.g. NaN has multiple representations). In any case, the number of exactly representable numbers is finite, above 0 starting at

$$V_{\text{denorm,min}} = \frac{1}{2^p} \cdot 2^{-b+1} \underbrace{\approx}_{\substack{\text{single} \\ \text{p.}}} 1.4 \cdot 10^{-45} \tag{10}$$

with the smallest normalized number being

$$V_{\text{norm,min}} = (1+0) \cdot 2^{-b} \underbrace{\approx}_{\substack{\text{single} \\ \text{p.}}} 1.2 \cdot 10^{-38} \tag{11}$$

and the largest normalized number being

$$V_{\text{norm,max}} = (1 + \frac{2^p - 1}{2^p}) \cdot 2^{E_{\max} - b} \underbrace{\approx}_{\substack{\text{single} \\ \text{p.}}} 3.4 \cdot 10^{38} \tag{12}$$

2.2.3 Machine Precision is finite

The smallest increment in the mantissa, in $1 + \frac{M}{2^p}$, is the **machine precision**

$$\epsilon_{\text{mach}} = \frac{1}{2^p} \underbrace{\approx}_{\substack{\text{single} \\ \text{p.}}} 1.2 \cdot 10^{-7} \tag{13}$$

Consider two floating point numbers $V_1, V_2 > 0$ *next to each other*

$$V_1 = \left(1 + \frac{M}{2^p}\right) \cdot 2^{E-b}, \quad V_2 = \left(1 + \frac{M+1}{2^p}\right) \cdot 2^{E-b} \tag{14}$$

so their relative difference is bound by

$$\frac{V_2 - V_1}{V_2} = \frac{\frac{1}{2^p} \cdot 2^{E-b}}{\left(1 + \frac{M+1}{2^p}\right) \cdot 2^{E-b}} \leq \epsilon_{\text{mach}} \tag{15}$$

2.2.4 Rounding and Pitfalls of Floating Point Arithmetic

In the IEEE standard, results of addition, subtraction, multiplication and division must equal to one where the arithmetic operations are assumed to be exact and then there is rounding to the nearest representable number (computation is done at higher (typically double or higher) precision). Therefore (mind the section before)

$$\text{ralative error } \frac{|x - \hat{x}}{|x|} \leq \epsilon_{\text{mach}}, \quad \text{number } x, \text{ number on machine } \hat{x} \tag{16}$$

with the common pitfalls

- **Limitation of machine precision:** $a + b = a$ typically for $|b| < \epsilon_{\text{mach}}|a|$, i.e. when b cannot be resolved by the mantissa of a, e.g. $(1 + 0.5\epsilon) - 0.5\epsilon$ in floating point arithmetic yields 0.9999999999999999 not 1.
- **Associativity is not guarantueed:** $(a+b)+c \underbrace{\neq}_{\text{i.A.}} a+(b+c)$, e.g. $(2.3+1e20)-1e20$ yields 0.0 but $2.3 + (1e20 - 1e20)$ yields 2.3

- **Problems of representability:** As e.g. 0.1 is not exactly representable in base $\beta = 2$, $x/10 \neq 0.1 \cdot x$ in general while $x/2.0 = 0.5 \cdot x$ is exact. The compiler may automatically choose the multiplication variant as multiplication is faster than division.
- **Cancellation:** For $x = a - b$ subtractive cancellation causes relative errors already present in $\hat{a}$ and $\hat{b}$ to be (relatively) amplified, when a and b are of similar size. Significant digits are lost and the relative error explodes. Consider e.g. $a = 1.75682, b = 1.75471$ with $\hat{a} = 1.76$ and $\hat{b} = 1.75$. While $\hat{a}, \hat{b}$ have small relative errors (3 digits precision[2] Note that here 0.123 ans 0.127 agree in two significant digits, where one intuitively might say this should be rather 1.), $a - b = 0.00211$ and $\hat{a} - \hat{b} = 0.01$ has a large relative error (no precise digit).
- **NaN and Inf:** All calculations including NaN yield NaN, calculations with inf mostly inf (except of course $1/\text{inf} = 0$, ...)

where we should

- **Rewrite calculations so that errors do not amplify:** For $x = 10^8, y = 10^5, z = -1 - 10^5$ we have $xy + xz = -1.0066 \cdot 10^8$ (problem in resolving the -1 in xz) but $x(y + z) = -1.0 \cdot 10^8$.
- **Compare floats based on a maximum relative error:** Instead of $x == y$ we should use e.g. $|x - y| \leq \epsilon_{\text{mach}} \cdot \max(|x|, |y|)$.
- **As avoid overflow to inf and nan:** E.g. in `float x = 1e20; float y = x * x; float z = y / x` z will be inf.

2.2.5 Rewriting Expressions to Avoid Cancellation I

Consider $f(x) = \frac{1-\cos x}{x^2}$. For $x_e = 10^{-4}$, we have (when we represent 6 figures)

$$c := \cos x_e, \quad \hat{c} = 0.999999, \quad 1 - \hat{c} = 10^{-6}, \quad \text{while } 1 - c \approx 5 \cdot 10^{-9} \tag{18}$$

$1 - c$ has only one significant digit, the relative error is enormously amplified and we get

$$\frac{1 - \hat{c}}{x_e^2} = 100, \quad \text{while in reality for } x \neq 0 : 0 \leq f(x) \leq \frac{1}{2} \tag{19}$$

[2] $\hat{x}$ is said to approximate x to the r-th digit, if the absolute error is at most $\frac{1}{2}$ in the r-th digit, so

$$\text{largest integer s so that } 10^s < |x|, \quad |x - \hat{x}| < 1/2 \cdot 10^{s-r+1} \tag{17}$$

To avoid cancellation we can rewrite using $\cos x = \cos^2 \frac{x}{2} - \sin^2 \frac{x}{2} = 1 - 2\sin^2 \frac{x}{2}$ to

$$f(x) = \frac{1}{2}\left(\frac{\sin \frac{x}{2}}{\frac{x}{2}}\right)^2 \tag{20}$$

A comparison of both versions in python can be found in figure 8, at some point (roughly below 10^{-8}), $\cos x$ is too close to 1 to be resolved by the mantissa, so the total result is 0, above that the magnified error is visible.

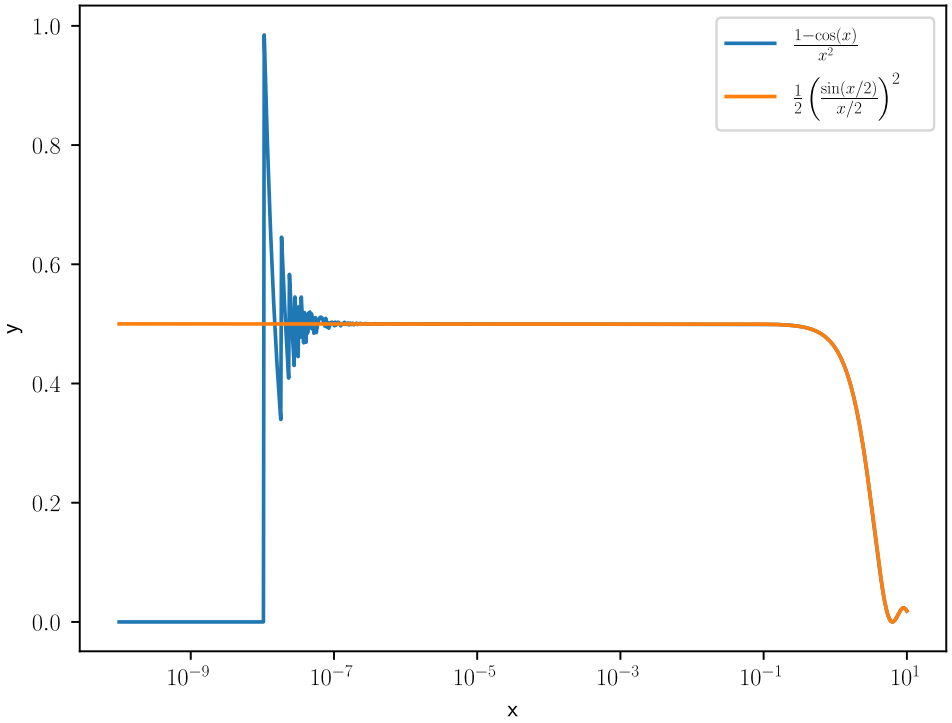

Figure 8: Comparison of the mathematically equivalent expressions $f(x) = \frac{1-\cos x}{x^2}$ and $f(x) = \frac{1}{2}\left(\frac{\sin \frac{x}{2}}{\frac{x}{2}}\right)^2$ in python.

2.2.6 Rewriting Expressions to Avoid Cancellation II

Consider the following expressions for the sample variance of $\{x_i\}_{i=1}^N$

$$\begin{aligned} &\text{two-pass formula: } \bar{x} = \frac{1}{N}\sum_{i=1}^{N-1} x_i, \quad \sigma_N^2 = \frac{1}{N}\sum_{i=1}^{N}(x_i - \bar{x})^2 \\ &\text{one-pass formula: } \sigma_N^2 = \frac{1}{N-1}\left(\sum_{i=1}^{N} x_i^2 - \frac{1}{N}\left(\sum_{i=1}^{N} x_i\right)^2\right) \\ &\qquad\qquad \text{as } \sigma^2 = E[(x-\bar{x})^2] = E[x^2] - E[x]^2 \end{aligned} \tag{21}$$

While for the one-pass formula, we can calculate all necessary sums in one pass through the data, it suffers heavily from cancellation: For $\{10000, 10001, 10002\}$, the two-pass formula in single precision correctly gives 1.0 while the one-pass formula yields 0.0 (cancellation) (there are better one-pass formulas though).

2.2.7 Accumulation of Round-off Errors

Consider the sum

$$\sum_{k=1}^{\infty} k^{-2} = \frac{\pi^2}{6} \tag{22}$$

which we want to approximate by finitely many summands. If we sum the terms just as the formula suggests from large to small, at some point, the small changes will not be resolved anymore - so better sum up from small to large. Summing up in single precision for $N = 10^7$ terms, one gets

$$\begin{aligned} &\text{big to small: } 1.644725323, \quad \text{small to big: } 1.644933939, \\ &\qquad\qquad \text{exact (till 9th digit): } 1.644934058 \end{aligned} \tag{23}$$

As expected the big-to-small summation is too small.

2.2.8 Higher Precision

The above pitfalls are less severe in higher precision. For instance in double precision (64-bit)

$$\begin{aligned} &p = 52(+1) \text{ mantissa bits}, \quad 11 \text{ exponent bits, with } e_{min} = -1022, e_{max} = 1023, \\ &\quad \text{smallest and largest repr. numbers } f_{min} \simeq 2.2 \cdot 10^{-308}, f_{max} \simeq 1.8 \cdot 10^{308}, \\ &\qquad\qquad |e_{min}| < |e_{max}| \to \frac{1}{f_{min}} < f_{max} \end{aligned} \tag{24}$$

with machine precision $\epsilon_{\text{mach}} \approx 2.2 \cdot 10^{-16}$. There is even quad-double precision (128-bit) (not supported on hardware though and therefore relatively slow as it has to be emulated). Packages for nearly arbitrary precision also exist.

2.3 A more general view on sources of numerical error

In numerical computation, the typical error sources are

- rounding
- data uncertainty
- truncation (of terms in numerical schemata, e.g. in the approximation of a function by its Taylor series)

where we have now discussed rounding errors and their effects to some extent.

2.4 Backward error, forward error and condition number

Consider we approximate $y = f(x)$ as $\hat{y}$ in an arithmetic of limited precision, with $f : \mathbb{R} \to \mathbb{R}$.

- **Forward error:** The absolute or relative error between $\hat{y}$ and y is the forward error (living in the output space)
- **Backward error:** The backward error is the smallest Δx (in the input space) so that $f(x + \Delta x) = \hat{y}$, so the smallest perturbation where the exact function gives our approximate result.

If this Δx is sufficiently small, e.g. as small as the uncertainty in the data in the first place, we speak of backward stability. A weaker formulation is the mixed forward-backward error

$$\hat{y} + \Delta y = f(x + \Delta x), \quad |\Delta y| \leq \epsilon |y|, \quad |\Delta x| \leq \eta |x| \tag{25}$$

In the context of rounding errors, we call the algorithm numerically stable if $\hat{y}$ is almost the right answer for almost the right data (ϵ, η small).

2.4.1 Conditioning

Backward and forward error are connected by the conditioning of a problem, the sensitivity of the solution to perturbations in the data. Assuming $\hat{y} = f(x + \Delta x)$ and f differentiable, we have

$$\hat{y} - y = f(x + \Delta x) - f(x) = f'(x)\Delta x + \mathcal{O}((\Delta x)^2) \tag{26}$$

so the relative error is

$$\frac{\hat{y}-y}{y} = \frac{f'(x)\Delta x}{f(x)} + \mathcal{O}((\Delta x)^2) \tag{27}$$

leading to the relative condition number

$$\kappa(x) \underbrace{=}_{\text{i.A.}} \lim_{\epsilon \to 0^+} \sup_{||\Delta x|| \leq \epsilon} \frac{||y-\hat{y}||/||y||}{||\Delta x||/||x||} = \left| \frac{x f'(x)}{f(x)} \right| \tag{28}$$

for small Δx measuring the relative change in the output over a relative change in the input. As a rule of thumb

$$\text{forward error} \lesssim \text{condition number} \cdot \text{backward error} \tag{29}$$

so ill-conditioned problems can have large forward errors.

Application on Matrices

Consider the linear system $\underline{\underline{A}}\underline{y} = \underline{x}, \underline{y} = \underline{\underline{A}}^{-1}\underline{x}, \underline{\hat{y}} = \underline{\underline{A}}^{-1}(\underline{x} + \underline{\Delta x})$. The condition number follows as

$$\begin{aligned}
\kappa(\underline{\underline{A}}) &= \max_{\underline{x}, \underline{\Delta x} \neq 0} \frac{||\underline{\underline{A}}^{-1}\underline{x} - \underline{\underline{A}}^{-1}(\underline{x} + \underline{\Delta x})||/||\underline{\underline{A}}^{-1}\underline{x}||}{||\underline{\Delta x}||/||\underline{x}||} \\
&= \max_{\underline{\Delta x} \neq 0} \frac{||\underline{\underline{A}}^{-1}\underline{\Delta x}||}{||\Delta x||} \max_{\underline{x} \neq 0} \frac{||\underline{x}||}{||\underline{\underline{A}}^{-1}\underline{x}||} \\
&= \max_{\underline{\Delta x} \neq 0} \frac{||\underline{\underline{A}}^{-1}\underline{\Delta x}||}{||\underline{\Delta x}||} \max_{\underline{y} \neq 0} \frac{||\underline{\underline{A}}\underline{y}||}{||\underline{y}||} \\
&= ||\underline{\underline{A}}^{-1}|| \cdot ||\underline{\underline{A}}||
\end{aligned} \tag{30}$$

where we used the definition of the matrix norm $||\underline{\underline{A}}|| = \max_{\underline{x} \neq 0} \frac{||\underline{\underline{A}}\underline{x}||}{||\underline{x}||}$. For large condition numbers, small perturbations in the input $\underline{x}$ lead to large changes in the solution $\underline{y}$.

Part II

Simulation Methods

The dynamical evolution of physical systems is described using differential equations. Numerical methods for solving differential equations and the rise of computers have allowed for accurate modeling of complex dynamical systems that could hardly be approached by analytical means even under the usage of perturbation theory (compare Moser, 1978).

Oftentimes, we face an initial value problem (IVP) where from initial values from the functions to solve and values for their derivatives as necessary, the evolution is sought to be calculated. In a boundary value problem a differential equation is given together with a set of additional constraints (e.g. Sturm-Liouville problems).

3 Integration of ordinary differential equations

Our aim is solving an ordinary differential equation (ODE) $\partial_t \underline{y} = \underline{f}\left(\underline{y}\right)$ with initial values $\underline{y}(t = t_0) = \underline{y}_0$. Notice that $\underline{f} = \underline{f}(\underline{y}, t)$ can be handled by augmenting $\tilde{\underline{y}} = \begin{pmatrix} \underline{y} \\ t \end{pmatrix}$ and $\tilde{\underline{f}}(\tilde{\underline{y}}) = \begin{pmatrix} \underline{f}(\tilde{\underline{y}}) \\ 1 \end{pmatrix}$.

3.1 Notes on ODEs

3.1.1 Converting to a first order system

Ordinary differential equations only contain derivatives with respect to one variable. Note, however, that higher order derivatives with respect to that variable can occur. We can get to the form $\partial_t \underline{y} = \underline{f}\left(\underline{y}\right)$ by converting to a coupled first order system.

Consider the n-th order ODE

$$\partial_t^n y(t) = f\left(y(t), \partial_t y(t), \ldots, \partial_t^{n-1} y(t), t\right), \quad f : U \subset \mathbb{R} \times \mathbb{K}^n \to \mathbb{K} \tag{31}$$

for instance a pendulum with damping

$$\partial_t^2 \phi = -\omega_0^2 \sin\phi - \gamma \partial_t \phi, \quad \gamma, \omega_0 \in \mathbb{R} \tag{32}$$

Now we define the variables

$$u_m = \partial_t^m y(t), \quad m \in \{0, \ldots, n-1\} \tag{33}$$

leading to the coupled first order system

$$\partial_t \begin{pmatrix} u_0 \\ u_1 \\ \vdots \\ u_{n-2} \\ u_n \end{pmatrix} = \begin{pmatrix} u_1 \\ u_2 \\ \vdots \\ u_{n-1} \\ f\left(t, u_0, u_1, \ldots, u_{n-1}\right) \end{pmatrix} \rightarrow \partial_t \underline{u} = \underline{f}\left(t, \underline{u}\right) \tag{34}$$

Using ϕ for the angle and $\omega = \partial_t \phi$ for the angular velocity, we can write the pendulum as

$$\partial_t \begin{pmatrix} \phi \\ \omega \end{pmatrix} = \begin{pmatrix} \omega \\ -\omega_0^2 \sin\phi - \gamma\omega \end{pmatrix} \tag{35}$$

3.1.2 Existence and uniqueness of an ODE solution for an initial value problem - Picard-Lindelöf and Lipschitz condition

For the initial value problem $\partial_t \underline{y} = \underline{f}\left(\underline{y}\right), \underline{y}(t_0) = \underline{y}_0$ to have a unique solution in the vicinity of $(\underline{y}_0, t_0)$, i.e. for the change around that point, to uniquely determine the development, this change must be *well-behaved*, $\underline{f}$ must be *Lipschitz-continuous*.

$$\forall(\underline{y}, t), (\underline{z}, t) \text{ in the vicinity of } (\underline{y}_0, t_0) : ||\underline{f}(\underline{y}, t) - \underline{f}(\underline{z}, t)|| \leq \lambda ||\underline{y} - \underline{z}|| \tag{36}$$

with $\lambda > 0$ and $||\cdot||$ being an arbitrary vector norm. The slope of the line connecting two close-by evaluations of $\underline{f}$ must be bounded by λ. This is guaranteed for $\underline{f}$ being continuous and sufficiently often differentiable with bounded derivatives and more so $\underline{f}$ analytic.

3.2 Introduction of Numerical Integration at the hand of the two-body problem

Our aim is computationally modelling the interaction of two-bodies. This lends itself well as an example, as stepping the system forward in time is easy to imagine visually, an analytic solution exists to which we might compare numerical solution and it guides us to the problem of conserved quantities and symplectic integrators.

3.2.1 The two-body problem

For the two-body problem (illustrated in figure 9) the equations of motion are

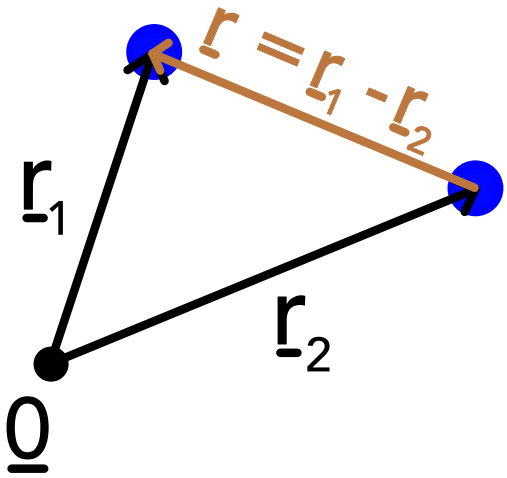

Figure 9: Illustration of the two-body problem.

$$\begin{aligned} m_1 \partial_t^2 \underline{r}_1 &= -G \frac{m_1 m_2}{|\underline{r}|^3} \underline{r} \\ m_2 \partial_t^2 \underline{r}_2 &= +G \frac{m_1 m_2}{|\underline{r}|^3} \underline{r} \end{aligned} \tag{37}$$

for $\underline{r} = \underline{r}_1 - \underline{r}_2$. Subtracting both yields

$$\partial_t^2 \underline{r} = -G \frac{M}{|\underline{r}|^3} \underline{r} \tag{38}$$

with $M = m_1 + m_2$. Which is equivalent to the equation of motion of a single body of mass $\mu = \frac{m_1 m_2}{M}$ in a potential $U(r) = -G\frac{m_1 m_2}{r} = -G\frac{M\mu}{r}$.

We can write this as the first order system

$$\partial_t \begin{pmatrix} \underline{r} \\ \underline{v} \end{pmatrix} = \begin{pmatrix} \underline{v} \\ -G\frac{M}{|\underline{r}|^3} \underline{r} \end{pmatrix} \tag{39}$$

3.2.2 Integrals of Motion

The following quantities are conserved along the trajectories of m_1 and m_2 and are therefore useful sanity checks for simulations.

- Total energy

$$E = T + U = \frac{\mu}{2} v^2 - \frac{GM}{r} \mu \tag{40}$$

- Angular momentum (perpendicular to the orbital plane)

$$\underline{L} = \underline{r} \times \underline{p} = \underline{r} \times \mu \underline{v} \tag{41}$$

- Laplace-Runge-Lenz vector (here in its dimensionless form, the eccentricity vector)

$$\underline{e} = \frac{\underline{v} \times \underline{j}}{GM} - \underline{\hat{e}}_r, \qquad \text{specific angular momentum } \underline{j} = \frac{\underline{L}}{\mu} \text{ eccentricity } e = ||\underline{e}|| \tag{42}$$

Note: The 1-body Kepler problem has 6 degrees of freedom (phase-space coordinates), of which one cannot be conserved, as nothing should be able to tell us the initial time of our motion. Therefore, only 5 quantities can be conserved and the Laplace-Runge-Lenz vector indeed only adds 1 more conserved degree of freedom (taking E and $\underline{L}$ as primary conserved quantities, $\underline{e}$ only has one degree of freedom).

Additional notes on the Laplace-Runge Lenz vector

The Lenz vector is conserved in all $\frac{1}{r}$-potentials, like the gravitational or Coulomb potential, for instance in the Hydrogen atom (but not for multi-electron atoms). Kepler-orbits are conic sections and the Laplace-Runge-Lenz vector is illustrated in figure 10.

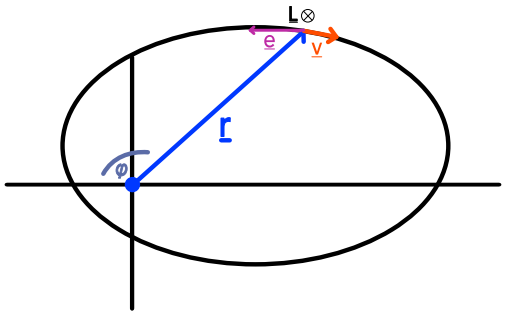

Figure 10: Illustration of the Laplace-Runge-Lenz vector.

From our pictorial evidence, we see that $\underline{e}$ is points along the semi-major axis. Note here we have drawn that $\underline{r} = \underline{r}_1 - \underline{r}_2$ follows a conic section. Likewise m_1 and m_2 move on conic sections with respect to the center of mass, $\underline{0} \underbrace{=}_{\text{o.b.d.A.}} \frac{1}{M}\left(m_1 \underline{r}_1 + m_2 \underline{r}_2\right)$ leading to $\underline{r}_1 = \frac{m_2}{M}\underline{r}$ and $\underline{r}_2 = -\frac{m_1}{M}\underline{r}$.

3.2.3 Kepler Orbits are Conic Sections

Depending on the total energy E, we have

- $E < 0 \rightarrow$ (closed) elliptic orbit

- $E = 0 \rightarrow$ parabolic orbit
- $E > 0 \rightarrow$ hyperbolic orbit

This dependence of the orbit form on the energy can be seen from writing

$$E = \frac{\mu}{2}(\partial_t \underline{r})^2 + U(r), \quad U(r) = -\frac{\alpha}{r}\mu, \quad \text{here } \alpha = GM \tag{43}$$

and using polar coordinates as the movement takes place on a planar surface

$$(\partial_t \underline{r})^2 = (\partial_t r)^2 + r^2(\partial_t \phi)^2 \tag{44}$$

with $\partial_t \phi$ expressed via the conserved angular momentum

$$\text{const.} \; = l = I\omega = \mu r^2 \partial_t \phi \quad \Rightarrow \quad \partial_t \phi = \frac{l}{\mu r^2} \tag{45}$$

so

$$\begin{aligned} E &= \frac{\mu}{2}(\partial_t \underline{r})^2 + U(r) \\ &= \frac{\mu}{2}(\partial_t r)^2 + \frac{\mu}{2} r^2 (\partial_t \phi)^2 + U(r) \\ &= \frac{\mu}{2}(\partial_t r)^2 + \underbrace{\frac{l^2}{2\mu r^2} + U(r)}_{U_{eff}} \end{aligned} \tag{46}$$

Note here that we have expressed the total energy as the sum of a kinetic part stemming from a change in distance between the two bodies (which we have already related to the individual positions) and an effective potential U_{eff}. Where the vertical line of constant energy intersects the effective potential, $\partial_t r$ must be zero so such a point must be a point of reversal of movement (see figure 11 and 12).

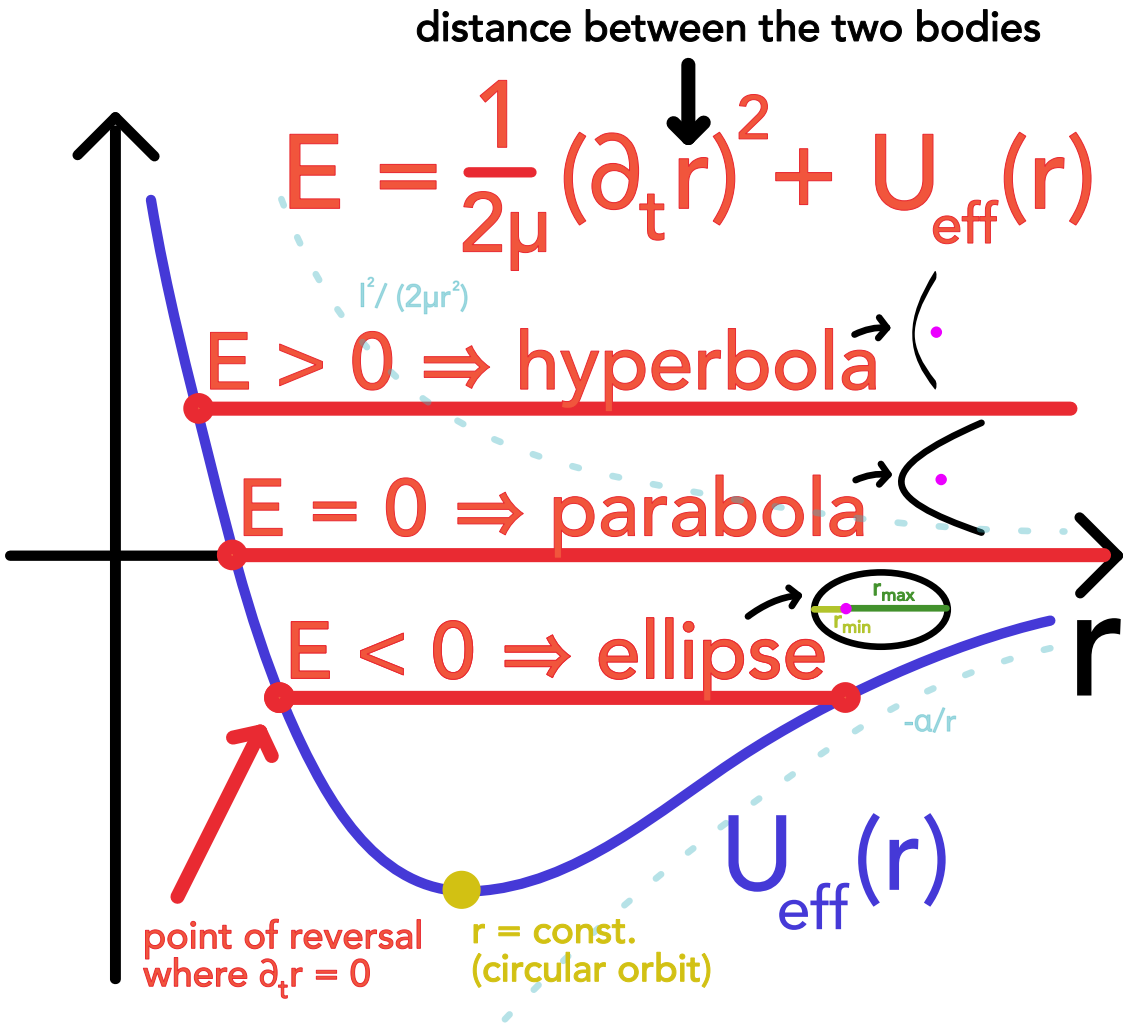

Figure 11: Illustration of the effective potential U_{eff} and the resulting orbits.

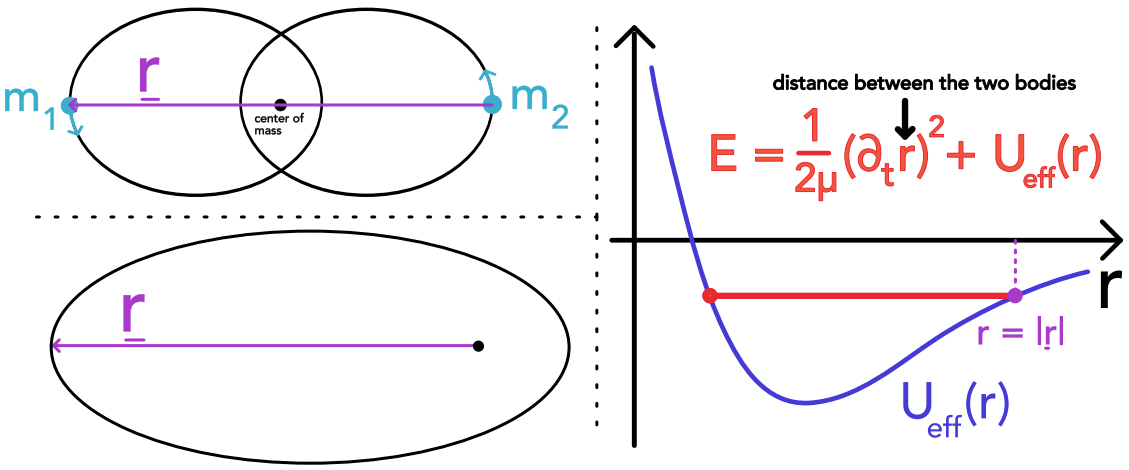

Figure 12: Connection between the different views on the two-body problem.

3.2.4 Connection of the Runge-Lenz vector to the eccentricity of a conic section

From multiplying $\underline{e}$ with $\underline{r}$ we obtain

$$\begin{aligned} \underline{e}\cdot\underline{r} = er\cos\varphi = \frac{(\underline{v}\times\underline{j})\cdot\underline{r}}{GM} - r \underset{\underline{a}\cdot(\underline{b}\times\underline{c})=\underline{b}\cdot(\underline{c}\times\underline{a})=\underline{c}\cdot(\underline{a}\times\underline{b})}{=} \frac{(\underline{r}\times\underline{v})\cdot\underline{j}}{GM} - r = \frac{j^2}{GM} - r \\ \rightarrow r(\varphi) = \frac{j^2/GM}{1+\epsilon\cos\varphi} \end{aligned} \tag{47}$$

3.2.5 Rescaling to Dimensionless variables

While the relative precision with which a number is stored on a computer is $\sim$ the machine precision, so independent of magnitude, we rescale our variables so that they predominantly fall into the range $[-1,1]$ so that different variables are on the same scale (so also their absolute precisions) (also making the problem statement more general).

$$\underline{r} \quad \rightarrow \quad \underline{s} := \frac{\underline{r}}{R_0}, \quad \text{characteristic length } R_0 \text{ e.g. initial separation} \tag{48}$$

$$\underline{v} \quad \rightarrow \quad \underline{w} := \frac{\underline{v}}{v_0}, \quad \text{characteristic velocity } v_0 = \left(\frac{GM}{R_0}\right)^{1/2} \tag{49}$$

v_0 is the velocity, a body circling one with mass M at distance R_0 would have ($F_{zp} = F_G$).

$$t \quad \rightarrow \quad \tau := \frac{t}{T_0}, \quad \text{characteristic time } T_0 = \frac{R_0}{v_0} = \left(\frac{R_0^3}{GM}\right)^{1/2} \tag{50}$$

With this we can write the equation of motion as

$$\frac{d\underline{s}}{d\tau} = \underline{w}, \quad \frac{d\underline{w}}{d\tau} = -\frac{\underline{s}}{|\underline{s}|^3} \tag{51}$$

3.2.6 Solving the two-body problem using explicit (aka forward) Euler

Let us discretize the derivatives with a simple difference quotient, where we probe the current slope by comparing the current position to the one a small time-step in the past or future.

$$\frac{d\underline{s}^{(n)}}{d\tau} = \frac{\underline{s}^{(n)} - \underline{s}^{(n-1)}}{h} + \mathcal{O}(h)(\text{backwards}) \quad \text{or} \quad \frac{d\underline{s}^{(n-1)}}{d\tau} = \frac{\underline{s}^{(n)} - \underline{s}^{(n-1)}}{h} + \mathcal{O}(h)(\text{forward}) \tag{52}$$

where $h = \tau^{(n)} - \tau^{(n-1)}$ is the step-size and the *forward* formulation gives an explicit scheme for $\underline{s}_n$ (only depending on already known values)

$$\begin{aligned} \underline{s}^{(n)} &= \underline{s}^{(n-1)} + h\frac{d\underline{s}^{(n-1)}}{d\tau} + \mathcal{O}(h^2) = \underline{s}^{(n-1)} + h\underline{w}^{(n-1)} + \mathcal{O}(h^2) \\ \underline{w}^{(n)} &= \underline{w}^{(n-1)} + h\frac{d\underline{w}^{(n-1)}}{d\tau} + \mathcal{O}(h^2) = \underline{w}^{(n-1)} - h\frac{\underline{s}^{(n-1)}}{|\underline{s}^{(n-1)}|^3} + \mathcal{O}(h^2) \end{aligned} \tag{53}$$

(explicit Euler)

and the *backward* formulation gives an implicit scheme for $\underline{s}_n$ (*implicit* as depending on the yet unknown $\underline{w}^{(n)}$).

$$\begin{aligned} \underline{s}^{(n)} &= \underline{s}^{(n-1)} + h\frac{d\underline{s}^{(n)}}{d\tau} + \mathcal{O}(h^2) = \underline{s}^{(n-1)} + h\underline{w}^{(n)} + \mathcal{O}(h^2) \\ \underline{w}^{(n)} &= \underline{w}^{(n-1)} + h\frac{d\underline{w}^{(n)}}{d\tau} + \mathcal{O}(h^2) = \underline{w}^{(n-1)} - h\frac{\underline{s}^{(n)}}{|\underline{s}^{(n)}|^3} + \mathcal{O}(h^2) \end{aligned} \tag{54}$$

This is also very clear just from first order Taylor expansion.

3.2.7 Probing the accuracy of an integration scheme - energy error of explicit Euler

We probe the accuracy, by checking on the conserved quantities (now dimensionless)

$$\begin{gathered} \text{total energy } E^{(n)} = \frac{\left(\underline{w}^{(n)}\right)^2}{2} + \frac{1}{s^{(n)}}, \qquad \text{angular momentum } \underline{j}^{(n)} = \underline{s}^{(n)} \times \underline{w}^{(n)} \\ \text{Laplace - Runge - Lenz vector } \underline{e}^{(n)} = \underline{w}^{(n)} \times \left(\underline{s}^{(n)} \times \underline{w}^{(n)}\right) - \underline{s}^{(n)} \end{gathered} \tag{55}$$

Wanted behavior: In a good integration scheme, the truncation errors (from the Taylor expansion) and rounding errors should be small or at least not accumulate without bound.

We calculate relative errors with respect to the initial values, e.g.

$$\epsilon^{(n)}(h) = \frac{|E^{(n)} - E^{(0)}|}{|E^{(0)}|}$$

Rough error estimation for explicit Euler: Each step has an error of $\mathcal{O}(h^2)$, an orbit takes $\sim \frac{T_0}{\Delta t} = \frac{1}{h}$ steps so we expect an error of $\mathcal{O}(h)$ per orbit, more on the problem of applying *non-symplectic* schemes onto *symplectic* problems follow later.

3.3 Explicit Euler and it's shortcomings

The simplest method for solving an ODE is the Explicit Euler method

$$\underline{y}^{(n+1)} = \underline{y}^{(n)} + \underline{f}\left(\underline{y}^{(n)}\right)\Delta t, \quad \text{where} \quad \underline{y}^{(0)} = \underline{y}_0$$

which is explicit as the computation of $\underline{y}^{(n+1)}$ only depends on already known states.

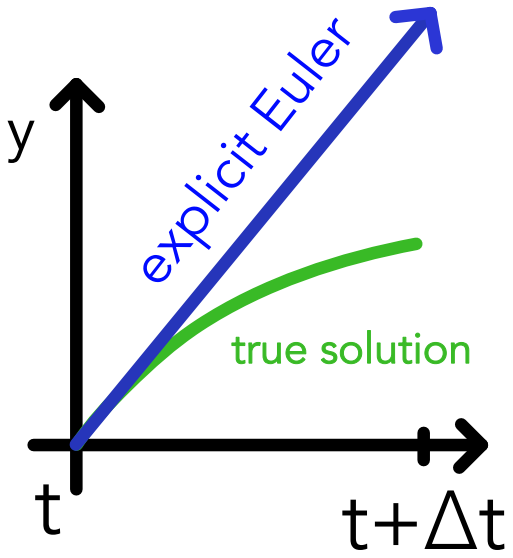

Figure 13: Illustration of one time step in the Explicit Euler scheme.

As illustrated in Figure 13 in every step we step forward along the current derivative $\underline{f}\left(\underline{y}^{(n)}\right)$.

3.3.1 Explicit Euler is only first order accurate | truncation error

A simple error approximation follows from Taylor expansion

$$\underline{y}(t+\Delta t) = \underline{y}(t) + \Delta t \underline{f}(t) + \mathcal{O}_s(\Delta t^2)$$

In each step we make an error $\mathcal{O}_s(\Delta t^2)$ so over some timespan T where we need $N_S = \frac{T}{\Delta t}$ steps we accumulate the error $N_S \mathcal{O}_S(\Delta t^2) = \mathcal{O}_T(\Delta t)$. We therefore call Explicit Euler first order accurate.

Note: For a global error scaling with $\mathcal{O}_T(\Delta t^n)$ (n-th order accurate scheme), the local truncation error (of the Taylor expansion) must be $\mathcal{O}_s(\Delta t^{n+1})$.

3.3.2 Explicit Euler has stability issues

Stability analysis is a broad field, and the interested reader can find details in chapter IV.3 of Hairer and Wanner, 1996. For now, consider the ODE $\partial_t y = \alpha y, Re(\alpha) < 0, y(0) = y_0$

with the solution $y(t) = y_0 e^{\alpha y}$.

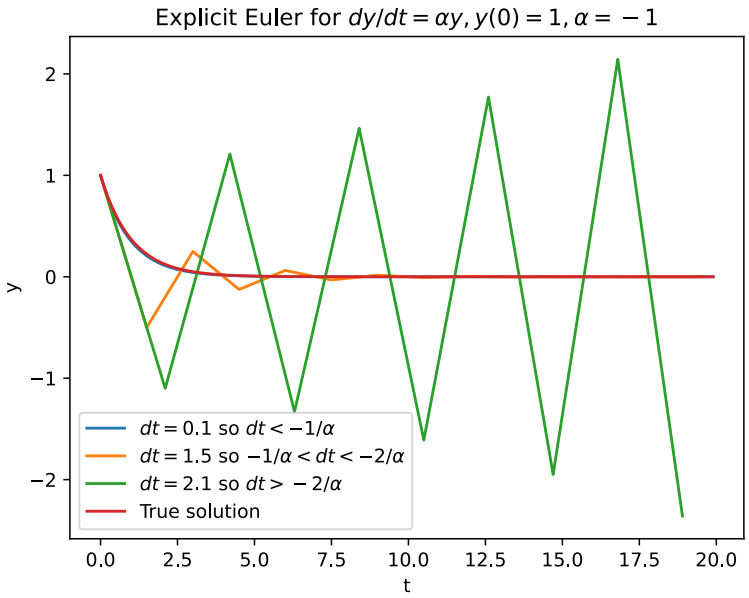

Figure 14: Linear stability of the Explicit Euler scheme.

The results of applying Explicit Euler for different step sizes Δt are shown in figure 14. At a small step size the correct solution is obtained, for a larger step size the numerical solution becomes oscillatory and for even larger step sizes it diverges. We can quantitatively explain this behavior by looking at the Euler steps

$$\begin{aligned} y^{(n+1)} &= y^{(n)} + \alpha y^{(n)} \Delta t \\ &= y^{(n)}(1 + \alpha \Delta t) \\ &= y^{(0)}(1 + \alpha \Delta t)^{n+1} \end{aligned}$$

- $\Delta t < -\frac{1}{\alpha} \rightarrow$ we observe monotonous decrease (ok)
- $-\frac{1}{\alpha} < \Delta t < -\frac{2}{\alpha} \rightarrow$ oscillation (regarding the sign) but still decrease in the absolute value (problematic)
- $-\frac{2}{\alpha} < \Delta t \rightarrow$ an increasing, oscillating solution (very bad)

The growth factor $R(\alpha \Delta t) = 1 + \alpha \Delta t$ in $y^{(n+1)} = R(\alpha \Delta t) y^{(n)}$ is called stability function and

$$\mathcal{D} := \{z \in \mathcal{C} : |R(z)| \leq 1\} \quad \text{so} \quad D_{Euler} = \{z = \alpha \Delta t \in \mathcal{C} : |1 + z| \leq 1\}$$

is called region of absolute stability or linear stability domain. D_{Euler} is a finite region of absolute stability in form of a circle on the left of the complex plane (see figure 15).

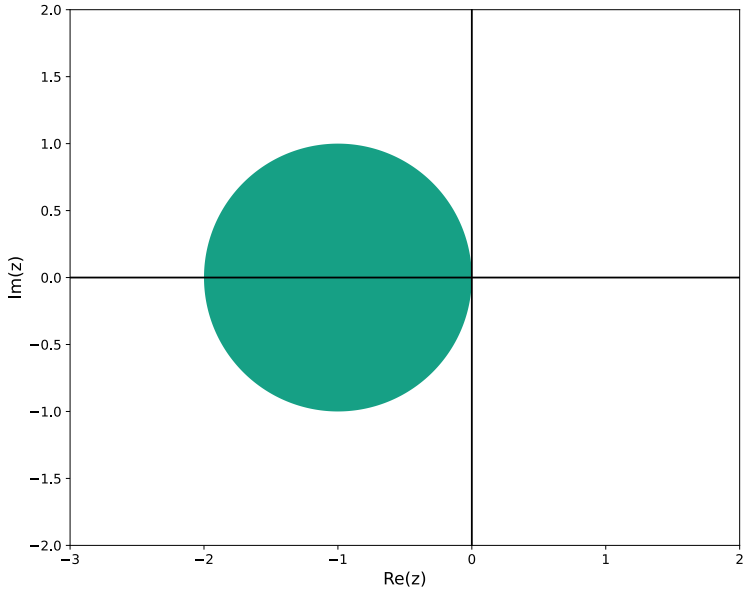

Figure 15: Region of absolute stability of the Explicit Euler method.

Problem: While in this example the stability constraint is easy to fulfill (we get a good solution for a reasonably large step-size), in problems with different timescales, with explicit Euler we must resolve the fastest one, even if its completely negligible (*stiff problems*).

More on stability, A-stable, L-stable, ...

3.4 Introduction of the Problem of Stiffness and Implicit Euler to the help

3.4.1 Introducing stiffness at the hand of a simple example

Consider the following ODE system (following Press et al., 2007, chapter 17.5)

$$\partial_t y_1 = 998 y_1 + 1998 y_2$$
$$\partial_t y_2 = -999 y_1 - 1999 y_2$$

with initial conditions $y_1(0) = 1$ and $y_2(0) = 0$. The system can be represented in matrix form as

$$\partial_t \begin{pmatrix} y_1 \\ y_2 \end{pmatrix} = \underline{\underline{A}} \begin{pmatrix} y_1 \\ y_2 \end{pmatrix}, \quad \underline{\underline{A}} = \begin{pmatrix} 998 & 1998 \\ -999 & -1999 \end{pmatrix}$$

The eigenvalues of $\underline{\underline{A}}$ are $\lambda_1 = -1$ and $\lambda_2 = -1000$. The eigenvectors are $\underline{e}_1 = \begin{pmatrix} 1 \\ -1 \end{pmatrix}$ and $\underline{e}_2 = \begin{pmatrix} 2 \\ -1 \end{pmatrix}$. The solution of the system is then

$$\begin{pmatrix} y_1(t) \\ y_2(t) \end{pmatrix} = \exp\left(\underline{\underline{A}}t\right) \begin{pmatrix} 1 \\ 0 \end{pmatrix} = \begin{pmatrix} 2 \\ -1 \end{pmatrix} \exp\left(-1t\right) + \begin{pmatrix} -1 \\ 1 \end{pmatrix} \exp\left(-1000t\right)$$

Let us now apply the Explicit Euler method to this system for different time-steps Δt. The result is shown in figure 16.

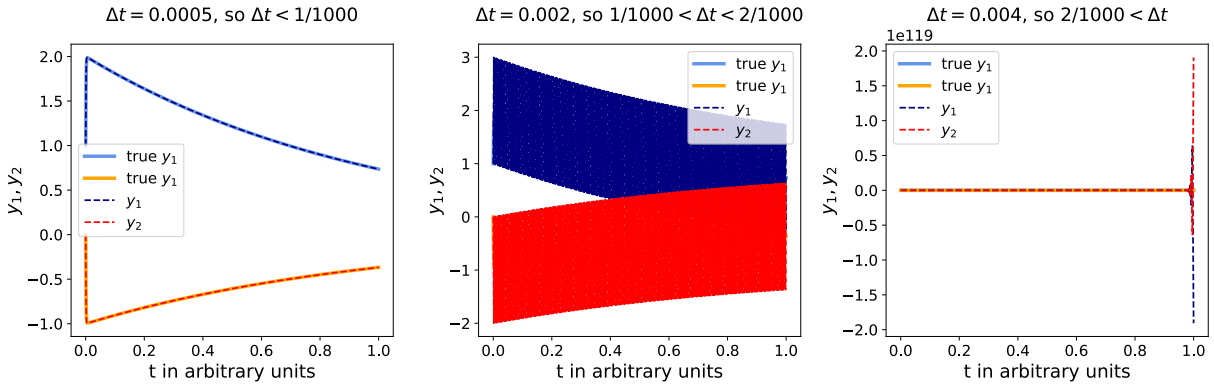

Figure 16: Numerical solution to the linear system $\partial_t \begin{pmatrix} y_1 \\ y_2 \end{pmatrix} = \underline{\underline{A}} \begin{pmatrix} y_1 \\ y_2 \end{pmatrix}$ with $\underline{\underline{A}} = \begin{pmatrix} 998 & 1998 \\ -999 & -1999 \end{pmatrix}$ and $y_1(0) = 1$, $y_2(0) = 0$ using the Explicit Euler method for different time-steps Δt. The left panel shows the solution for $\Delta t = 0.0005$, the central one for $\Delta t = 0.002$ and the right one for $\Delta t = 0.004$.

Let us think back to the linear stability analysis of the Explicit Euler scheme for $\partial_t y = \alpha y, Re(\alpha) < 0, y(0) = y_0$. We had obtained

- $\Delta t < -\frac{1}{\alpha} \rightarrow$ we observe monotonous decrease (ok)
- $-\frac{1}{\alpha} < \Delta t < -\frac{2}{\alpha} \rightarrow$ oscillation (regarding the sign) but still decrease in the absolute value (problematic)
- $-\frac{2}{\alpha} < \Delta t \rightarrow$ an increasing, oscillating solution (very bad)

The same result holds in principle for our linear system - but with α replaced by the eigenvalue of largest magnitude of $\underline{\underline{A}}$, here $\lambda_2 = -1000$ (for the proof see Press et al., 2007, chapter 17.5).

As we move away from the origin, the fastest decreasing term $\propto \exp\left(-\lambda_2 t\right)$ in the true solution is completely negligible. However, in the explicit scheme it still sets the timescale

that has to be resolved for a stable solution.

In the setting of $\partial_t y = \alpha y, Re(\alpha) < 0$ the stability constraint for Δt is not too problematic because the resulting step-size is reasonable compared to the timescale of the problem. In the case of an ODE with different timescales in the solution, however, we are often interested in the timescale of the slowest processes but in the explicit scheme we still need to resolve the fastest timescale which quickly becomes infeasable. This is the problem of stiffness and can - in such a linear setting with all negative eigenvalues of $\underline{\underline{A}}$ - be characterized by the stiffness ratio

$$\text{stiffness ratio} := \frac{\max_{\text{eigenvalues } \lambda_i \text{ of } \underline{\underline{A}}} |\text{Re } \lambda_i|}{\min_{\text{eigenvalues } \lambda_i \text{ of } \underline{\underline{A}}} |\text{Re } \lambda_i|} = \frac{\lambda_2}{\lambda_1} = 1000$$

A large stiffness ratio indicates that an explicit scheme like the Explicit Euler method would be very inefficient for following the slowest process.

3.4.2 A *definition* of stiffness

As discussed in Lambert, 1991 a hard mathematical definition of stiffness is difficult and we therefore resort to the broad practical definition (Lambert, 1991, chapter 6)

> »If a numerical method with a finite region of absolute stability, applied to a system with any initial conditions, is forced to use in a certain interval of integration a step length which is excessively small in relation to the smoothness of the exact solution in that interval, then the system is said to be stiff in that interval.«

An example for a numerical method with a finite region of absolute stability is the Explicit Euler method (see figure 15). In the example above, in spite of the fact that the solution is very smooth and the term $\propto \exp(-\lambda_2 t)$ is quickly negligible, we have to use excessively small steps.

3.4.3 Implicit Euler to the help

At the core of dealing with stiffness are implicit methods, the simplest representative being Implicit Euler.

An Implicit Euler step for solving $\partial_t \underline{y} = \underline{f}\left(\underline{y}\right)$ is given by

$$\underline{y}^{(n+1)} = \underline{y}^{(n)} + \underline{f}\left(\underline{y}^{(n+1)}\right)\Delta t \quad \text{where} \quad \underline{y}^{(0)} = \underline{y}_0$$

which is an implicit equation as $\underline{f}$ is evaluated at the new time step $\underline{y}^{(n+1)}$.

Intuition behind implicit Euler: We can write the implicit Euler step as $\underline{y}^{(n+1)} - \underline{f}\left(\underline{y}^{(n+1)}\right)\Delta t = \underline{y}^{(n)}$, so which is the point where when I sit on it and shoot back with the corresponding slope, I get back to where I am coming from. This is illustrated in figure 17.

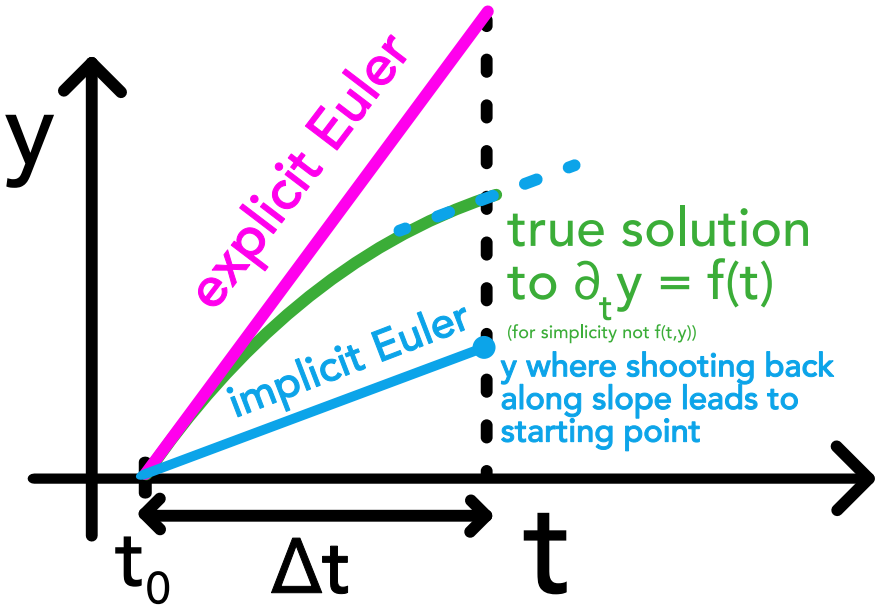

Figure 17: Illustration of the implicit Euler step.

Note: Implicit Euler is often referred to as backward Euler and the explicit Euler as forward Euler.

Problem: Note that implicit Euler is also a first order accurate scheme.

Region of absolute stability of the Implicit Euler method

As for the Explicit Euler method, we perform a linear stability analysis of the Implicit Euler method for $\partial_t y = \alpha y, Re(\alpha) < 0, y(0) = y_0$. We obtain

$$y^{(n+1)} = y^{(n)} + \alpha y^{(n+1)}\Delta t \quad \Rightarrow \quad y^{(n+1)} = \frac{1}{1-\alpha\Delta t} y^{(n)}$$

which decreases for any $\Delta t > 0$ (illustrated in figure 18a). For large time-steps, the result is inaccurate (Implicit Euler is a first order scheme) but the solution remains stable. As of the stability function $R(z) = \frac{1}{1-z}$ the region of absolute stability is given by

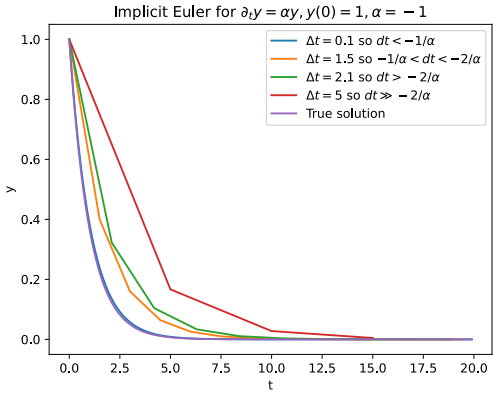

(a) Linear stability of Implicit Euler.

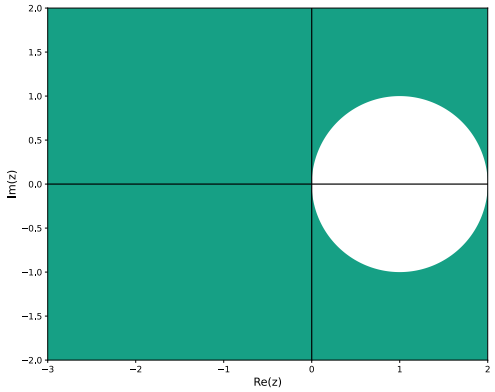

(b) Region of absolute stability of the Implicit Euler method (shaded in green).

Figure 18: Stability of the Implicit Euler scheme.

$$\mathcal{D}_{\text{implicit euler}} = \{z \in \mathbb{C} \mid |R(z)| < 1\} = \{z \in \mathbb{C} \mid |1 - z| > 1\}$$

which is illustrated in figure 18b. The whole left half plane is included in the region of absolute stability and the method is therefore unconditionally stable.

Implicit Euler for stiff linear ODEs

As Implicit Euler is unconditionally stable, the fast oscillating terms resulting from

$$\partial_t \begin{pmatrix} y_1 \\ y_2 \end{pmatrix} = \underline{\underline{A}} \begin{pmatrix} y_1 \\ y_2 \end{pmatrix}, \quad \underline{\underline{A}} = \begin{pmatrix} 998 & 1998 \\ -999 & -1999 \end{pmatrix}$$

with initial conditions $y_1(0) = 1$ and $y_2(0) = 0$ are no problem as illustrated in figure 19, where in spite of the relatively large time-step a good approximation of the solution is obtained.

The implicit step for such a linear system $\partial_t \underline{y} = \underline{\underline{A}}\underline{y}$ is

$$\underline{y}^{(n+1)} = \underline{y}^{(n)} + \underline{\underline{A}}\underline{y}^{(n+1)}\Delta t \quad \Rightarrow \quad \left(\underline{\underline{1}} - \underline{\underline{A}}\Delta t\right) \underline{y}^{(n+1)} = \underline{y}^{(n)}$$

which means that to make a step we have to solve a linear system which is usually done by matrix decomposition (like LU decomposition).

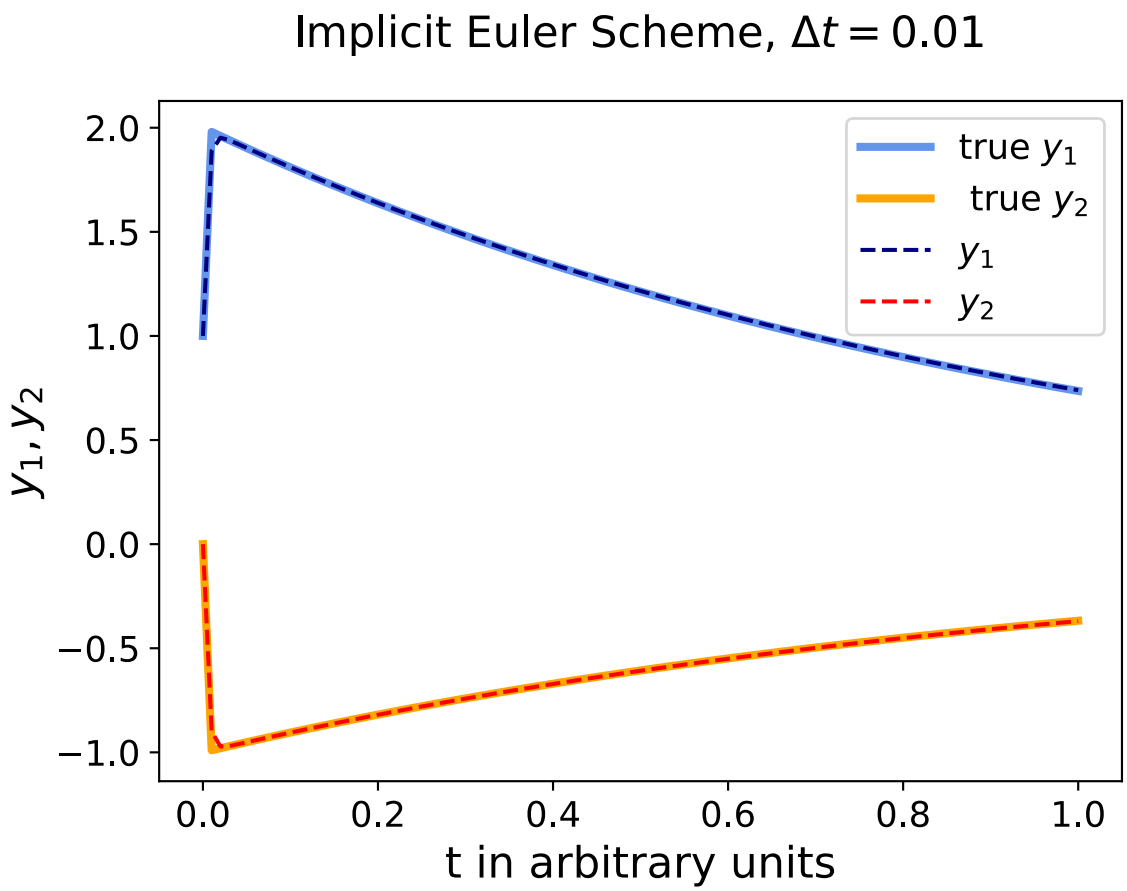

Figure 19: The same problem as in figure 16 is now approached using the Implicit Euler method and a relatively large time-step of $\Delta t = 0.01$.

But how can we approach non-linear ODEs using the Implicit Euler method?

To perform an implicit step

$$\underline{y}^{(n+1)} = \underline{y}^{(n)} + \underline{f}\left(\underline{y}^{(n+1)}\right) \Delta t$$

for a non-linear system $\partial_t \underline{y} = \underline{f}\left(\underline{y}\right)$ like the Davis-Skodje equation

$$\begin{aligned} \dot{y}_1(t) &= -y_1(t) \\ \dot{y}_2(t) &= -\gamma y_2(t) + \frac{(\gamma - 1) y_1(t) + \gamma y_1^2(t)}{(1 + y_1(t))^2} \end{aligned}$$

where γ is a measure for the stiffness (see Heiter, 2012, chapter 2.4) we reformulate the implicit step as a root-finding problem

$$\underline{0} = \underline{y}^{(n+1)} - \underline{y}^{(n)} - \Delta t \underline{f}\left(\underline{y}^{(n+1)}\right), \quad \underline{g}\left(\underline{\xi}\right) := \underline{\xi} - \underline{y}^{(n)} - \Delta t \underline{f}\left(\underline{\xi}\right)$$
$$\rightarrow \underline{0} = \underline{g}\left(\underline{\xi}\right) \Leftrightarrow \underline{\xi} = \underline{y}^{(n+1)}$$

where each of those time-steps is solved using Newton's method (or quasi-Newton)

$$\underline{\xi}_{k+1} = \underline{\xi}_k - \underline{\underline{J}}_{\underline{g}}^{-1}\left(\underline{\xi}_k\right) \underline{g}\left(\underline{\xi}_k\right), \quad \underline{\underline{J}}_{\underline{g}} = \underline{\underline{1}} - \Delta t \gamma \left(\underline{\xi}_k\right) \underline{\underline{J}}_{\underline{f}}$$

$$\underline{\xi}_0 = \underline{y}^{(n)}, \quad \underline{\xi}_m \rightarrow \underline{y}^{(n+1)} \quad \text{for} \quad m \rightarrow \infty$$

where $\underline{\underline{J}}_{\underline{f}}$ is the Jacobian of $\underline{f}$. In Quasi-Newton the Jacobian is only recalculated once per time-step in the Euler method

$$\underline{\xi}_{k+1} = \underline{\xi}_k - \underline{\underline{J}}_{\underline{g}}^{-1}\left(\underline{\xi}_0\right) \underline{g}\left(\underline{\xi}_k\right)$$

For the Davis-Skodje problem mentioned above some Implicit Euler steps are drawn into the stream plot of the equation in figure 20. Here, one can also see the intuition behind Implicit Euler steps: One searches a point where the derivative is such that shooting back with this slope leads back to the point we are coming from, as

$$\underline{y}^{(n)} = \underline{y}^{(n+1)} - \underline{f}\left(\underline{y}^{(n+1)}\right) \Delta t$$

The steps of the Newton iteration done for each Implicit Euler step can most intuitively be understood in the formulation as the linear equation

$$\underline{b} := \underline{g}\left(\underline{\xi}_k\right) = \underline{\underline{J}}_{\underline{g}}\left(\underline{\xi}_k - \underline{\xi}_{k+1}\right) = \underline{\underline{J}}_{\underline{g}} \underline{a}, \quad \underline{a} := \underline{\xi}_k - \underline{\xi}_{k+1}$$

which is also the equation solved on the computer using matrix decomposition. $\underline{\underline{J}}_{\underline{g}} \underline{a}$ is the directional derivative of $\underline{g}$ in the direction of $\underline{a}$ and in a step of the Newton iteration we search for a step $\underline{a}$ that gets us from $\underline{0}$ to $\underline{b}$ in other words $\underline{\xi}_{k+1} = \underline{\xi}_k - \underline{a}$.

Problem: While the Implicit Euler method is unconditionally stable, performing the implicit step for non-linear ODEs requires solving a non-linear equation with some root-finding algorithm, which can be even more costly than doing small explicit steps if no proper care (e.g. smart forward differentiation in the root finding) is taken.

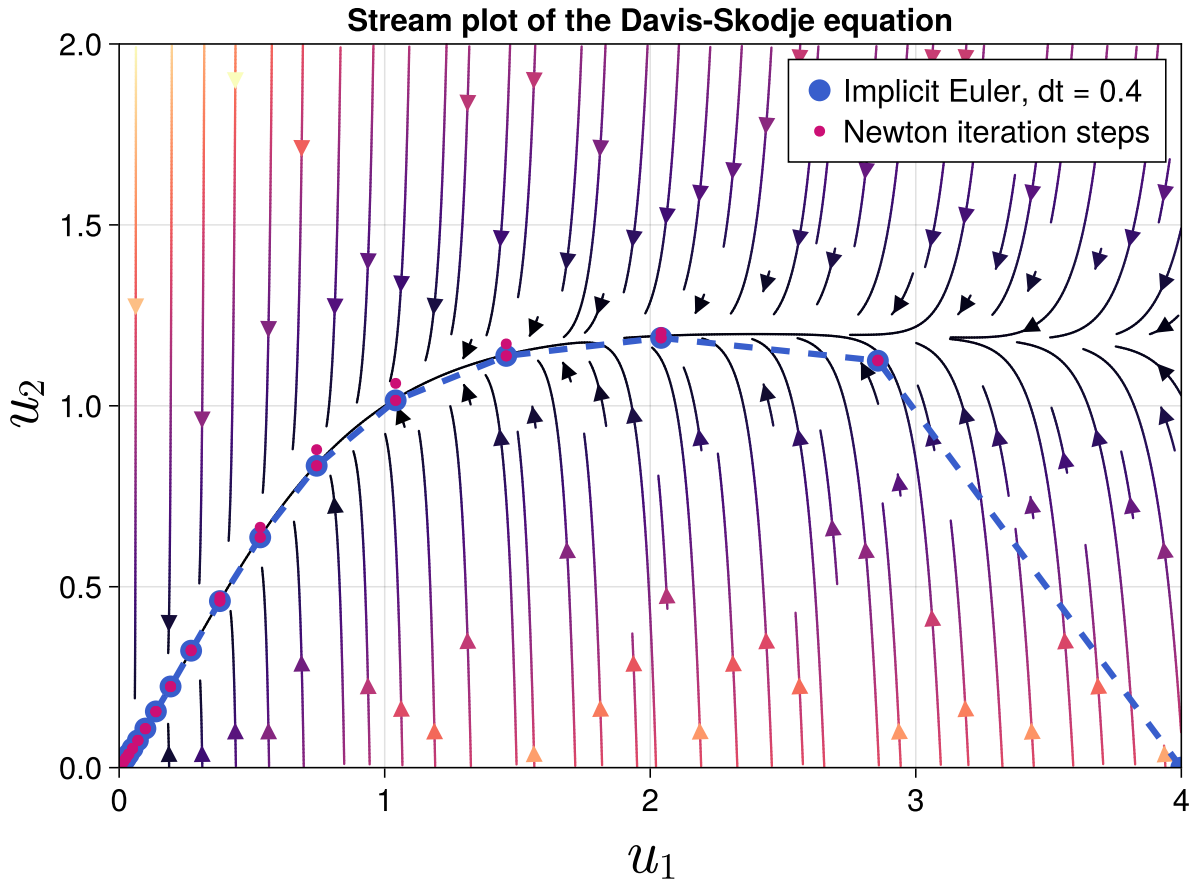

Figure 20: Stream plot of the Davis-Skodje equation with some Implicit Euler steps also drawn. The direction of the Implicit Euler steps is from right (starting at (4, 0)) to left.

3.5 Construction of higher-order methods

The two basic kinds of numerical methods for ODEs are

- one-step methods using one starting value at each step (in a step we want to get from $y^{(n)}$ to $y^{(n+1)}$)
- multistep methods using e.g. also $y^{(n-1)}, y^{(n-2)}$ to get from $y^{(n)}$ to $y^{(n+1)}$

In this subsection, we essentially only deal with one-step methods.

3.5.1 Meaning of going to higher order

Let us first understand, why we would want a higher order method. We still want to solve $\underline{f} = \underline{f}(\underline{y}, t)$ with $\underline{y}(t^{(0)}) = \underline{y}^{(0)}$ and our scheme approximates $\underline{y}(t^{(0)} + h)$ as $\underline{y}^{(1)}$. The scheme has order p if

$$||\underline{y}(t^{(0)} + h) - \underline{y}^{(1)}|| \leq Kh^{p+1} \tag{56}$$

for sufficiently smooth problems, so if the Taylor series for the exact solution $\underline{y}(t^{(0)}+h)$ and for $\underline{y}^{(1)}$ coincide up to (and including) h^p.

Computational advantage: Our basic unit of cost are function evaluations of $\underline{f}(\underline{y},t)$, where explicit Euler takes one function evaluation per step and has $p=1$. Now imagine we can construct a second order scheme ($p=2$) with some constant number of function evaluations per step. While halving the step-size still doubles the integration cost over an interval for $p=2$ it quarters the error, so at some point the higher order scheme will be advantageous.

3.5.2 Approaches to constructing a higher order method

Higher order schemes can either be constructed using Taylor expansion so higher order derivatives (can be costly) or by the weighted combination of simple derivatives of multiple points and clever substeps.

3.5.3 Construction by Taylor expansion

The most obvious way to get a higher order truncation error, is to build a scheme based on higher order Taylor expansion.

We start by expanding $y(t)$ around some time t.

$$y(t+h) = y(t) + h\,\partial_t y\big|_t + \frac{h^2}{2}\,\partial_t^2 y\big|_t + \frac{h^3}{6}\,\partial_t^3 y\big|_t + \mathcal{O}(h^4) \tag{57}$$

The expansion up to the first order is just our explicit Euler scheme. As of our problem statement (1st order ODE)

$$\partial_t y = f(y,t), \quad y(t^{(0)}) = y^{(0)}, \quad t^{(n)} = t^{(0)} + hn, \quad \text{stepsize } h \tag{58}$$

(with the solutions defining 2D trajectories $(t, y(t))$ and we approximate $(t^{(n)}, y^{(n)})$), we can express the higher order derivatives in the Taylor expansion as (chain rule)

$$\begin{gathered}\partial_t^k y\big|_t = \left(\frac{d}{dt}\right)^{k-1} f\Big|_{y(t),t} =: f^{(k-1)}(y,t) \\ f^{(k)}(y,t) = \partial_t f^{(k-1)}(y,t) + (\partial_t y)\partial_y f^{(k-1)}(y,t) = \partial_t f^{(k-1)}(y,t) + f\partial_y f^{(k-1)}(y,t)\end{gathered} \tag{59}$$

Problem: The higher order derivatives have to be calculated recursively e.g. with forward differentiation at the ground level which is complicated and slow.

Problem: In high-order Taylor expansion, the individual terms can be numerically problematic, e.g. in

$$\cos(x)|_{x=0} \approx 1 - \frac{x^2}{2} + \frac{x^4}{4!} + \dots \tag{60}$$

all polynomial terms diverge while the infinite sum is bound in $[-1, 1]$ as expected to the cosine.

3.5.4 Runge-Kutta (RK) Integration schemes I: General Idea

Consider instead of a 1st order ODE problem $\partial_t y = f(y, t)$ we had a quadrature problem $\partial_t y = f(t)$. Then a step would be

$$y(t + h) = y(t) + \int_t^{t+h} f(t')dt' \tag{61}$$

where we could approximate, e.g. using the trapezoidal rule

$$y^{(n+1)} = y^{(n)} + h\frac{f^{(n+1)} + f^{(n)}}{2}, \quad f(n) = f(t^{(0)} + hn) \tag{62}$$

We can't just apply this to the ODE $\partial_t y = f(y, t)$, because to calculate $f^{(n+1)}$ there we need $y^{(n+1)}$ which is what we are searching for. But what if we would approximate $y^{(n+1)}$ for $f^{(n+1)}$ with an Euler step? We would then have

$$\begin{aligned} k_1 &= f\left(y^{(n)}, t^{(n)}\right) \\ k_2 &= f\left(y^{(n)} + hk_1, t^{(n)} + h\right) \\ y^{(n+1)} &= y^{(n)} + \frac{h}{2}\left(k_1 + k_2\right) + \mathcal{O}\left(h^3\right) \end{aligned} \tag{63}$$

where the central advantage roughly is, that k_2 which includes the Euler approximation of $\mathcal{O}(h^2)$ is multiplied by h in the expression for $y^{(n+1)}$ so the error becomes less important. This already is the *RK2* scheme. The more general idea is illustrated in figure 21.

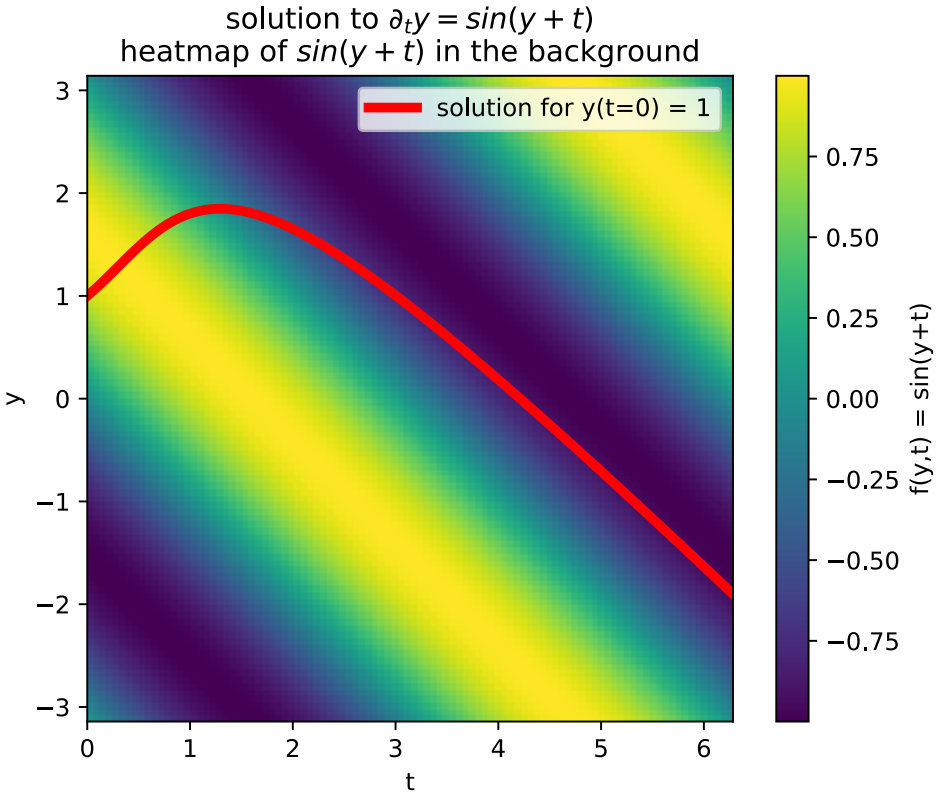

Figure 21: For a step in t the corresponding step in y equals the integration of $f(y,t)$ over the correct path. The correct path, however, is unknown. So we approximate points along the path to get a better approximation of the step as an approximation of the integral over $f(y,t)$.

3.5.5 Runge-Kutta (RK) Integration schemes II: Derivation of the general RK scheme

Using clever substeps, we want to construct an accurate and cost-efficient scheme, to solve the initial value problem $\partial_t \underline{y} = f(\underline{y}, t)$ with $y(t^{(0)}) = y^{(0)}$. We make the ansatz

$$\begin{aligned}
\underline{y}(t+h) &= \underline{y}(t) + \left[\underline{y}(t+h) - \underline{y}(t)\right] \\
&= \underline{y}(t) + \int_t^{t+h} \partial_t \underline{y}\big|_{t'}\, dt' \\
&= \underline{y}(t) + h \int_0^1 \partial_t \underline{y}\big|_{t+\tau h}\, d\tau \\
&= \underline{y}(t) + h \int_0^1 \underline{f}(\underline{y}(t+\tau h), t+\tau h) d\tau
\end{aligned} \tag{64}$$

which will later allow us to extrapolate $\underline{y}$ according to the ODE. We approximate the integral by a quadrature rule of the form

$$\begin{aligned} &\int_0^1 g(\tau)d\tau \approx \sum_{i=1}^m \beta_i g(\gamma_i), \quad \text{RK weights } \beta_i, \quad \text{RK nodes } \gamma_i \\ &\sum_{i=1}^m \beta_i = 1 \quad \rightarrow \quad \text{correct integration of unity } g \equiv 1, \quad \text{scheme order } m \end{aligned} \tag{65}$$

Application to the ansatz (64) yields

$$\underline{y}(t+h) \approx \underline{y}(t) + h \sum_{i=1}^m \beta_i \underline{f}(\underline{y}(t+\gamma_i h), t+\gamma_i h) \tag{66}$$

Problem: We don't know $\underline{y}(t+\gamma_i h)$ yet.

Idea: Use an analogous quadrature rule to get approximations to $\underline{y}(t+\gamma_i h)$ with the γ_i as nodes again - quadrature in quadrature.

$$\begin{aligned} &\underline{y}(t+\gamma_i h) = \underline{y}(t) + h \int_0^{\gamma_i} \partial_t \underline{y}\big|_{t+\tau h} d\tau \approx \underline{y}(t) + h \sum_{l=1}^m \alpha_{i,l}\, \partial_t \underline{y}\big|_{t+\gamma_l h} \\ &\sum_{i=1}^m = \gamma_i \quad \rightarrow \quad \text{correct integration of unity } g \equiv 1, \quad i = 1, \dots, m \end{aligned} \tag{67}$$

We define

$$\underline{k}_l := \partial_t \underline{y}\big|_{t+\gamma_l h} = \underline{f}\left(\underline{y}(t+\gamma_l h), t+\gamma_l h\right) \tag{68}$$

But what have we won, we still need the $\underline{y}(t+\gamma_l h)$, right? By setting $\alpha_{i,l} = 0$ for $l \leq i$, we gain an explicit scheme where $\underline{y}(t+\gamma_l h)$ is constructed only based on previous substeps.

1. Starting with $\underline{y}^{(0)} = \underline{y}(t^{(0)})$ and $\underline{k}_1 = \underline{f}(\underline{y}^{(0)}, t^{(0)})$ we approximate $\underline{y}(t^{(0)} + \gamma_1 h)$ from which we calculate $\underline{k}_1 = \underline{f}(\underline{y}(t^{(0)}+\gamma_1 h), t^{(0)}+\gamma_1 h)$, then based on k_0, k_1 we approximate $\underline{y}(t^{(0)} + \gamma_2 h)$ and thus k_3 and so on.
2. Based on $\underline{k}_1, \dots, \underline{k}_m$, we approximate $\underline{y}^{(1)} = \underline{y}^{(0)} + h \sum_{i=1}^m \beta_i \underline{k}_i$
3. ...

3.5.6 Runge-Kutta (RK) Integration schemes III: General m-substep RK method

In general, we have obtained

$$\begin{aligned} \underline{y}^{(n+1)} &= \underline{y}^{(n)} + h \sum_{i=1}^{m} \beta_i \underline{k}_i \\ \underline{k}_i &= f\left(\left(\underline{y}^{(n)} + h \sum_{l=1}^{m-1} \alpha_{i,l} \underline{k}_l\right), t_n + \gamma_i h\right), \quad i = 1, \ldots, m \\ \sum_{l=1}^{m} \alpha_{i,l} &= \gamma_i, \quad \alpha_{i,l} = 0 \text{ for } l \geq i \rightarrow \text{ explicit method} \end{aligned} \tag{69}$$

where for $\alpha_{i,l} = 0$ for $l \geq i$, $\underline{k}_i$ only depends on $\underline{k}_l, l < i$.

3.5.6.1 Butcher-Tableau for visualizing the RK coefficients

The general Butcher-Tableau is given in figure 22, for an explicit scheme, the α's form a lower left triangular matrix ($\alpha_{i,l} = 0$ for $l \geq i$, $\underline{k}_i$).

Examples for butcher tableaus of explicit RK methods are given in table 3.

Explicit Euler (1st order)	Implicit Euler (1st order)	RK2 (2nd order)	RK4 (4th order)
$\begin{array}{c\|c} 0 & \\ \hline & 1 \end{array}$	$\begin{array}{c\|c} 0 & 1 \\ \hline & 1 \end{array}$	$\begin{array}{c\|cc} 0 & & \\ 1 & 1 & \\ \hline & \frac{1}{2} & \frac{1}{2} \end{array}$	$\begin{array}{c\|cccc} 0 & & & & \\ \frac{1}{2} & \frac{1}{2} & & & \\ \frac{1}{2} & 0 & \frac{1}{2} & & \\ 1 & 0 & 0 & 1 & \\ \hline & \frac{1}{6} & \frac{1}{3} & \frac{1}{3} & \frac{1}{6} \end{array}$

Table 3: Butcher-Tableau for explicit RK methods.

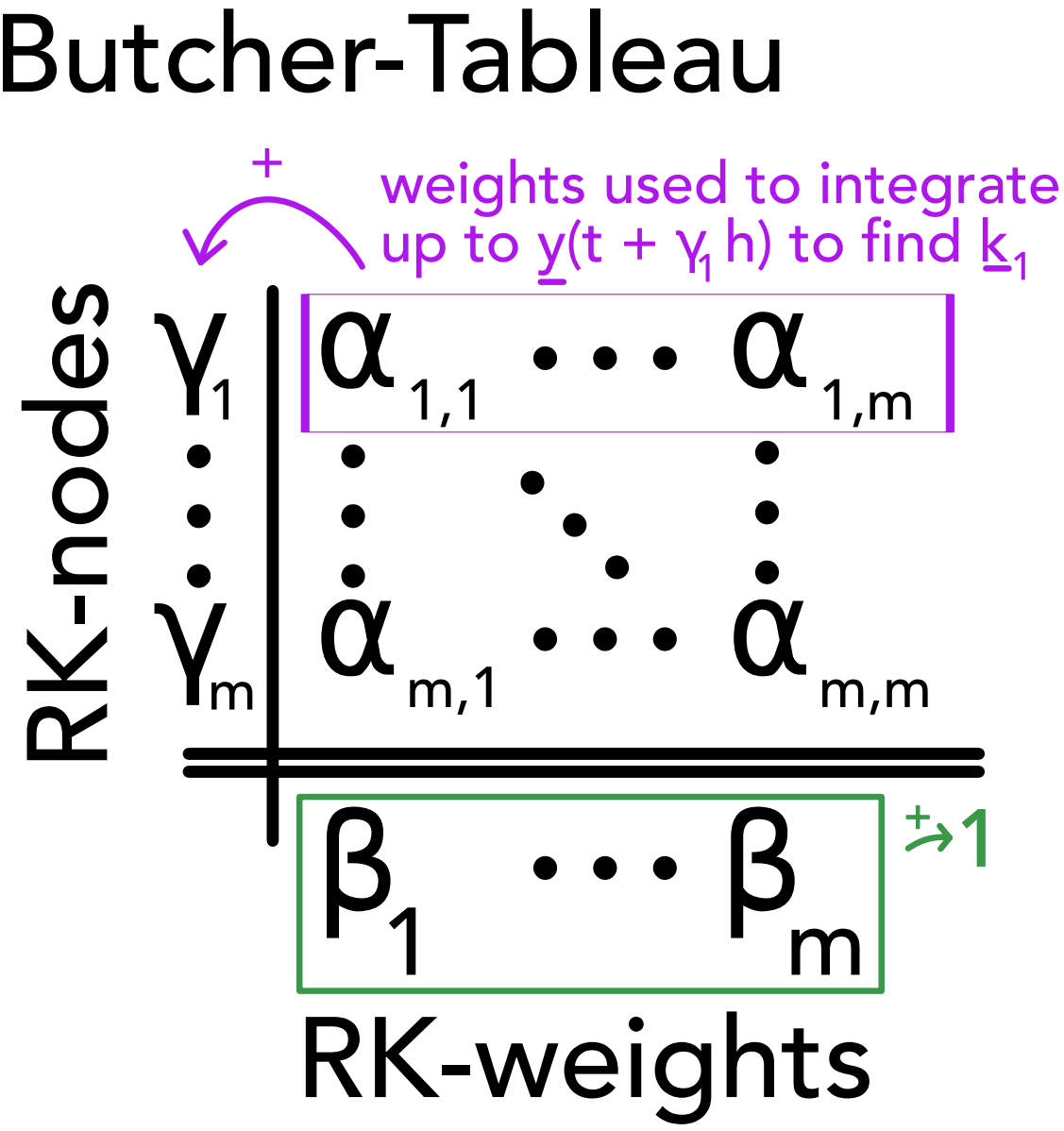

Figure 22: Butcher-Tableau for the general m-substep RK method.

3.5.7 Runge-Kutta (RK) Integration schemes IV: Taylor expansion to identify RK parameters for 2nd order schemes

3.5.7.1 Comparison of coefficients

We want to find appropriate α's and β's such that the RK scheme follows the **Taylor expansion**

$$\begin{aligned} y(t^{(n+1)}) &= y^{(n+1)} \\ &= y^{(n)} + h\partial_t y + \frac{h^2}{2}\partial_t^2 y + \mathcal{O}(h^3) \\ &= y^{(n)} + hf + \frac{h^2}{2}\frac{d}{dt}f + \mathcal{O}(h^3) \\ &= y^{(n)} + hf + \frac{h^2}{2}\left((\partial_y f)\partial_t y + \partial_t f\right) + \mathcal{O}(h^3) \\ &\boxed{= y^{(n)} + hf + \frac{h^2}{2}\left(f\partial_y f + \partial_t f\right) + \mathcal{O}(h^3)} \end{aligned} \tag{70}$$

where if not specified differently, the evaluation is at (y_n, t_n), so that we know that the error per step is $\mathcal{O}(h^3)$.

Now let us bring the explicit RK ansatz for $m = 2$ ($\rightarrow$ only $\alpha_{2,1} \neq 0$ so $\gamma_1 = 0$ and $\gamma_2 = \alpha_{2,1}$) into the form of the Taylor expansion. We start with

$$\begin{aligned} y^{(n+1)} &= y^{(n)} + h(\beta_1 k_1 + \beta_2 k_2) \\ &= y^{(n)} + h(\beta_1 f + \beta_2 f\left((y^{(n)} + h\alpha_{2,1}f), t^{(n)} + \gamma_2 h\right)) \end{aligned} \tag{71}$$

and first order expand k_2 to

$$f\left((y^{(n)} + h\alpha_{2,1}f), t^{(n)} + \gamma_2 h\right) = f + h\alpha_{2,1}f\partial_y f + \gamma_2 h\partial_t f \tag{72}$$

Using $\gamma_2 = \alpha_{2,1}$ yields a form that allows comparison of coefficients

$$\begin{aligned} y^{(n+1)} &= y^{(n)} + h \cdot (\beta_1 f + \beta_2 \left(f + h\alpha_{2,1}f\partial_y f + \alpha_{2,1}h\partial_t f\right)) \\ &\boxed{= y^{(n)} + hf \cdot (\beta_1 + \beta_2) + h^2\beta_2\alpha_{2,1}\left(f\partial_y f + \partial_t f\right)} \end{aligned} \tag{73}$$

Comparing the boxed equations yields two equations for three variables $(\beta_1, \beta_2, \alpha_{2,1})$

$$\beta_1 + \beta_2 = 1, \quad \beta_2\alpha_{2,1} = \frac{1}{2} \quad \rightarrow \quad \text{choose } \beta_2 = q \tag{74}$$

so

$$\beta_1 = 1 - q, \quad \beta_2 = q, \quad \alpha_{2,1} = \frac{1}{2q} \tag{75}$$

3.5.7.2 Resulting integration formula with free parameter q

We get the integration formula

$$t^{(n+1)} = t^{(n)} + h, \quad y^{(n+1)} = y^{(n)} + h\left[(1-q)f + qf\left((y^{(n)} + \frac{h}{2q}f), t^{(n)} + \frac{h}{2q}\right)\right] \tag{76}$$

3.5.7.3 Different integration schemes based on the choice of q

Depending on q we can yield different schemes, with examples shown in table 4.

Only based on two function evaluations of f, the midpoint rule and RK2 are already second order accurate.

$q = 0$	$q = \frac{1}{2}$	$q = 1$
Forward Euler	2nd order Runge-Kutta (RK2) (aka Heun-method)	Midpoint-Rule
$k_1 = f(y^{(n),t^{(n)}})$ $y^{(n+1)} = y^{(n)} + hk_1 + \mathcal{O}(h^2)$	$k_1 = f(y^{(n),t^{(n)}})$ $k_2 = f(y^{(n)} + hk_1, t^{(n)} + h)$ $y^{(n+1)} = y^{(n)} + \frac{h}{2}(k_1 + k_2) + \mathcal{O}(h^3)$	$k_1 = f(y^{(n),t^{(n)}})$ $k_2 = f(y^{(n)} + \frac{h}{2}k_1, t^{(n)} + \frac{h}{2})$ $y^{(n+1)} = y^{(n)} + hk_2 + \mathcal{O}(h^3)$
Shoot along a tangent from the starting point.	• Using k_1 Euler-approximate $y(t+h)$ • Find k_2 using this approximation • Shoot with the mean of k_1 and k_2	Approximate y at the midpoint of the interval and use the slope there for shooting across the whole interval.
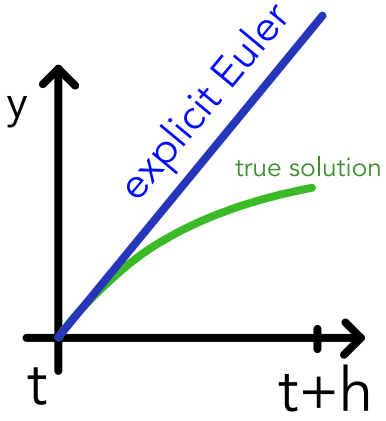	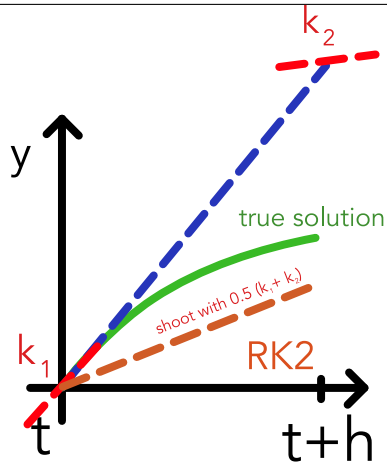	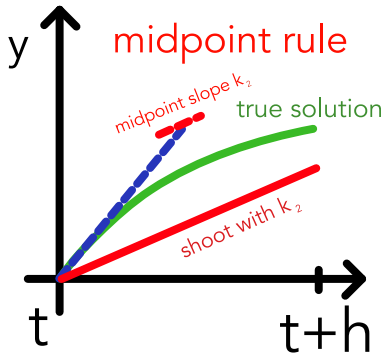

Table 4: Different schemes based on the choice of q.

3.5.8 Runge-Kutta (RK) Integration schemes V: Classical 4th order RK scheme (RK-4)

$$\begin{aligned} \underline{k}_1 &= \underline{f}(\underline{y}^{(n)}, t^{(n)}), \quad \underline{k}_2 = \underline{f}(\underline{y}^{(n)} + \frac{h}{2}\underline{k}_1, t^{(n)} + \frac{h}{2}), \\ \underline{k}_3 &= \underline{f}(\underline{y}^{(n)} + \frac{h}{2}\underline{k}_2, t^{(n)} + \frac{h}{2}), \quad \underline{k}_4 = \underline{f}(\underline{y}^{(n)} + h\underline{k}_3, t^{(n)} + h) \\ \underline{y}^{(n+1)} &= \underline{y}^{(n)} + \frac{h}{6}\left(\underline{k}_1 + 2\underline{k}_2 + 2\underline{k}_3 + \underline{k}_4\right) + \mathcal{O}(h^5) \end{aligned} \tag{77}$$

Note: Here we need 4 function evaluations of f per step. Depending on the situation, lower order schemes with smaller stepsize might be more efficient. Choosing an appropriate step-size might is very important.

An example application of RK4 with the corresponding evaluation points of k_2, k_3, k_4 is shown in figure 23.

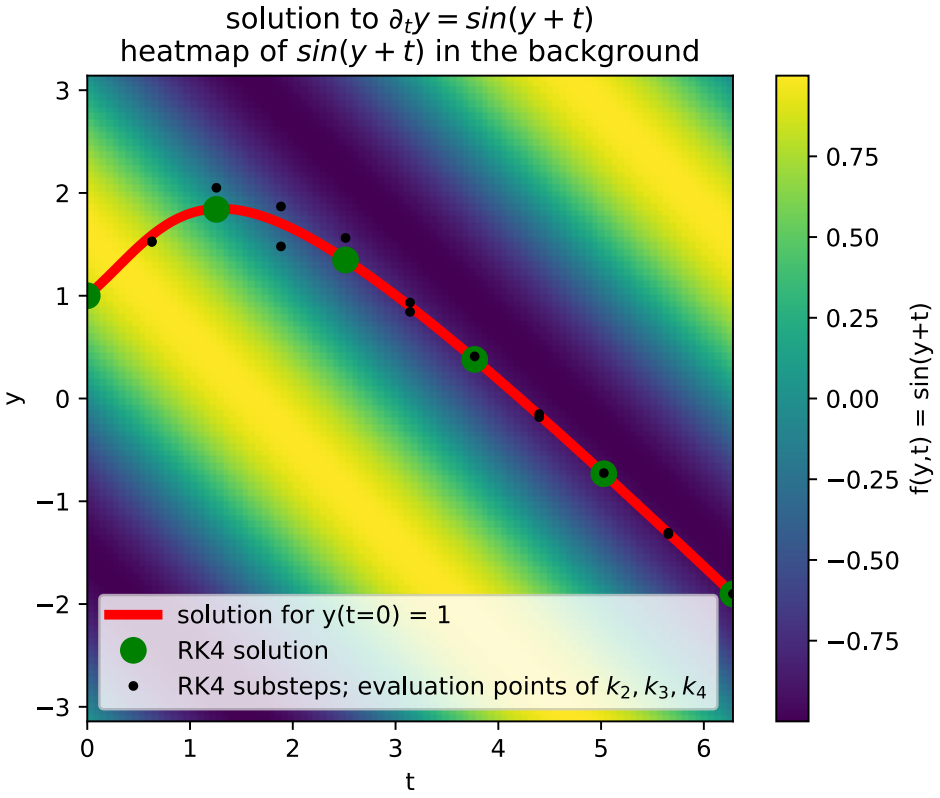

Figure 23: RK4 applied to the problem $\partial_t y = f(y,t)$ with $f(y,t) = \sin(y+t)$ and $y(0) = 1$. The evaluation points of k_2, k_3, k_4 are marked in black.

3.6 Adaptive Step Sizes

Problem: While in one region of a problem a relatively large step-size might suffice in others we might need a very small one. Using the large step size everywhere does not work but taking the small one everywhere is a waste of compute.

Idea: Take steps of adaptive size, striking a balance between accuracy, stability and efficiency. The adaptation is based on the estimation of a local integration error and a user-specified wanted upper bound on it. For an example see figure 24.

When we simulate e.g. hydrogen in space we might even want to use different step-sizes in different local regions of the problem (smaller timesteps in denser regions).

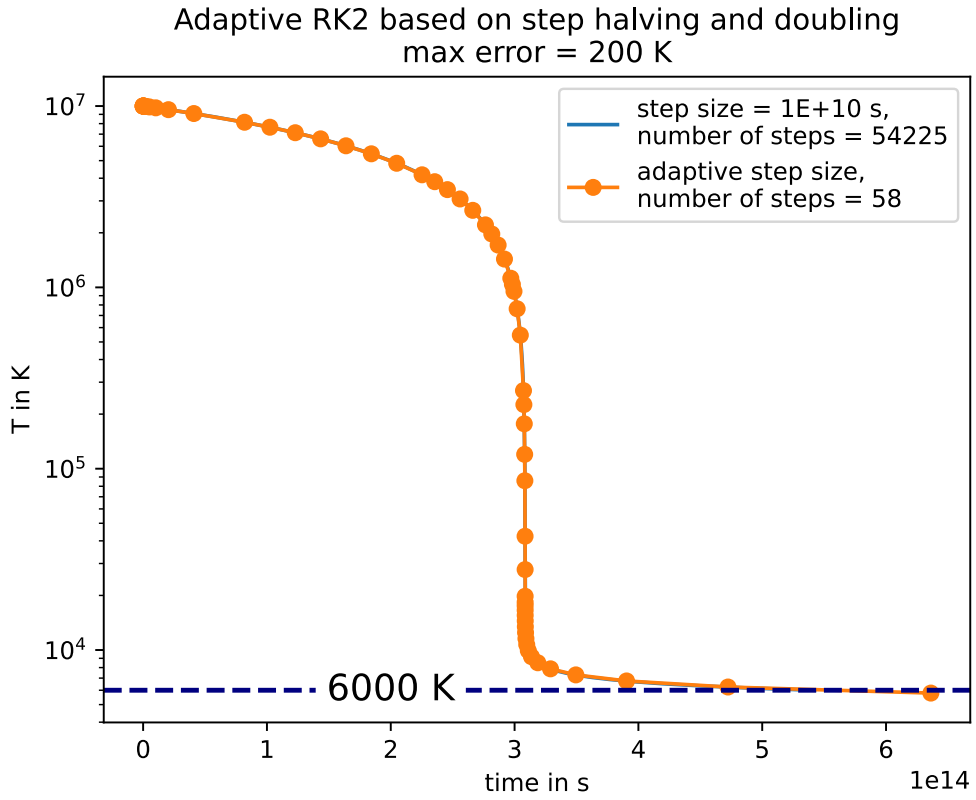

Figure 24: Example of adaptive step sizes.

3.6.1 Step halving and doubling method

We can estimate the local integration error by

- performing one step of size h to obtain y_a
- performing two steps of size $\frac{h}{2}$ to obtain y_b

from the same starting point and then comparing the results.

With this, the **halving and doubling scheme** given the user-specified local upper error bound ϵ_0 is

1. Calculate y_a, y_b and $\epsilon = |y_a - y_b|$
2. If $\epsilon > \epsilon_0$ discard the step and try again with $h' = \frac{h}{2}$
3. If $\epsilon \ll \epsilon_0$, keep y_b and use $h' = 2h$ for the next step (doubling)
4. Else if $\epsilon < \epsilon_0$, keep y_b and retain h for the next step

Advantage of the halving and doubling scheme in spatio-temporal simulations: Consider some hydrogen simulation. In a halving-doubling scheme we can use different step sizes in different spatial regions and still have results in sync - for every point on the coarse time-grid we will also have a result from the finer grids in time, see figure 25

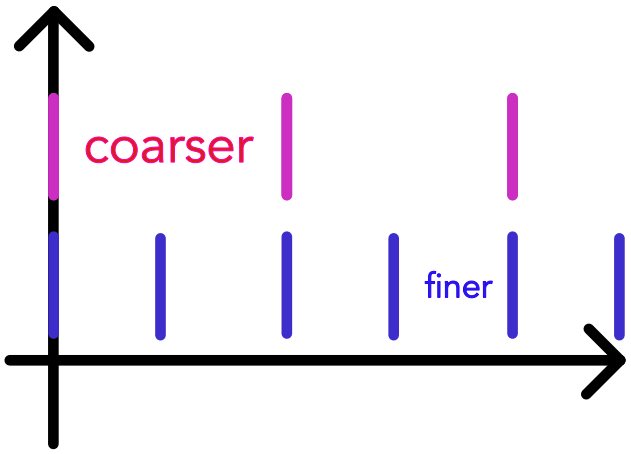

Figure 25: Different step sizes in time but still results in sync in the halving-doubling scheme.

Note: We said we want to double h for the next step for $\epsilon \ll \epsilon_0$. A more concise criterion is even if we double we would expect an error lower than the user-specified upper bound. For this we first make a remark on the local accuracy.

3.6.2 Note on the Local accuracy

As a p-th order scheme is locally accurate to the $p+1$-th order, we can write the local errors as

$$\begin{aligned} y_a - y(t^{(0)} + h) &= \alpha h^{p+1} + \mathcal{O}(h^{p+2}) \\ y_b - y(t^{(0)} + h) &= 2\alpha \left(\frac{h}{2}\right)^{p+1} + \mathcal{O}(h^{p+2}) \end{aligned} \tag{78}$$

yielding an error estimate of

$$\epsilon = |y_a - y_b| = \alpha h^{p+1}(1 - 2^{-p}) \tag{79}$$

3.6.3 When does doubling make sense?

For a doubled time-step, we expect the error ($h \to 2h$ in (79)) to be

$$\epsilon' = \alpha(2h)^{p+1}(1 - 2^{-p}) = 2^{p+1}\epsilon \tag{80}$$

which we still want to be smaller than ϵ_0 so we double if

$$\epsilon' = 2^{p+1}\epsilon < \epsilon_0 \tag{81}$$

so when the expected error after doubling is below our error bound.

3.6.4 Adaptively choosing ϵ_0

Problem: The smaller the time-step the more steps we need to cover a certain timespan, the more error can accumulate.

Idea: Set ϵ_0 adaptively, taking into account how many timesteps one would need to cover the total integration time with the current h, so

$$\epsilon_0 = \frac{h}{T}\epsilon_0^{\text{global}}, \quad \text{total integration time } T, \quad \text{prescribed global error bound } \epsilon_0^{\text{global}} \tag{82}$$

3.6.5 Continuous time step adjustment

While the halving-doubling is nicely suited for being able to use different step-sized in different spatial regions of a simulation, often we want a more flexible continuous adjustment.

Idea: For the next step use a step-size h^{new} such that we would assume this step-size to just hit the error bound in our current step (with some safety factor.)

The next timestep is scaled according to the current error, such that for h^{desired} we have $\epsilon' = \epsilon_0$ so

$$\begin{aligned} \epsilon_0 = \epsilon' = \alpha \cdot \left(h^{\text{desired}}\right)^{p+1} \cdot (1 - 2^{-p}) = \left(\frac{h^{\text{desired}}}{h}\right)^{p+1} \epsilon \\ \rightarrow h^{\text{desired}} = h\left(\frac{\epsilon_0}{\epsilon}\right)^{\frac{1}{p+1}}, \quad \text{error } \epsilon \text{ if step with size } h \text{ is taken} \end{aligned} \tag{83}$$

Note that we have used the error formula for the halving-doubling scheme but more generally assuming $\mathcal{O}(\epsilon) = h^{p+1}$ we get the same result for h^{desired} from

$$\frac{\epsilon_0}{\epsilon} = \left(\frac{h^{\text{desired}}}{h}\right)^{p+1} \tag{84}$$

3.6.5.1 Continuous adaptive time step control scheme

We get to the scheme

1. Advance the system by a step h and extimate the error of the step, we assume a p-th

order scheme with $\mathcal{O}(\epsilon) = h^{p+1}$

2. Calculate the new step size as

$$h^{\text{new}} = \beta h \left(\frac{\epsilon_0}{\epsilon}\right)^{\frac{1}{p+1}} \tag{85}$$

with some safety factor $\beta \sim 0.9$

3. If $\epsilon < \epsilon_0$ accept the step, otherwise discard it and repeat with the new step-size

But is there a more efficient way to estimate ϵ than the halving-doubling scheme?

3.6.5.2 Embedded Runge-Kutta schemes for cheaper error estimates

In embedded Runge-Kutta schemes like Runge-Kutta-Fehlberg (e.g. RKF45), based on the same function evaluations and respectively $\underline{k}_i$ schemes of different order are constructed and from the difference of their results, the error is estimated.

For instance RK45 is illustrated in figure 26.

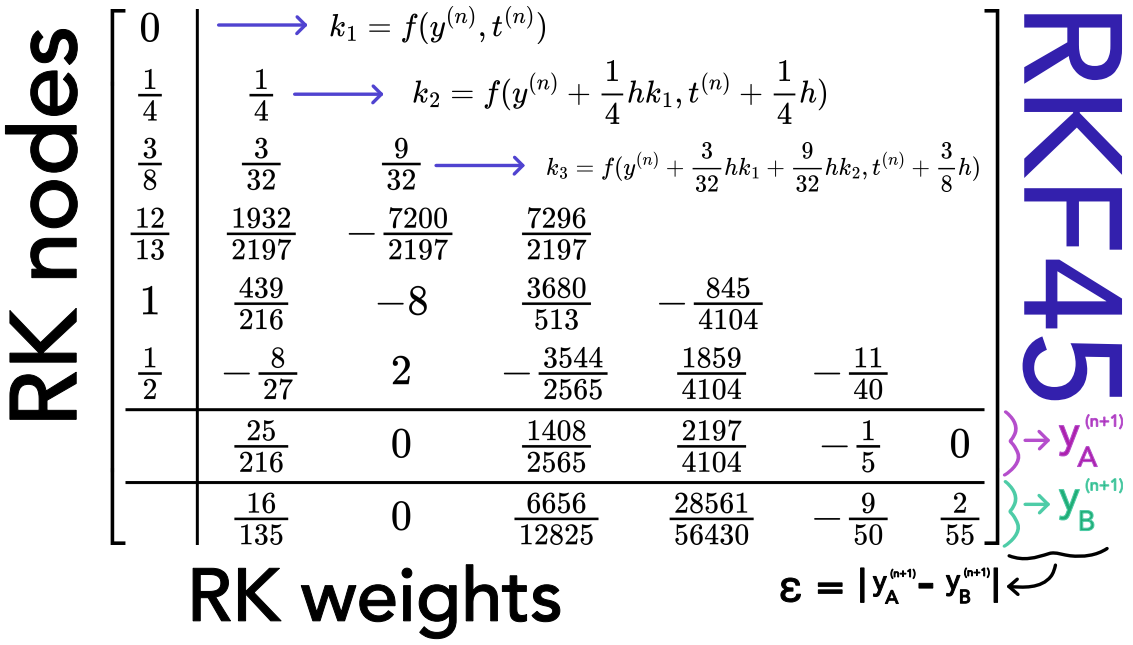

Figure 26: Embedded Runge-Kutta scheme RK45.

3.7 The problem of conserved quantities | Symplectic Integrators

3.7.1 Hamiltonian Systems and Symplecticity

Evolutions of classical physical systems can very generally be stated in terms of equations of motion derived from a real-valued, smooth Hamiltonian $H(\underline{p}, \underline{q})$

$$\begin{aligned}\partial_t \underline{p} &= -\underline{\nabla}_{\underline{q}} H(\underline{p},\underline{q}) \\ \partial_t \underline{q} &= \underline{\nabla}_{\underline{p}} H(\underline{p},\underline{q})\end{aligned} \quad \text{or} \quad \partial_t \underline{y} = \underline{\underline{J}}^{-1} \underline{\nabla} H(\underline{y}), \underline{y} = \begin{pmatrix}\underline{p}\\ \underline{q}\end{pmatrix}, \quad \underline{\underline{J}} = \begin{pmatrix} 0 & \underline{\underline{1}} \\ -\underline{\underline{1}} & 0 \end{pmatrix} \in \mathbb{R}^{2d} \tag{86}$$

where $\underline{p} \in \mathbb{R}^d$ is the generalized momentum and $\underline{q} \in \mathbb{R}^d$ are the generalized coordinates. The Hamiltonian can be followed as the legendre transform of the Lagrangian.

Hamiltonian systems

- conserve energy, i. e. $H(\underline{p},\underline{q})$ is conserved along a trajectory if the Hamiltonian does not explicitly depend on time
- show *symplecticity*, which is most intuitively understood as area conservation in phase space Hairer, Wanner, and Lubich, 2006, phase space volumina spanned by trajactories remain constant (see the following examples) / the phase space ditribution function is constant along trajectories

3.7.1.1 Poisson brackets and constants of motion (first integrals)

The Poisson brackets are

$$\{f,g\} = \{f,g\}_{qp} = \sum_{k=1}^{d} \frac{\partial f}{\partial q_k}\frac{\partial g}{\partial p_k} - \frac{\partial f}{\partial p_k}\frac{\partial g}{\partial q_k} \tag{87}$$

and we can find the **total derivation of a variable** $F(p,q,t)$ **along physical trajectories** as

$$\frac{dF(p(t),q(t),t)}{dt} = \{F,H\} + \partial_t F \tag{88}$$

so F is a constant of motion if $\{F,H\} = 0$ and $\partial_t F = 0$

3.7.1.2 Canonical transformations

Consider a coordinate transform in phase space

$$(p,q,t) \quad \rightarrow \quad (P,Q,t), \quad Q_i = Q_i(p,q,t), \quad P_i = P_i(p,q,t), \quad i = 1,\ldots,d \tag{89}$$

and the corresponding transformation of the Hamiltonian

$$H(p,q,t) \quad \rightarrow \quad \tilde{H}(P,Q,t) \tag{90}$$

Then if the coordinate transformation is a **canonical transformations** it necessarily leaves the Hamiltonian equations of movement invariant.

$$\begin{aligned} \partial_t \underline{P} &= -\underline{\nabla}_{\underline{Q}} \tilde{H}(\underline{P}, \underline{Q}) \\ \partial_t \underline{Q} &= \underline{\nabla}_{\underline{P}} \tilde{H}(\underline{P}, \underline{Q}) \end{aligned} \tag{91}$$

Closely connected are the Hamilton-Jacobi equations.

3.7.1.3 Definition of symplectic transformations

Linear maps: A linear map in 2D $F : \mathbb{R}^{2d} \to \mathbb{R}^{2d}$ is called symplectic if $\forall \underline{\xi}, \underline{\eta} \in \mathbb{R}^{2d}$: $\omega(\underline{\underline{F}}\underline{\xi}, \underline{\underline{F}}\underline{\eta}) = \omega(\underline{\xi}, \underline{\eta})$, where ω gives the area of the parallelogram spanned by both vectors.

Differentiable maps: $g : U \to \mathbb{R}^{2d}$ is symplectic if its Jacobian matrix $\underline{\underline{J}}_g$ is everywhere symplectic, so $\omega(\underline{\underline{J}}_g \underline{\xi}, \underline{\underline{J}}_g \underline{\eta}) = \omega(\underline{\xi}, \underline{\eta})$.

Connection to canonical transformations: In Hamiltonian systems, symplectic transformations are canonical transformations.

Compositions: Compositions of symplectic transformations are symplectic again.

Poincare's recurrence theorem: The time-evolution generated by a Hamiltonian in phase space is a symplectic transformation.

Idea: If the Hamiltonian evolution is symplectic, maybe its advantageous if our integrator is symplectic too.

3.7.2 Runge-Kutta methods do not conserve energy and are not symplectic

Let us now apply RK2 to the two-body-problem reduced to a dimensionless one-body-problem as described by

$$\frac{d\underline{s}}{d\tau} = \underline{w}, \quad \frac{d\underline{w}}{d\tau} = -\frac{\underline{s}}{s^3}$$

where $\underline{s}$ is the position and $\underline{w}$ the velocity. The numerical solution obtained using RK2 can be seen in figure 27. One can see that neither the energy nor the angular momentum nor the Runge-Lenz vector are conserved. Every step in the scheme is erroneous, and those errors add up leading to our quantities of interest not being conserved.

Let us look at another physical problem, the pendulum, as it lends itself well to phase space visualization. We see in figure 28 that the phase space area, the area spanned by the test points as they propagate in time, is not preserved as it should be for Hamiltonian flow.

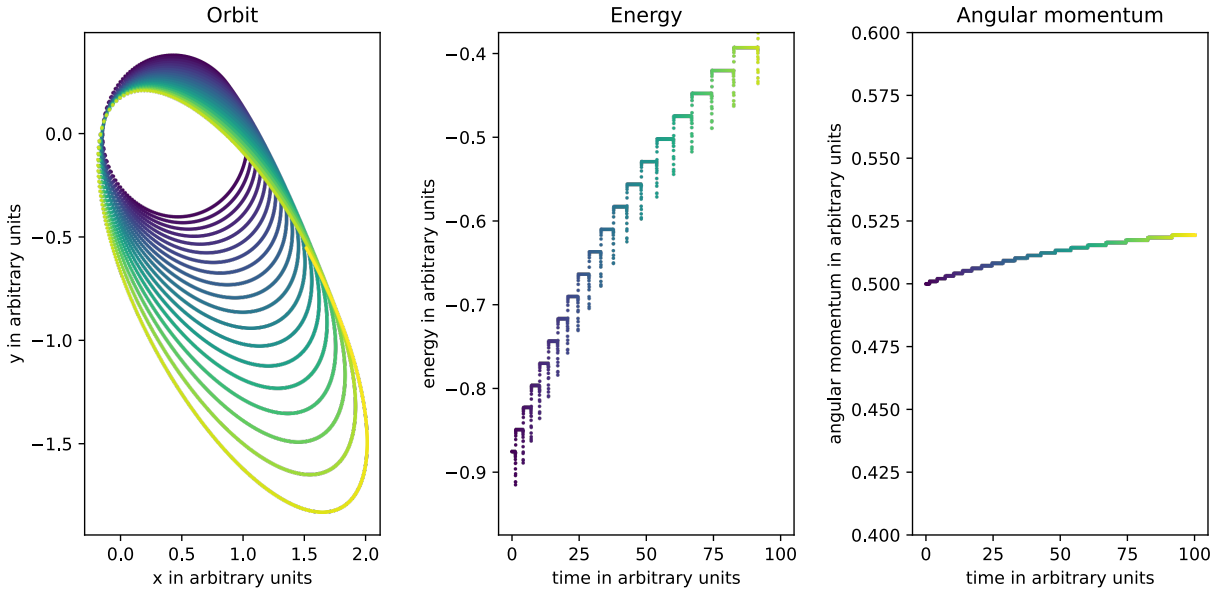

Figure 27: Numerical solution of the two-body-problem using RK2. The left panel shows the orbit, the central one the energy and the right one the angular momentum. Time is also encoded in the form of color, going from a dark blue to yellow.

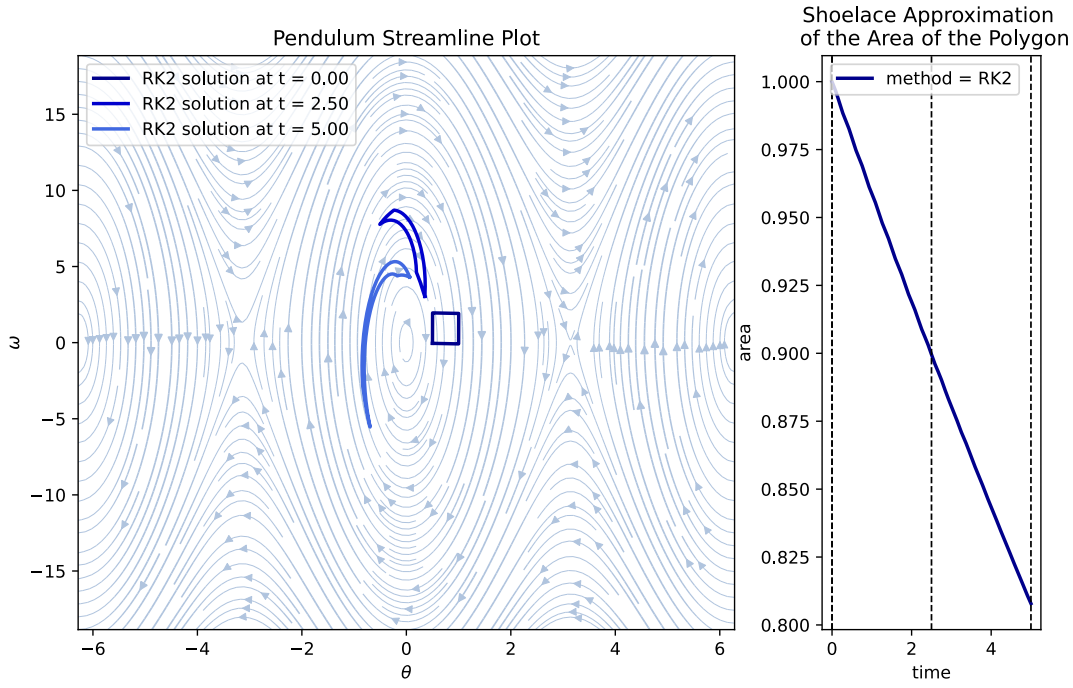

Figure 28: The left panel shows solutions to the pendulum problem at different points in time for different initial values as obtained by the RK2 scheme. The initial values are chosen so that they initially span a square in phase space. The right panel shows the phase space area spanned by the solutions as a function of time.

We need to switch to a whole other class of integrators.

3.7.3 Symplectic integrators to the help

This leads us to geometric integrators which are numerical methods preserving geometric properties of the exact flow of ODEs (Hairer, Wanner, and Lubich, 2006). More specifically for Hamiltonian systems we use **Symplectic Integrators** which produce a flow in phase space that is symplectic just as the flow of the exact solution (Hairer, Wanner, and Lubich, 2006, chapter VI).

Symplectic integrators

- are *structure preserving*
- nearly conserve properties of Hamiltonian systems, e.g. *first integrals* (variables $F(p, q)$ constant along the motion as dictated by the Hamiltonian)
- conserve phase-space (as prescribed by the Liouville theorem)
- more generally conserve all the Poincare invariants

It turns out that preserving symplecticity and energy at the same time is very difficult (Hairer, 2006). However, symplectic integrators still have good energy conservation properties without much long-term drifts. The general idea behind the connection between symplecticity and energy conservation is that geometric properties of the integrator (e.g. phase space conservation) translate into structure preservation on the level of modified equations (Hairer, Wanner, and Lubich, 2006, preface and chapters X through XII).

Problem: Symplectic integrators do not come without caveats:

- Using adaptive time-steps and keeping symplecticity is a problem.
- Non-conservative forces (those which cannot be described by a potential) like radiation forces (depending on velocity not only position) might be important, e.g. for debris in space and particles in planetary rings but then the central requirement of a Hamiltonian system breaks down
- The propagation of floating-point errors might be non-optimal

So the rebound N-body simulation package actually uses IAS15 (implicit integrator with adaptive time-stepping, 15th order) as the default (Rein and Spiegel, 2014).

Note: The default integrator in the N-body-simulator rebound is IAS15, a non-symplectic integrator

3.7.4 Verlet Scheme

Consider we want to solve the Newtonian equation of movement

$$\partial_t^2 \underline{s} = \underline{a}(\underline{s}) \tag{92}$$

- a classical physical problem with a particle at position $\underline{s}$ with velocity $\underline{v}$ and an acceleration $\underline{a}$ that depends only on the position.

Note: In the following we will introduce the Störmer-Verlet, velocity Verlet and Leapfrog scheme which differ in their formulations but are essentially the same. In molecular dynamics it is mostly called Verlet method, in the context of partial differential equations of wave propagation leapfrog method (Hairer, Lubich, et al., 2003).

We can derive a two-step scheme based on a Taylor expansion forward by Δt and backward by $-\Delta t$

$$\begin{aligned} \underline{s}(t+\Delta t) &= \underline{s}(t) + \underline{v}(t)\Delta t + \frac{1}{2}\underline{a}\Delta t^2 + \frac{1}{6}\underline{b}(t)\Delta t^3 + \mathcal{O}(\Delta t^4) \\ \underline{s}(t-\Delta t) &= \underline{s}(t) - \underline{v}(t)\Delta t + \frac{1}{2}\underline{a}\Delta t^2 - \frac{1}{6}\underline{b}(t)\Delta t^3 + \mathcal{O}(\Delta t^4) \end{aligned} \tag{93}$$

with

$$\begin{gathered} \text{position } \underline{s}, \quad \text{velocity } \underline{v}, \quad \text{acceleration} \underline{a} = -\frac{1}{m}\nabla V(\underline{s}) \\ \text{some potential } V, \quad \text{jerk } \underline{b} = \frac{d\underline{a}}{dt} \end{gathered} \tag{94}$$

Adding both equations yields a scheme 4th order accurate in time

$$\underline{s}(t+\Delta t) = 2\underline{s}(t) - \underline{s}(t-\Delta t) + \underline{a}(t)\Delta t^2 + \mathcal{O}(\Delta t^4) \tag{95}$$

where terms with odd powers of Δt were eliminated. This is a two-step scheme as for $\underline{s}(t+\Delta t)$, $\underline{s}(t)$ and $\underline{s}(t-\Delta t)$ are used (sometimes this form is called Störmer-Verlet).

Problem: What if we are also interested in calculating the velocity $\underline{v}$? What if $\underline{a}$ also depends on $\underline{v}$ as in the Lorentz and we need $\underline{v}$ to calculate $\underline{a}$?

From subtracting the equations 93, we can find

$$\underline{v}(t) = \frac{\underline{s}(t+\Delta t) - \underline{s}(t-\Delta t)}{2\Delta t} - \frac{1}{6}\underline{b}(t)\Delta t^2 + \mathcal{O}(\Delta t^3) \tag{96}$$

but this is problematic as

- only accurate to the third order
- an implicit equation as we do not know the future $\underline{s}(t+\Delta t)$ at the current timepoint
- we would need to know the jerk at the current timestep which could itself depend on $\underline{v}(t)$, we could ignore the jerk, but then the accuracy is only $\mathcal{O}(\Delta t^2)$

3.7.4.1 Velocity Verlet algorithm

Idea: Starting again from the Taylor expansion, we omit the jerk and extrapolate the velocity $\underline{v}(t+\Delta t)$ using the average of the accelerations at t and $t+\Delta t$

$$\begin{aligned}\underline{s}(t+\Delta t) &= \underline{s}(t) + \underline{v}(t)\Delta t + \mathcal{O}(\Delta t)^3 \\ \underline{v}(t+\Delta t) &= \underline{v}(t) + \frac{\underline{a}(t) + \underline{a}(t+\Delta t)}{2} + \mathcal{O}(\Delta t)^2\end{aligned} \tag{97}$$

Note: Again, we use $\underline{a}(t+\Delta t)$ to get $\underline{v}(t+\Delta t)$ which is not possible if $\underline{a}$ depends on v. If we would take only $\underline{a}(t)$ instead of the average, we would just have explicit Euler.

In steps we can write

1. calculate the new position: $\underline{s}(t+\Delta t) = (\underline{s})(t) + \underline{v}(t)\Delta t + \frac{1}{2}\underline{a}(t)\Delta t^2$
2. update the acceleration: $\underline{a}(t+\Delta t) = -\frac{1}{m}\nabla V|_{\underline{s}(t+\Delta t)}$
3. calculate the new velocity: $\underline{v}(t+\Delta t) = \underline{v}(t) + \frac{\underline{a}(t)+\underline{a}(t+\Delta t)}{2}\Delta t$
4. update the time: $t \to t+\Delta t$

Introducing half timesteps, we can write the Verlet scheme as a combination of 1st order steps

1. $\underline{v}\left(t+\frac{1}{2}\Delta t\right) = \underline{v}(t) + \frac{1}{2}\underline{a}(t)\Delta t$
2. $\underline{s}(t+\Delta t) = \underline{s}(t) + \underline{v}\left(t+\frac{1}{2}\Delta t\right)\Delta t$
   (note that plugging (1) into (2) yields the previous step (1))
3. $\underline{a}(t+\Delta t) = -\frac{1}{m}\nabla V|_{\underline{s}(t+\Delta t)}$
4. $\underline{v}\left(t+\Delta t\right) = \underline{v}\left(t+\frac{1}{2}\Delta t\right) + \frac{1}{2}\underline{a}(t+\Delta t)\Delta t$
   (note that plugging (1) into (4) yields the previous step (3))
5. $t \to t+\Delta t$

This is illustrated in figure 29. Here the last step can be called *implicit* as it depends on $\underline{a}(t + \Delta t)$, so a result at the same time as it is supposed to deliver a result at - we have a semi-implicit Euler scheme.

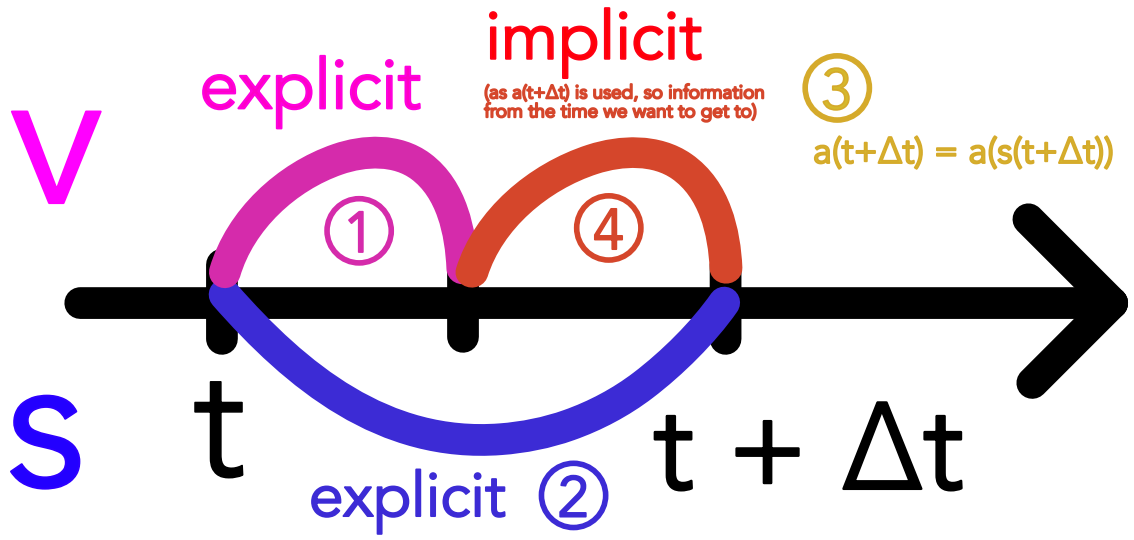

Figure 29: Illustration of the velocity Verlet scheme.

3.7.5 The Leapfrog Method

We will now introduce the Leapfrog scheme and at its hand what it means for a method to be symplectic.

The leapfrog scheme can then be written as

$$\begin{aligned} \underline{s}(t + \frac{1}{2}\Delta t) &= \underline{s}(t - \frac{1}{2}\Delta t) + \underline{v}(t)\Delta t + \mathcal{O}(\Delta t^3) \\ \underline{v}(t + \Delta t) &= \underline{v}(t) + \underline{a}(t + \frac{1}{2}\Delta t)\Delta t + \mathcal{O}(\Delta t^3) \end{aligned} \tag{98}$$

The position and velocity are updated at alternating half time steps as illustrated in figure 30, just as the name suggests (the velocity is "leaping" over the position and vice versa (*Bockspringen*)).

Note: To start the scheme or to save the position and velocity at the same time, a half step needs to be performed, e.g. using half standard explicit Euler.

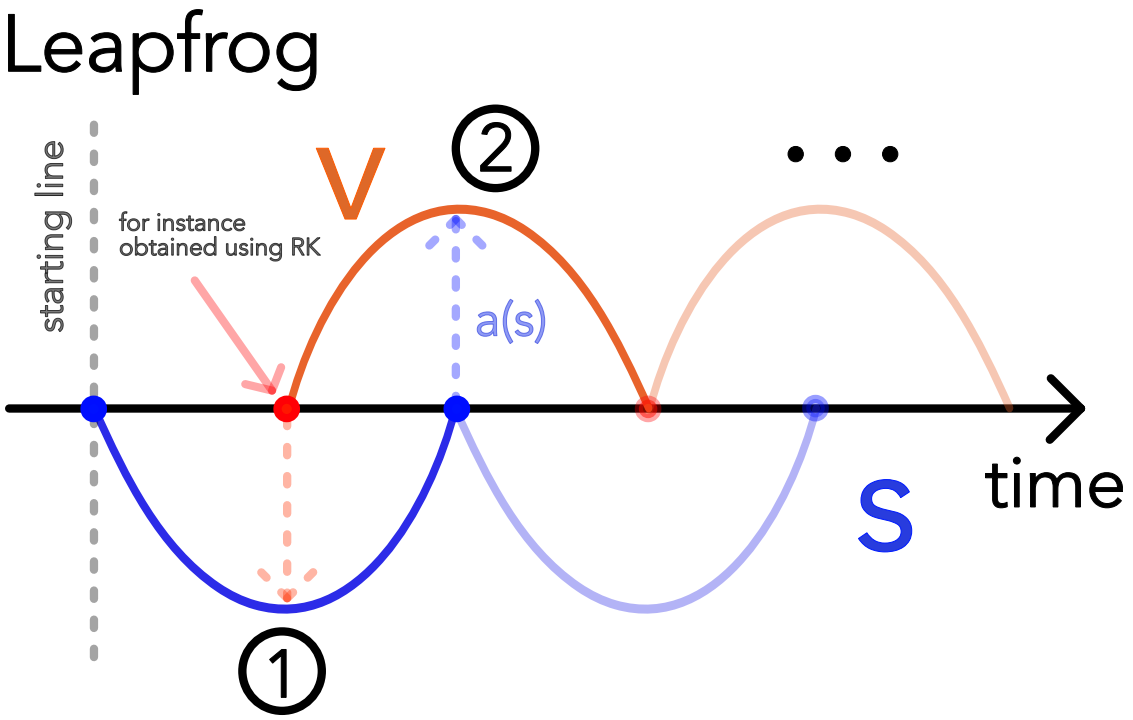

Figure 30: Illustration of the leapfrog scheme.

3.7.5.1 Connection between Leapfrog and Velocity Verlet

We can combine steps $4, 5, 1$ in the velocity Verlet scheme in the half-step formulation to get

$$\begin{aligned} \underline{s}(t+\Delta t) &= \underline{s}(t) + \underline{v}\left(t+\frac{1}{2}\Delta t\right)\Delta t \\ \underline{v}(t+\frac{3}{2}\Delta t) &= \underline{v}(t+\frac{1}{2}\Delta t) + \underline{a}(t+\Delta t)\Delta t \end{aligned} \tag{99}$$

which if we shift everything by $\frac{1}{2}\Delta t$ yields the aforementioned leapfrog scheme. Phrased differently velocity Verlet is leapfrog with Euler-kickoff built-in.

3.7.5.2 Kick-drift-kick and Drift-kick-drift Leapfrog formulations to have velocity and position information at the same time

Problem: One problem of the Leapfrog scheme in this form is that velocity and position information are not available at the same time. This is for instance problematic if we want to calculate the energy which depends on both or if we want to change the step-size adaptively without destryoing the interlacement (see figure 31).

Idea: We rearrange and split the interlaced integration by a full time step into a half step in first variable, full step in second variable, half step in first variable.

There are two possible schemes.

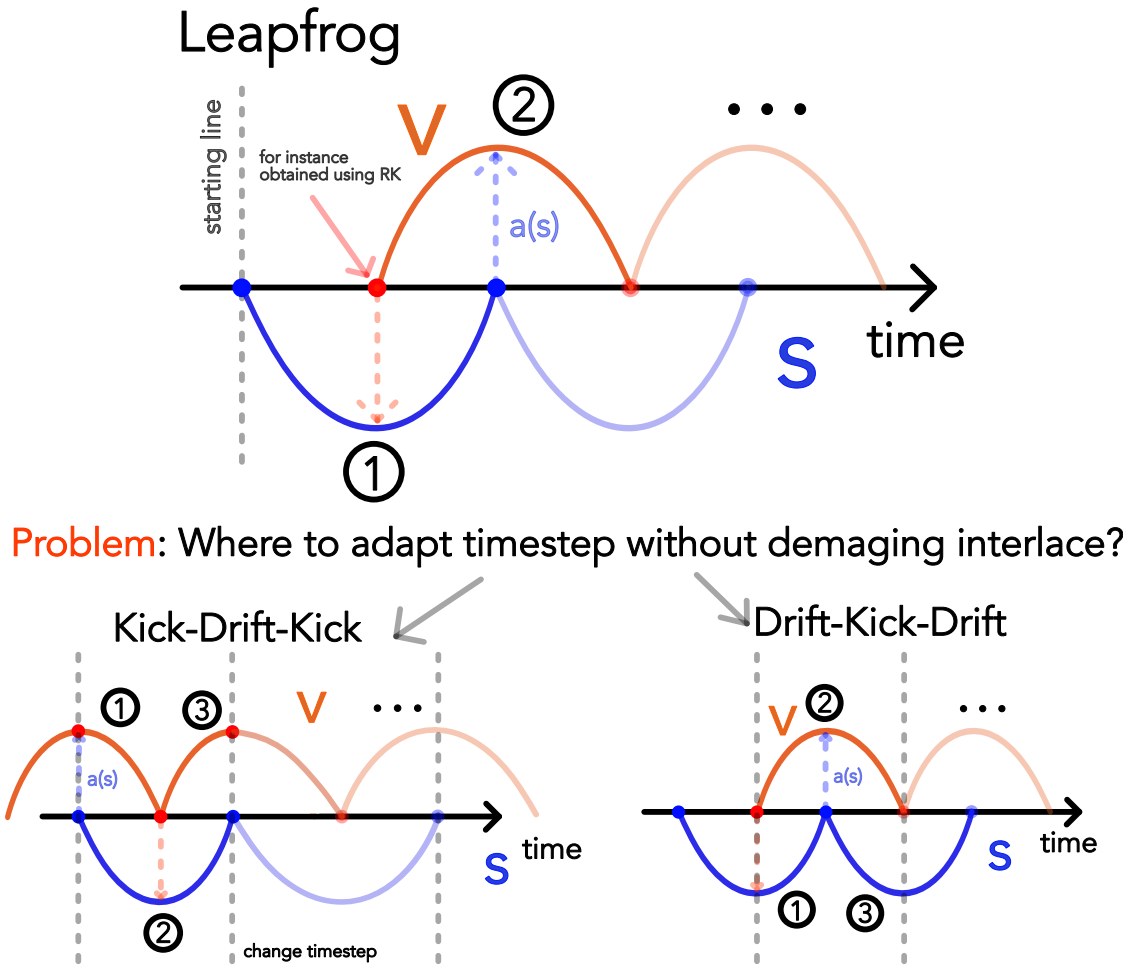

Figure 31: Illustration of the problem of changing the step-size in the leapfrog scheme and the solutions - kick-drift-kick and drift-kick-drift.

In the **kick-drift-kick formulation**, positions are stored at full, velocities at half time steps (equivalent to the velocity Verlet).

$$
\begin{aligned}
&\underline{v}(t+\frac{1}{2}\Delta t) = \underline{v}(t) + \underline{a}(t)\frac{\Delta t}{2} \quad \text{kick, half-step in first variable} \\
&\underline{s}(t+\Delta t) = \underline{s}(t) + \underline{v}(t+\frac{1}{2}\Delta t)\Delta t \quad \text{drift, full-step in second variable} \\
&\underline{v}(t+\Delta t) = \underline{v}(t+\frac{1}{2}\Delta t) + \underline{a}(t+\Delta t)\frac{\Delta t}{2} \quad \text{kick, half-step in first variable} \\
&\text{possibly adapt step-size here} \\
&t \to t + \Delta t
\end{aligned}
\tag{100}
$$

where a *drift* is a change of the position with constant velocity and a *kick* is a change of the velocity with constant acceleration.

In the **drift-kick-drift formulation**, velocities are stored at full, positions at half time steps.

$$\begin{aligned}
&\underline{s}(t+\frac{1}{2}\Delta t) = \underline{s}(t) + \underline{v}(t)\frac{\Delta t}{2} \quad \text{drift, half-step in first variable} \\
&\underline{v}(t+\Delta t) = \underline{v}(t) + \underline{a}(t+\frac{1}{2}\Delta t)\Delta t \quad \text{kick, full-step in first variable} \\
&\underline{s}(t+\Delta t) = \underline{s}(t+\frac{1}{2}\Delta t) + \underline{v}(t+\Delta t)\frac{\Delta t}{2} \quad \text{drift, half-step in first variable} \\
&\text{possibly adapt step-size here} \\
&t \to t+\Delta t
\end{aligned} \tag{101}$$

3.7.5.3 Advantages of the Leapfrog scheme

The leapfrog scheme is second order accurate, symmetric (time reversible), symplectic, has good energy conservation properties and is time reversible (proofs in Springel et al., 2023, chapter 2.8).

Second order accuracy may be surprising as we seemingly only Taylor approximate up to the first order - but note the interlacement and connection to velocity Verlet.

3.7.5.4 Leapfrog is symmetric (time reversible)

In terms of the one-step map $\Phi_h : (\underline{s}_n, \underline{v}_n) \to (\underline{s}_{n+1}, \underline{v}_{n+1})$ symmetry means that $\Phi_{-h}^{-1} = \Phi_h$ so going one step forward and then back leads us back to where we came from, $n \rightleftharpoons n+1$.

We integrate from $\left(\underline{s}_n, \underline{v}_{n-\frac{1}{2}}\right)$ to $\left(\underline{s}_{n+1}, \underline{v}_{n+\frac{1}{2}}\right)$ and return.

$$\begin{aligned}
\underline{s}_{\text{fin}} &= \underline{s}_{n+1} - \underline{v}_{n+\frac{1}{2}}\Delta t = \underline{s}_n + \underline{v}_{n+\frac{1}{2}}\Delta t - \underline{v}_{n+\frac{1}{2}}\Delta t = \underline{s}_n \\
\underline{v}_{\text{fin}} &= \underline{v}_{n+\frac{1}{2}} - \underline{a}_n\Delta t = \underline{v}_{n+\frac{1}{2}} + \underline{a}_n\Delta t - \underline{a}_n\Delta t = \underline{v}_{n-\frac{1}{2}}
\end{aligned} \tag{102}$$

So leapfrog is symmetric (time-reversible), different from e.g. explicit Euler (see figure 32).

Advantages of symmetric methods: Symmetric methods applied to *integrable and near-integrable* **reversible systems** share similar properties to symplectic methods applied to *(near)-integrable* Hamiltonian systems: linear error growth and long-time near-conservation of first integrals. For a non-reversible system, a symmetric but non-symplectic method (e.g. Lobatto IIIB) will have no good conservation properties though.

Note: Not every symplectic method is symmetric. For instance symplectic Euler is symplectic but not symmetric.

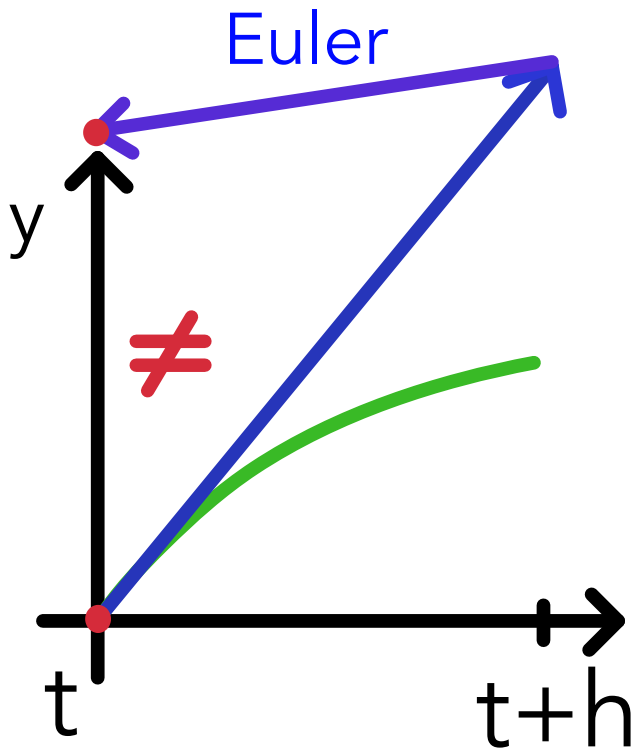

Figure 32: Explicit Euler is not symmetric (time-reversible).

3.7.5.5 Symplecticity of the leapfrog scheme I: Intuition and Meaning

Symplecticity (so area conservation in phase space) is illustrated at the hand of the pendulum in figure 33 and energy conservation at the hand of the two-body-problem in figure 34. The area in phase space does not change at all while the energy shows small fluctuations but no overall drift (compare Hairer, Lubich, et al., 2003, theorem 5.5). The angular momentum is exactly conserved in the leapfrog solution to the two-body-problem (details on the conservation of specific *quadratic first integrals* can be found in Hairer, Lubich, et al., 2003, theorem 3.5). As visible in the changing orientation of the orbit in figure 34 the leapfrog scheme does not preserve the orientation of the Runge-Lenz vector.

3.7.5.6 Symplecticity of the leapfrog scheme II: Proof

Consider the separable Hamiltonian

$$\begin{aligned} H(q,p) &= H_{\text{kin}}(p) + H_{\text{kin}}(q) \\ &\underbrace{=}_{\text{here}} \frac{p^2}{2m} + U(q) \end{aligned} \tag{103}$$

Procedure: We solve both parts of the Hamiltonian separately (operator splitting) and construct Leapfrog as the concatenation of these solutions (proving symplecticity) and then

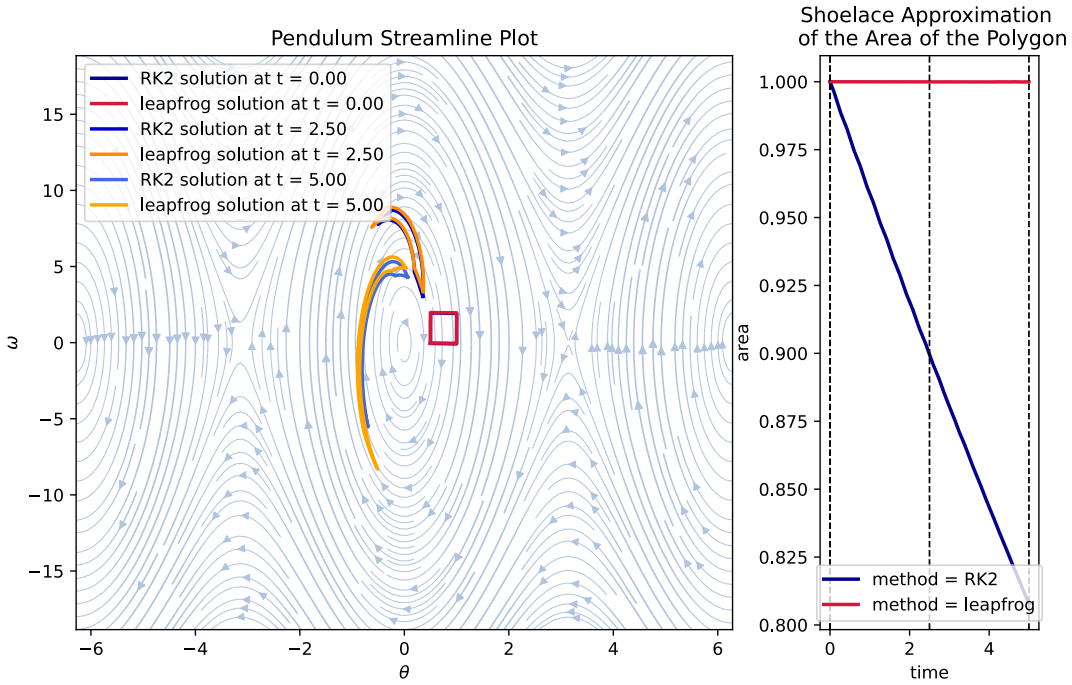

Figure 33: The same situation as in figure 28 is shown but now with the result of the leapfrog method added. The leapfrog scheme preserves the area in phase space while the RK2 scheme does not.

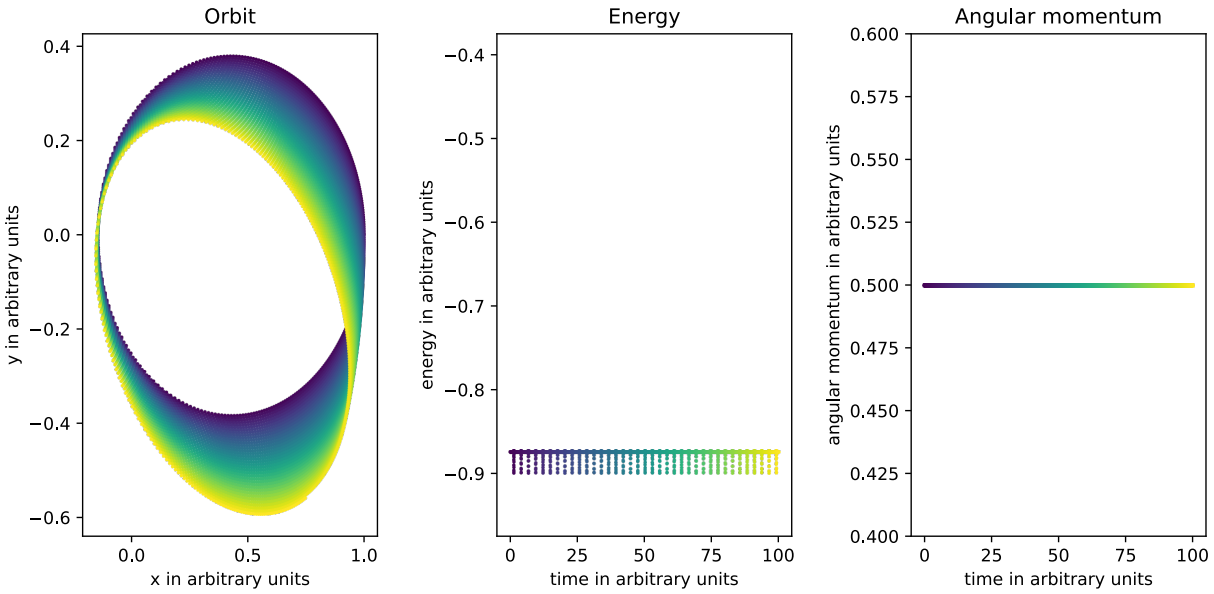

Figure 34: Numerical solution of the two-body-problem using the leapfrog method in the kick-drift-kick scheme. The left panel shows the orbit, the central one the energy and the right one the angular momentum. Time is also encoded in the form of color, going from a dark blue to yellow.

calculate an error Hamiltonian.

Operator splitting From the Hamiltonian equations of the kinetic and potential part, we find update steps.

For the kinetic part H_{kin} we find

$$\left.\begin{array}{c} \partial_t q = \partial_p H_{\text{kin}} = \frac{p}{m} \\ \partial_t p = -\partial_q H_{\text{kin}} = 0 \end{array}\right\} \rightarrow \left\{\begin{array}{c} q^{(n+1)} = q^{(n)} + \frac{p^{(n)}}{m}\Delta t \\ p^{(n+1)} = p^{(n)} \end{array}\right. \tag{104}$$

and for the potential part

$$\left.\begin{array}{c} \partial_t q = \partial_p H_{\text{pot}} = 0 \\ \partial_t p = -\partial_q H_{\text{pot}} = -\partial_q U \end{array}\right\} \rightarrow \left\{\begin{array}{c} q^{(n+1)} = q^{(n)} \\ p^{(n+1)} = p^{(n)} - \partial_q U \Delta t \end{array}\right. \tag{105}$$

Note: Independent of Δt the schemes found are exact; and symplectic as brought forward by Hamiltonians.

Constructing leapfrog Let $\phi_{\Delta t}(H)$ describe making a step Δt governed by H in phase-space (a time evolution operator). Then leapfrog (kick-drift-kick version) is given as

$$\phi_{\Delta t}(H) = \phi_{\frac{\Delta t}{2}}(H_{\text{pot}}) \odot \phi_{\frac{\Delta t}{2}}(H_{\text{kin}}) \odot \phi_{\Delta t}(H_{\text{pot}}) \tag{106}$$

so Leapfrog is symplectic as a concatenation of symplectic operators, so

- there is no secular (long-lasting, non-oscillatory) drift in e.g. the Energy of e.g. the Kepler orbits
- the longer the timespan to simulate, the more it makes sense to use leapfrog over Runge Kutta schemes (e.g. the explicit Euler scheme always overshoots the orbits leading to increasing total energy and unbound states)

Note: »Yes, symplectic integrators do not exactly conserve energy. It is a common misconception that they do. What symplectic integrators actually do is solve for a trajectory which rests on a symplectic manifold that is perturbed from the true solution's manifold by the truncation error. This means that symplectic integrators do not experience (very much) longtime drift, but their orbit is not exactly the same as the true solution in phase space, and thus you will see differences in energy that tend to look periodic. There is a small drift which grows linearly and is related to floating-point error, but this drift is much less than standard methods. This is why symplectic methods are recommended for longtime integration.« (Rackauckas, Sciemon, et al., 2022)

Error Hamiltonian Indeed, it turns out that the leapfrog scheme exactly solves the modified Hamiltonian

$$H_{leap} = H + H_{err}, \quad H_{err} \propto \frac{\Delta t^2}{12} \left\{ \{H_{kin}, H_{pot}\}, H_{kin} + \frac{1}{2} H_{pot} \right\} + \mathcal{O}(\Delta t^3) \tag{107}$$

where H_{kin} and H_{pot} are the kinetic and potential part of the original Hamiltonian (Springel et al., 2023, chapter 2.8). The curly brackets denote the Poisson bracket.

Notes on the derivation of the Error Hamiltonian The time evolution of a phase space function $F(p, q)$ under the flow generated by a Hamiltonian H fulfills $-\partial_t F = -\{H, F\} = -\hat{H}F$ and similar to the time-development operator in Quantum Mechanics, we can write

$$F(t) = \exp\left(\hat{H}t\right) F(0) \tag{108}$$

and for the leapfrog scheme with $H_{leap} = H + H_{err}, H = H_{kin} + H_{pot}$ we have

$$\exp\left(\left(H + H_{\text{err}}\right) \Delta t\right) = \exp\left(H_{\text{pot}} \frac{\Delta t}{2}\right) \exp\left(H_{\text{kin}} \Delta t\right) \exp\left(H_{\text{pot}} \frac{\Delta t}{2}\right) \tag{109}$$

where using the the Baker-Campbell-Hausdorff formula lets us find H_{err}.

3.8 Extrapolation method: Bulirsch-Stoer algorithm

Our goal is still to obtain highly accurate and cheap solutions to ODEs. The ingedriends of Bulirsch-Stoer are

1. we integrate across a whole interval with length H multiple times with a sequence of decreasing substep-sizes h_j each yielding a final result $F(h_j)$

2. we extrapolate $F(h)$ to $h = 0$ asking ourselves *What would be the solution, if we had taken infinitely many, infinitely small steps?*, for instance using polynomial extrapolation or Richardson extrapolation[3] with rational functions

with the method being most-appropriate for differential equations containing smooth (cheap to evaluate) functions. An illustration is given in figure 35.

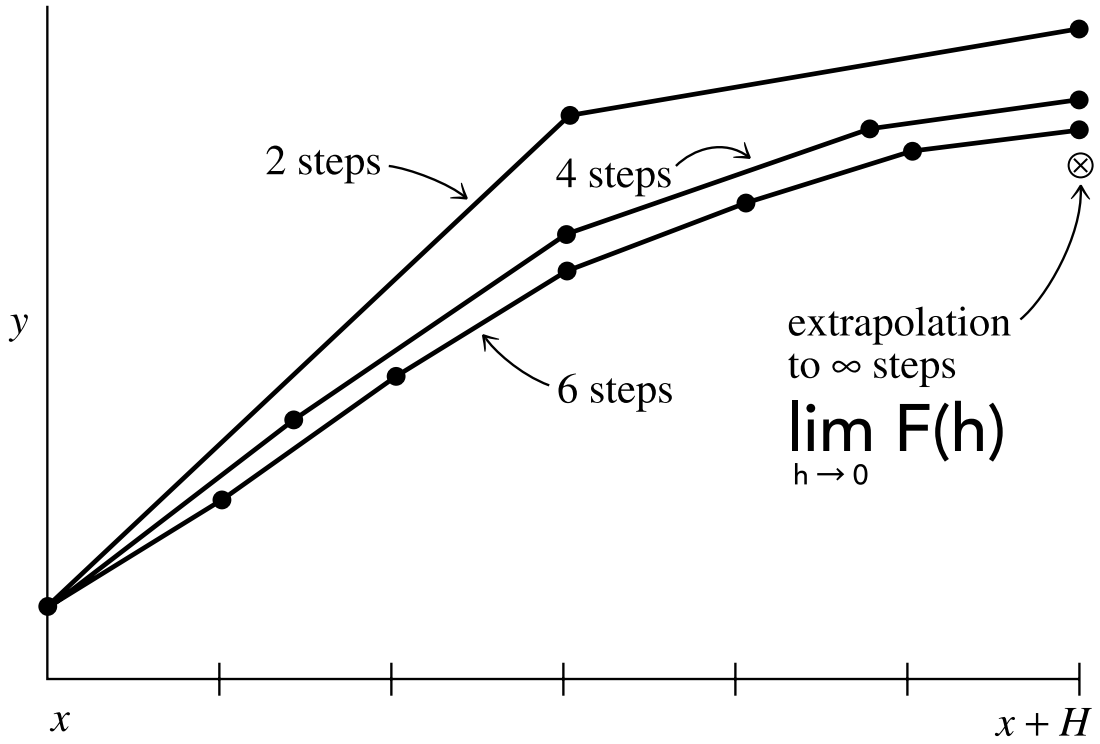

Figure 35: Illustration of the Bulirsch-Stoer algorithm.

While the idea of this method is very beautiful, its usage is disputed, with e.g. W. Van Snyder writing: extrapolation methods are almost always substantially inferior to Runge-Kutta, Taylor's series, or multistep methods.

A single step taking us from x to $x + H$ (large distance H) consists of many substeps using the modified midpoint rule.

[3] A sequence acceleration method to improve the convergence of a sequence $F^* = \lim_{h \to 0} F(h)$

3.8.1 Basic integration method | second order method with $\mathcal{O}(h^2)$; midpoint rule $\rightarrow$ modified midpoint rule

The midpoint rule is given by

$$\begin{aligned} k_1 &= f(y_i, x_i) \\ k_2 &= f\left(y_i + \frac{h}{2}k_1, x_i + \frac{h}{2}\right) \\ x_{i+1} &= x_i + h \\ y_{i+1} &= y_i + hk_2 + \mathcal{O}(h^3) \end{aligned} \tag{110}$$

as illustrated in figure 36.

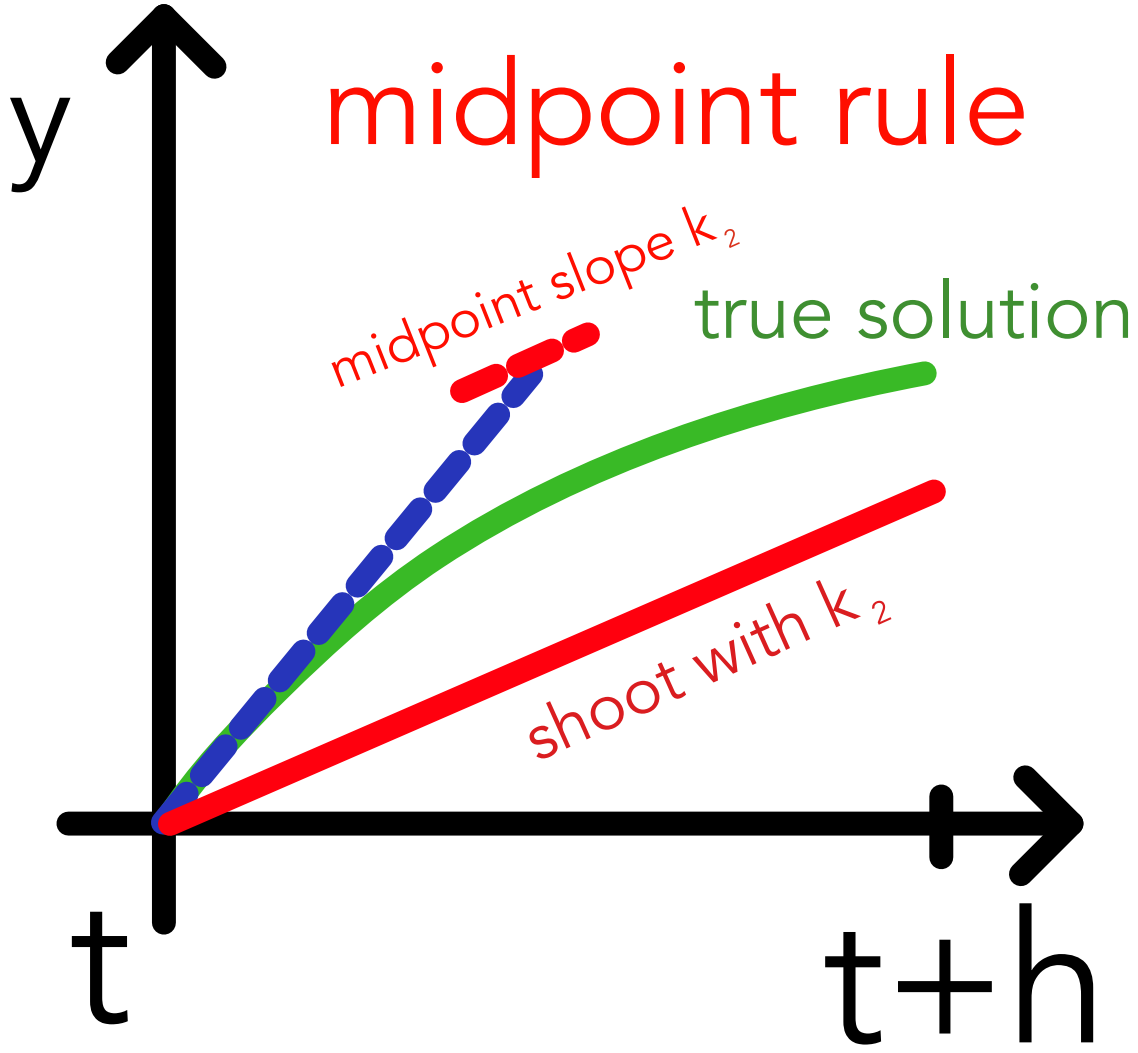

Figure 36: Illustration of the midpoint rule.

3.8.1.1 Modified midpoint rule

We advance from x to $x + H$ using n substeps of size $h = \frac{H}{n}$. Except for the first and last step, we advance using the midpoint rule.

Advantage of the midpoint rule over RK2: We only need one evaluation of f per step h instead of two.

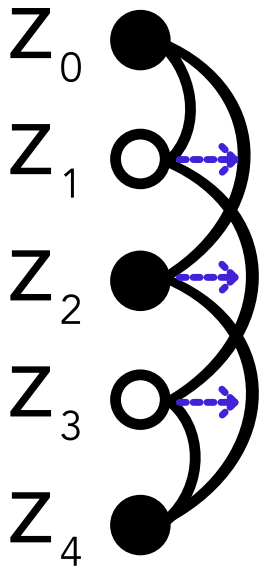

Figure 37: Modified midpoint rule.

$$
\begin{aligned}
z_0 &= y(x) \\
z_1 &= z_0 + hf(z_0, x) \text{ not midpoint} \\
z_2 &= z_0 + 2hf(z_1, x + h) \text{ midpoint with stepsize } 2h \\
z_3 &= z_1 + 2hf(z_2, x + 2h) \text{ midpoint with stepsize } 2h \\
&\vdots \\
z_m &= z_{m-2} + 2hf(z_{m-1}, x + (m-1)h) \\
z_{m+1} &= z_{m-1} + 2hf(z_m, x + mh), \quad m = 4, \ldots, n-1 \\
&\vdots \\
y(x + H) \approx y_n &= \frac{1}{2}\left[z_n + \underbrace{z_{n-1} + hf(z_n, x + H)}_{\text{euler Step from } z_{n-1}} \right]
\end{aligned}
\tag{111}
$$

3.8.1.2 Combining modified midpoint calculations with different h; advantage of modified midpoint

Remember that the midpoint rule is of 2nd order so the error when covering an interval H with multiple steps is $\mathcal{O}(h^2)$. Central to the advantage of the modified midpoint rule is (not proven here)

$$
y(x + H) - y_n = \sum_{i=1}^{\infty} \alpha_i h^{2i} \tag{112}
$$

so the error between the true $y(x + H)$ and our numerical result y_n expressed as a power series in h only contains even powers of h. We can therefore combine results with different step-sizes to gain two oders at a time.

Example Let us combine a version with n steps h and one with $2n$ steps $2h$.

$$\begin{aligned} n: &\quad y(x+H) - y_n = \alpha_1 h^2 + \alpha_2 h^4 \\ 2n: &\quad y(x+H) - y_{2n} = \alpha_1 \left(\frac{h}{2}\right)^2 + \alpha_2 \left(\frac{h}{2}\right)^4 \end{aligned} \tag{113}$$

from which we obtain

$$y(x+H) = \frac{4y_{2n} - y_n}{3} + \mathcal{O}(h^4) \tag{114}$$

which is 4th order accurate like RK4 but at less cost (function evaluations).

3.8.1.3 What extrapolation nodes to choose? - how to inrease n (or rather decrease h)

Let us remember

$$F(h_n) = y_n \quad \text{with } n = \frac{H}{h} \tag{115}$$

We cross the large interval H using multiple substeps multiple times with decreasing substep size. Each iteration delivers a result $F(h_n)$ and we have already seen that such results can be combined smartly - and extrapolation to $h \to 0$ is even better. But what evalutation nodes for $F(h)$ should we choose?

$$\begin{aligned} \text{Romberg}: &\quad n = [2, 4, 8, 16, \ldots, 1024] \\ \text{Bulirsch}: &\quad n = [2, 4, 6, 8, 12, 16, \ldots, 96] \\ \text{Deufelhard}: &\quad n = [2, 4, 6, 8, 10, \ldots, 24] \end{aligned} \tag{116}$$

3.8.1.4 How to extrapolate from multiple $F(h_n)$ to the limit $h \to 0$?

One option is polynomial interpolation (two points define a line, ..., n points define a polynomial of (max) degree $n-1$), so we do polynomial regression and evaluate it at zero.

There is also the approach to use rational functions, which can also capture poles and divergence regions between the interpolation points (which polynomials will never do), so

$$R_{m+1}(x) = \frac{P_\mu(x)}{Q_\nu(x)} = \frac{p_0 + p_1 x + p_2 x^2 + \cdots + p_\mu x^\mu}{q_0 + q_1 x + q_2 x^2 + \cdots + q_v x^v}, \quad m+1 = v + \mu + 1 \tag{117}$$

Hairer, Wanner, and Nørsett, 1993 write: »Many authors in the sixties claimed that it is better to use rational functions instead of polynomials. Later numerical experiments (Deuflhard 1983) showed that rational extrapolation is nearly never more advantageous than polynomial extrapolation.«. One reason I can imagine is that the more complex rational model is more unstable and harder to appropriately fit.

3.9 Predictor-corrector methods

Multistep idea: While a one-step method only uses the differential value and the ODE itself in a step, multistep methods also include information from previous steps (e.g $x, x-h, x-2h$) to obtain better estimates for the next step $(x+h)$. The method is e.g. kicked off using Runge-Kutta steps.

Let us start by writing an advance in an ODE $\partial_x y = f(y(x), x)$ as

$$y_{n+1} = y_n + \int_{x_n}^{x_{n+1}} f(x', y(x'))dx' \tag{118}$$

the problem is that different from an integration problem, we would need to know $y(x)$ to use this formula to calculate $y(x)$ or rather y_{n+1} - so what have we won?

Consider we are in the multistep setting and already have approximations $y_n, y_{n-1}, \dots$ at $x_n, x_{n-1}, \dots$. We can then approximate $f(x, y)$ by a polynomial passing through those points and yield

$$y_{n+1} = y_n + h \cdot (\beta_0 f(x_{n+1}, y_{n+1}) + \beta_1 f(x_n, y_n) + \beta_2 f(x_{n-1}, y_{n-1}) + \dots) \tag{119}$$

But wait - we used y_{n+1} in the RHS which we do not know. We could get an explicit scheme by setting $\beta_0 = 0$ but the formula screams fixpoint iteration (as in Picard iteration) - **predictor-corrector method**.

1. **predictor step:** obtain a good estimate for y_{n+1}
2. **corrector step(s):** plugging the result of the predictor step into eq. 119 gives an improved estimate for y_{n+1}

For correction to make sense, the first prediction must be sufficiently good.

3.9.1 One-step predictor-corrector method: RK2 and $P(EC)^k$

Indeed standard RK2 is a predictor-corrector method

$$\begin{aligned} k_1 &= f\left(y_n, x_n\right) \\ k_2 &= f\left(\underbrace{y_n + hk_1}_{\text{predictor}}, x_n + h\right) \\ \underbrace{y_{n+1} &= y_n + \frac{h}{2}\left(k_1 + k_2\right) + \mathcal{O}\left(h^3\right)}_{\text{corrector}} \end{aligned} \tag{120}$$

Different notation and $P(EC)^k$ method We write the predictor P step as

$$\tilde{y}^P_{n+1,[0]} = y_n + hf(y_n, x_n) \tag{121}$$

and can then write the evaluation / corrector step EC as

$$\tilde{y}^{EC}_{n+1,[1]} = y_n + \frac{h}{2}\left[f(y_n, x_n) + f(\tilde{y}^P_{n+1,[0]}, x_{n+1})\right] \tag{122}$$

which we can repeat

$$\begin{aligned} \tilde{y}^{EC}_{n+1,[2]} &= y_n + \frac{h}{2}\left[f(y_n, x_n) + f(\tilde{y}^{EC}_{n+1,[1]}, x_{n+1})\right] \\ \tilde{y}^{EC}_{n+1,[k]} &= y_n + \frac{h}{2}\left[f(y_n, x_n) + f(\tilde{y}^{EC}_{n+1,[k-1]}, x_{n+1})\right] \end{aligned} \tag{123}$$

until convergence $|\tilde{y}^{EC}_{n+1,[k]} - \tilde{y}^{EC}_{n+1,[k-1]}| \leq \epsilon_0$ (some error tolerance ϵ_0) where our final approximation is $y_{n+1} = \tilde{y}^{EC}_{n+1,[k]}$. This is the $P(EC)^k$ method.

3.9.2 4th order Adams-Bashforth-Moulton

Here we used the multistep principle as introduces above. In the 4th order Adams-Bachforth-Moulton approach we use three previous timesteps. It is a 4th order method.

The predictor step has weights designed so it gives the correct result for cubic polynomials

$$\tilde{y}_{n+1} = y_n + \frac{h}{24}\left[55f(y_n, x_n) - 59f(y_{n-1}, x_{n-1}) + 37f(y_{n-2}, x_{n-2}) - 9f(y_{n-3}, x_{n-3})\right] + \mathcal{O}(h^5) \tag{124}$$

the evaluation / corrector step EC is

$$y_{n+1} = y_n + \frac{h}{24}\left[9f(\tilde{y}_{n+1}, x_{n+1}) + 19f(y_n, x_n) - 5f(y_{n-1}, x_{n-1}) + f(y_{n-2}, x_{n-2})\right] + \mathcal{O}(h^5) \tag{125}$$

containing $\tilde{y}_{n+1}$ (*implicit*) and can be repeated for higher accuracy (plug in y_{n+1} instead of $\tilde{y}_{n+1}$ in the next EC step). We start the scheme with three RK steps.

3.10 Shooting | adapting parameters until boundary conditions are fulfilled

3.10.1 Remark on ODE solutions in phase space

There are infinitely many solutions to an ODE but only one unique to a initial value problem. Those solutions are streamlines through phase space that

- do not start / end
- do not cross

3.10.2 Examplary Shooting Problem

Consider the motion of a projectile from a canon, given by

$$\partial_t^2 \begin{pmatrix} x \\ y \end{pmatrix} = \begin{pmatrix} 0 \\ -g \end{pmatrix} - b\partial_t \begin{pmatrix} x \\ y \end{pmatrix} \tag{126}$$

where the canon sits at $(0, 1)$ and shoots with a give velocity v_{canon} at an angle α to the horizontal. Our aim is hitting a target at $(x_{\text{target}}, y_{\text{target}})$ (boundary condition). This is illustrated in figure 38.

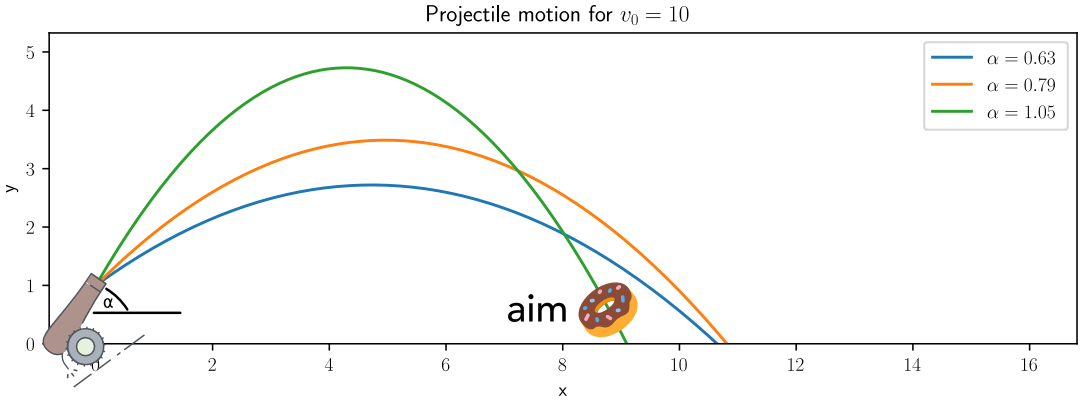

Figure 38: Illustration of the shooting problem. Trajectories gained by converting the system to first order ($\underline{q} = (x, y, v_x, v_y), f = (v_x, v_y, -bv_x, -g - bv_y)$) and then applying RK2.

3.10.3 Shooting

In the shooting method a boundary value problem is reduced to an initial value problem. We solve the initial value problem for different choices of parameters until the given boundary conditions are satisfied – we shoot trajectories in different directions from one boundary until we find one that hits the other boundary condition. For a neutron star we could know the central density and density at the surface and seek some process parameters.

4 Simulation of Physical Systems - from Quantum Mechanics to Fluid Dynamics

4.1 Different levels of modelling from Quantum Mechanics to Kinetic Gas theory

Our aim is simulating real-world physical systems with two of our fundamental tools being modeling and model order reduction. When we model a fluid, we will probably not model every particle let alone the underlying quantum mechanics[4].

Starting off with Quantum Mechanics Consider we would model the whole wave function of a system of particles $\Phi(\underline{x}_1, \ldots, \underline{x}_N)$ (giving the joint probability $|\Phi|^2$ of finding all particles at $\underline{x}_1, \ldots, \underline{x}_N$ with single particle probabilities being the margins) with possibly more degrees of freedom (like spin) and evolve it using e.g. the Schrödinger equation with particle interaction being represented in the potential of the Hamiltonian. If we would discretize each dimension with 1000 cells, the simulation would have 1000^{3N} cells - quickly infeasible (we model a too large probability space). First reduction steps could be

- use symmetries, e.g. particles of a type are indistinguishable reducing the degrees of freedom
- in given potentials approximate the particle wave as a sum of standing waves and evolve the coefficients
- ...

Molecular dynamics Quantum mechanical simulation is infeasible (and unnecessary) for larger systems. A first step is to decouple the electrons and protons (Born-Oppenheimer approximation) as the electrons move on much quicker timescales and describe the atoms as localized particles in phase-space. Based on the positions of the nuclei forming a fixed potential, we can calculate the lowest energy wave function of the electrons (which will occur in *no time* for the protons), from there forces on the nuclei with which we move them and so on. The next step is to model the interatomic interactions using inter-atomic potentials (e.g. Morse, Lenard-Jones) with the potential parameters for instance adapted to match quantum mechanical simulations or for a system as a whole to portray correct behavior.

[4]Except for instance when we want to analyse shocks in Warm Dense Matter in Neutron Stars or inertial confinement fusion based on Quantum hydrodynamics (Graziani et al., 2022)

Kinetic Gas theory Let us assume, the "free flight" between interactions is much larger than the interaction time. We can model *molecule-particles* with some effective interaction radius which only exhibit collisions. Note that while when modeling the potentials, at a sufficiently large collision parameter, particles do a kind of slingshot maneuver (attractive potential), which can never be modelled in a pure collision system. But this can be fine - with the right parameters our system can work globally in spite of local differences.

4.2 From a classical particle description to the Boltzmann equation

Consider we start of with classical point-like particles in phase space (e.g. the molecules) $\{\underline{x}_i, \underline{p}_i\}_{i=1}^N$ with a force term

$$\frac{d}{dt}\underline{p}_i = \underline{f}(\underline{x}_i(t), t) \underbrace{=}_{\substack{\text{e.g.}\\ \text{for}\\ \text{ions}}} q_i \cdot \left(\underline{E}_m(\underline{x}_i(t), t) + \frac{1}{m_i}\underline{p}_i(t) \times \underline{B}_m(\underline{x}_i(t), t) \right) \tag{127}$$

where the forces depend on the particle positions and momenta themselves (e.g. via Maxwells equations where the particle positions inform the charge density and thus the electric field and the velocities the currents and thus the magnetic field).

For as many particles as in a fluid (a mol has $\sim 6 \cdot 10^{23}$ particles and e.g. water has roughly 18 grams per mol) this is still unfeasible for simulation. It turns out to be smarter to model a phase space density. The exact classical phase space density is

$$\mathcal{F}(\underline{x}, \underline{p}, t) = \sum_{i=1}^{N} \delta(\underline{x} - \underline{x}_i)\delta(\underline{p} - \underline{p}_i) \tag{128}$$

Phase space conservation (Liouville theorem) (previously visualized for the pendulum) means that

$$\frac{d}{dt}\mathcal{F}(\underline{x}, \underline{u}, t) = \partial_t \mathcal{F} + \underline{v} \underline{\nabla}_{\underline{x}} \mathcal{F} + \underline{\mathcal{A}} \underline{\nabla}_{\underline{u}} \mathcal{F} = 0 \tag{129}$$

with the local acceleration $\underline{\mathcal{A}}$ following from the local force and mass. Let us use a mean phase space density and acceleration instead.

$$\begin{aligned} \mathcal{F}(\underline{x}, \underline{u}, t) &= f(\underline{x}, \underline{p}, t) + \delta\mathcal{F}(\underline{x}, \underline{u}, t), \quad f(\underline{x}, \underline{u}, t) = \langle \mathcal{F}(\underline{x}, \underline{u}, t) \rangle \\ \underline{\mathcal{A}}(\underline{x}, \underline{u}, t) &= \underline{a}(\underline{x}, \underline{u}, t) + \delta\underline{\mathcal{A}}(\underline{x}, \underline{u}, t), \quad \underline{a}(\underline{x}, \underline{u}, t) = \langle \underline{\mathcal{A}}(\underline{x}, \underline{u}, t) \rangle \end{aligned} \tag{130}$$

which we have also done for the acceleration, separating a mean effect on a *fluid parcel* from the direct particle-particle interactions. With this we get

$$\partial_t f + \underline{v} \cdot \underline{\nabla}_{\underline{x}} f + \underline{a} \cdot \underline{\nabla}_{\underline{u}} f = -\langle \delta \underline{\mathcal{A}} \cdot \underline{\nabla}_{\underline{u}} \delta \mathcal{F} \rangle =: \left. \frac{df}{dt} \right|_c \tag{131}$$

which is the Boltzmann equation, where we identified the local fluctuations with collisions $\left.\frac{df}{dt}\right|_c$ from a kinetic gas theory perspective.

4.3 Emergence of irreversibility in the Boltzmann equation

Consider a classical simulation of colliding spheres (interaction time $\ll$ free flight time), where we start out with the particles concentrated at the center of our box. As of their thermal motion, the particles will spread out and fill the box. Now consider we start with this end state and reverse all velocities - the particles will clump up - anti-dissipation. Such things can happen miscroscopically, they are simply very unlikely.

Something unlikely miscroscopically is virtually impossible macroscopically.

But based on the Boltzmmann equation, this will never happen - the Boltzmann equation is *irreversible* and will never show anti-dissipation.

»The derivation of the Boltzmann equation (BE) from the Hamiltonian equations of motion of a hard spheres gas is a key topic on irreversibility (Sklar 1993, p.32; Uffink 2007, Section 4). Although the Hamiltonian equations of motion are invariant under time reversal, the BE is not. Moreover, this equation allows us to derive the H-theorem, which states that a function H monotonically decreases with time, and thus, that the minus-H function increases, in agreement with the second law of thermodynamics. The derivation of the BE thus raises the question of irreversibility, since this equation exhibits irreversibility even though the microscopic description of the gas is based on reversible equations.« from Ardourel, 2017 where the emergence of irreversibility is discussed in detail.

We can try to understand the emergence of irreversibility based on going from the exact information of the positions and momenta of the particles to an averaged phase space density:

»In other words, when the particles are described by the Boltzmann equation, our knowledge is incomplete, since the positions and momenta of all the particles remain unknown, in contrast to the description by means of Hamilton canonical equations or Liouville equation. And this lack of knowledge makes the evolution of the one-particle distribution function f irreversible. The irreversibility is then explicitly expressed by the collision integral in the Boltzmann equation. The second law of thermodynamics thus emerges from completely reversible dynamics when our description is incomplete (not seeing all positions and momenta of the particles).« from Kincl and Pavelka, 2023

5 Basic Fluid Dynamics

Fluids (gases or liquids[5]) react to tangential (aka shear) stress with flow, a deformation rate depending on the viscosity, as opposed to solids which deform. Many systems from galaxies to lab plasmas can - on the right scale - be successfully modelled as fluids.

5.1 Basic notes on fluid description - the fluid from the view of a parcel

Physical systems can be described on different level: from a wave function in quantum physics, over a collection of point-like particles in classical physics to a **continuous fluid**.

5.1.1 When is a fluid description valid?

We want to describe the fluid in terms of macroscopic position and time dependent quantities like: mass density ρ, temperature T, velocity $\underline{u} = \underline{v} + \underline{w}$ where $\underline{v} = \langle \underline{u} \rangle$ is the mean (bulk) velocity of the local fluid element and $\underline{w}$ is the random velocity defining the temperature.

5.1.1.1 Connection between temperature and random movement

As of the equipartition theorem, each exitable degree of freedom adds $\frac{k_B T}{2}$ to the internal energy, so

$$\langle \frac{1}{2} m w_i^2 \rangle = \frac{1}{2} k_B T \quad \rightarrow \quad \langle ||\underline{w}||^2 \rangle = \frac{3 k_B T}{m} \tag{132}$$

5.1.1.2 Continuum Hypothesis

Q: When does it make sense to describe a physical system by a continuous fluid? A: When we can construct a volume small compared to the region of the fluid but big compared to the molecular free path. When we consider a fluid in terms of **parcels** with constant mass and particle number

$$\text{parcel mass } m_p = \int_V \rho dV, \quad \text{parcel volume } V, \quad \text{parcel density } \rho \tag{133}$$

we postulate that every fluid quantity (bulk quantity of the parcel) tends to a limit as the size of the volume approaches zero, before molecular fluctuation kicks in (**continuum hypothesis**), see figure 39.

[5] In gases, time between interactions is so much longer than time of interactions that they can often be described by kinetic gas theory. At higher temperatures there are more collsions and the gas is more viscous while in liquids at higher temperatures *bonds are easier to break* so the liquid is less viscous.

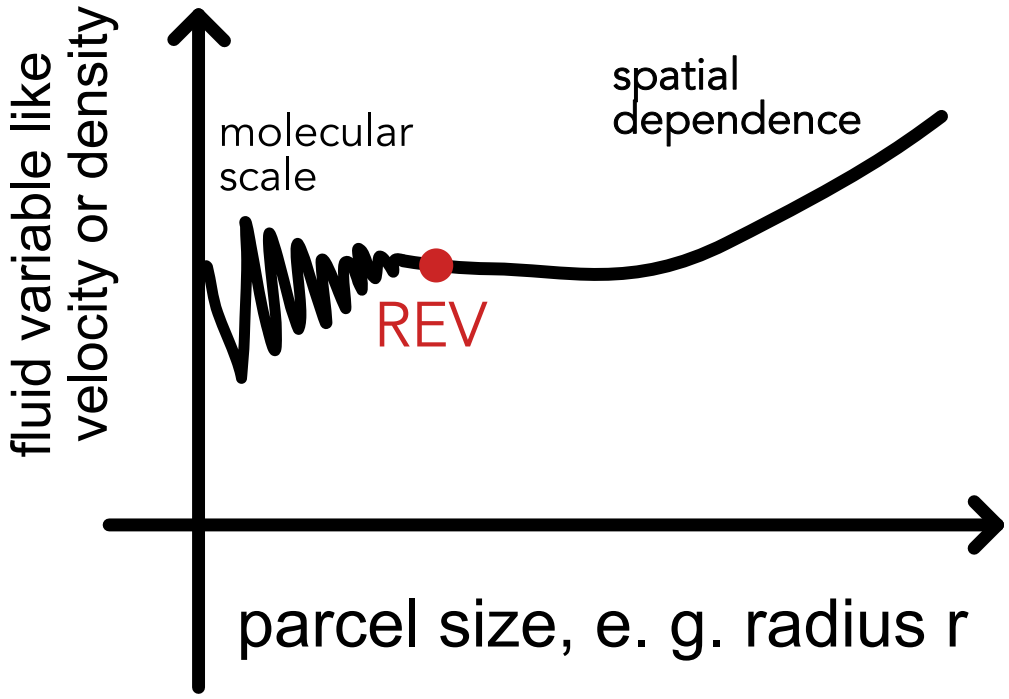

Figure 39: Continuum hypothesis; REV = representative elementary volume

A fluid description is thus justified if

$$\text{Knudsen number } Kn = \frac{\text{mean free path of particles } \lambda_{mfp}}{\text{characteristic system length } L} \ll 1 \tag{134}$$

5.1.2 Example: the plasma in the intercluster medium can be considered a fluid*

5.1.2.1 Mean free path in a model of colliding spheres

Consider a particle has a collisional cross-section of σ (in m^2) and moves with root mean square velocity $\bar{v}$ in a medium with number density n (in m^{-3}). Note that the mean relative velocity between particles is larger than the mean velocity per particle

$$\langle v_{rel}^2 \rangle = \langle (v - v')^2 \rangle = \langle v^2 \rangle - \underbrace{2\langle v v' \rangle}_{\substack{=0, \\ \text{as} \\ \text{uncor-} \\ \text{related}}} + \langle v'^2 \rangle = 2\langle v'^2 \rangle = 2\bar{v}^2 \quad \rightarrow \quad v_{rel} = \sqrt{2}\bar{v} \tag{135}$$

A particle thus in a time τ probes the volume $V = \sigma v_{rel} \tau$, so interacts with $N = nV$ particles. We are interested in the time till one interaction so the case $N = 1$, so $\tau = \frac{1}{n v_{rel} \sigma}$.

The path the particle itself has moved during that time is

$$\lambda_{mfp} = \tau \bar{v} = \frac{1}{\sqrt{2} n \sigma} \tag{136}$$

Note: The electrons though are much more mobile than the protons ($\frac{m_e}{m_p} \approx \frac{1}{1836}, m_e \approx 10^{-30}$ kg) so for electron-ion collisions the simpler $\lambda_{mfp} = \frac{1}{n\sigma}$ (assuming stationary nuclei) is probably better.

5.1.2.2 Collisional cross-section of an electron in a plasma and first approximation of λ_{mfp}

We approximate $\sigma = \pi r_{eff,e}^2$. We can approximate this radius by the distance where the electrostatic potential (in the electron-ion or electron-electron interaction) is only as relevant as the thermal energy, so (Z for the nucleic charge, relevant for the ion-electron interaction)

$$\frac{Ze^2}{r_{eff,e}} \sim m_e w_e^2 \sim k_B T_e \tag{137}$$

We can therefore approximate an electron mean free path

$$\begin{aligned} \lambda_{mfp,e} &\simeq \frac{1}{n\sigma} \sim \frac{1}{n\pi r_{eff,e}^2} \sim \frac{1}{\pi n} \left(\frac{k_B T_e}{Ze^2} \right) \\ &\sim 1.5 \times 10^{22} \left(\frac{n}{10^{-3}\,\mathrm{cm}^{-3}} \right)^{-1} \left(\frac{k_B T_e}{1\,\mathrm{keV}} \right) \mathrm{cm} \end{aligned} \tag{138}$$

where we assumed $Z = 1$.

Note: Most *collisions* in (strongly ionized) plasmas are Coulomb interactions with very small deflections (so collision parameters mostly larger than $r_{eff,e}$). Therefore, we define the collision rate and collisional cross-section based on a total deflection of $\frac{\pi}{2}$.

5.1.2.3 A better approximation to the mean free path in an ionized plasma

More careful considerations take into account the smaller deflections. The integral over $\frac{1}{b}$ (impact parameter b) yields the Coulomb logarithm

$$\log \Lambda = \log \frac{b_{max}}{b_{min}} \tag{139}$$

where for b_{max} we take the Debye length

$$\lambda_{D\xi} = \left(\frac{\epsilon_0 k_B T_\xi}{n_\xi e^2} \right)^{\frac{1}{2}}, \quad \xi = \text{ion, electron,} \quad \text{in plasma } n_i \approx n_e \tag{140}$$

(where the potential of a *Überschussladung* drops to $\frac{1}{e}\phi_0$ (e here Euler's number)) and for b_{min} e.g. $\pi r_{eff,e}$. One finally gets

$$\lambda_{mfp,e} = \frac{\bar{v_e}}{\nu_{ei}} \approx 64\pi\lambda_D \frac{\Lambda}{\log \Lambda} \propto \frac{T_e^2}{n_e} \gg \lambda_D \tag{141}$$

with ν_{ei} being the electron-ion collision rate. Examples of mean free paths are given in table 5.

Plasma	Solar Wind ($n \sim 1\,\mathrm{cm}^{-3}, T =$ some eV)	Ionosphere	Gas molecule in air under standard conditions
mean free path λ_{mfp}	1 AU	1 km	68 nm

Table 5: Mean free paths

The plasma in the intercluster medium can be considered a fluid. The solar wind can hardly be considered a fluid on a reasonable scale.

5.1.3 Fluid description based on fluid parcels

The modes of motion in a fluid are

- motion of macroscopic fluid parcels
- random walk between fluid parcels (diffusion, very slow)

The most important fluid equation, the **Navier Stokes equation** *falls out of the* Boltzmann equation but can also be *understood* as an equation of movement for a fluid parcel.

- mass conservation $\Longleftrightarrow$ continuity equation
- mass conservation + momentum conservation $\Longleftrightarrow$ Navier Stokes equation

5.1.3.1 Eulerian and Lagrangian fluid dynamics

Lagrangian and Eulerian view are presented in table 6.

The rate of change in the Eulerian view is the **material derivative**, the rate of change of a physical quantity (like temperature) of a material element that is subjected to a macroscopic

Lagrangian description	Eulerian description
Coordinate system comoves with the fluid element (we sit on the fluid parcel)	Coordinate system is fixed in space
The temporal evolution of fluid quantities is described along the trajectory of the movement of a fluid parcel	The temporal evolution of fluid quantities is described at a fixed locations over accounting volumes
e.g. measurement on a weather balloon following the wind flow	e.g. measurement by ground stations

Table 6: Lagrangian and Eulerian fluid dynamics

velocity field $\underline{v}$. Let $\Psi_L(t)$ describe the evolution of a fluid quantity along the parcel motion (Lagrangian) and $\Psi_E(\underline{x}, t)$ the evolution of a fluid quantity at a fixed location (Eulerian). Then the material derivative is

$$D_t\Psi_L = \frac{D\Psi_L}{Dt} = \partial_t\Psi_L = \underbrace{\partial_t\Psi_E}_{\substack{\text{local}\\ \text{change}}} + \underbrace{\underline{v}\cdot\underline{\nabla}_{\underline{x}}\Psi_E}_{\substack{\text{convective}\\ \text{change}}} = D_t\Psi_E \tag{142}$$

(derive $\Psi(\underline{x}(t), t)$ with respect to time and use the chain rule). Generally

$$D_t = \partial_t + \underline{v}\cdot\underline{\nabla} \tag{143}$$

5.1.3.2 Continuity equation

As of mass conservation, the change of mass m_V in a volume V can only be due to flux $\underline{j} = \rho\underline{v}$ through the surface ∂V.

$$\partial_t m_V = \partial_t \int_V \rho dV = -\int_{\partial V} \underline{j}\cdot d\underline{A} \underbrace{=}_{\text{Gauss}} -\int_V \underline{\nabla}\cdot\underline{j} dV \quad \rightarrow \quad \boxed{\partial_t\rho + \underline{\nabla}\cdot(\rho\underline{v}) = 0} \tag{144}$$

which is the continuity equation.

5.1.3.3 Incompressible fluids

An incompressible fluid is one, where the density of a fluid parcel never changes with time $\frac{d\rho}{dt} = 0$ (there can still be gradients in the density). From the Lagrangian form of the continuity equation

$$0 = \frac{d\rho}{dt} = \partial_t\rho + \underline{v}\cdot\underline{\nabla}\rho \underbrace{=}_{\substack{\text{cont.}\\ \text{eq.}}} \quad \rightarrow \quad \boxed{\underline{\nabla}\cdot\underline{v} = 0} \tag{145}$$

For $\underline{\nabla} \cdot \underline{v} < 0$ we have a sink, for $\underline{\nabla} \cdot \underline{v} > 0$ a source. The divergence of the velocity field of incompressible fluids vanishes (divergence free flow) (e. g. rotational flow) Note in a 3D flow horizontal convergence can be balanced by vertical divergence.

Interpretation of $\underline{\nabla} \cdot \underline{v} = 0$ A divergence free flow does not mean that the velocity does not change over space as one can easily see from flow along a narrowing tube. Consider a tube with flow tangential to it.

$$\begin{aligned} \underline{\nabla} \cdot \underline{v} = 0 \xrightarrow{\text{integrate over tube}} 0 = \int_V \underline{\nabla} \cdot \underline{v} dV \underset{\text{Gauss}}{=} \int_{\partial V} \underline{v} d\underline{A} \\ \xrightarrow[\text{only opposing flux trough } A_1 \text{ and } A_2]{} v_1 A_1 - v_2 A_2 = 0 \\ \rightarrow v_1 A_1 = v_2 A_2 \end{aligned} \tag{146}$$

5.1.3.4 Equation of motion of a fluid parcel, general path towards Navier-Stokes

Consider a fluid parcel with constant mass m. The equation of motion is

$$\underline{F} = \frac{d\underline{p}}{dt} = m\frac{d\underline{V}}{dt} = \rho V \frac{d\underline{v}}{dt}, \quad \underline{a} = \frac{\underline{F}}{\rho V} = \frac{\underline{f}}{\rho} = \frac{d\underline{v}}{dt} \tag{147}$$

Using the material derivative, we can write

$$\frac{d\underline{v}}{dt} = \partial_t \underline{v} + \underbrace{\underline{v} \cdot \underline{\nabla} \underline{v}}_{\substack{\text{non-linear advective term} \rightarrow \text{chaotic behavior}}} = \underline{a} = \frac{\underline{f}}{\rho} \tag{148}$$

where one can find (leading to a simplified **Navier Stokes equation**)

$$\underline{f} = \underbrace{\underline{f}_g}_{\substack{\text{gravi.} \\ \text{force}}} + \underbrace{\underline{f}_p}_{\substack{\text{pressure} \\ \text{force}}} + \underbrace{\underline{f}_f}_{\substack{\text{friction} \\ \text{force}}} = \rho \underline{g} - \underline{\nabla} p + \rho \nu \underline{\nabla}^2 \underline{v} \tag{149}$$

where the viscous friction $\underline{f}_v$ (viscosity ν) is an approximation for an incompressible isotropic Newtonian fluid. While pressure is a force per area, only when there are different pressures acting on the sides of a fluid parcel (a gradient), there is net movement. The friction term can be understood as diffusion of momentum when there is a velocity gradient (which only leads to a local change when when $\underline{\nabla}^2 \underline{v} \neq 0$, otherwise there is the same momentum diffusion in and out of the parcel).

5.2 Basic Gas Dynamics

Aim: Our aim is to derive equations for the evolution of variables of the fluid, like density, velocity and temperature. For instance how do perturbation (e.g. by a jet) propagate through the fluid?

5.2.1 Distribution function and Boltzmann equation

Idea: Let us derive the fluid equations based on the Boltzmann equation for the distribution function.

The distribution function $f(\underline{x}, \underline{u}, t)$ is defined so that

$$f(\underline{x}, \underline{u}, t) d^3x d^3u \tag{150}$$

is (depending on the normalization) the probability of finding a particle in the phase space volume $d^3x d^3u$ around $(\underline{x}, \underline{u})$ at time t or the expected number or particles therein, so in total

$$N = \int \int f(\underline{x}, \underline{u}, t) d^3x d^3u, \quad \text{total number of particles } N \tag{151}$$

Phase space conservation (Liouville theorem) (particles are neither created nor destroyed) is captured in the Boltzmann equation

$$\frac{d}{dt} f(\underline{x}, \underline{u}, t) = \partial_t f + \underline{\dot{x}} \underline{\nabla}_{\underline{x}} f + \underline{\dot{u}} \underline{\nabla}_{\underline{u}} f = \left. \frac{df}{dt} \right|_c, \quad \text{with } \underline{\dot{x}} = \underline{u}, \underline{\dot{u}} = \underline{g} \tag{152}$$

where $\left. \frac{df}{dt} \right|_c$ is the change in f due to *collisions*.

Note: One can understand this in the sense of dicontinupus motion (instantaneous velocity changes) kicking a particle out of a phase space volume. More aligned with our previous derivation, we can see this as a simplification of the correlation term between forces and accelerations (also capturing the particle interaction) (see subsection 4.2).

In the case of a sufficiently large collision term $\left. \frac{df}{dt} \right|_c$ (in the fluid limit $\lambda_m f p \ll L$) $f(\underline{u})$ becomes Mawellian. Near the sun for instance Coulomb collisions are incapable of isotropizing the velocity distribution of the ions in the solar wind (cigar shape).

5.2.2 Retrieving information from the Boltzmann equation

By taking the moments of the distribution function over velocity space

$$M_n(\underline{x},t) = \int \underline{v}^n f(\underline{x},\underline{u},t)d^3u \tag{153}$$

we find out on the quantities of interest in space as

- density (0th moment)

$$\begin{gathered} n = \int f(\underline{x},\underline{u},t)d^3u, \quad \rho = nm, \quad \text{particle mass } m \\ \rightarrow \text{mass weighted average } \langle q\rangle(\underline{x},t) = \frac{1}{\rho(\underline{x})}\int q(\underline{x},\underline{u},t)f(\underline{x},\underline{u},t)d^3u \end{gathered} \tag{154}$$

- mean velocity (1st moment)
- pressure tensor as of the fluctuations of the velocity around the mean ($\rightarrow$ temperature in case of a Maxwell distribution) (2nd moment)
- heat tensor (3rd moment)

The development of those quantities in time is given by the balance (/conservation) equations obtained from taking the appropriate moments of the Boltzmmann equation (mass, momentum and energy are conserved).

$$\text{form of balance equations: } \partial_t\text{conserved quantity} + \underline{\nabla}\text{corrsp. flux} = \text{source term} \tag{155}$$

5.2.3 Mass conservation | continuity equation (1st moment)

By following the steps

- multiply the Boltzmann equation by m and integrate over d^3u
- using Gauss divergence theorem and assuming $f \rightarrow 0$ for $u \rightarrow \infty$
- local mass conservation $\int m \left.\frac{df}{dt}\right|_c d^3u = 0$ (collisions only shift discontinuously on velocity space)

one follows the mass continuity equation

$$\partial_t\rho + \underline{\nabla}\cdot(\rho\cdot\underline{v}) = 0, \quad \underline{u} = \underline{v} + \underline{w}, \quad \underline{v} = \langle\underline{u}\rangle \tag{156}$$

By taking the volume integral (d^3x) we find $\frac{dm}{dt} = 0$, i.e. mass conservation.

5.2.3.1 Derivation of the continuity equation*

From

$$\underbrace{\int m\partial_t f d^3u}_{\partial_t\rho(\underline{x},t)} + \underbrace{\underline{\nabla}_{\underline{x}}\int m\underline{u} f d^3u}_{\substack{\text{using } r,u \text{ indep.;}\\ =\underline{\nabla}_{\underline{x}}(\rho\underline{v})}} + \underbrace{\int m\underline{\nabla}_{\underline{u}}(\underline{g}f)d^3u}_{\substack{\text{assume acc. } \underline{g}\\ \text{indep. } \underline{u}}} = \underbrace{\int m\left.\frac{df}{dt}\right|_c d^3u}_{\substack{=0 \text{ (local}\\ \text{particle}\\ \text{conserv.)}}} \tag{157}$$

where the third term also vanishes (apply Gauss, assume $f \to 0$ (e.g. Maxwellian $\exp(-u^2)$) for $u \to \infty$), we get the result from above.

5.2.4 Momentum conservation | Navier Stokes equation (2nd moment)

By following the steps

- multiply Boltzmann equation with momentum ($m\underline{u}$) and integrate over d^3u
- using that collisions conserve momentum
- using the continuity equation

one obtains the Navier-Stokes equation

$$\partial_t(\rho\underline{v}) + \underline{\nabla}\cdot(\rho\underline{v}\underline{v}^T + P\underline{\underline{1}} - \underline{\underline{\Pi}}) = \rho\underline{g} \tag{158}$$

which using the continuity equation becomes

$$\partial_t\underline{v} + (\underline{v}\cdot\underline{\nabla})\underline{v} = \underline{g} - \frac{1}{\rho}\underline{\nabla}P + \frac{1}{\rho}\underline{\nabla}\cdot\underline{\underline{\Pi}} \tag{159}$$

with

$$\begin{gathered}\text{(isotropic) pressure } P = \frac{1}{3}\rho\langle||\underline{w}||^2\rangle\\ \text{anisotropic viscous stress tensor } \Pi_{ij} = P\delta_{ij} - p\langle w_i w_j\rangle \text{ (symmetric and traceless)}\\ \text{acceleration } \underline{g} \text{ from external sources}\end{gathered} \tag{160}$$

Viscosity opposes shearing motion and interprenetation (diffusion of momentum on shear).

Taking the volume integral over the Navier-Stokes equation and applying Gauss theorem, we see that in the absence of an external force ($\underline{g} = 0$), the momentum is conserved.

5.2.4.1 Notes on the derivation of the Navier-Stokes equation

Take a look at the terms in

$$\partial_t \int m\underline{u} f d^3u + \underline{\nabla}_{\underline{x}} \int m\underline{u}\underline{u}^T f d^3u + \int m\underline{g}\underline{u}^T \underline{\nabla}_{\underline{u}} f du^3 = \int m\underline{u} \left.\frac{\partial f}{\partial t}\right|_c d^3u \tag{161}$$

- first term: $\partial_t \int m\underline{u} f d^3u = \partial_t(\rho \underline{v})$ by definition of $\underline{v}$
- second term: $\underline{\nabla}_{\underline{x}} \int m\underline{u}\underline{u}^T f d^3u = \underline{\nabla}_{\underline{x}} \left(\rho \langle \underline{u}\underline{u}^T \rangle\right)$ using $\underline{u} = \underline{v} + \underline{w}$ this becomes $\underline{\nabla}_{\underline{x}} \left(\rho \underline{v}\underline{v}^T\right) + 2\underline{\nabla}_{\underline{x}} \left(\rho \underline{v} \langle \underline{w} \rangle^T\right) + \underline{\nabla}_{\underline{x}} \left(\rho \langle \underline{w}\underline{w}^T \rangle\right) = \underline{\nabla}_{\underline{x}} \left(\rho \underline{v}\underline{v}^T\right) + \underline{\nabla}_{\underline{x}} \left(\rho \langle \underline{w}\underline{w}^T \rangle\right)$ as $\langle \underline{w} \rangle = \underline{0}$.
- third term: assuming $\underline{g}$ does not depend on $\underline{u}$, $\underline{g} \int m\underline{u}^T \underline{\nabla}_{\underline{u}} f du^3 = -\rho \underline{g}$ as by the chain rule $\underline{u}^T \underline{\nabla}_{\underline{u}} f = \underline{\nabla}_{\underline{u}} (\underline{u}^T f) - f \underline{\nabla}_{\underline{u}} \underline{u}^T$ where the integral over the first term vanishes by the same reasoning as before
- the right-hand side vanishes, because collisions conserve momentum

Finally, $\left(\rho \langle \underline{w}\underline{w}^T \rangle\right)$ (so the correlation matrix of the random fluctuations (?)) is split into an isotropic contribution from pressure P and an anisotropic viscous stress tensor $\underline{\underline{\Pi}}$. The continuity equation can be used to get (first apply chain rule) $\partial_t(\rho \underline{v}) + \underline{\nabla}_{\underline{x}} \left(\rho \underline{v}\underline{v}^T\right) = \rho \left(\partial_t \underline{v} + (\underline{v} \cdot \nabla)\underline{v}\right)$

5.2.4.2 Interpretation and viscous stress tensor for a Newtonian fluid

Our result

$$\frac{d\underline{v}}{dt} = \partial_t \underline{v} + (\underline{v} \cdot \underline{\nabla})\underline{v} = \underline{g} - \frac{1}{\rho} \underline{\nabla} P + \frac{1}{\rho} \underline{\nabla} \cdot \underline{\underline{\Pi}} \tag{162}$$

already looks similar to our intuitive result. We have

- some acceleration from external forces $\underline{g}$ (e.g. gravity)
- pressure force, where on the pressure we now also have a microscopic unterstanding $P = \frac{1}{3} \rho \langle ||\underline{w}||^2 \rangle$
- some viscous force as described by $\frac{1}{\rho} \underline{\nabla} \cdot \underline{\underline{\Pi}}$

Intuition for viscosity and momentum diffusion: Viscosity is an every-day phenomenon - but how can we understand it miscroscopically? Consider a fluid with bulk velocity $\underline{v}$ only in x-direction. Now imagine v_x increases with z (maybe because im pulling a plate on top of my container). The molecules constantly bump into each other, and it is much more probabable that a particle from higher up z will give x- momentum to one from lower down in a collision than vice versa. Therefore x-momentum diffuses down. However if the x-velocity increases linearly with z, $v_x(z)$ will not change, as there is as much momentum transport in as out of a given slice along x at some height z. Therefore the simplest diffusion equation for momentum is $\rho\partial_t v_x(z) = \nu\rho\partial_z^2 v_x$ (for a positive curvature more momentum diffuses down from the top then goes out of the bottom). Speaking in terms of the fluctuations $\underline{w}$ from the bulk velocity $\underline{v}$, in the above scenario we expect particles with high *random* downward velocity $-w_z$ to be faster than their surrounding (high w_x), so we expect $-\langle w_z w_x\rangle > 0$.

With the above intuition, it should make sense that

$$\Pi_{ij} = P\delta_{ij} - p\langle w_i w_j\rangle \tag{163}$$

and that we might make the ansatz of Π_{ij} being linear in $\frac{\partial v_i}{\partial x_j}$

$$\begin{aligned}\Pi_{ij} &= \eta D_{ij} + \xi\delta_{ij}(\underline{\nabla}\cdot\underline{v})\\ D_{ij} &= \frac{\partial v_i}{\partial x_j} + \frac{\partial v_j}{\partial x_i} - \frac{2}{3}\delta_{ij}(\underline{\nabla}\cdot\underline{v})\end{aligned} \tag{164}$$

with D_{ij} being the deformation tensor that vanishes for uniform expansion or contraction, η and ξ are the coefficients of shear and bulk viscosity respectively, with units $g\,\mathrm{cm}^{-1}\,\mathrm{s}^{-1}$.

- ηD_{ij} represents the resistance to shearing motion
- $\xi\delta_{ij}\left(\underline{\nabla}\cdot\underline{v}\right)$ represents the resistance in volume, remember that for $\underline{\nabla}\cdot\underline{v} = 0$ we have an incompressible fluid

5.2.5 Energy conservation (3rd moment)

By the following steps

- multiply the Boltzmann equation by $m\underline{u}^2$ and integrate over d^3u
- use that collisions conserve energy
- use the continuity equation

one follows

$$\rho\frac{de_{th}}{dt} \equiv \partial_t(\rho e_{th}) + \underline{\nabla}\cdot(\rho e_{th}\cdot\underline{v}) = -P\underline{\nabla}\cdot\underline{v} + \Psi - \underline{\nabla}\cdot\underline{Q}$$
$$\text{specific internal energy } e_{th} \equiv \frac{1}{2}\langle||\underline{w}||^2\rangle$$
$$\text{viscous dissipation rate (bulkmotion } \rightarrow \text{ internal energy) } \Psi \equiv \sum_{i,j=1}^{N}\Pi_{ij}\frac{\partial v_i}{\partial x_j} \tag{165}$$
$$\text{conductive heat flux } \underline{Q} = \frac{1}{2}\rho\langle\underline{w}||\underline{w}||^2\rangle$$

5.2.5.1 Notes on the conductive heat flux

There is only conductive heat flux $\underline{Q}$ is $\underline{w}$ is asymmetric around the bulk motion (hotter (*faster* in the sense of $||\underline{w}||$) particles drift relative to cold ones). The conductive flux is in most cases produced by a temperature gradient

$$\underline{Q} = -\xi\underline{\nabla}T, \quad \text{with } \chi \simeq 6\times10^{-7}T^{\frac{5}{2}}\,\mathrm{erg\,s^{-1}\,cm^{-1}\,K^{-1}}$$
$$\text{proper diffusion coefficient } \kappa = \frac{\chi T}{P} \text{ in } \mathrm{cm^2\,s^{-1}} \tag{166}$$

(by collisions and random movement, wiggling spreads, stochastically along the gradient of T). As always, there is only change in a volume if there is different in- and outflux, so if $\underline{\nabla}\cdot\underline{Q} \neq 0$.

5.2.5.2 Evolution equation for the total specific energy $e = e_{th} + \underline{v}^2/2$

We are interested in

$$\frac{de}{dt} = \frac{de_{th}}{dt} + \frac{d}{dt}\left(\frac{1}{2}\underline{v}^2\right) \tag{167}$$

where we already know $\frac{de_{th}}{dt}$. So let us consider

$$\begin{aligned}\partial_t\left(\frac{\rho\underline{v}^2}{2}\right) &= \frac{\underline{v}^2}{2}\partial_t\rho + \rho\underline{v}\partial_t\underline{v}\\ &= \frac{\underline{v}^2}{2}\left(-\underline{\nabla}(\rho\underline{v})\right) + \rho\underline{v}\left(-(\underline{v}\cdot\underline{\nabla})\underline{v} + \underline{g} - \frac{1}{\rho}\underline{\nabla}P + \frac{1}{\rho}\underline{\nabla}\cdot\underline{\underline{\Pi}}\right)\end{aligned} \tag{168}$$

where we used the continuity equation and Navier-Stokes equation. Based on

$$(\underline{v}\cdot\underline{\nabla})\underline{v} \equiv \frac{1}{2}\underline{\nabla}\underline{v}^2, \quad \rho\underline{v}\frac{1}{2}\underline{\nabla}\underline{v}^2 + \frac{\underline{v}^2}{2}\underline{\nabla}\rho\underline{v} = \underline{\nabla}\cdot\left(\frac{1}{2}\rho\underline{v}^2\underline{v}\right) \tag{169}$$

this becomes

$$\frac{d}{dt}\left(\frac{\rho \underline{v}^2}{2}\right) = \partial_t\left(\frac{\rho \underline{v}^2}{2}\right) + \underline{v}\cdot\left(\frac{1}{2}\rho \underline{v}^2 \underline{v}\right) = \rho \underline{v}\cdot\underline{g} - \underline{v}\cdot\underline{\nabla} P + \underline{v}\cdot\left(\underline{\nabla}\cdot\underline{\underline{\Pi}}\right) \tag{170}$$

so we finally get the evolution equation for the total specific energy $e = e_{th} + \underline{v}^2/2$

$$\partial_t(\rho e) + \underline{\nabla}\cdot\left[(\rho e + P)\underline{v} - \underline{\underline{\Pi}}\cdot\underline{v} + \underline{Q}\right] = \rho \underline{v}\cdot\underline{g} \tag{171}$$

where taking the volume integral and applying Gauss theorem shows energy conservation if $\underline{g} = \underline{0}$.

5.2.6 Entropy conservation

Note: Heat conduction and viscous friction change the entropy and entropy is conserved is those processses are absent.

From the first law of thermodynamics in its specific form (specific volume $\tilde{V} = 1/\rho$)

$$de_{th} = dw + dq = -P d\tilde{V} + T ds = \frac{P}{\rho^2} d\rho + T ds \tag{172}$$

we find (*divide* by dt and insert the continuity and energy equation)

$$\rho T \frac{ds}{dt} = -\underline{\nabla}\cdot\underline{Q} + \Psi \tag{173}$$

proving the statement in the note.

5.3 Euler Equation and Navier-Stokes equation

Ideal gas dynamics, where we assume internal friction and heat conduction to be absent, are described by the Euler equations. Those assumptions are well justified for gas flow in astrophysics, which are often of extremely low density.

If viscosity is relevant, we use the hydrodynamical equations inclusind viscosity, the Navier-Stokes equation.

We will later discuss fluid instabilities in the absence of viscosity.

5.3.1 Euler Equations

Assuming (valid for non-dense media like air)

- no thermal conductivity
- no internal friction
- no external forces

the balance equations obtained from the moments of the Boltzmann equation simplify to the Euler equations (table 7).

Continuity equation	Balance of momentum	Balance of energy
$\partial_t \rho + \underline{\nabla} \cdot (\rho \underline{v}) = 0 \quad (174)$	$\partial_t(\rho \underline{v}) + \underline{\nabla} \cdot (\rho \underline{v}\underline{v}^T + P \underline{\underline{1}}) = 0$ (175)	$\partial_t(\rho e) + \underline{\nabla} \cdot \left[(\rho e + P)\underline{v}\right] = 0$ with $e = e_{th} + \frac{1}{2}\underline{v}^2$ $\frac{\text{total energy}}{\text{unit mass}}$ (176)

Table 7: Euler equations

The equations form a set of hyperbolic conservation laws (all continuity equations, one for mass, one for momentum, one for energy).

Hierarchy and closure The equations are in a hierarchy that in one equations occur quantities following from the next higher one (velocity in the continuity equation, ...) - we need a further closure relation making the energy balance unnecessary, for an ideal gas this is

$$P = (\gamma - 1)\rho e_{th}, \quad \gamma = \text{ specific heat ratio } = \frac{c_p}{c_v}, \quad \text{for monoatomic gas } \gamma = \frac{f+2}{f} = \frac{5}{3} \tag{177}$$

5.3.2 Navier-Stokes equation

In real fluids, viscosity transforms relative motion into heat. For

- vanishing conductivity
- vanishing external forces

we have (table 8)

$\underline{\underline{\Pi}}$ is the viscous stress tensor, a material property. For a vanishing stress tensor, we recover the Euler equations. To first order $\underline{\underline{\Pi}}$ must be linear in the velocity derivatives, where the

Continuity equation	Balance of momentum	Balance of energy
$\partial_t \rho + \underline{\nabla} \cdot (\rho \underline{v}) = 0$ (178)	$\partial_t(\rho \underline{v}) + \underline{\nabla} \cdot (\rho \underline{\underline{v}} \underline{\underline{v}}^T + P \underline{\underline{1}}) = \underline{\nabla} \cdot \underline{\underline{\Pi}}$ (179)	$\partial_t(\rho e) + \underline{\nabla} \cdot \left[(\rho e + P)\underline{v}\right] = \underline{\nabla} \cdot \left(\underline{\underline{\Pi}} \cdot \underline{v}\right)$ (180)

Table 8: Navier stokes equations

most general rank-2 tensor of this type can be written as

$$\underline{\underline{\Pi}} = \eta \left[\underline{\nabla} \underline{v}^T + (\underline{\nabla} \underline{v}^T)^T - \frac{2}{3} (\underline{\nabla} \cdot \underline{v}) \underline{\underline{1}} \right] + \xi (\underline{\nabla} \cdot \underline{v}) \underline{\underline{1}}$$

$$\eta \text{ scales the traceless part, describes shear viscosity} \tag{181}$$

$$\xi \text{ scales the trace, describes bulk viscosity}$$

$$\text{possibly } \eta, \xi \text{ depend on } \rho, T, \ldots$$

5.3.2.1 Simplification of the Navier-Stokes equations for incompressible fluids ($\underline{\nabla} \cdot \underline{v} = 0$)

In the case $\underline{\nabla} \cdot \underline{v} = 0$ only shear forces matter (no bulk compression), and we have

$$\frac{1}{\eta} (\underline{\nabla} \cdot \underline{\underline{\Pi}})_x = \left(\underline{\nabla} \cdot \left[\underline{\nabla} \underline{v}^T + (\underline{\nabla} \underline{v}^T)^T \right] \right)_x = \underline{\nabla}^2 v_x \tag{182}$$

(hint: write the component out and use $\partial_x^2 v_x + \partial_y \partial_x v_y + \partial_z \partial_x v_z = \partial_x (\partial_x v_x + \partial_y v_y + \partial_z v_z) = 0$). Introducing the kinematic viscosity $\nu \equiv \frac{\eta}{\rho}$, we get

$$\frac{d\underline{v}}{dt} = \partial_t \underline{v} + (\underline{v} \cdot \underline{\nabla}) \underline{v} = -\frac{\underline{\underline{\nabla}} P}{\rho} + \nu \underline{\nabla}^2 \underline{v} \tag{183}$$

so the simplified expression from the beginning. The bulk motion responds to pressure gradients and viscous forces.

5.3.2.2 Characterizing flow | Reynolds number

Consider a flow problem with characteristic length scale L_0, velocity V_0 and density scale ρ_0. Let us define dimensionsless fluid variables and operators

$$\begin{aligned} \underline{\hat{v}} = \frac{\underline{v}}{V_0}, \quad \underline{\hat{x}} = \frac{\underline{x}}{L_0}, \quad \hat{P} = \frac{P}{\rho_0 V_0^2} \\ T_0 = \frac{L_0}{V_0}, \quad \hat{t} = \frac{t}{T_0}, \quad \hat{\rho} = \frac{\rho}{\rho_0}, \quad \underline{\hat{\nabla}} = L_0 \underline{\nabla} \end{aligned} \tag{184}$$

where for the pressure mind that pressure is also an energy density and the kinetic energy density is $\frac{1}{2}\rho_0 V_0^2$.

Plugging this the incompressible Navier-Stokes equation (183) we get

$$\frac{d\underline{\hat{v}}}{d\hat{t}} = -\frac{\underline{\hat{\nabla}} P}{\hat{\rho}} + \frac{\nu}{L_0 V_0} \underline{\hat{\nabla}}^2 \underline{\hat{v}} \tag{185}$$

involving the Reynolds number

$$Re \equiv \frac{L_0 V_0}{\nu} \tag{186}$$

We can understand the Reynolds number as the ratio between the chaotic advective term in the Navier-Stokes equation and the frictional term, so

$$Re = \frac{\text{advective term}}{\text{frictional term}} = \frac{|(\underline{v} \cdot \underline{\nabla})\underline{v}|}{\nu \underline{\nabla}^2 \underline{v}} \tag{187}$$

Note: Connection between the Reynolds number and turbulence: The quadratic (in the velocity) term $(\underline{v} \cdot \underline{\nabla})\underline{v}$ generates turbulence (deterministic chaos) while the viscous term $\nu \underline{\nabla}^2 \underline{v}$ destroys it via dissipation. In terms of energy

$$Re \sim \frac{V_0 L_0}{\nu} = \frac{\rho L^3 U^2}{\mu L^2 U} = \frac{2E_{kin}}{W_{friction}}, \quad \text{as } W_{friction} \sim F_{friction} \cdot L_0 = V \rho \nu \underline{\nabla}^2 \underline{v} \cdot L_0 = \mu V_0 L_0^2 \tag{188}$$

(with the kinematic viscosity $\nu = \frac{\mu}{\rho}$ in $m^2\,s^{-1}$). In general, the higher the Reynolds number the more turbulence, for

$$Re > R_c \sim 10^3 \tag{189}$$

we have turbulent flow (figure 40). For $Re \sim 1$ viscosity dominates, for $Re \to \infty$ we approach an ideal gas.

Re = 1 (domination of viscous friction)	Re = 26	Re = 41	Re = 105 (still regular)	Re > 10^3 Turbulence (higher Re → turbulence on smaller scales)
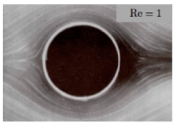	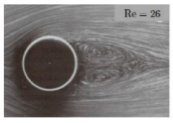	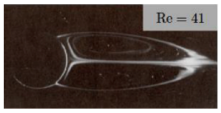		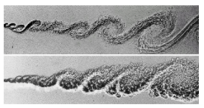

Figure 40: Reynolds number

5.4 Shocks

In hydrodynamical flows, shock waves can develop, where the fluid variables

- density ρ
- velocity $\underline{v}$
- temperature T
- specific entropy s

jump by finite amounts. In the frame of the Euler equations these are true mathematical discontinuities, while exhibiting a finite width in the Navier Stokes equations. A shock wave

- propagates faster than the signal speed for compressible waves c_s
- produces and irreversible change to the fluid change (increase in entropy)

A shock wave is a region of small thickness over which the properties of the flow change rapidly.

5.4.1 Propagation of disturbances 1: Speed of sound

Microscopic Intuition: Consider a higher density region in a fluid. Probabalisticly there is more momentum in the direction of lower density, so (by collisions) the higher density will spread out. The characteristic speed of on which density information propagates is related to the jiggling of the particles, i.e. their themperature. This characteristic speed of sound is roughly derived in the following.

Soundwaves are messengers, carrying density and pressure fluctuations. Imagine you're driving in fog towards a traffic jam - if you're so quick no messenger can quickly enough reach you, you will have a shock.

Consider the Euler equation for momentum without internal forces or friction in 1D in a steady state with constant flux $j = \rho v$, so $0 = d(\rho v) \rightarrow \rho dv = -v d\rho$. We get

$$\frac{dv}{dt} = -\frac{1}{\rho}\frac{dP}{dx} \quad \rightarrow \quad dP = -(\rho dv)\frac{dx}{dt} = (v d\rho)v \quad \rightarrow \quad v^2 \equiv c_s^2 = \frac{dP}{d\rho} \tag{190}$$

(note is relative to the bulk motion, so in the local rest frame of the flow, more later).

Now we use that for an adiabatic process, $P\rho^{-\gamma} = \text{const.}$ (and $T\rho^{1-\gamma} = \text{const.}$) so taking the logarithm and differentiating with respect to ρ yields

$$\frac{dP}{d\rho} = \frac{\gamma p}{\rho} \tag{191}$$

so using the ideal gas law

$$P = nk_BT = \frac{\rho}{m_p\mu}k_BT \quad \text{with } \mu \text{ being a mean molecular weight} \tag{192}$$

we get

$$c_s^2 = \frac{\gamma k_B T}{m_p \mu} \tag{193}$$

so based on $T\rho^{1-\gamma} = \text{const.}$ we can write

$$c_s^2 \propto \rho^{\gamma-1} \tag{194}$$

5.4.2 Characteristics of Perturbations

Idea: Our aim is to find the characteristics, lines in the (x, t) plane along which perturbations propagate.

Let us start with the continuity equation in 1D

$$\text{cont.:} \ \frac{1}{\rho}\left(\frac{\partial \rho}{\partial t} + v\frac{\partial \rho}{\partial x}\right) = 0 \tag{195}$$

With $c_s^2 = \frac{\partial P}{\partial \rho}$ we can write the Euler equation for momentum as

$$\text{Euler:} \ \frac{\partial v}{\partial t} + v\frac{\partial v}{\partial x} = -\frac{1}{\rho}\frac{\partial P}{\partial x} = -\frac{c_s^2}{\rho}\frac{\partial \rho}{\partial x} \tag{196}$$

Based on $c_s^2 \propto \rho^{\gamma-1}$, we can replace $\partial\rho$ in those equations using

$$\frac{d\rho}{\rho} = \frac{2}{\gamma-1}\frac{dc_s}{c_s} \tag{197}$$

With this replace $\partial\rho$ in the continuity and Euler equation. From adding and subtracting the Euler and continuity equation, we get

$$\begin{aligned}\left[\partial_t + (v+c_s)\,\partial_x\right]\left(u + \frac{2}{\gamma-1}c_s\right) &= 0\\ \left[\partial_t + (v-c_s)\,\partial_x\right]\left(u - \frac{2}{\gamma-1}c_s\right) &= 0\end{aligned} \tag{198}$$

Defining

$$\begin{aligned}\xi_+ \equiv u + \frac{2}{\gamma-1}c_s \quad &\rightarrow \quad \frac{d}{dt}\xi_+(x(t),t) = \left[\partial_t + (\partial_t x)\partial_x\right]\xi_+(x(t),t) = 0 \text{ for } \partial_t x = v + c_s\\ \xi_- \equiv u - \frac{2}{\gamma-1}c_s \quad &\rightarrow \quad \frac{d}{dt}\xi_-(x(t),t) = \left[\partial_t + (\partial_t x)\partial_x\right]\xi_-(x(t),t) = 0 \text{ for } \partial_t x = v - c_s\end{aligned} \tag{199}$$

where we applied the *method of characteristics*.

> From this we can see that (*as expected*) in a fluid with bulk motion v, perturbations propagate along characteristics with velocity $v \pm c_s$.

These characeteristic equations are the same no matter the aplitude of the perturbations.

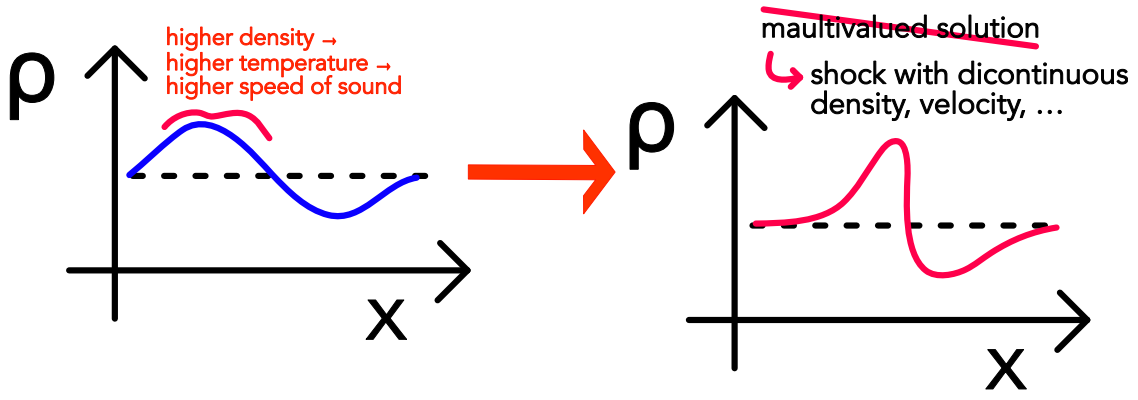

Figure 41: Formation of a shock

5.4.3 Formation of a shock

5.4.3.1 Formation as a pressure driven compressive disturbance

Consider a fluid with base density ρ_0. For small perturbation in density, we can to first order use

$$c_s = \left(\frac{\partial P}{\partial \rho}\right)^{\frac{1}{2}} \simeq \frac{\gamma p_0}{\rho_0} \tag{200}$$

But now consider a larger perturbation. Adiabatically the temperature scales with $T \propto \rho^{\gamma-1}$, and as c_s^2 scales linearly with the temperature, we have

$$c_s^2 \propto T \propto \rho^{\gamma-1} \tag{201}$$

Therefore, the "waves crest overtakes the valley" (figure 41) but as the hydrodynamic equations don't allow for multivalued solutions, we get a shock with discontinuities in ρ, v, T and s. For an isothermal gas $c_s = \text{const.}$ but steepening can happen nonetheless as of the non-linearity of the Euler / Navier-Stokes equations (?).

5.4.3.2 Causes for shocks

- supersonic compressible disturbance
- supersonic collision of two streams of fluids
- non-linear interaction of subsonic compressible modes (nonliear wave interaction)

5.4.4 Collisional and collisionless shocks | shock front

The »discontinuous« change normally happens over a scale proportional to the *effective* mean free path λ_{eff}.

- Collisional shocks: Coulomb-collisions determine λ_{eff}
- Collisionless plasma like solar wind: λ_{eff} is reduced by electromagnetic viscosities $\lambda_{eff} \ll \lambda_{coulomb}$

The shock front or transition layer is of the scale of λ_{eff}. Here, viscous effects are important - they dissipate kinetic energy, generating heat and entropy. Outside this layer viscous effects are small on scales $L \gg \lambda_{eff} \rightarrow \underline{\underline{\Pi}} = \underline{\underline{0}}$.

Note: This scale violates the assumptions under which the Navier-Stokes equations are derived from the Boltzmann equation. »It would be more than 50 years before computer simulation and laboratory experiments would show that physical shocks are measured to be twice the width predicted by theory, validating Becker's assertion that something beyond the Navier-Stokes description is needed.« (Margolin and Lloyd-Ronning, 2023)

5.4.5 Properties at fluid discontinuities

External gravitational forces and conductive heat flux are way slower than the transition time of fluid discontinuities and can thus be neglected.

We consider the propagating fluid discontinuity in its rest frame (i.e. upstream is ahead of the shock).

We distinguish two types of fluid discontinuities

- shocks characterized by mass flux through their interface
- contact dicontinuities without such mass flux

5.4.5.1 (Rankine-Hugoniot) Jump conditions I: Assumptions

Relative to the shock, fluid moves from upstream to downstream and we would like to relate upstream conditions ρ_1, v_1, T_1 to downstread conditions ρ_2, v_2, T_2 by *jump conditions*, see figure 42.

We assume

- the velocity to be perpendicular to the surface of the discontinuity (we later generalize)
- a steady state $\partial_t = 0$
- a 1D situation $\underline{\nabla} \to \partial_x$

5.4.5.2 (Rankine-Hugoniot) Jump conditions II: Jump condition from the continuity equation

From the above assumption and the continuity equation, we following

$$\begin{gathered}\frac{d}{dx}(\rho v) = 0 \to \rho v = \text{const.} \to \rho_1 v_1 = \rho_2 v_2 = j, \quad \text{mass flux } j \\ v_1, v_2 \text{ measured in frame of the discontinuity} \\ \text{notation for up-downstream-difference: } \boxed{[\rho v] = 0}\end{gathered} \tag{202}$$

The mass flux is constant across the discontinuity.

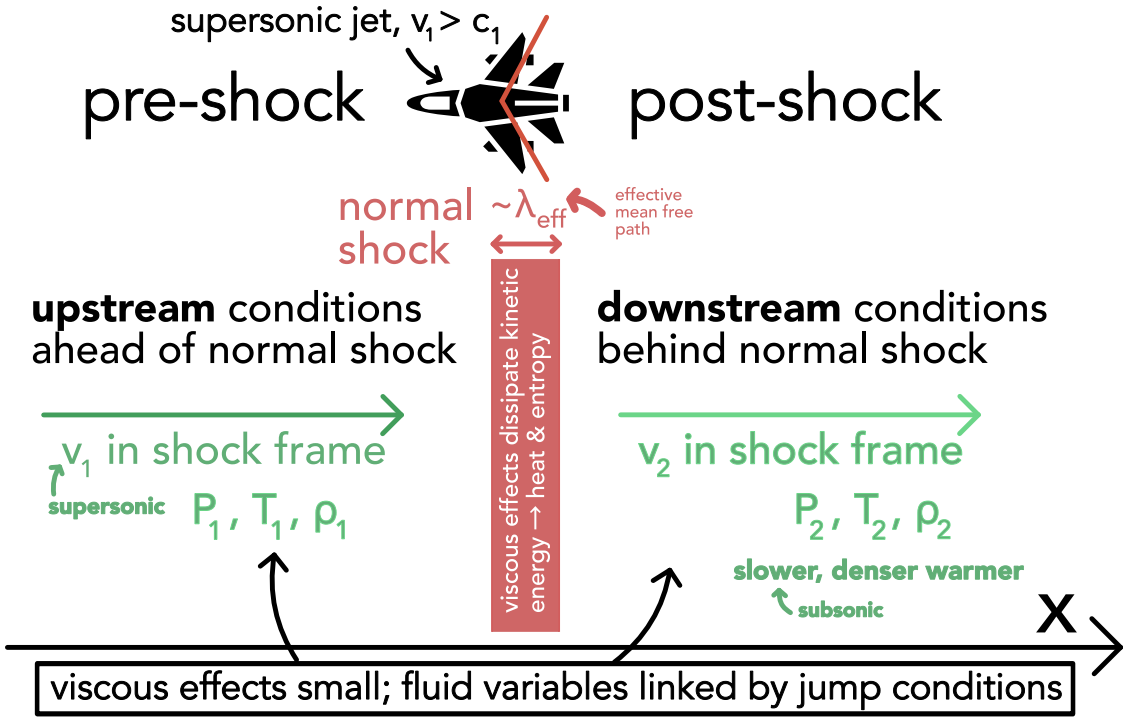

Figure 42: Normal shock

5.4.5.3 (Rankine-Hugoniot) Jump conditions III: Jump condition from the momentum equation

One obtains (for the pre and post shock zones)

$$\frac{d}{dx}(\rho v^2 + P) = 0 \quad \rightarrow \quad \boxed{[\rho v^2 + P] = 0} \tag{203}$$

Note: We consider the difference in the pre- and post-shock-zones, where viscosity effects can be neglected ($\xi, \eta = 0$) and also $\frac{dv}{dx} = 0$. Note that as the transition zone is typically of a scale λ_{mfp}, we would have to resort to kinetic theory (or plasma particle in cell-codes) there anyways.

5.4.5.4 (Rankine-Hugoniot) Jump conditions IV: Jump condition from the energy equation

We obtain

$$0 = \frac{d}{dx}\left((\rho e + P)v\right) = \frac{d}{dx}\left(\rho v\left(e_{th} + \frac{v^2}{2} + \frac{P}{\rho}\right)\right)$$
$$= \rho v \frac{d}{dx}\left(\left(e_{th} + \frac{v^2}{2} + \frac{P}{\rho}\right)\right) + \frac{d(\rho v)}{dx}\left(\left(e_{th} + \frac{v^2}{2} + \frac{P}{\rho}\right)\right) \underbrace{=}_{[\rho v]=0} \rho v \frac{d}{dx}\left(\left(e_{th} + \frac{v^2}{2} + \frac{P}{\rho}\right)\right)$$
$$\rightarrow \boxed{\left[\frac{v^2}{2} + e_{th} + \frac{P}{\rho}\right] = 0} \tag{204}$$

Marked in the boxes are the Rankine-Hugoniot Jump conditions.

We can plug in the closure $e_{th,i} = P_i / \left(\rho_i \cdot (\gamma_i - 1)\right)$ into the energy jump condition where theoretically γ_i can be different in the pre- and post-shock zones, e.g. when molecules are dissociated.

5.4.5.5 Types of dicontinuities: contact discontinuity vs. shock

The continuity of mass flux allows two scenarios

- **tangential discontinuity**: $\rho_1 v_1 = \rho_1 v_2 = 0$ so as $\rho_1, \rho_2 \neq 0$ in general, $v_1 = v_2 = 0$ so $[P] = 0$ as of $[\rho v^2 + P] = 0$. The pre- and post-shock zones move with the same velocity as the shock, there is no mass-flux through the shock. If the tangential velocities are also continuous ($[v_y] = [v_z] = 0$) (which we do not consider by our current assumptions), this is called a contact dicontinuity. The density may jump but as of $[P] = 0$, T then has to do the *opposite* jump. A contact discontinuity is a surface separating two fluids with different physical properties.
- **shock**: for $\rho_1 v_1 = \rho_1 v_2 \neq 0$ we have mass flux and thus a shock. Shock waves do propagate with respect to the fluid because of the mass flux in the normal.

5.4.6 Characterizing the Shock strength - Mach number

Note: In the shock's frameof reference, the unshocked material is moving at speed v_1 and the shocked material at speed v_2.

The (pre-shock) Mach number is the ratio between the upstream (with respect to the shock) velocity to the upstream sound speed, characterizing the strength of a shock ($\rho_1 v_1 \neq 0$) (in

case of a jet causing the upstream velocity, the jets velocity is used[6])

$$\mathcal{M}_1 \equiv \frac{v_1}{c_{s,1}} \underbrace{=}_{c_s^2=\frac{\gamma P}{\rho}} \sqrt{\frac{\rho_1 v_1^2}{\gamma P_1}} \underbrace{=}_{P=\frac{\rho}{m}k_B T} \sqrt{\frac{m v_1^2}{\gamma k_B T_1}} \tag{205}$$

we can analogously define a post-shock Mach number $\mathcal{M}_2$.

$$\mathcal{M}_2 \equiv \frac{v_2}{c_{s,2}} \tag{206}$$

Equivalently, the Mach number is

- ratio of ram pressure ρv^2 (pressure as of fluids bulk motion, not the thermal motion) to thermal pressure (for $\mathcal{M}_1$ in the pre-shock zone)
- and (as pressure is also an energy density) the kinetic thermal energy density

Note: Below $\mathcal{M} = 1$ there is no shock, the flow is subsonic. A shock occurs, when supersonic flow (e.g. Solar Wind) encounters an obstacle forcing a change in velocity (e.g. the Earth's magnetosphere $\rightarrow$ bow shock).

5.4.6.1 Occurence of the Mach number in the continuity equation

Rewriting $\partial_t \rho + \underline{\nabla}\left(\rho \underline{v}\right) = 0$ using $\frac{D}{Dt} = D_t = \partial_t + \underline{v} \cdot \underline{\nabla}$ to $-\frac{1}{\rho}\frac{D\rho}{Dt} = \underline{\nabla} \cdot \underline{v}$ and using the adiabatic $dp = c_s^2 d\rho$ we get

$$-\frac{1}{\rho c_s^2}\frac{D\rho}{dt} = \underline{\nabla} \cdot \underline{v} \quad \xrightarrow{\text{dimensionless form}} \quad -\mathcal{M}^2 \frac{1}{\hat{\rho}}\frac{D\hat{\rho}}{D\hat{t}} = \hat{\underline{\nabla}} \cdot \hat{\underline{v}} \tag{207}$$

So in the limit $\mathcal{M} \rightarrow 0$ we have incompressible flow.

5.4.6.2 Rewriting the Rankine-Hugoniot jump conditions in terms of $\mathcal{M}_1$ - relating pre- and post-shock quantities

One can rewrite the jump conditions in terms of the Mach number $\mathcal{M}_1$ (assume $\gamma_1 = \gamma_2 = \gamma$) (here without proof)

[6]If a jet is flying sufficiently fast, some of its energy goes into compressing the air in front. If the jet itself moves faster than c_s, the information speed in the air, shock waves form as of those compressions (they cannot spread suffieciently fast for there not to be a shock).

$$\begin{aligned}
\frac{\rho_2}{\rho_1} &= \frac{v_1}{v_2} = \frac{(\gamma+1)\mathcal{M}_1^2}{(\gamma-1)\mathcal{M}_1^2+2} \xrightarrow{\gamma=1} \mathcal{M}_1^2 \\
\frac{P_2}{P_1} &= \frac{\rho_2 k_\mathrm{B} T_2}{\rho_1 k_\mathrm{B} T_1} = \frac{2\gamma\mathcal{M}_1^2-(\gamma-1)}{\gamma+1} \xrightarrow{\gamma=1} \mathcal{M}_1^2 \\
\frac{T_2}{T_1} &= \frac{\left[(\gamma-1)\mathcal{M}_1^2+2\right]\left[2\gamma\mathcal{M}_1^2-(\gamma-1)\right]}{(\gamma+1)^2\mathcal{M}_1^2} \xrightarrow{\gamma=1} 1
\end{aligned} \tag{208}$$

from which we for a strong shock ($\mathcal{M}_1 \gg 1$)[7] can find (use $\gamma = 5/3$ for an ideal non-relativistic gas)

$$\begin{aligned}
\frac{\rho_2}{\rho_1} &= \frac{v_1}{v_2} \approx \frac{\gamma+1}{\gamma-1} = 4, \\
P_2 &\approx \frac{2\gamma}{\gamma+1}\mathcal{M}_1^2 P_1 = \frac{2}{\gamma+1}\rho_1 v_1^2 = \frac{3}{4}\rho_1 v_1^2, \\
k_\mathrm{B} T_2 &\approx \frac{2\gamma(\gamma-1)}{(\gamma+1)^2} k_\mathrm{B} T_1 \mathcal{M}_1^2 = \frac{2(\gamma-1)}{(\gamma+1)^2} m v_1^2 = \frac{3}{16} m v_1^2,
\end{aligned} \tag{209}$$

In the shock frame, the post-shock medium is slower, denser, has higher-pressure and is warmer, see figure 43.

5.4.6.3 Conversion of kinetic to thermal energy in the shock

Based on the above relations for $\mathcal{M}_1 \gg 1, \gamma = 5/3$ we can write

$$\begin{aligned}
\text{post-shock specific kinetic energy: } & \frac{1}{2}v_2^2 \approx \frac{1}{16}\frac{1}{2}v_1^2 \\
\text{post-shock specific thermal energy: } & \frac{3}{2}\frac{k_B T_2}{m} \approx \frac{9}{32}v_1^2 = \frac{9}{16}\frac{1}{2}v_1^2
\end{aligned} \tag{210}$$

We find that in the shock frame, roughly half of the pre-shock kinetic energy ($\frac{9}{16}$) is converted to thermal energy.

5.4.6.4 Conservation of energy in the shock

In the pre-shock flow (for a strong shock) we can neglect the thermal energy, so $e_1 = \frac{v_1^2}{2}$ (specific energy per particle).

In

$$\frac{1}{2}v_2^2 + \frac{3}{2}\frac{k_B T_2}{m} \approx \frac{10}{16}\frac{v_1^2}{2} \tag{211}$$

(in the shock rest frame) one is missing the pdV work, which is done by the shock to compress the post-shock gas and amounts to $k_B T_2 \approx \frac{6}{16}\frac{1}{2}v_1^2$.

[7] In a strong shock $v_1^2 \gg c_1^2$, so the thermal pressure of the unshocked gas is negligible to its ram pressure.

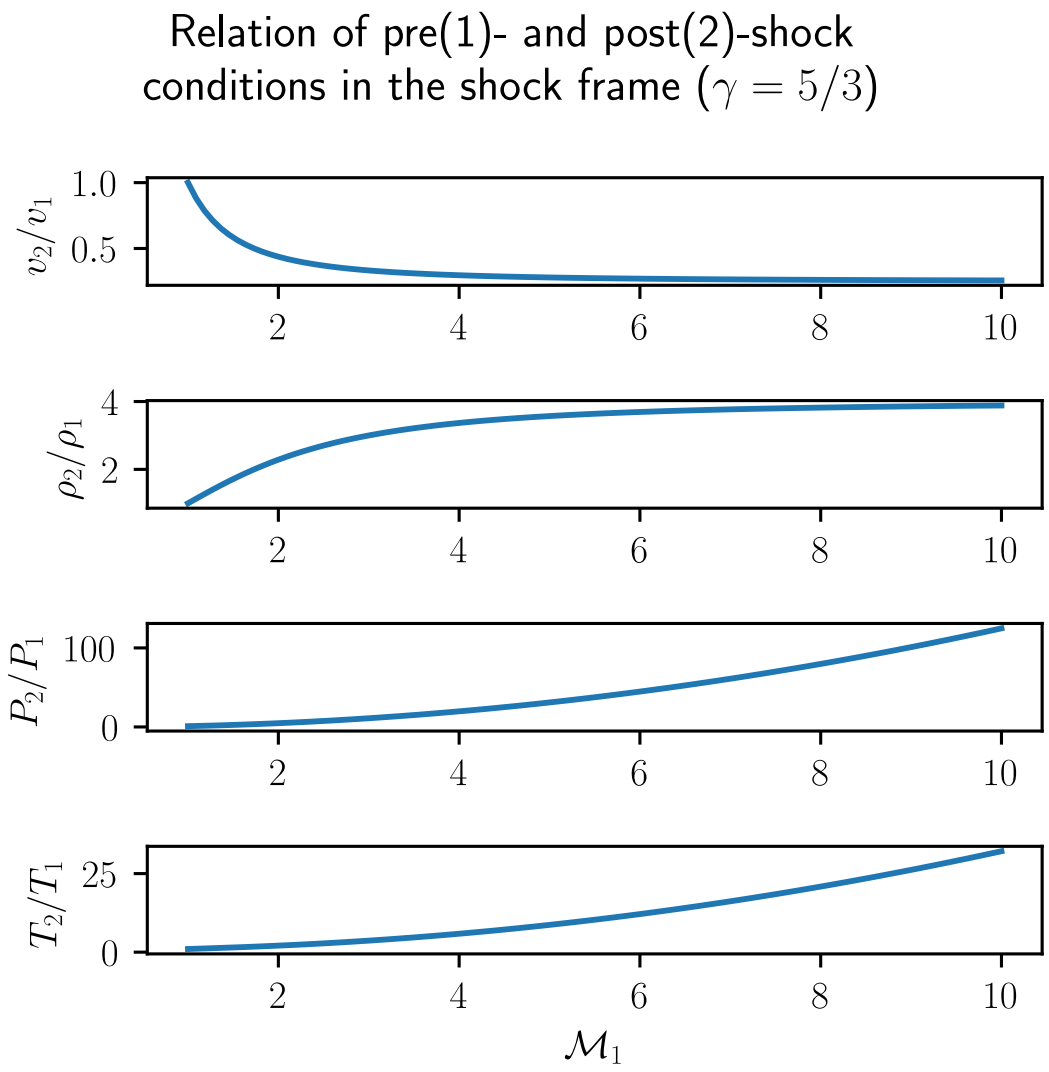

Figure 43: Relation of pre- and post-shock quantities (shock $\rightleftarrows \mathcal{M}_1 = \frac{v_1}{c_1} > 1$). v_1 is the velocity of the upstream (pre-shock) fluid with respect to the shock.

Note: The sum of enthalpy (thermal energy + pdV work) and kinetic energy is conserved in adiabatic flow (even when non-adiabatic processes like shocks occur between the two sections). Enthalpy plays the same role in a flowing system that internal energy takes in a non-flowing one, taking care of the energy associated with flow work in / out of the control volume.

Note: There are also radiative shocks, where in the transition through the shock energy is radiated away.

Note: In the rest frame of the post-shock gas there is no PdV term.

5.4.6.5 Connection between pre- and post-shock Mach number

We can write the post-shock Mach number as

$$\mathcal{M}_2 = \frac{v_2}{c_2} = \frac{v_1}{c_1}\frac{v_2}{v_1}\frac{c_1}{c_2}\underbrace{=}_{c^2 \propto T}\mathcal{M}_1\frac{v_2}{v_1}\left(\frac{T_1}{T_2}\right)^{\frac{1}{2}} \tag{212}$$

Plugging in the jump condition for T_2/T_1, in the strong shock limit we get

$$\mathcal{M}_2 = \left(\frac{\gamma-1}{2\gamma}\right)^{\frac{1}{2}}\underbrace{\approx}_{\gamma=5/3} 0.45 \tag{213}$$

Summary: Supersonic gas is slowed down (to subsonic), compressed (density, pressure and temperature increase) by a shock.

5.4.6.6 Shock adiabatic curve*

Note: In shocks, the post-shock entropy is increased with respect to the pre-shock entropy - the shock shifts the gas to a higher adiabatic curve.

The shock is a non-adiabatic process ($\delta Q \neq 0 \rightarrow dS = \frac{\delta Q}{T} \neq 0$). Based on the first law of thermodynamics $\delta Q = dE + PdV$, the ideal gas law and $dE = \nu c_V dT$ (number of mols ν), we can one can find for an ideal polytropic gas that $s = c_V \ln\left(\frac{p}{\rho^\gamma}\right)$, so here

$$s_2 - s_1 = c_V \ln\left(\frac{p_2}{p_1}\left(\frac{\rho_1}{\rho_2}\right)^\gamma\right) = c_V \ln\left(\frac{K_2}{K_1}\right) \tag{214}$$

The shock shifts the gas to a higher adiabatic curce $K = P\rho^{-\gamma}$. Note that one finds using the jump conditions, that $s_2 - s_1 > 0$ only for $\mathcal{M}_1 > 1$, so there is only a shock for $\mathcal{M}_1 > 1$.

Based on $j = \rho_1 v_1 = \rho_2 v_2$ and $[\rho v^2 + P] = 0$ the slope of the shock adiabatic curve in a PV-diagram is

$$\frac{j^2}{m} = \frac{P_2 - P_1}{V_1 - V_2} \tag{215}$$

$P = \text{const.} \times \rho^\gamma$ on either side of the shock (where we assume equilibrium), but with different constants.

Note: The jump conditions are *reversible* - if we interchange post- and pre-shock flow conditions, so $v_1 < v_2$, then density, pressure and temperature would decrease across the shock and so the entropy, excluding a shock with deceleration.

5.4.6.7 Oblique shocks

The fluid might not impact the shock perpendicular to the shock front, but at an oblique angle. **Result:** The shock deflects the flow away from the shocks normal direction (towards the shock's surface), the final velocity may remain supersonic. Only the velocity component normal to the shock front changes, V_t is continuous across the shock (see figure 44).

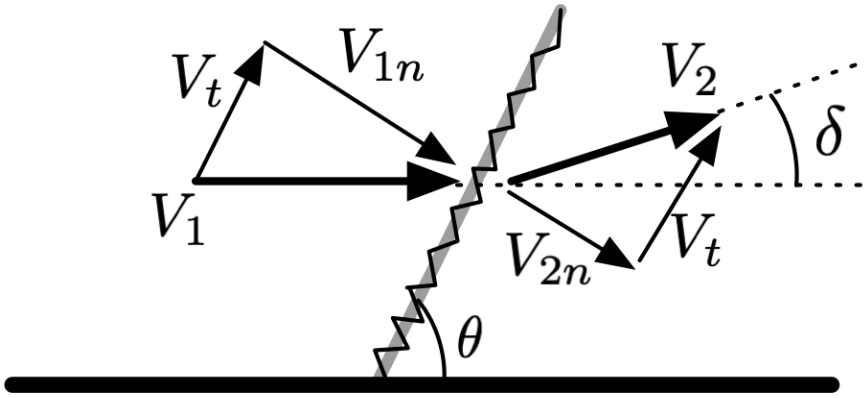

Figure 44: Oblique shock

Derivation - oblique jump conditions: Let $\underline{n}$ (here $= \hat{\underline{e}}_x$) be the shock normal, so $v_\parallel = \underline{v} \cdot \underline{n}$ is the component of the fluid velocity v parallel and $v_\perp$ the one perpendicular to $\underline{n}$. The Navier-Stokes equation describes conservation of momentum in form of a continuity equation and as such contains a momentum current. This current across the shock, $\rho \underline{v}(\underline{v} \cdot \underline{n})$, is continuous across the shock, yielding

$$\begin{aligned} [\rho v_x^2 + P] &= 0 \\ [\rho v_x v_y] &= 0 \\ [\rho v_x v_z] &= 0 \end{aligned} \tag{216}$$

As we are dealing with a shock with momentum flux $[\rho v_x] \neq 0$, we get

$$[v_y] = 0, \quad [v_z] = 0 \tag{217}$$

so as stated, the tangential velocities are continuous across the shock, $v_{1,\perp} = v_{2,\perp} = v_\perp$ and for $v_{2,\parallel}$ we have $v_{2,\parallel} = v_{1,\parallel} \frac{\rho_1}{\rho_2}$ ($\rho_2 > \rho_1$). So if the component parallel to the shock normal gets smaller and the one perpendicular remains the same, we are deflected away from the shock normal.

5.5 Fluid instabilities

Instabilities are the rapid growth of small perturbations, tapping into a source of free energy.

5.5.1 Stability of a shear flow

We consider two flows counterpropagating side by side (see figure 45). Using perturbation theory, the stability of the flow can be analyzed - if the dispersion relation for a perturbation yields a positive imaginary part (not just yeal oscillation) such modes grow exponentially - the flow is unstable.

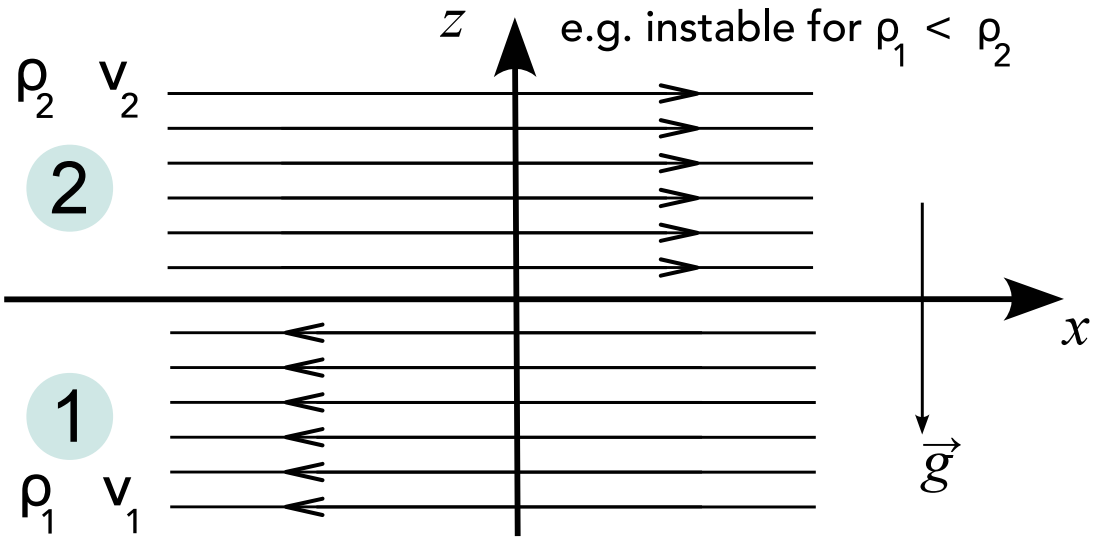

Figure 45: Shear flow

5.5.2 Rayleigh-Taylor instability

Here we consider a fluid at rest, i. e. $v_1 = v_2 = 0$. If the denser fluid lies on top, there are unstable solution - Rayleigh-Taylor instability. The instability is driven by the buoyancy of the lighter fluid or rather the release of potential energy with respect to the external force $\underline{g}$ (see figure 46). If the denser fluid is on the bottom, the interface is stable and will only oscillate if perturbed. There is also the Rayleigh-Taylor instability in plasmas.

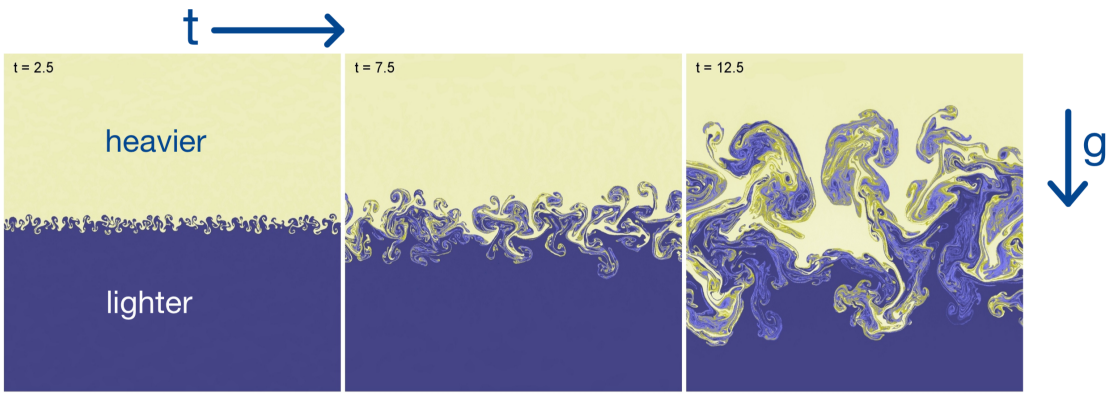

Figure 46: Rayleigh-Taylor instability

5.5.3 Kelvin-Helmholtz instability

Consider the case without the gravitational field $\underline{g} = 0$. In an ideal gas, small wave like perturbances will grow into large waves (with largest growth for large k, so small wavelengths) - Kelvin-Helmholtz-Billows, which subsequently roll up to vortex-like structures. Sharp velocity gradients are unstable - we can create turbulence. Some modes can be stabilized against the instability if we have the gravitational field, the heavy part is on the bottom (otherwise Rayleigh-Taylor instability) and the velocity difference $(v_2 - v_1)^2$ is sufficiently small.

5.5.4 Further instabilities

- **Richtmyer-Meshkov instability**: at suddenly accelerated interfaces
- **Jeans-instability**: in self-gravitating fluids, where denser regions can grow and collapse under their own attraction
- **Thermal instbaility**: ...

5.6 Turbulence

»Big whirls have little whirls that feed on their velocity, and little whirls have lesser whirls and so on to viscosity.« - Lewis Fry Richardson

Both laminar and turbulent flow are solutions to the deterministic Navier-Stokes equations, however turbulent flow is chaotic, laminar not (see table 9 and figure 47).

Laminar flow	**Turbulent flow**
Fluid flows in parallel layers with no disruption between those layers	Unsteady, chaotic flow with varying velocity and pressure in position and time
similar conditions → similar solutions	infinitesimal difference in conditions → vastly different solutions (deterministic chaos[8])

Table 9: Laminar vs. turbulent flow

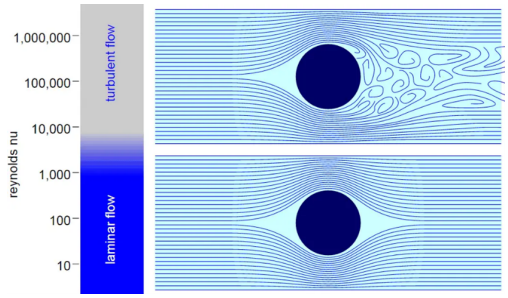

Figure 47: Laminar vs. turbulent flow

5.6.1 Subsonic (incompressible) turbulence, low Mach numbers | rotational modes

For subsonic turbulence, the information speed is far higher than the transport speed limiting the naturally occuring compressions (no shocks), so we can assume the fluid to be incompressible, $\underline{\nabla} \cdot \underline{v} = 0$.

In Fourier space the nabla operator becomes $\underline{\nabla} \to \underline{k}$, so $\underline{k} \cdot \underline{v} = 0$, so there are no longitudinal disturbances (aka soundwaves) but only solenoidal, i.e. source free motion, so shear flow and rotational turbulence (swirling eddies as for instance produces by the Kelvin-Helmholtz instability).

$\underline{v} \cdot \underline{v} = 0$ also implies subsonic flow as supersonic velocities would cause shocks coming with compression of the post-shock fluid.

Incompressible turbulence is described by Kolmogorov's theory of incompressible turbulence.

Incompressible flow is governed by the Navier-Stokes equation for an incompressible fluid, so

$$\partial_t \underline{v} + \overbrace{(\underline{v} \cdot \underline{\nabla})\underline{v}}^{\text{advective transport}} = \underline{g} \underbrace{-\frac{1}{\rho}\underline{\nabla} P}_{\text{pressure force}} + \overbrace{\nu \nabla^2 \underline{v}}^{\text{viscous dissipation}} \tag{218}$$

5.6.2 How to quantify turbulence? - Reynolds number

Let us come back to the Reynolds number characterizing the ratio of the advective to the friction term in the Navier-Stokes equation

$$\begin{gathered} Re = \frac{\text{advective term}}{\text{frictional term}} = \frac{|(\underline{v}\cdot\underline{\nabla})\underline{v}|}{\nu\underline{\nabla}^2\underline{v}} = \frac{V_0 L_0}{\nu} \\ \text{with } V_0 = \text{characteristic velocity}, \quad L_0 = \text{characteristic length scale}, \\ \nu = \text{kinematic viscosity} = \frac{\eta}{\rho} \sim \lambda_{mfp} v_{th} \\ \text{with } \lambda_{mfp} = \text{mean free path}, \quad v_{th} = \text{thermal velocity} \end{gathered} \tag{219}$$

Although counterintuitive, the viscosity increases with larger mean free path, intuitively as shear stress information is transported over larger distances.

In this view a high Reynolds number means that turbulence is generated faster by the chaotic advective term than is descroyed via dissipation.

For approximately $Re > 3.5 \cdot 10^3$ turbulence is expected, the interstellar medium has $Re \sim 10^8$. Oceans (viscosity of water $\sim 10^{-6}\,\mathrm{m^2\,s^{-1}}$) and atmosphere are always turbulent, except for boundary layers (with small characteristic length scale).

5.6.2.1 Reynolds number as the ratio between advection and dissipation timescale

Most simply by dimensional analysis, one can yield (ν in units of $\frac{m^2}{s}$, a diffusion coefficient)

$$t_{adv} = \frac{L_0}{V_0}, \quad t_{dis} = \frac{L_0^2}{\nu} \quad \rightarrow \quad Re = \frac{t_{dis}}{t_{adv}} = \frac{L_0 V_0}{\nu} \sim \frac{L_0 V_0}{\lambda_{mfp} v_{th}} \tag{220}$$

where a high Reynolds number means that advection is faster than dissipation, thus dissipation cannot stabilize the growth of turbulence sufficiently and we have turbulent flow. In the equation we can also see that the Reynolds number is the product of the macroscopic-to-microscopic length and velocity scales.

5.6.3 Supersonic turbulence, shocks $\mathcal{M} \gg 1$ | rotational and compressive modes

Depending on the dimensionality, we have

- 1D: 1 compressive mode
- 2D: 1 compressive mode, 1 solenoidal mode
- 3D: 1 compressive mode, 2 solenoidal modes

5.6.4 Schematic concept of turbulence

In 3D

- **injection range** energy is injected on macroscopic scales, typical scale L, velocity v
- **inertial range** large eddies break up into smaller eddies and energy is transferred to smaller scales, vorticity ($\underline{\zeta} = \underline{\nabla} \times \underline{v}$) is conserved and no energy is dissipated
- **dissipation range** at the microscopic viscous scale (λ_{visc}, roughly the mean free path λ_{mfp}) energy is dissipated into viscous heat

In 2D the energy flow is reverted from small to large (inverse cascade).

5.6.5 Kolmogorov scales of turbulence

In the following consider

$$\begin{gathered} \text{largest eddy scale: } L_S, \quad \text{dissipation scale: } L_k \\ \text{rate of energy dissipation on small scales, energy flow in the inertial range: } \epsilon \\ \text{some eddy size: } \lambda, \quad \text{velocity on that scale: } v_\lambda \\ \text{fluid viscosity: } \nu \text{ in } \frac{m^2}{s} \end{gathered} \tag{221}$$

5.6.5.1 Dissipation scale - smallest scale to be resolved in a simulation

Assume high Reynolds number and start at the small scale. At the small scale, turbulent motions are statistically isotropic (different from the large scales L_S) and Kolmogorov postulates the statistics to be universally determined by ν and ϵ (in $\mathrm{m}^2\,/\,\mathrm{s}^3$). From dimensional analysis (physical units), one can then get

$$L_K \sim \left(\frac{\nu^3}{\epsilon}\right)^{\frac{1}{4}} \tag{222}$$

Note: This is the smallest scale to be resolved in a classical simulation, for an airplane with chord length 2 m this is $\mathcal{O}(10^{-6})$ m - quite a problem for simulations.

5.6.6 Scaling of the eddy velocity and vorticity in the inertial range

Energy flow ϵ must be constant in the inertial range (otherwise accumulation). We approximate the energy flow by the kinetic energy of an eddy divided by its characeteristic time

scale

$$\epsilon \approx \left(\frac{v_\lambda^2}{2}\right)\left(\frac{v_\lambda}{\lambda}\right) \approx \frac{v_\lambda^3}{\lambda} \underbrace{\approx}_{\epsilon=\text{const.}} \frac{v_{L_S}^3}{L_S} \tag{223}$$

therefore, we get

$$v_\lambda \approx v_{L_S}\left(\frac{\lambda}{L_S}\right)^{\frac{1}{3}} \tag{224}$$

Note: The largest eddies have highest velocities.

But as the size scales down quicker than the velocity, smallest eddies have the highest vorticity

$$|\underline{\zeta}_\lambda| \approx \frac{v_\lambda}{\lambda} \approx \frac{v_{L_S}}{(\lambda^2 L_S)^{\frac{1}{3}}} \tag{225}$$

Note: As the vorticity increases with decreasing scale but overall vorticity is approximately constant ($\sim$ conservation of angular momentum) on smaller scales less volume is filled with turbulent eddied.

5.6.7 Power spectrum of Kolmogorov turbulence

The dissipation is reflected by the energy spectrum of Kolmogorov turbulence, see figure 48.

The constant energy transfer through the cascade is described by

$$\begin{aligned} &\text{incompressible fluid, subsonic: } E(k) \propto k^{-\frac{5}{3}} \\ &\text{compressible, shock-dominated: } E(k) \propto k^{-2} \end{aligned} \tag{226}$$

Note: Including the the dissipation range, based on Kolmogorovs assumption that the statistics for small scale motion are universal, one might make the ansatz $E(k) = C\epsilon^{\frac{2}{3}}k^{-\frac{5}{3}}f_\eta(k\eta)$ with $f_\eta(x) = 1$ for $x \ll 1$ and $f_\eta(x) \to 0$ for $x \to \infty$.

5.6.7.1 Derivation of the energy spectrum of Kolmogorov turbulence

See Springel et al., 2023.

Maybe add derivation of Kolmogorov spectrum.

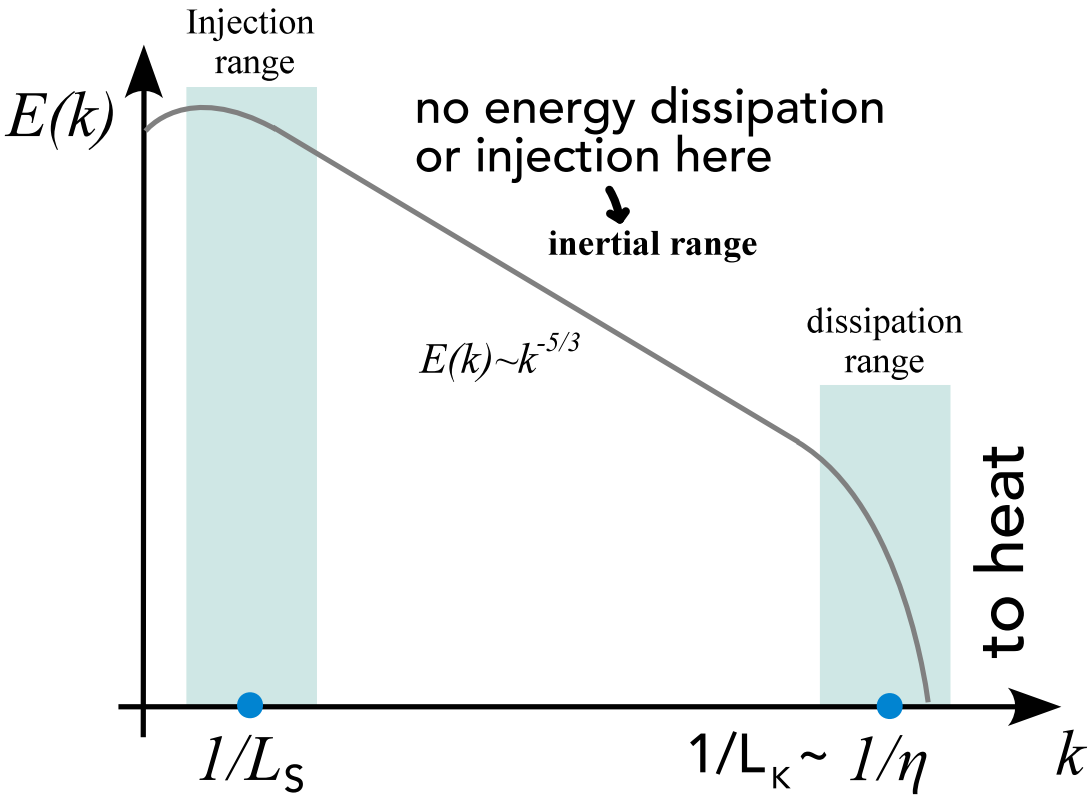

Figure 48: Kolmogorov energy spectrum

6 Eulerian Hydrodynamics | Solving PDEs

As our overarching aim is simulating physical systems (e.g. how do perturbations evolve in a fluid) and most physical systems are described by partial differential equations (PDEs) (like the Euler equations), we turn our heads towards numerically solving PDEs. We search for functions complying to $\mathcal{P}[u] = 0$ (and boundary conditions) with $\mathcal{P}$ being a differential operator.

Note: This section focuses on solvers following fluid variables on a fixed grid - eulerian hydrodynamics.

6.1 Introductory notes on PDEs

Partial differential equations (like Euler and Navier Stokes equation, Maxwell's equation, ...) describe relations between partial derivatives of a dependent variable (e.g. fluid density) with respect to several independent variables (e.g. time and position), like

$$\partial_t u = \partial_x^2 u, \quad \text{dependent variable } u(x,t), \quad \text{independent variables } x, t \tag{227}$$

(a kind of 1D diffusion equation).

Note: There is no general approach for solving PDEs.

6.2 Types of PDEs

PDEs are classified by

- Order of the PDE: Order of the highest occuring derivative
- Linearity: If the dependent variable and all its derivatives only occur linearly (no $\sqrt{\partial_x u}$), the PDE is linear and if u_1 and u_2 are solutions to the PDE, $c_1 u_1 + c_2 u_2$ are as well (superposition)
- Homogeneity: The PDE is homogeneous, if all terms contain the dependent variable or its derivatives, so if there is no source term

6.2.1 Classification of linear 2nd order PDEs in analogy with conic sections

PDEs can be distinguished into different types which give clues about appropriate solution strategies as well as appropriate initial and boundary conditions and the smoothness of the solution.

Consider a 2nd order linear PDE with two independent variables, so generally

$$a\frac{\partial^2 u}{\partial x^2} + b\frac{\partial^2 u}{\partial x \partial y} + c\frac{\partial^2 u}{\partial y^2} + d\frac{\partial u}{\partial x} + e\frac{\partial u}{\partial y} + fu = g, \quad a, b, c \text{ not all zero} \tag{228}$$

6.2.1.1 Derivation | homogeneous solutions are conic section in k-space

The unknown function u is expanded into plane waves (Fourier transformation)

$$u(\underline{x}) = \frac{1}{(2\pi)^2} \int \hat{u}(\underline{k}) \exp(-i\underline{k} \cdot \underline{x}) d^2k, \quad \underline{k} =: \begin{pmatrix} k \\ l \end{pmatrix} \tag{229}$$

Plugging this into the PDE yields

$$-\frac{1}{(2\pi)^2} \int \left(ak^2 + bkl + cl^2 + idk + idk - f \right) \hat{u}(\underline{k}) \exp\left(-i\underline{k} \cdot \underline{x}\right) d^2k = g \tag{230}$$

For the homogeneous solution ($g = 0$) this must be zero, so

$$\underline{k}^T \underline{\underline{\Delta}} \underline{k} + i \begin{pmatrix} d \\ e \end{pmatrix}^T \underline{k} - f = 0, \quad \underline{\underline{\Delta}} = \begin{pmatrix} a & b/2 \\ b/2 & c \end{pmatrix} \tag{231}$$

which is the matrix representation of a conic section in $\underline{k}$-space (why?).

6.2.1.2 Classification into elliptic, parabolic, hyperbolic

$$\text{The PDE is } \begin{cases} \text{hyperbolic if } D > 0 \\ \text{parabolic if } D = 0, \\ \text{elliptic if } D < 0 \end{cases} \quad \Delta = \begin{vmatrix} a & b/2 \\ b/2 & c \end{vmatrix}, \quad D = -4\Delta = b^2 - 4ac \tag{232}$$

6.2.1.3 Qualitative differences on the types of PDEs

- Elliptic
  - often describe static problems (no time dependence) like the Poisson equation ($\underline{\nabla}^2\phi = -\frac{\rho}{\epsilon}$)
  - as smooth as coefficients allow in the interior region where the equation and solutions are defined (independent of the smoothness of the boundary conditions)
- Parabolic
  - often of second order, describing slowly changing processes like diffusion, becoming smoother with time
  - the problem is described using an initial state $u(x, t_0)$ as well as boundary conditions
  - all parabolic PDEs can be transformed into a form analogous to the heat equation by change of independent variables
- Hyperbolic
  - typically describe dynamical processes in physics
  - initial conditions are specified by $u(x, t_0)$, $\frac{\partial u}{\partial x}(x, t_0)$ and higher derivatives as necessary as well as boundary conditions
  - disturbances have finite propagation speed
  - solutions can develop steep regions and real discontinuities

Boundary types: Fixed function values on the boundaries = Dirichlet boundary; fixed value of the derivative = van Neumann boundary.

Equation	Classification
Laplace equation $$\underline{\nabla}^2 u = \partial_x^2 u + \partial_y^2 u = 0 \quad (a=1, b=0, c=1) \tag{233}$$	Elliptic
1D Heat conduction equation (diffusion equation) $$\partial_t u - \lambda^2 \partial_x^2 u = 0 \quad (a=0, b=0, d=1, c=-\lambda^2) \tag{234}$$	Parabolic
1D Wave equation $$\partial_t^2 u - c_s^2 \partial_x^2 u = 0 \quad (a=1, b=0, c=-c_s^2) \tag{235}$$	Hyperbolic

Table 10: Typical examples and classification of homogeneous 2nd order PDEs

6.2.2 Typical examples and classification of homogeneous 2nd order PDEs

Note: The classification scheme introduced is for 2nd order PDEs with two variables, it is not made e.g. for the advection equation $\partial_t u + v\partial_x u = 0$ which is first order and hyperbolic.

6.2.3 Classification of linear 2nd order PDEs with more unknowns

For the general from

$$\sum_{i,j=1}^{n} A_{ij} \frac{\partial^2 u}{\partial x_i \partial x_j} + \sum_{i=1}^{n} b_i \frac{\partial u}{\partial x_i} + cu + d = 0, \quad \underline{\underline{A}} \text{ with entries } A_{ij} \tag{236}$$

regarding the eigenvalues of $\underline{\underline{A}}$ (following from $\underline{\underline{A}}\underline{v} = \lambda \underline{v} \rightarrow \det(\underline{\underline{A}} - \lambda \underline{\underline{I}}) = 0$) it holds that

$$\text{The PDE is } \begin{cases} \text{hyperbolic if one negative, rest postitive or one positive, rest negative} \\ \text{parabolic if one zero, others all positive or all negative} \\ \text{elliptic if all positive or all negative} \end{cases} \tag{237}$$

Note that this classification is not exhaustive, the occurrence of multiple different signs is sometimes called ultra-hyperbolic.

Task to the reader: Check that for $n = 2$ this classification scheme is equivalent to the previous one.

6.2.4 Linear systems of 1st order homogeneous PDEs

Question: When is a 1st order homogeneous PDE hyperbolic?

A first order homogeneous PDE is of the form

$$\partial_t u_i + \sum_{j=1}^{n} A_{ij} \partial_{x_j} u_i = 0, \quad i = 1, \dots, n \tag{238}$$

with short-hand notation

$$\partial_t \underline{u} + \left(\underline{\underline{A}} \underline{\underline{\nabla}}_{\underline{x}} \right) \underline{u} = 0, \quad \underline{\underline{A}} \text{ with entries } A_{ij}, \quad \underline{\underline{\nabla}}_{\underline{x}} = \mathrm{diag}(\partial_{x_1}, \dots, \partial_{x_n}) \tag{239}$$

where **the system is hyperbolic if $\underline{\underline{A}}$ has real eigenvalues and is diagonizable**.

6.2.4.1 Extension to conservation laws

We extend this to conservation laws

$$\partial_t \underline{u} + \underline{\nabla}_{\underline{x}} \cdot \underline{\underline{F}}(\underline{u}) = \partial_t \underline{u} + (\underline{\underline{\nabla}}_{\underline{u}} \underline{F}(\underline{u})) \underline{\underline{\nabla}}_{\underline{x}} \underline{u} = 0 \tag{240}$$

with conserved variable $\underline{u}$ and flux matrix $\underline{\underline{F}}(\underline{u})$. IF $\underline{\underline{\nabla}}_{\underline{u}} \underline{F}(\underline{u})$ is diagonizable with real eigenvalues, the system is hyperbolic.

Consider e.g. the Navier-Stokes equation

$$\partial_t(\rho \underline{v}) + \underline{\nabla} \cdot (\rho \underline{v} \underline{v}^T + P \underline{\underline{I}} - \underline{\underline{\Pi}}) = \rho \underline{g} \tag{241}$$

where $\underline{\nabla} \cdot$ here is a matrix divergence (a vector) with entries as expected for such a matrix vector multiplication.

Note: The classification introduced has its limits: What type the Navier-Stokes equation is seems different to tell, often *hyperbolic* is used as *advection-dominated* (the advection equation is hyperbolic) and *parabolic* as *diffusion-dominated* (the diffusion equation is parabolic) and then the Navier stokes equation can be either depending on the Reynolds number.

6.3 Solution schemes for PDEs

There is no general approach but mutltiple general methods for different types or even only a certain PDE. Common methods are

- Finite difference methods: Differential operators are approximated by finite difference operators, usually on a regular (Cartesian) mesh
- Finite volume methods: Useful for hyperbolic conservation laws. We consider quantities averaged over finite volumes around mesh cells where divergence terms in a PDE turn into fluxes through the cells surface ($\rightarrow$ conservative method, fluxes are not lost). Exact expressions for the average value of the solution over some volumes are calculated and from these averages solutions within the cells can be reconstructed. This **contrasts with finite difference methods where derivatives are approximated based on nodal values and finite element methods where local approximations are made using local data** and stitched together to a global solution.
- Spectral methods: The PDE is converted into an algebraic form (e.g. by Fourier transform), the solution is represented by a linear combination of functions (e.g. the plane waves from the inverse Fourier transform).
- Method of lines: All derivatives but one are approximated by finite differences, leading to an ODE system, where we can use ODE solvers. **Time-dependent problems:** Consider a time-dependent problem on a 1D grid, $x_i, i = 1, ..., N$. Each point yields and ODE for the time evolution of the solution at that point, dependent on e.g. the solution on neighboring points $\rightarrow N$ coupled ODEs.
- Finite element methods: The simulation domain is divided into cells (elements, arbitrary shape, unstructured mesh) and the solution on each cell approximated in form of a simple (polynomial) function. The solutions from the cells are linearly combined and we solve for the coefficients.

Example for the method of lines: Consider the 1D heat equation

$$\partial_t u - \lambda^2 \partial_x^2 u = 0 \tag{242}$$

How to discretize the 2nd order derivative $\partial_x^2 u$?: Second order Taylor expansion yields

$$\begin{aligned} u(x + \Delta x) &= u(x) + \Delta x \partial_x u(x) + \frac{1}{2}\Delta x^2 \partial_x^2 u(x) + \mathcal{O}(\Delta x^3) \\ u(x - \Delta x) &= u(x) - \Delta x \partial_x u(x) + \frac{1}{2}\Delta x^2 \partial_x^2 u(x) + \mathcal{O}(\Delta x^3) \end{aligned} \tag{243}$$

where adding both yields

$$\partial_x^2 u(x) \approx \frac{u(x + \Delta x) - 2u(x) + u(x - \Delta x)}{\Delta x^2} \tag{244}$$

We therefore get

$$\partial_t u_i - \lambda^2 \frac{u_{i+1} - 2u_i + u_{i-1}}{h^2} = 0, \quad i = 1, \ldots, N \tag{245}$$

which we could for instance approach using the Euler method. The grid is illustrated in fig. 49.

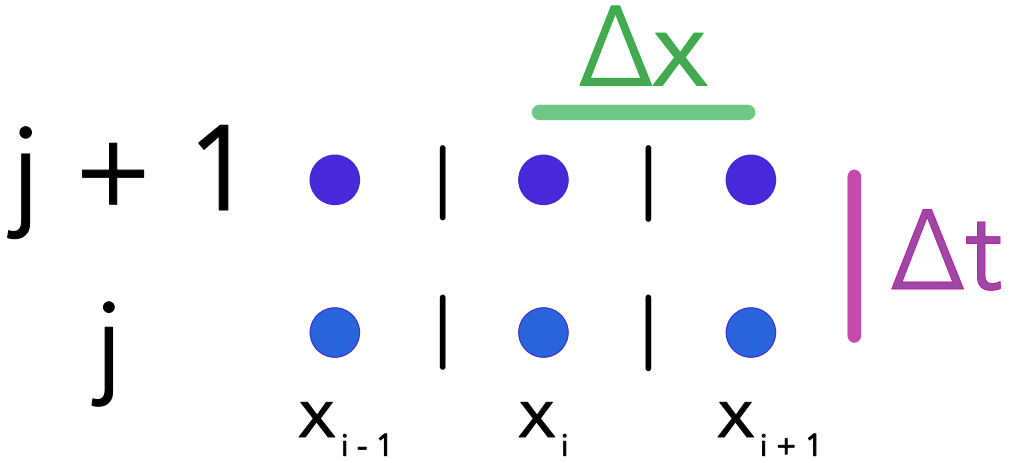

Figure 49: 1D grid

Problem: This scheme might not be stable.

6.4 Advection - Keep information flow in the physical system in mind

Consider the first-order hyperbolic advection equation

$$\partial_t u + v\partial_x u = 0, \text{we seek } u(x,t), \quad v \text{ constant parameter} \tag{246}$$

which is hyperbolic as of the real and *diagonizable* coefficient matrix (a scalar).

6.4.0.1 Analytic solution to the advection equation

For any function $q(x)$, the function $u(x,t) = q(x - vt)$ is a solution to the advection equation ($\partial_t u = -v\partial_x q$) (see fig. 50).

Interpreting $u(x, t = 0) = q(x)$ as an initial condition, the solution at a later time is just a shifted (by vt along x) copy of $q(x)$.

While for the advection problem we know the analytic solution, it helps us uncover the basic cavets of numerically solving PDEs.

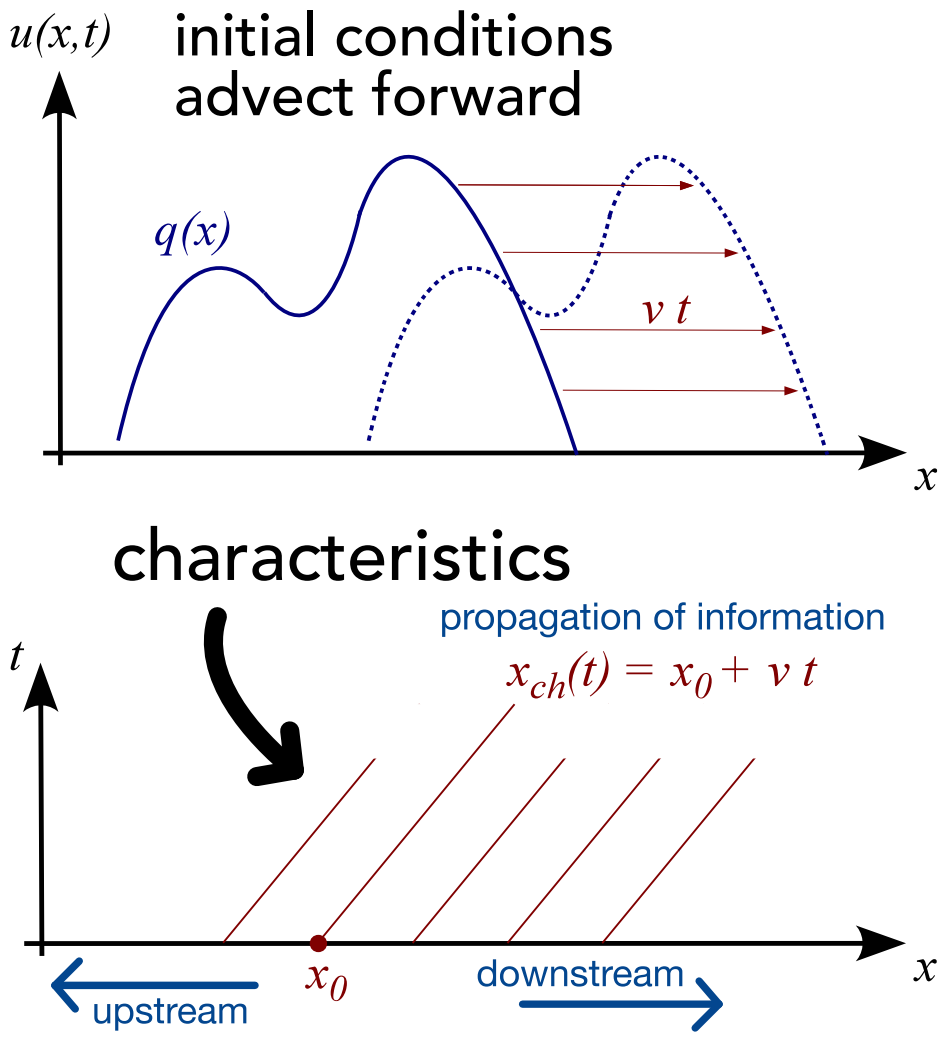

Figure 50: Advection

6.4.0.2 Simple but wrong approach | we need to consider the flow of information

Let us replace the derivative in space by a central difference with respect to the neighboring grid points

$$\frac{\partial u_i}{\partial t} + v\frac{u_{i+1} - u_{i-1}}{2h} = 0 \tag{247}$$

and step in time using explicit Euler

$$u_i^{(n+1)} = u_i^{(n)} - v\frac{u_{i+1}^{(n)} - u_{i-1}^{(n)}}{2h}\Delta t \tag{248}$$

Problem: This is violently unstable (illustrated in 51), as (based on the characteristics) information should only travel downstream but in the central differencing, we use upstream information $u_{i+1}^{(n)}$

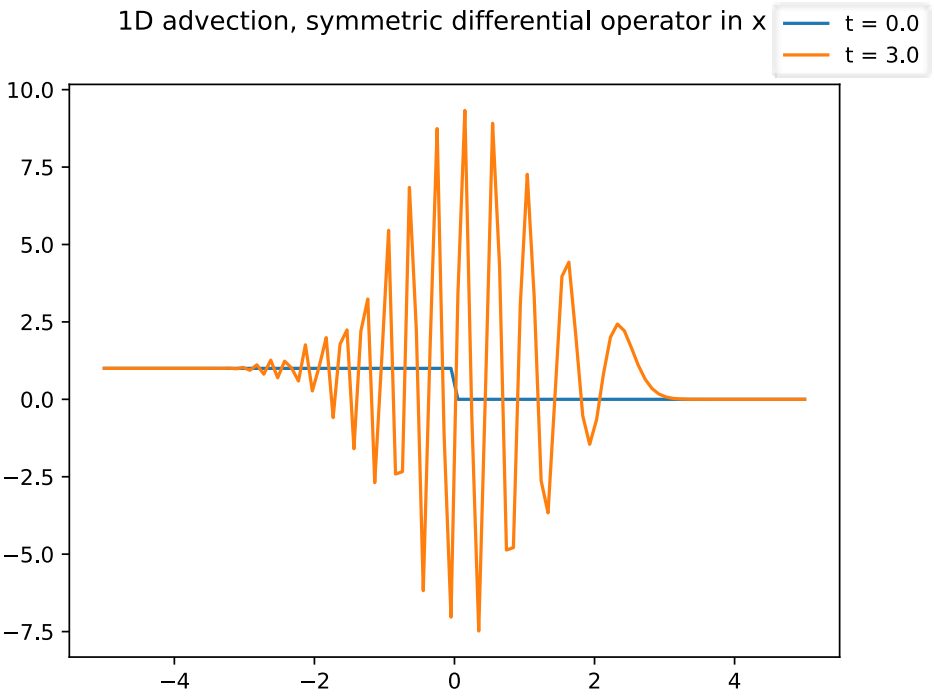

Figure 51: Advection with central differencing, violently unstable

6.4.0.3 Directional splitting / upwind scheme to the rescue

Let us only use downstream information, so (mind the sign of v)

$$\begin{aligned} v > 0 : u_i^{(n+1)} &= u_i^{(n)} - v\frac{u_i^{(n)} - u_{i-1}^{(n)}}{h}\Delta t \\ v < 0 : u_i^{(n+1)} &= u_i^{(n)} - v\frac{u_{i+1}^{(n)} - u_i^{(n)}}{h}\Delta t \end{aligned} \tag{249}$$

An example application is given in fig. 52.

Problem: The solution is smeared out (smoothed).

6.4.0.4 Where does the smoothing in the upwind scheme come from?

Our numerical algorithm (that lead to stability) introduced numerical diffusion as a byproduct.

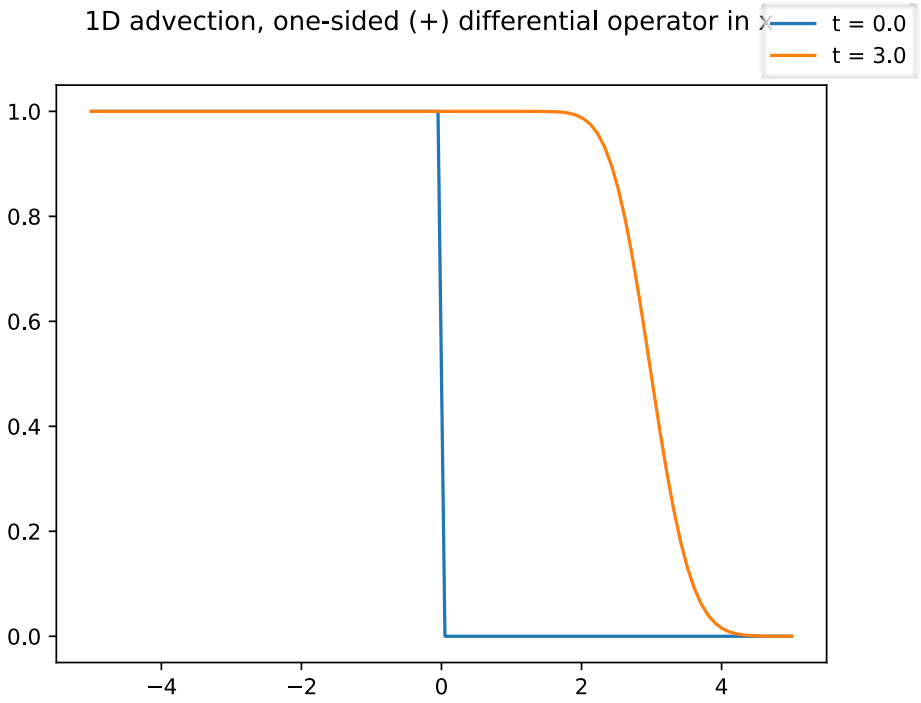

Figure 52: Advection with upwind scheme

Using

$$\frac{u_i - u_{i-1}}{h} = \frac{u_{i+1} - u_{i-1}}{2h} - \frac{u_{i+1} - 2u_{i+1} + u_{i-1}}{2h} \tag{250}$$

we can rewrite the upwind scheme for $v > 0$ as

$$\begin{aligned} 0 = \partial_t u_i + v\frac{u_i - u_{i-1}}{h} = \partial_t u_i + v\frac{u_{i+1} - u_{i-1}}{2h} - \underbrace{\frac{vh}{2}}_{D}\underbrace{\frac{u_{i+1} - 2u_{i+1} + u_{i-1}}{h^2}}_{\text{discretization of } \partial_x^2 u} \\ \text{so } \partial_t u_i + v\frac{u_i - u_{i-1}}{h} = D\frac{u_{i+1} - 2u_{i+1} + u_{i-1}}{h^2} \end{aligned} \tag{251}$$

which is the the central difference version of a advection-diffusion equation

$$\partial_t u + v\partial_x u = D\partial_x^2 u \tag{252}$$

where the diffusion term smears out the solution.

The numerical diffusion term $D = \frac{vh}{2}$ is small for

- fine grids ($h \to 0$)
- small velocities ($v \to 0$), stronger advection $\to$ stronger diffusion

The diffusion term dampens all post-shock oscillations / oscillations connected to steep

gradient and can thus also be useful for stabilization.

6.4.0.5 What is the maximum timestep we can take? | Courant-Friedrichs-Lewy (CFL) criterion

Consider the advection problem. Information travels with velocity v. Consider you would take a timestep $\Delta t > \frac{h}{v}$. Then in the upwind scheme, we would not only need to consider u_{i-1} (assuming $v > 0$) but also u_{i-2}, which we do not do - leading to catastrophic instability, as illustrated in fig. 53.

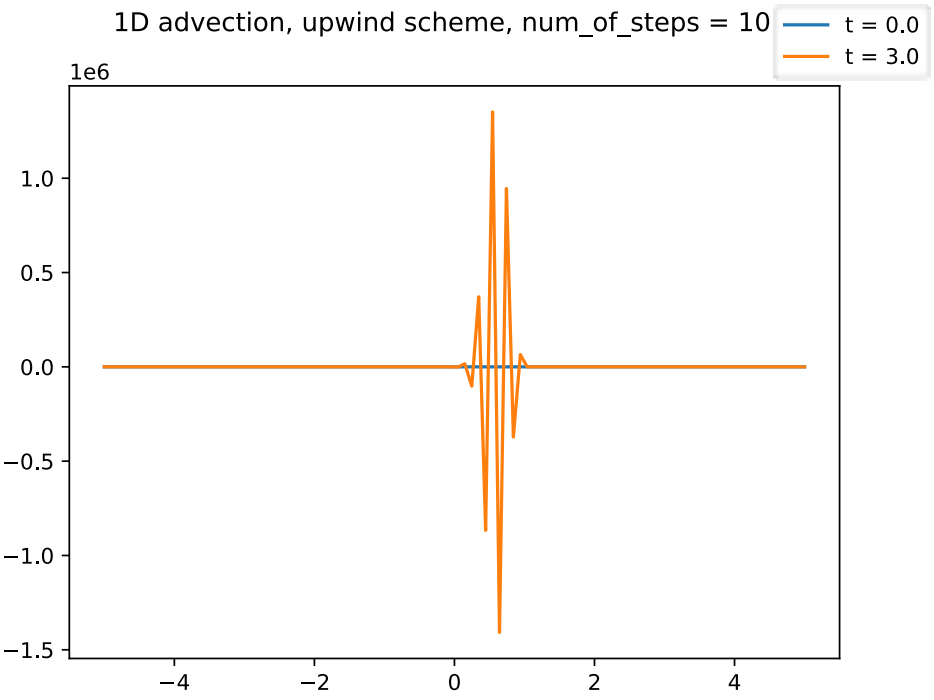

Figure 53: Advection with upwind scheme, violating the CFL criterion

The CFL criterion therefore reads

$$\Delta t \leq \frac{h}{v} \tag{253}$$

a necessary but not suffiecient condition for the stability of explicit methods regarding hyperbolic conservation laws (here for the advection case, might generally take different forms)

Note: Integrating hyperbolic conservation laws in time needs sufficiently small integration steps, as there is a finite speed of information travel in such hyperbolic problems.

6.4.0.6 Hyperbolic conservation laws | changing upwind direction

Consider the continuity equation

$$\partial_t \rho + \underline{\nabla} \cdot \underline{F} = 0, \quad \text{mass flux } \underline{F} = \rho \underline{v} \tag{254}$$

While this is essentially an advection problem, $\underline{v}$ can vary over space, $\underline{v} = \underline{v}(\underline{x})$.

In a naive discretization of space and time

$$\frac{\rho_i^{(n+1)} - \rho_i^{(n)}}{\Delta t} + \frac{F_{i+1}^{(n)} - F_{i-1}^{(n)}}{2\Delta x} = 0 \rightarrow \rho_i^{(n+1)} = \rho_i^{(n)} + \frac{\Delta t}{2\Delta x}\left(F_{i+1}^{(n)} - F_{i-1}^{(n)}\right) \tag{255}$$

the solution is highly unstable as of not accounting for the direction of flow of information (here flow of mass). We need to choose the correct discretization depending on the direction of the characteristic / sign of mass flux.

6.4.0.7 What if identifying the local characteristics is very difficult?

In general (non-linear PDE) situations, information about the local solution and local characteristics is obtained using Riemann solvers.

6.5 Intermezzo: CFL like criterion and connection to stiffness in a reaction diffusion system

Introduction to the example problem - the Brusselator

As our example, we use a simplified *Brusselator* as introduced in Hairer, Wanner, and Nørsett, 1993, chapter I.16 and further discussed in Hairer and Wanner, 1996, chapter IV.1 (originally introduced in Lefever and Nicolis, 1971).

Some details on the Brusselator and all of our implementations regarding numerical methods for solving it can be found in the accompanying Julia notebook.

Here, it is sufficient to know that we consider a non-linear chemical-reaction-diffusion partial differential equation in one dimension of the form

$$\begin{aligned}
\frac{\partial u}{\partial t} &= A + u^2 v - (B+1)u + \alpha \frac{\partial^2 u}{\partial x^2} \\
\frac{\partial v}{\partial t} &= Bu - u^2 v + \alpha \frac{\partial^2 v}{\partial x^2}
\end{aligned}$$

where $u(x,t)$ and $v(x,t)$ are the concentrations of chemical substances, α is a diffusion constant and A and B are fixed concentrations of other substances.

From discretizing the differentiation in space (i.e. using the method of lines for approaching this partial differential equations) we follow (with $x_i = \frac{i}{N+1} (1 \leq i \leq N), \Delta x = \frac{1}{N+1}$, $A = 1$, $B = 3$, $\alpha = \frac{1}{50}$)

$$\begin{aligned} u_i' &= 1 + u_i^2 v_i - 4u_i + \frac{\alpha}{(\Delta x)^2} \left(u_{i-1} - 2u_i + u_{i+1} \right), \\ v_i' &= 3u_i - u_i^2 v_i + \frac{\alpha}{(\Delta x)^2} \left(v_{i-1} - 2v_i + v_{i+1} \right) \\ u_0(t) &= u_{N+1}(t) = 1, \quad v_0(t) = v_{N+1}(t) = 3 \\ u_i(0) &= 1 + \sin\left(2\pi x_i\right), \quad v_i(0) = 3, \quad i = 1, \ldots, N. \end{aligned} \tag{256}$$

where some boundary conditions and initial conditions have been chosen. The constant boundary values are enforced using so-called ghost-cells in the implementation.

We compactly write the differential equation system as

$$\underline{y} = \underline{f}\left(\underline{y}\right), \quad \underline{y} = \begin{pmatrix} u_0 \\ \vdots \\ u_{N+1} \\ v_0 \\ \vdots \\ v_{N+1} \end{pmatrix}$$

where $\underline{f} : \mathbb{R}^{2N} \to \mathbb{R}^{2N}$ follows from equation 256.

The occurrence of stiffness

Let us start by applying the Explicit Euler method to the simplified Brusselator with $N = 40$ grid points and a step size $dt = 0.01$. The result is shown in figure 54a and is in agreement with the literature results (Hairer and Wanner, 1996, chapter IV.1).

But if we increase N to $N = 400$, i.e. we decrease the spacing between the grid points $\Delta x = \frac{1}{N+1}$, the Explicit Euler scheme yields a diverging result (see figure 54b).

We can get back to a stable solution by decreasing the step size but notice that we have to use a much smaller step size, e.g. $dt = 0.0001$ (see figure 54c), in spite of the solution still being very smooth.

In fact even a more sophisticated explicit method like the Tsitouras 5/4 Runge-Kutta method from the DifferentialEquations.jl package (Rackauckas and Nie, 2017) will use excessively many steps (e.g. to cover a time interval of length 10 (dimensionless as of our problem

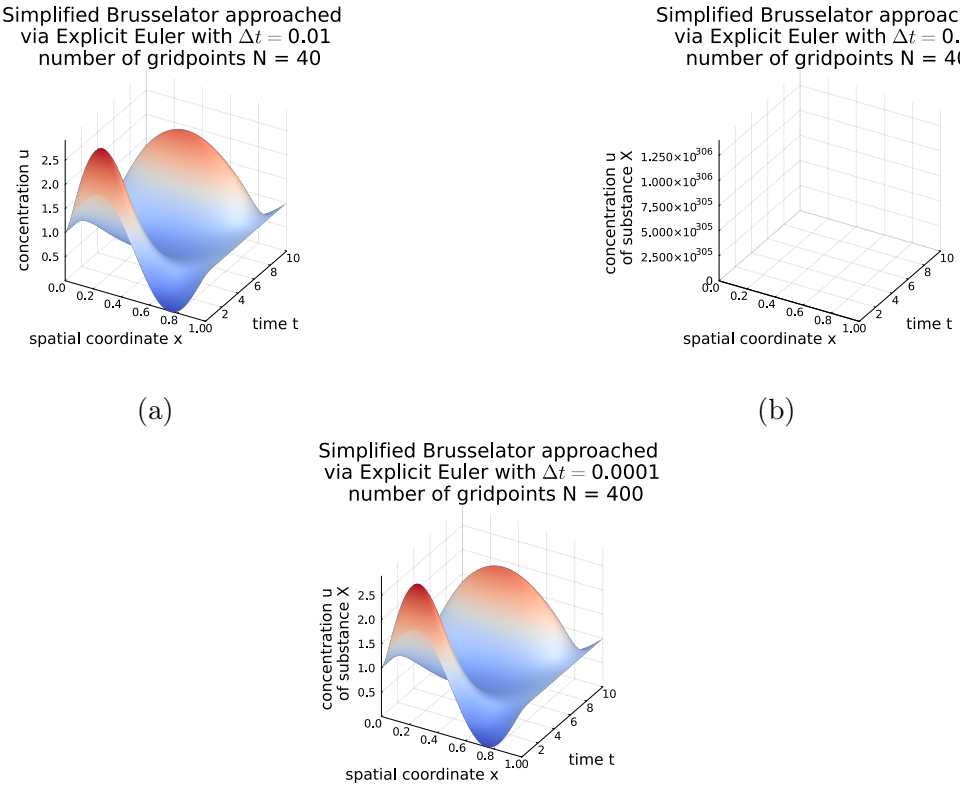

Figure 54: Numerical solutions to a simplified Brusselator using the Explicit Euler method with different numbers N of grid points and time-steps Δt.

formulation) using the default settings 220047 evaluations of $\underline{f}$ are used). The problem of stiffness as described in section 3.4.2 has occurred.

Understanding stiffness in a diffusive context

The transport process at play is diffusion. For a diffusive process we know the spreading of some concentration to follow $\sigma = \sqrt{2\alpha t}$. Now in each Euler step we do, only neighboring cells have an effect on each other (compare the discretized ODE we introduced in the beginning). Therefore - in the style of a Courant-Friedrichs-Levy criterion (Courant et al., 1928) - we can propose the stability constraint

$$\Delta x > \sigma(\Delta t) = \sqrt{2\alpha t}$$

so $\Delta t < \frac{\Delta x^2}{2\alpha}$. If we want to double N (cut in half Δx) we need $\mathcal{O}(N^2)$ more time-steps with the complexity of a function evaluation scaling with $\mathcal{O}(N)$ resulting in a $\mathcal{O}(N^3)$ scaling - calculations quickly become unfeasible.

Let us note that in the simplified Brusselator at hand it is the diffusive term causing stiffness,

but in a more complex model the chemical reactions could be an additional factor of stiffness (see e.g. Chou et al., 2007).

6.6 Riemann problem | Riemann solvers

Consider a hyperbolic system. At time $t = 0$ we start out with two piecewise constant states (in the fluid variables) meeting at a plane. The Riemann problem is to determine the subsequent evolution.

Note: One reason the Riemann problem is important is that when we discretize a fluid into cells with constant values, we effectively have Riemann problems in-between.

Consider the Riemann problem for the Euler equations (ideal gas dynamics). The two constant states can be uniquely described by

$$\underline{U}_L = \begin{pmatrix} \rho_L \\ P_L \\ \underline{v}_L \end{pmatrix}, \quad \underline{U}_R = \begin{pmatrix} \rho_R \\ P_R \\ \underline{v}_R \end{pmatrix}, \quad \text{mass density } \rho, \quad \text{pressure } P, \quad \text{velocity } \underline{v} \tag{257}$$

alternative primitive variables: density, momentum density, energy density

with a hydrodynamic discontinuity in between (illustrated in 55). This can be solved analytically (but not be written down explicitly, requires numerical root-finding for an implicit equation).

The shock tube (for $\underline{v}_L = \underline{v}_R = 0$) is a common test for Riemann solvers. There is no smooth information transport across the shock (but many collisions) and hydrodynamics breaks down.

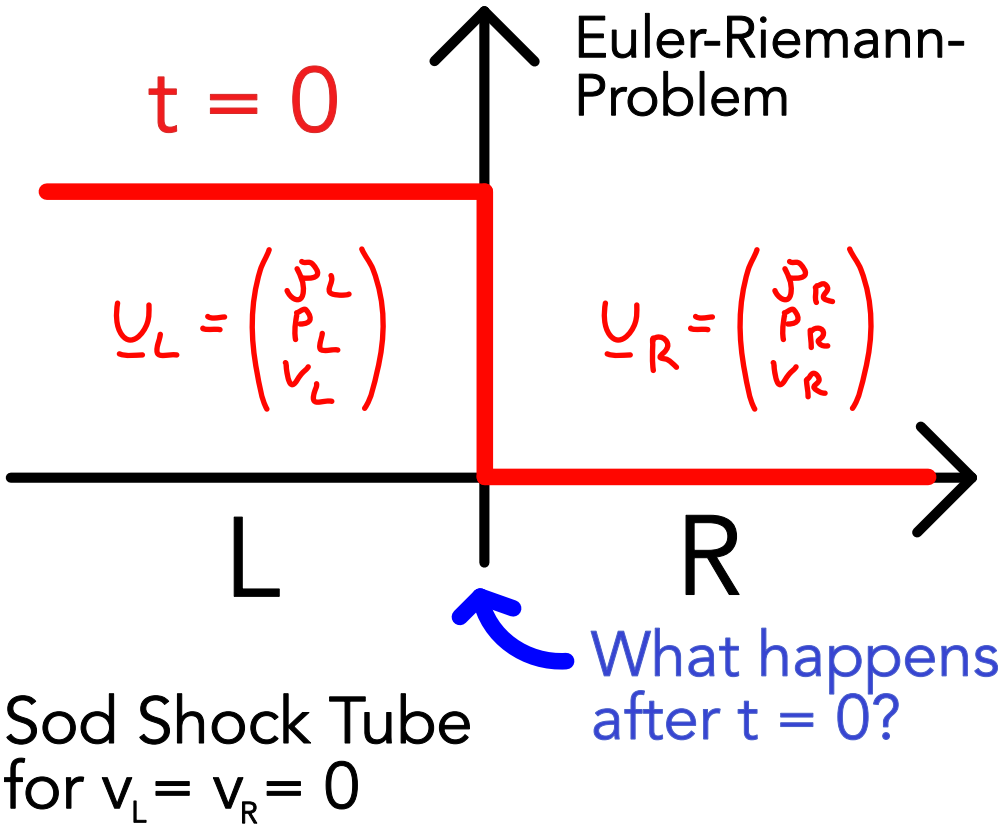

Figure 55: Riemann problem

6.6.1 Structure of the solution of the Euler-Riemann-Problem

In general, the solution to an Euler-Riemann problem always contains three waves

- **contact wave / discontinuity**: a middle wave marking the boundary between the original fluid phases
- on either side of the contact wave there can either be a **shock** or **rarefaction wave** (rather rarefaction fan with continuously changing variables). Shock or rarefaction on both sides is also possible.

where all three waves propagate with constant speed. At $x = 0$ the fluid quantities (ρ, P, v) (in the region containing the interface) are constant in time for $t > 0$.

6.6.1.1 Characteristics of the three waves

The characteristics are shown in fig. 56.

6.6.1.2 Example Riemann-Problem situation

An example with marked rarefaction fan, contact discontinuity and shock is shown in fig. 57.

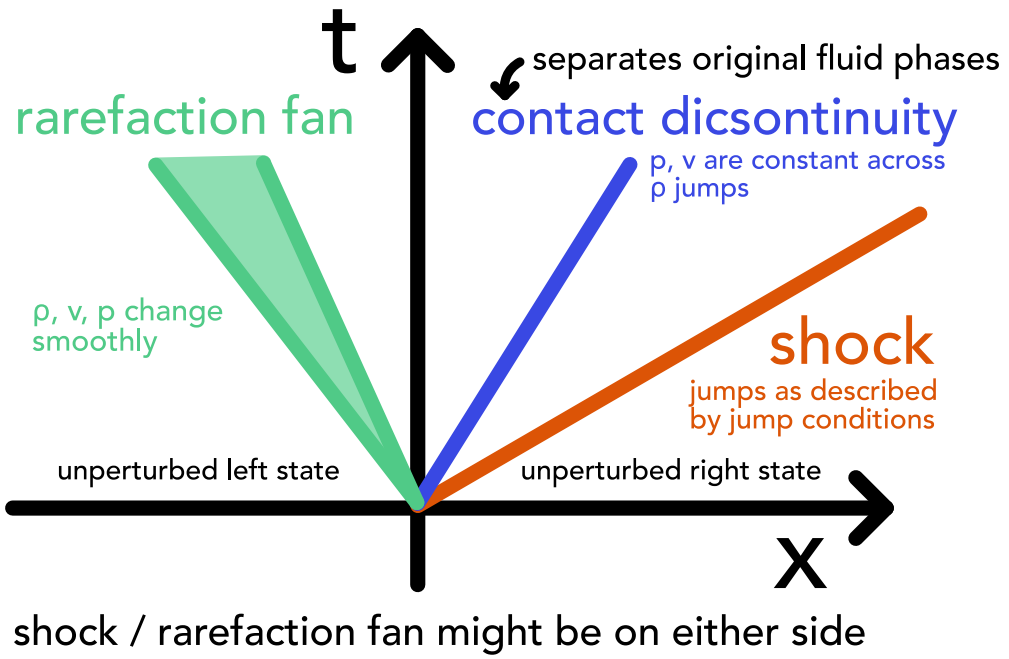

Figure 56: Characteristics of the three waves

6.6.1.3 Properties of shock, contact discontinuity and rarefaction wave

- Shock: Normal velocity, pressure, denseity, entropy change discontinuously. In the rest frame of the shock fast upstream fluid is converted to slow downstream one. The fluid is compressed and kinetic energy tuned into heat (addition of entropy).
- Contact discontinuity: Traces the original seperating plane between the two originally seperated fluid phases.
  - constant across the contact: pressure, normal velocity
  - can jump: density, entropy, temperature
- Rarefaction wave: smooth transition between two states, no discontinuities

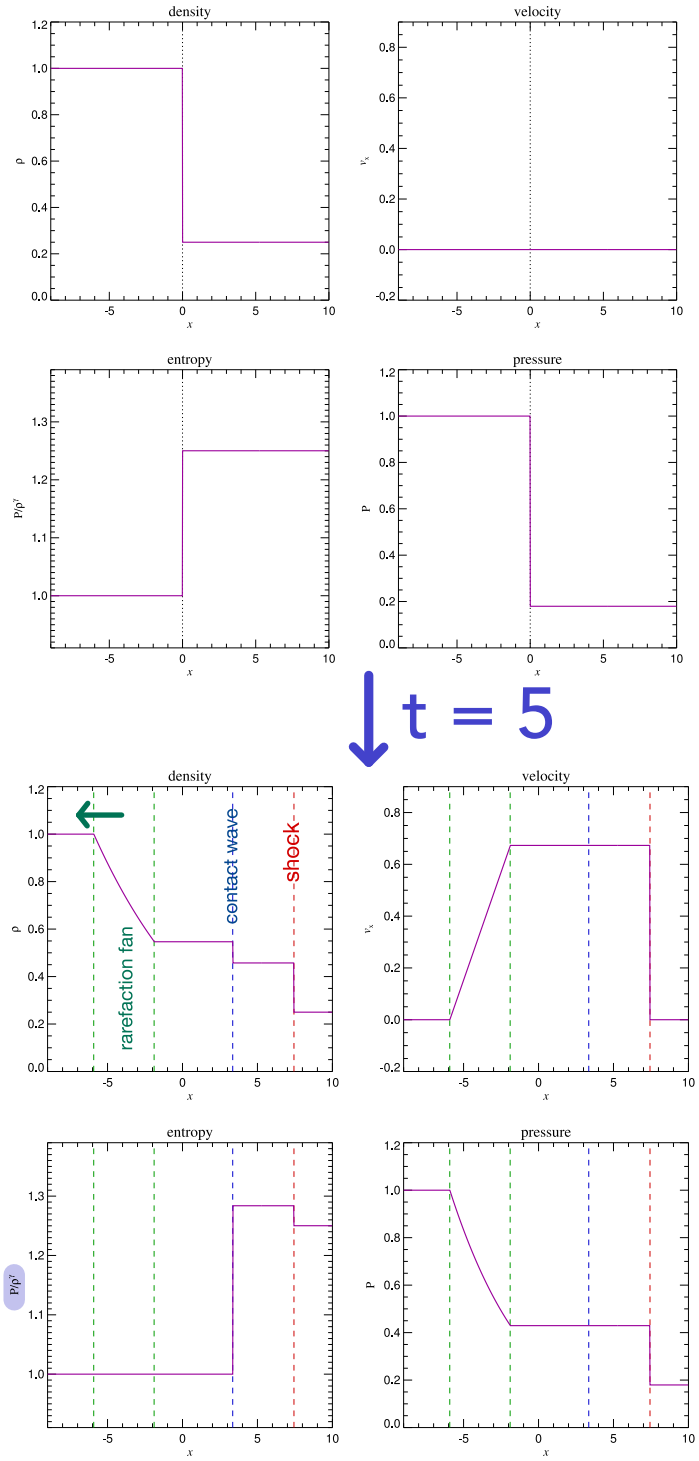

Figure 57: Example Riemann-Problem situation

6.7 Finite volume discretization | Reducing a hyperbolic conservation law to a Riemann problem | Godunov scheme

Idea: If we discretize the fluid into finite volumes and assume constant fluid variables on them, at each cell interface we have a Riemann problem. We are now more concerned with cell boundaries than centers. In the - conservative, finite volume - Godunov method, exact or approximate Riemann problems are solved at the boundaries and no flux is lost.

6.7.1 Problem | solve a hyperbolic conservation law PDE

We want to solve the conservation law

$$\partial_t \underline{U} + \partial_{\underline{x}} \cdot \underline{\underline{F}}(\underline{U}) = 0, \quad \text{state vector } \underline{U}, \quad \text{flux matrix } \underline{\underline{F}} \tag{258}$$

for instance for the Euler equations with

$$\underline{U} = \begin{pmatrix} \rho \\ \rho \underline{v} \\ \rho e \end{pmatrix}, \quad \underline{\underline{F}} = \begin{pmatrix} \rho \underline{v} \\ \rho \underline{v}\underline{v}^T + P \underline{\underline{1}} \\ (\rho e + P)\underline{v} \end{pmatrix}, \quad e = e_{th} + \frac{\underline{v}^2}{2}, \quad P = (\gamma - 1)\rho e_{th} \text{ closure} \tag{259}$$

6.7.2 Deriving a finite volume scheme where only Riemann problems are left to solve

In a finite volume method, the state of the cell is an average over the fluid quntities over the cell

$$\underline{U}_i = \frac{1}{V_i} \int_{\text{cell}i} \underline{U}(\underline{x}) dV \tag{260}$$

Aim: We want to derive an update scheme for the cell averages $\underline{U}_i$ (the vector of the fluid variables), where no intercell flux is lost.

We derive the update scheme in 1D, so $\underline{F}$ is a vector ($\underline{v}\underline{v}^T$ is a scalar) (see figure 58).

Step 1: Integrate the conservation law over a cell and timestep and recognize the average defined in 260.

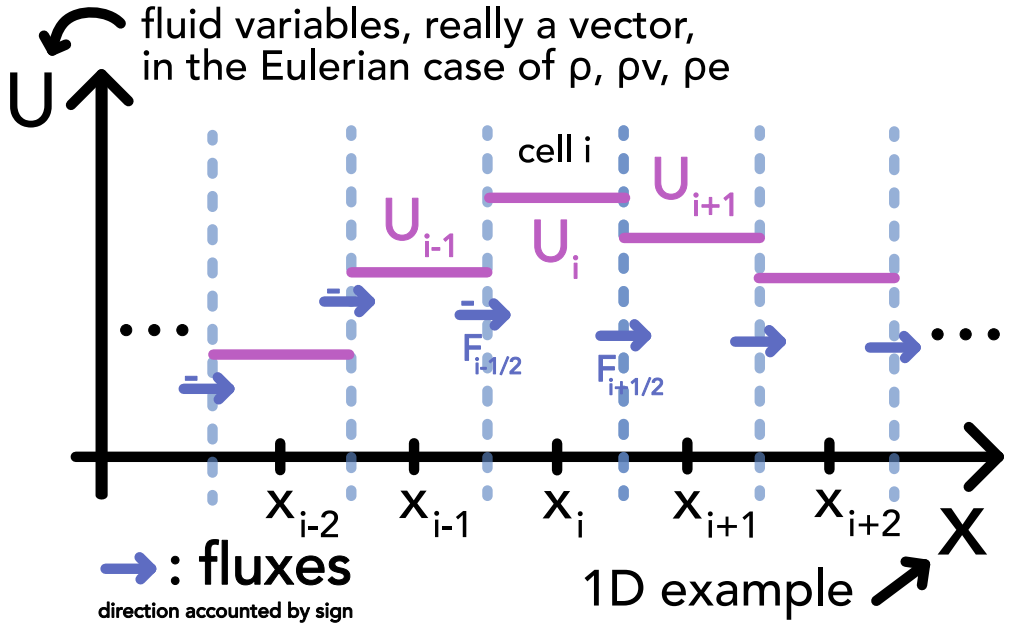

Figure 58: Finite volume scheme

$$\int_{x_{i-\frac{1}{2}}}^{x_{i+\frac{1}{2}}} \int_{t_n}^{t_{n+1}} \left(\frac{\partial \underline{U}}{\partial t} + \frac{\partial \underline{F}}{\partial x} \right) dt dx = 0$$

$$\underbrace{=}_{\text{carry out simple integrals}} \int_{x_{i-\frac{1}{2}}}^{x_{i+\frac{1}{2}}} \left[\underline{U}\left(x, t_{n+1}\right) - \underline{U}\left(x, t_n\right) \right] dx + \int_{t_n}^{t_{n+1}} \left[\underline{F}\left(x_{i+\frac{1}{2}}, t\right) - \underline{F}\left(x_{i-\frac{1}{2}}, t\right) \right] dt$$

$$\underbrace{=}_{\text{recognize avg}} \Delta x \left[\underline{U}_i^{(n+1)} - \underline{U}_i^{(n)} \right] + \int_{t_n}^{t_{n+1}} \left[\underline{F}\left(x_{i+\frac{1}{2}}, t\right) - \underline{F}\left(x_{i-\frac{1}{2}}, t\right) \right] dt = 0 \tag{261}$$

Step 2: In the frame of discrete cell averages, between any two cells we essentially have a Riemann problem from which solution we can follow the flux between the cells.

$\underline{F}(x_{i+\frac{1}{2}}, t)$ for $t > t_n$ = solution of Riemann problem with left state $\underline{U}_i^{(n)}$ and right state $\underline{U}_{i+1}^{(n)}$ (262)

Note: At the cell interface, the solution of the Riemann problem is constant in time, so

$$\underline{F}(x_{i+\frac{1}{2}}, t) = \underline{F}^*_{i+\frac{1}{2}} = \underline{F}_{\text{Riemann}}(\underline{U}_i^{(n)}, \underline{U}_{i+1}^{(n)}) \text{ from Riemann solution at interface} \tag{263}$$

Step 3: As the solution at the interface is constant, without approximation, we can

write the Godunov scheme (based on eq. 261) as

$$\underline{U}_i^{(n+1)} = \underline{U}_i^{(n)} + \frac{\Delta t}{\Delta x}\left[\underbrace{\underline{F}^*_{i-\frac{1}{2}}}_{\text{flux from left into cell}} - \underbrace{\underline{F}^*_{i+\frac{1}{2}}}_{\text{out on the right}}\right] \tag{264}$$

This defined an update scheme for the fluid variables on the cells (with some appropriate initial and boundary conditions). $\underline{F}^*_{i-\frac{1}{2}}$ and $\underline{F}^*_{i+\frac{1}{2}}$ are black-boxes for now - to find the fluxes we need to solve the Riemann problem, later e.g. done with the approximate HLL solver.

6.7.2.1 Caveats of the Godunov scheme

CFL needs to be obeyed: We can only assume the Riemann problems at the interfaces to be independent, if the timestep is short enough, so that no information has travelled from one interface to the other → CFL: $\frac{\Delta x}{\Delta t} \leq c_{max}$.

$\underline{U}$ is not piecewise constant in reality: Even if we start out with piecewise constant $\underline{U}$ in reality, this will change. Therefore the flux we calculate between the cells is also only an approximation.

6.7.3 Godunov's method and Riemann solver | reconstruct - evolve - average (REA)

Godunov's method can be seen as a REA scheme of a hydrodynamical system discretized on a mesh

1. Reconstruct: A global solution is constructed from the cell averaged quantities, simples approach: piecewise-constant
2. Evolve: The reconstructed state is evolved by Δt (mind the CFL criterion), in the Gudonov scheme based on the intercell Riemann problems
3. Average: $\underline{U}_i^{(n+1)}$ is calculatted from the evolved state, in the Godunov scheme, evolving and averaging are combined as we directly calculate the new average based on accounting the fluxes entering and leaving the cell (an implicit average over the new state)

But how can the Riemann problem giving us the fluxes be solved?

6.8 Approximate Riemann solvers | HLL solver

6.8.1 1D Riemann problem to solve

Let us again formulate the Riemann problem in 1D. Given the conservation law

$$\partial_t u(x) + \partial_x f(u) = 0 \tag{265}$$

with piecewise initial values

$$u(x, t=0) = \begin{cases} u_L \text{ for } x < 0 \\ u_R \text{ for } x \geq 0 \end{cases}, \quad \text{cell interface at } x = 0 \tag{266}$$

we want to solve for our fluid quantity u. The characteristics, i.e. where information from point $x = 0$ (discontinuity) can travel in some time, are shown in figure 59.

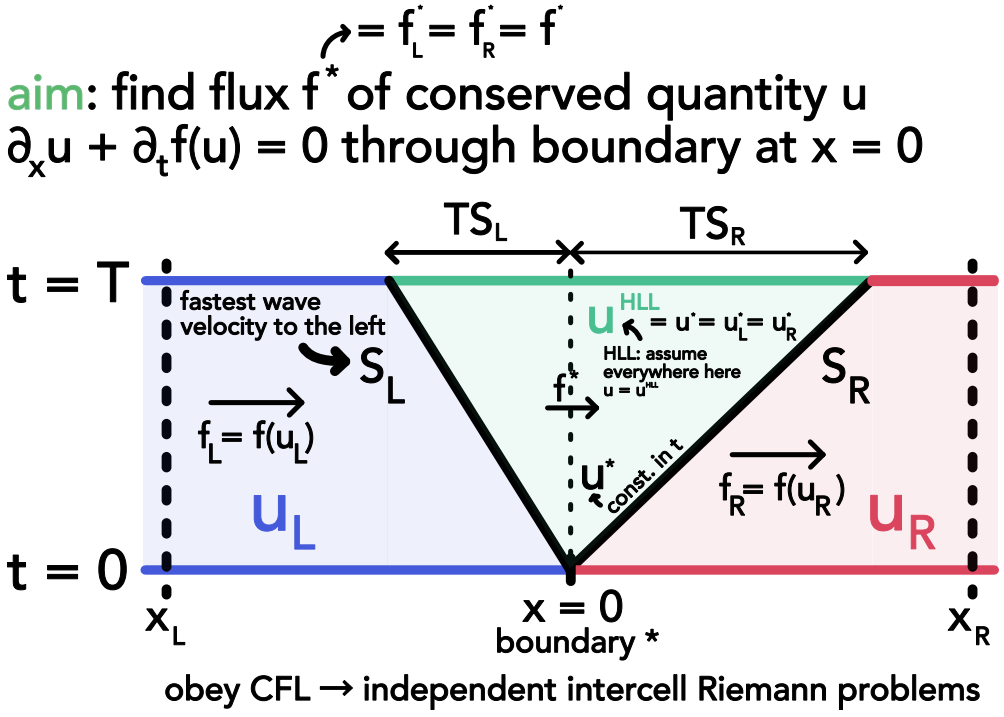

Figure 59: Characteristics of the Riemann problem and HLL approach.

6.8.2 Basic HLL assumptions and problem statement

In the HLL scheme we assume to know

- the fastest moving wave velocity to the left S_L and right S_R
- the left and right state u_L and u_R and therefore the fluxes f_L and f_R

Based on the CFL criterion (no interaction with other cells), we can assume the following quantities to be constant in time $t \in [0, T]$:

$$u_L = u(x_L, t), \quad u_R = u(x_R, t), \quad f_L = f(u_L), \quad f_R = f(u_R) \tag{267}$$

and we make the simplifying assumption that

$$\forall x \in [S_R t, S_L t] : u(x,t) = u^{HLL} = u_L^* = u_R^* = u^* \underbrace{=}_{\text{at interface}} \text{const.}, \quad f^{HLL} = f^* = f_L^* = f_R^* \tag{268}$$

Aim: Find expressions for u^* and f^*.

6.8.3 Deriving the solution of the Riemann problem in the HLL scheme

Idea: u is conserved, so the spatial integral over u at some point in time is the same as at another point in time plus / minus the in- and outcoming fluxes during that time-interval. Based and the flux balance in our whole region $[x_L, x_R]$ we can first find an expression for u^{HLL} and then based on the same balance in the left and right region $[S_R T, 0]$ and $[0, S_L T]$ we can find an expression for f^{HLL}.

6.8.3.1 Derivation of the middle state u^{HLL} at $t = T$

Remember, we assume the middle state u^{HLL} hold for the whole interval $[S_R T, S_L T]$, where information could have spread.

We can therefore write

$$u^{HLL} = \frac{1}{T \cdot (S_R - S_L)} \int_{TS_R}^{TS_L} u(x,T)dx \tag{269}$$

we can find this integral from considering the spatial integral over the whole domain at time T

$$\begin{aligned} \int_{x_L}^{x_R} u(x,T)dx &= (TS_L - x_L)\, u_L + \int_{TS_R}^{TS_L} u(x,T)dx + (x_R - TS_R)\, u_R \\ &\underbrace{=}_{u \text{ conserved}} \int_{x_L}^{x_R} u(x,0)dx + \underbrace{\int_0^T f(u_L)\, dt}_{\text{flux in from left}} - \underbrace{\int_0^T f(u_R)\, dt}_{\text{flux out to right}} \\ &= u_R x_R - u_L x_L + f_L T - f_R T \end{aligned} \tag{270}$$

We therefore find an expression for our integral and thus for u^{HLL}:

$$u^{HLL} = \frac{S_R u_R - S_L u_L + f_L - f_R}{S_R - S_L} \tag{271}$$

Which is a pretty simple balance we could have seen directly.

6.8.3.2 Deriving the intercell flux $f^{HLL} = f^*$

We consider the integral over u in the left region where the information can have propagated to, so $x \in [S_R T, 0]$ and in the right region $x \in [0, S_L T]$.

Idea: As before the integral of u over space at some time t must be the same as at an earlier time plus / minus the fluxes in / out since then.

For the left ($x \in [S_R T, 0]$) we have

$$\begin{aligned} -TS_L u^{HLL} &= \int_{TS_L}^{0} u(x,T)dx \\ &= \underbrace{-TS_L u_L}_{\text{at t=0}} + \underbrace{T \cdot (f_L - f_L^*)}_{\text{fluxes since then}} \end{aligned} \tag{272}$$

For the right ($x \in [0, S_L T]$) we have

$$\begin{aligned} TS_R u^{HLL} &= \int_{0}^{TS_R} u(x,T)dx \\ &= \underbrace{TS_R u_R}_{\text{at t=0}} + \underbrace{T \cdot (f_R^* - f_R)}_{\text{fluxes since then}} \end{aligned} \tag{273}$$

The fluxes at the interface must be equal, $f_L^* = f_R^* = f^{HLL}$, so

$$f^{HLL} = f_L + S_L \left(u^{HLL} - u_L\right) = f_R + S_R \left(u^{HLL} - u_R\right) \tag{274}$$

6.8.4 Final HLL solution

There are three states after the step T in the HLL scheme

$$u(x,T) = \begin{cases} u_L \text{ for } x < S_L t \\ u^{HLL} \text{ for } S_L t \leq x \leq S_R t \\ u_R \text{ for } x > S_R t \end{cases} \tag{275}$$

and the interface flux is

$$f^{HLL} = \frac{S_R f_R - S_L f_L + S_L S_R (u_R - u_L)}{S_R - S_L}$$
$$\text{maximum velocity to the left } S_L, \quad \text{maximum velocity to the right } S_R$$
$$\text{initial state on the left } u_L, \quad \text{initial state on the right } u_R \tag{276}$$
$$f_L = f(u_L), \quad f_R = f(u_R)$$

6.8.5 Mind that the extreme velocities can point into the same direction

Both extreme velocities can be to the left, both to the right, or on to the left and one to the right. For instance in figure 60 characteristics for advection are drawn.

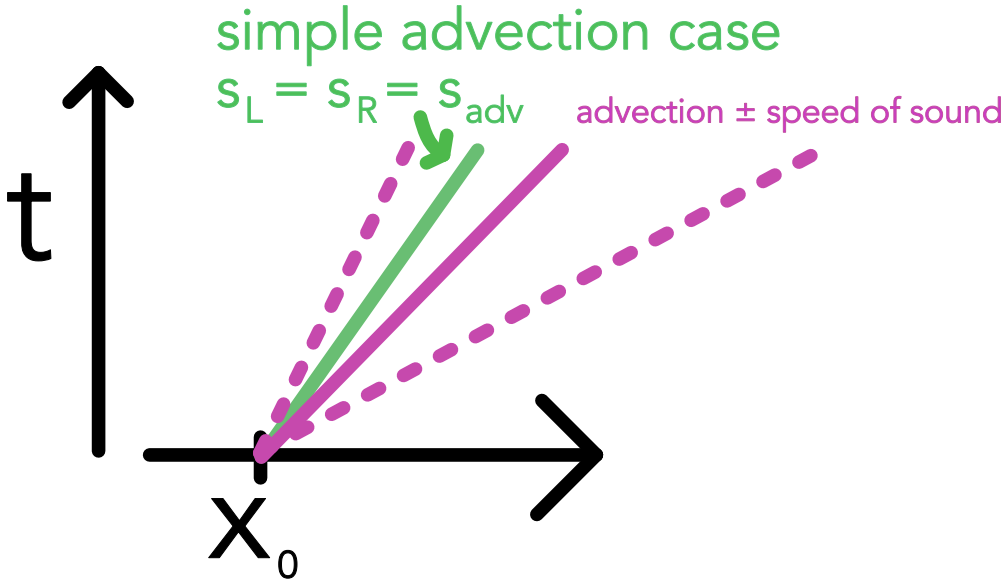

Figure 60: Advection characteristics, once the simple advection case with only the advection speed and once with information travelling from the advected state to the left and right with the speed of sound.

6.8.6 Godunov scheme with HLL solver

For the Godunov scheme

$$U_i^{(n+1)} = U_i^{(n)} + \frac{\Delta t}{\Delta x}\left[F^*_{i-\frac{1}{2}} - F^*_{i+\frac{1}{2}}\right] \tag{277}$$

the flux we choose depends on the orientation of S_L and S_R (eveloping the *Lichtkegel*). This is illustrated for unidirectional information flow to the right in figure 61.

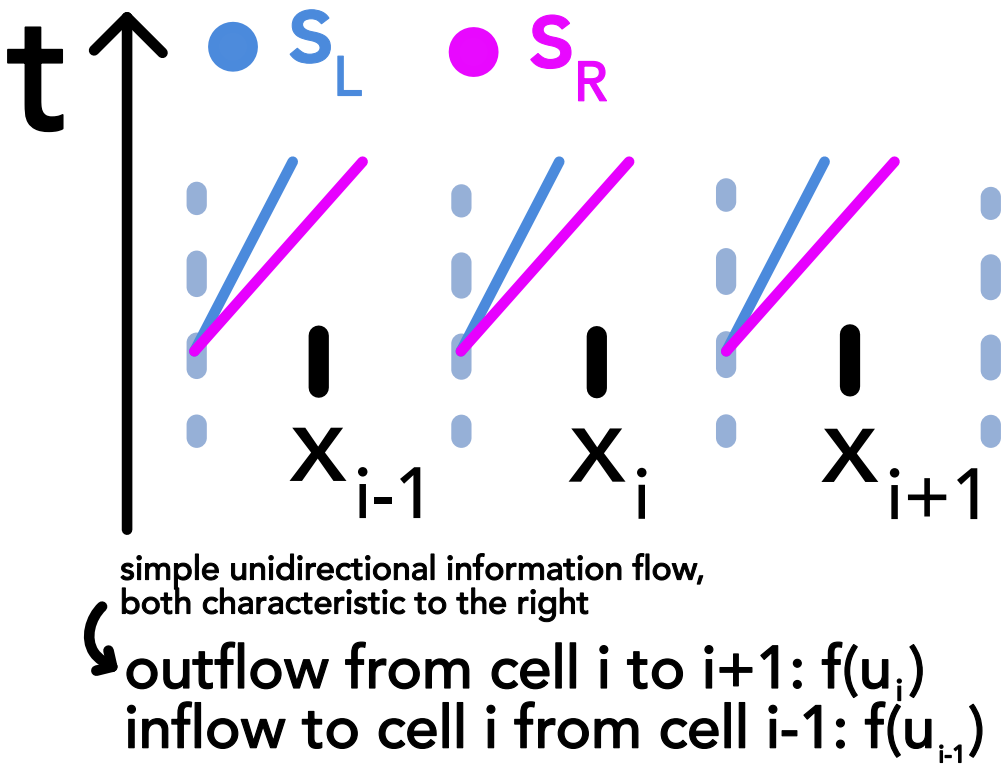

Figure 61: Godunov scheme with HLL solver for unidirectional information flow to the right.

We get

$$F^*_{i+\frac{1}{2}} = \begin{cases} F_i \text{ for } 0 < S_L \\ F^{HLL}_{i+\frac{1}{2}} \text{ for } S_L \leq 0 \leq S_R \\ F_{i+1} \text{ for } 0 > S_R \end{cases}, \quad F^*_{i-\frac{1}{2}} \text{ from } i \to i-1 \tag{278}$$

with

$$F^{HLL}_{i+\frac{1}{2}} = \frac{S_R F_{i+1} - S_L F_i + S_L S_R \left(U_{i+1} - U_i\right)}{S_R - S_L} \tag{279}$$

where we can combine this expression and the cases above to

$$F^{HLL}_{i+\frac{1}{2}} = \frac{S^+_R F_{i+1} - S^-_L F_i + S^-_L S^+_R \left(U_{i+1} - U_i\right)}{S^+_R - S^-_L}, \quad S^+_R = \max(0, S_R), \quad S^-_L = \min(0, S_L) \tag{280}$$

6.8.7 Pointers to extensions of the HLL scheme

- in HLLC an additional velocity between S_L and S_R is considered
- HLLD used for magnetohydrodynamics (MHD)

6.8.8 Ansätze for the maximum wave velocities S_L and S_R

Consider the gas velocity v as given by part of the state vector and sound speed c_s (given by the problem, here denoted a_L and a_R), then possible estimates are

- $S_L = v_L - a_L, S_R = v_R + a_R$
- $S_L = \min(v_L - a_L, v_R - a_R), S_R = \max(v_R + a_R, v_R + a_R)$
- Roe average, where we weigh dense areas as more important to the communication (leading to less smearing but instability) of information.

$$\begin{aligned}
S_L &= \tilde{u} - \tilde{a} \\
S_R &= \tilde{u} + \tilde{a} \\
\tilde{u} &= \frac{\sqrt{\rho_L} u_L + \sqrt{\rho_R} u_R}{\sqrt{\rho_L} + \sqrt{\rho_R}} \\
\tilde{a} &= \left[(\gamma - 1) \left(\widetilde{H} - \frac{1}{2} \tilde{u}^2 \right) \right]^{\frac{1}{2}} \text{ with the enthalpy} \\
H &= (e + P)/\rho \text{ and} \\
\widetilde{H} &= \frac{\sqrt{\rho_L} H_L + \sqrt{\rho_R} H_R}{\sqrt{\rho_L} + \sqrt{\rho_R}}
\end{aligned} \tag{281}$$

6.9 Extension of Eulerian hydrodynamics to multiple dimensions

Based on our previous results, we can simulate the 1D conservation law

$$\partial_t \underline{U} + \partial_x \underline{F}(\underline{U}) = 0 \tag{282}$$

e.g. for an isothermal gas (so constant sound speed c_s) with

$$\underline{U} = \begin{pmatrix} \rho \\ \rho v_x \end{pmatrix}, \quad \underline{F} = \begin{pmatrix} \rho v_x \\ \rho v_x^2 + P \end{pmatrix}, \quad P = c_s^2 \rho \tag{283}$$

Let us formulate the Euler equations for a 3D fluid (see eq. 259) by seperating the flux by direction

$$\partial_t \underline{U} + \partial_x \underline{F} + \partial_y \underline{G} + \partial_z \underline{H} = 0 \tag{284}$$

with

$$\underline{F}: \text{ flux vector along } \hat{\underline{e}}_x, \quad \underline{G}: \text{ flux vector along } \hat{\underline{e}}_y, \quad \underline{H}: \text{ flux vector along } \hat{\underline{e}}_z$$

$$\underline{F} = \begin{pmatrix} \rho u \\ \rho u^2 + P \\ \rho uv \\ \rho uw \\ u(\rho e + P) \end{pmatrix}, \quad \underline{G} = \begin{pmatrix} \rho v \\ puv \\ \rho v^2 + P \\ \rho vw \\ v(\rho e + P) \end{pmatrix}, \quad \underline{U} = \begin{pmatrix} \rho w \\ puw \\ \rho vw \\ \rho w^2 + P \\ w(\rho e + P) \end{pmatrix} \tag{285}$$

$$\text{state vector } \underline{U} = \begin{pmatrix} \rho \\ \rho u \\ \rho v \\ \rho w \\ \rho e \end{pmatrix}$$

and

$$\text{total specific energy per uni mass } e = e_{th} + \frac{1}{2}\left(u^2 + v^2 + w^2\right)$$

$$\text{pressure } P = (\gamma - 1)\rho e_{th}, \quad \text{thermal energy per unit mass } e_{th}$$

$$u: \text{ velocity in } \hat{\underline{e}}_x \text{ direction}, \quad v: \text{ velocity in } \hat{\underline{e}}_y \text{ direction}, \quad w: \text{ velocity in } \hat{\underline{e}}_z \text{ direction} \tag{286}$$

6.9.1 Dimensional splitting Ansatz

Idea: Seperately update dimensions (using our 1D solver) and combine.

From eq. 284 we make the following separation ansatz

$$\partial_t \underline{U} + \partial_x \underline{F} = \underline{0}, \quad \partial_t \underline{U} + \partial_y \underline{G} = \underline{0}, \quad \partial_t \underline{U} + \partial_z \underline{H} = \underline{0} \tag{287}$$

Note: While the state vector and fluxes are still $\in \mathbb{R}^5$ (the velocities in the other directions appear), we effectively have *augmented* 1D problems (the flux along x is not as directly coupled to w as it is to u)

To forward our state in 3D we have to sequence multiple augmented 1D steps (sweeps). For 2D this is illustrated in figure 62.

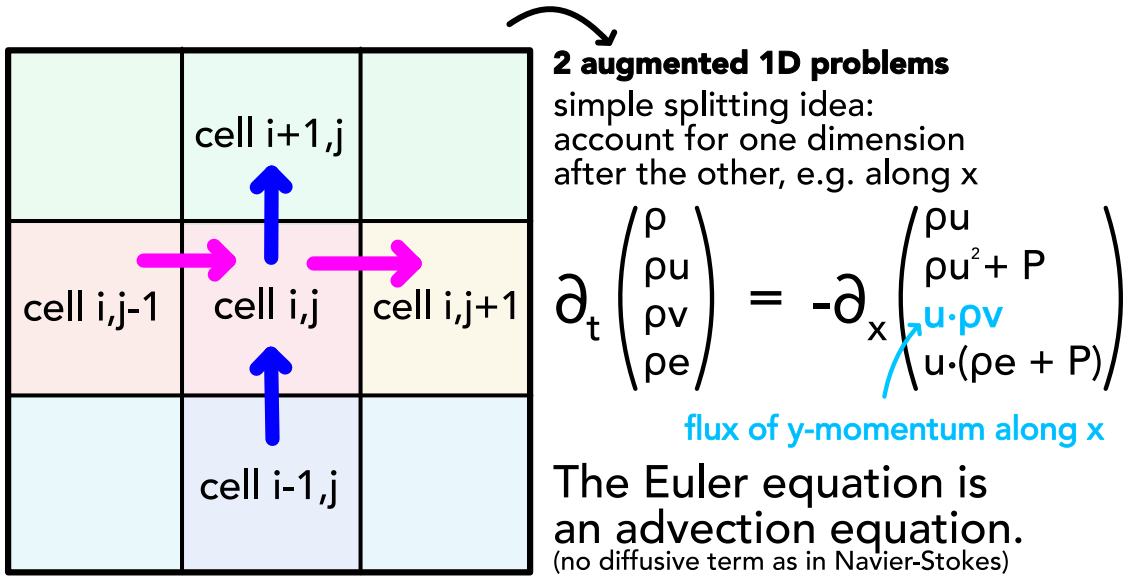

Figure 62: Splitting Ansatz for 2D

6.9.1.1 1st order ansatz

Assuming we already have a method to advance in one dimension then

$$\underline{U}^{(n+1)} = \mathcal{X}(\Delta t)\mathcal{Y}(\Delta t)\mathcal{Z}(\Delta t)\underline{U}^{(n)}, \quad \text{time evolution operators} \mathcal{X}, \mathcal{Y}, \mathcal{Z} \tag{288}$$

is a dimensionally split update scheme, which is exact for linear advection but not so for any higher order problem (first order reduction) as the steps in the dimensions are done separately.

6.9.1.2 2nd order accurate in 2D examples

$$\begin{aligned} \underline{U}^{(n+1)} &= \frac{1}{2}[X(\Delta t)\mathcal{Y}(\Delta t) + \mathcal{Y}(\Delta t)\mathcal{X}(\Delta t)]\underline{U}^{(n)} \\ \text{or } \underline{U}^{(n+1)} &= X\left(\frac{\Delta t}{2}\right)\mathcal{Y}(\Delta t)\mathcal{X}\left(\frac{\Delta t}{2}\right)\underline{U}^{(n)} \end{aligned} \tag{289}$$

6.9.2 2nd order accurate in 3D example

$$\underline{U}^{(n+1)} = x\left(\frac{\Delta t}{2}\right)\mathcal{Y}\left(\frac{\Delta t}{2}\right)z(\Delta t)\mathcal{Y}\left(\frac{\Delta t}{2}\right)\mathcal{X}\left(\frac{\Delta t}{2}\right)\underline{U}^{(n)} \tag{290}$$

where the 2nd order is based on the alternating reverse order application of the time evolution operators.

6.9.3 Unsplit schemes

Consider rectangular 2D cells. In a dimensionally split scheme we would make updates to a cell based on the information flow in only one direction and then the other based on the changed situation. In an unsplit scheme we apply both fluxes simultaneously.

In the case of rectangular cells in 2D, we have

$$\underline{U}_{i,j}^{(n+1)} = \underline{U}_{i,j}^{(n)} + \frac{\Delta t}{\Delta x}\left(\underline{F}_{i-\frac{1}{2},j} - \underline{F}_{i+\frac{1}{2},j}\right) + \frac{\Delta t}{\Delta y}\left(\underline{G}_{i,j-\frac{1}{2}} - \underline{G}_{i,j-\frac{1}{2}}\right) \tag{291}$$

In the situation of an unstructured mesh, we generally have

$$\underline{U}^{(n+1)} = \underline{U}^{(n)} - \frac{\Delta t}{V}\int \underline{F}\cdot d\underline{S} \quad \text{integral over cell surface, } d\underline{S} \text{ is the surface element vector, pointing outward} \tag{292}$$

which makes sense intuitively (the change coming from the borders distributes over the cells).

The situations are illustrated in figure 63.

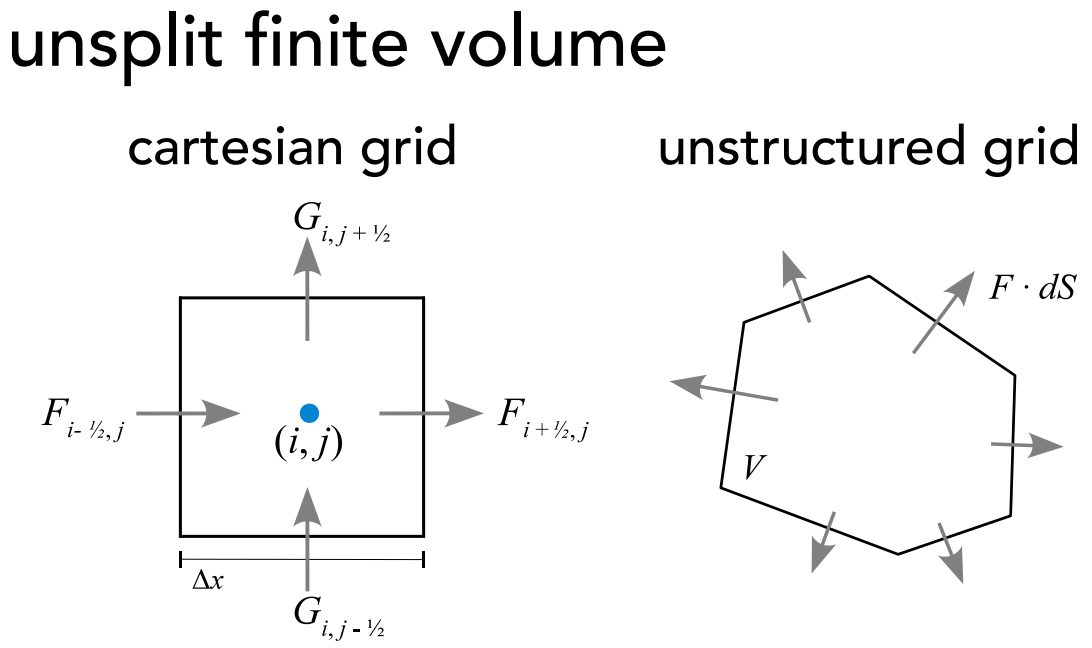

Figure 63: Unsplitting Ansatz Grids

6.10 Extensions for high-oder accuracy

6.10.1 What even is a schemes order?

Consider our numerical solution ρ_i sits on a grid of N points x_i, $i = 1, \dots, N$. Let $\rho(x)$ be the true solution. Then based on the mean L1 error

$$L1 = \frac{1}{N} \sum_{i=1}^{N} |\rho_i - \rho(x_i)| \tag{293}$$

we call a method

- first order accurate if $L1 \propto \Delta x \propto N^{-1}$ with $\Delta x = \frac{L}{N}$
- second order accurate if $L1 \propto \Delta x^2 \propto N^{-1}$
- ...

In the 2nd order accurate scheme, doubling the number of cells will quarter our error.

6.10.2 2nd order extension to Godunov's scheme by changing the reconstruction step from piecewise-constant to linear

1. Estimate the fluid variables gradients, e.g. $\partial_x \rho$ (e.g. based on the averages on the neighboring cells)
2. Slope limit these gradients as otherwise we could introduce quite extreme values of the fluid variables at the cell boundaries, especially in case real fluid discontinuities are present
3. Estimate the values of the fluid variables at one interface by linear extrapolation

$$\rho^L_{i+\frac{1}{2}} = \rho_i + \frac{\Delta x}{2}(\partial_x \rho)_i, \quad \rho^R_{i+\frac{1}{2}} = \rho_{i+1} - \frac{\Delta x}{2}(\partial_x \rho)_{i+1} \tag{294}$$

   See figure 64 for an illustration.

4. Based on the extrapolated fluid variable values at the interface we apply our Riemann solver to find the flux and update the cell averages (although we do not have the piecewise-constant Riemann situation)

Problem: Above we have done a linear extrapolation to the boundary $\rho^L_{i+\frac{1}{2}}$ based on the gradient at the center $(\partial_x \rho)_i$. Note, however, that over our timestep Δt, ρ_i changes, so also our value at the boundary.

$$d\rho(x,t) = (\partial_x \rho)dx + (\partial_t \rho)dt \tag{295}$$

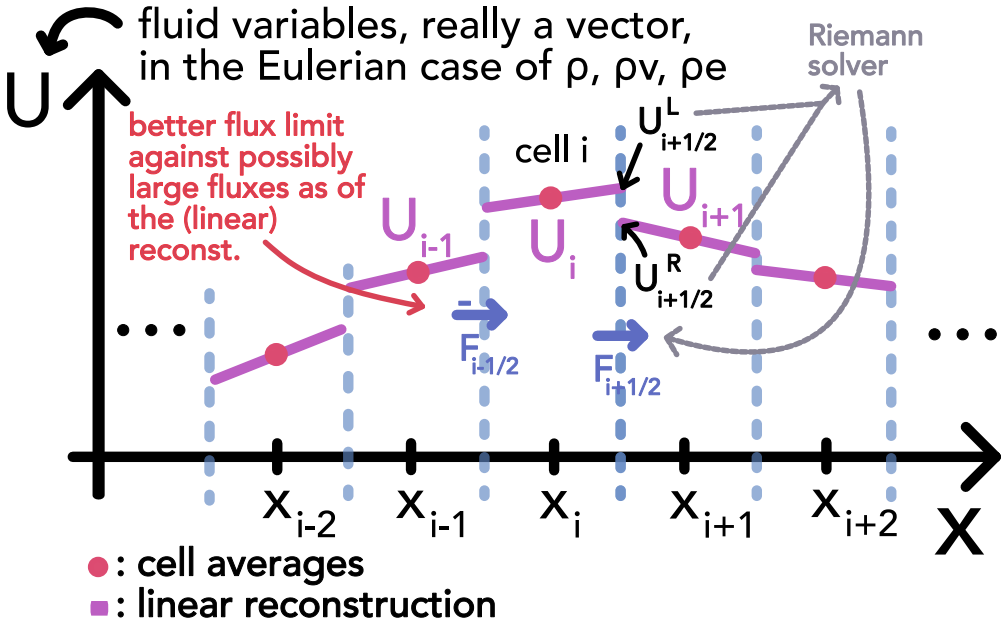

Figure 64: Linear extrapolation of the fluid variables to the cell interface.

For more stability (and 2nd order accuracy), we do the extrapolation based on the gradient but also include the effect of $(\partial_t \rho)_i$ up intil half a timestep (as a proxy to the situation throughout the timestep).

$$\rho^L_{i+\frac{1}{2}} = \rho_i + (\partial_x \rho)_i \frac{\Delta x}{2} + (\partial_t \rho)_i \frac{\Delta t}{2}, \quad \rho^R_{i+\frac{1}{2}} = \rho_{i+1} - (\partial_x \rho)_{i+1} \frac{\Delta x}{2} + (\partial_t \rho)_{i+1} \frac{\Delta t}{2}$$
$$\rightarrow \text{ flux estimate } \underline{F}_{\text{Riemann}}\left(\underline{U}^L_{i+\frac{1}{2}}, \underline{U}^R_{i+\frac{1}{2}}\right) \text{ effectively at half-timestep} \tag{296}$$

So for the entire state $\underline{U}$ we have

$$\underline{U}^L_{i+\frac{1}{2}} = \underline{U}_i + \left(\partial_x \underline{U}\right)_i \frac{\Delta x}{2} + \left(\partial_t \underline{U}\right)_i \frac{\Delta t}{2}, \quad \underline{U}^R_{i+\frac{1}{2}} = \underline{U}_{i+1} - \left(\partial_x \underline{U}\right)_{i+1} \frac{\Delta x}{2} + \left(\partial_t \underline{U}\right)_{i+1} \frac{\Delta t}{2}$$
$$\left(\partial_x \underline{U}\right)_i \text{ calculated from finite difference approach + slope limiting} \tag{297}$$

Idea of the MUSCL-Hancock scheme: Cell averages of the primitive fluid quantities are used to predict the values at the cell boundaries as $t + \frac{\Delta t}{2}$ and then use these prediction to calculate the fluxes and with them the primitive fluid quantities at $t + \Delta t$.

6.10.2.1 How to estimate the time derivatives $(\partial_t \underline{U})_i$? | MUSCL-Hancock scheme

Let us use the Euler equation in 1D (x is a scalar)

$$\partial_t \underline{U} + \partial_x \underline{F}(\underline{U}) \underbrace{=}_{\text{quasi-linear form}} \partial_t \underline{U} + \underline{\underline{J}}_{\underline{U}}(\underline{F}) \cdot \partial_x \underline{U} = 0 \rightarrow \boxed{\partial_t \underline{U} = -\underline{\underline{J}}_{\underline{u}}(\underline{F}) \cdot \partial_x \underline{U}} \tag{298}$$

with Jacobian matrix $\underline{\underline{J}}_{\underline{U}}(\underline{F})$ of $\underline{F}(\underline{U})$ with respect to $\underline{U}$, $\underline{\underline{J}}_{\underline{U}}(\underline{F})\Big|_{\underline{U}=\underline{U}} =: \underline{\underline{A}}(\underline{U})$

We can therefore estimate the derivative in time based on our estimation $\partial_x \underline{U}$ of the derivative in space, yielding the MUSCL-Hancock scheme

$$\begin{aligned} \underline{U}^L_{i+\frac{1}{2}} &= \underline{U}_i + \left[\frac{\Delta x}{2}\underline{\underline{1}} - \underline{\underline{A}}(\underline{U})\frac{\Delta t}{2}\right](\partial_x \underline{U})_i \\ \underline{U}^R_{i+\frac{1}{2}} &= \underline{U}_{i+1} + \left[-\frac{\Delta x}{2}\underline{\underline{1}} - \underline{\underline{A}}(\underline{U})\frac{\Delta t}{2}\right](\partial_x \underline{U})_{i+1} \end{aligned} \tag{299}$$

- a 2nd order accurate extension of Godunov's scheme.

6.10.3 Idea and discussion of even higher order methods

We can

- use higher order polynomial reconstruction as in piecewise parabolic methods (also mind information transport by characteristic waves), see figure 65 (high order methods tend to create post shock oscillations → add dissipation mechanism / some flattening[9] to PPM)
- even higher order polynomials are used in methods like ENO and WENO (find polynomials based on values from multiple cells (*larger stencil*))

Note: Independent of the order, we only **store** one value (per variable) per cell in finite volume methods. In **finite element methods**, per cell polynomial representations of the state vector are stored (discontinuities are harder to capture though).

6.10.3.1 Discussion of higher order methods

Advantages and disadvantages of higher order methods can be found in table 11, those of lower order methods in table 12.

[9] Which essentially means that locally we go back to lower order.

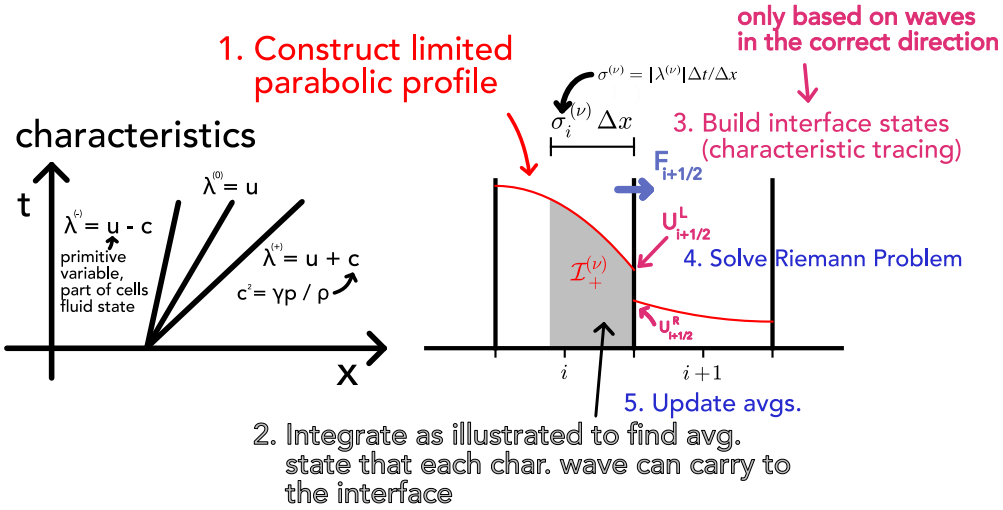

Figure 65: Piecewise parabolic reconstruction.

Pro higher	Con higher
• sharp solution • more accurate (sharper solutions alone can be inaccurate, e.g. when the bulk position is inaccurate)	• more expensive • strong oscillations at discontinuities (principle illustrated in figure 66) • crash at high Mach numbers

Table 11: Advantages and disadvantages of higher order methods.

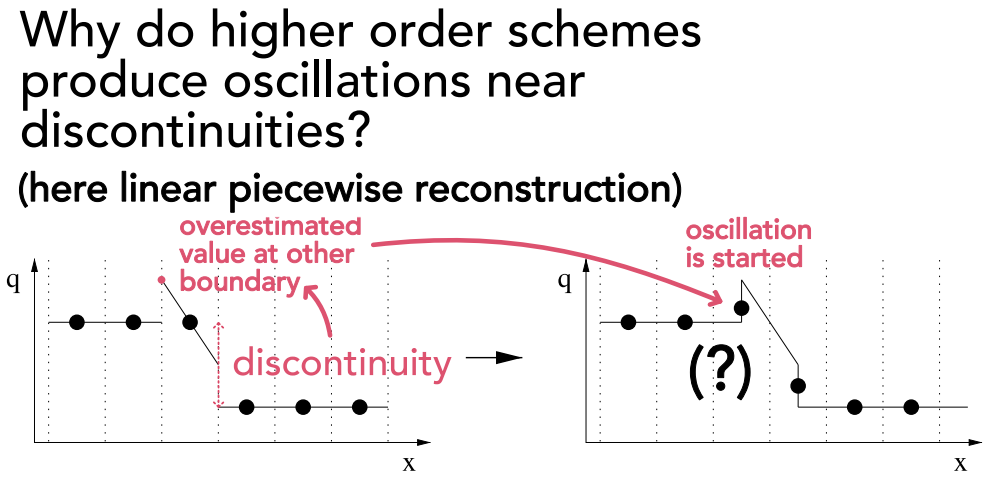

Figure 66: Illustration of the principle of oscillations at discontinuities in higher order methods.

Pro lower	Con lower
• stable for complex flows • no ocillations at discontinuities • do not crash at high Mach numbers	• smear out solutions • slower convergence to accurate solutions • less accurate

Table 12: Advantages and disadvantages of lower order methods.

6.11 Flux / slope limiters | adaptively switching between a high and low order method

Problem: A system can contain very boring and strongly dynamic parts. It is very difficult to choose which solver is best for the global problem for all timesteps.

Idea: Dynamically switch between orders and solvers. Use 2nd order where possible and 1st order where necessary (e.g. for discontinuities).

Let us for simplicity consider a 1D problem with a single state variable u, e.g. the viscous Burgers equation

$$\partial_t u + \partial_x \left(\frac{1}{2} u^2 - \nu \partial_x u \right) = 0 \tag{300}$$

(which can be analytically solved using the Cole-Hopf transform $u = -2\nu \frac{1}{\phi} \partial_x \phi$[10]).

Let $\mathcal{F}^H_{i+\frac{1}{2}}$ be a high-order flux computation and $\mathcal{F}^L_{i+\frac{1}{2}}$ be a low-order flux computation. We use the flux

$$\begin{gathered} F^{(n)}_{i+\frac{1}{2}} = \mathcal{F}^{L,(n)}_{i+\frac{1}{2}} \left(U_i, U_{i+1} \right) + \phi^{(n)}_{i+\frac{1}{2}}(r) \cdot \left(\mathcal{F}^{H,(n)}_{i+\frac{1}{2}} \left(U_i, U_{i+1} \right) - \mathcal{F}^{L,(n)}_{i+\frac{1}{2}} \left(U_i, U_{i+1} \right) \right) \\ \text{high order for } \phi^{(n)}_{i+\frac{1}{2}}(r) = 1, \quad \text{low order for } \phi^{(n)}_{i+\frac{1}{2}}(r) = 0 \end{gathered} \tag{301}$$

with

$$\text{flux limiter } \phi^{(n)}_{i+\frac{1}{2}}(r) \text{ based on the ratio } r = \frac{U_i - U_{i-1}}{U_{i+1} - U_i}$$

large if the jump of interest between U_i and U_{i+1} is large compared to the jump between U_{i-1} and U_i (302)

with and exemplary flux limiter being

$$\phi_{\text{minmod}} = \max(0, \min(1, r)), \quad r > 1 \to \phi_{\text{minmod}} = 1 \to \text{high order} \tag{303}$$

(illustrated in figure 67) where it makes sense that for a big r we use the higher order method: If the jump between i and $i+1$ is small compared to the jump between $i-1$ and i, we can assume that the solution is smooth and use the higher order method (no dicontinuity expected).

[10] This is nice if we want to test different flux limiters against a ground-truth result.

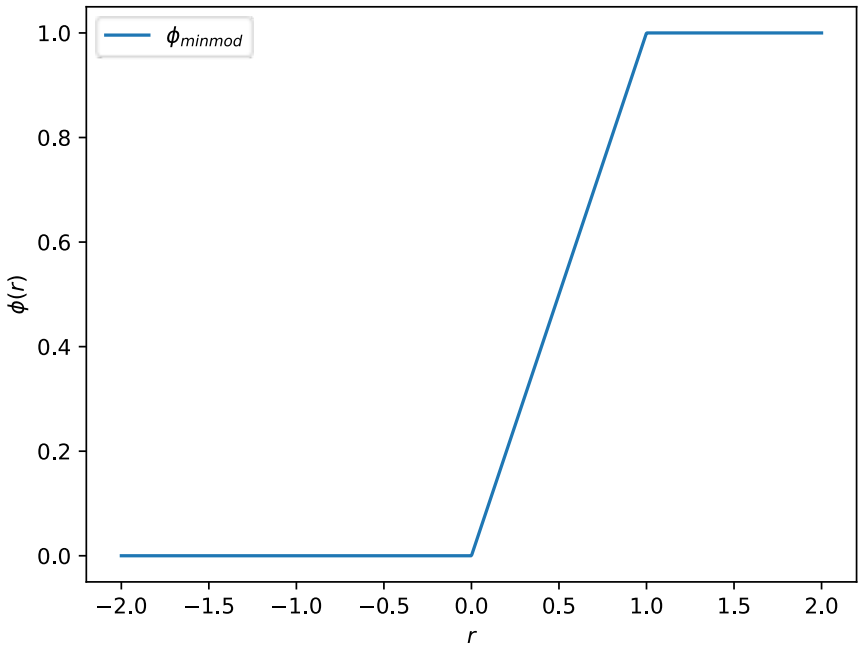

Figure 67: Minmod flux limiter.

Why is ϕ called a flux limiter? Higher order schemes can have larger slopes and predict larger fluxes, taking the lower order will has less of this problem.

6.11.1 Possibly advantageous properties of the flux limiter

It is often advantageous for the limiters to be symmetric with the property

$$\frac{\phi(r)}{r} = \phi\left(\frac{1}{r}\right) \tag{304}$$

so that the switch works the same for forward and backward facing gradients (mind the definition of r) (?).

Another property is based on the total variation

$$\mathrm{TV}(\underline{U}) = \sum_i |U_{i+1} - U_i| \tag{305}$$

(where here $\underline{U}$ is the vector over the grid points not fluid variables), called total variation diminishing (TVD) property

$$\mathrm{TV}(\underline{U}^{(n+1)}) \leq \mathrm{TV}(\underline{U}^{(n)}) \tag{306}$$

which means no oscillation will appear but real ocscillations in the system will also not grow

but rather smeared out. Minmod is TVD.

7 Smoothed Particle Hydrodynamics - Lagrangian Particle Method

Idea: In Smoothed Particle Hydrodynamics (SPH) we approximately solve the fluid equations numerically by replacing the fluid with a set of particles, we call *SPH-particles*[a]. The equations of motion and properties of those particles are followed from the Lagrangian form of the continuity equations for the fluid. We then forward these particles in time using e.g. the leapfrog or semi-implicit Euler scheme.

[a]Characterized by their position and velocity. Additionally, hydrodynamic variables, e.g. ρ_i, T_i, are derived at the particles positions $\underline{x}_i$. Not to be confused with the real particles making up the fluid.

From this it makes sense that the main ingredients to the baseline scheme will be

- formulate the fluid equations in their Lagrangian[11] form
- formulate an algorithm to update the SPH-particles positions and velocities based on the Lagrangian fluid equations
- find expressions for the quantities used in the update-steps which goes hand in hand with finding how to get from the SPH-particle-perspective to continuous fluid quantities

Such a mesh-free scheme has some key advantages

- This particle representation of SPH has great conservation features - energy, linear momentum, angular momentum mass and specific thermodynamic entropy (more later; if we do not add artificial viscosity) are conserved (as we follow particles there is no loss of mass etc.).
- No advection errors, scheme is fully Galilean invariant (unlike mesh-based Eulerian techniques)
- As of the Lagrangian character, the local resolution of SPH follows the mass flow automatically → adaptive resolution, good for problems with vastly different densities

[11]Co-moving with the flow rather than fixed as in the Eulerian perspective.

7.1 Lagrangian fluid equations (i.e. as material derivatives)

7.1.1 Continuity equation

Written as a material derivative, the continuity equation is

$$D_t\rho = -\rho(\underline{\nabla}\cdot\underline{v}), \quad \text{fluid mass density } \rho, \quad \text{fluid velocity } \underline{v} \tag{307}$$

which is zero for an incompressible fluid.

7.1.2 Navier-Stokes equation | Conservation law of Linear Momentum

A natural extension of Newtons 2nd law to continua is (including internal and external forces)

$$\begin{gathered}\rho D_t\underline{v} = \sum \text{forces} = -\underline{\nabla}P + \underline{\nabla}\cdot\underline{\underline{\Pi}} + \rho\underline{g} \\ \text{stress tensor } \underline{\underline{\Pi}}, \quad \text{pressure } P, \quad \text{external accelerations } \underline{g}\end{gathered} \tag{308}$$

where a general approach to $\underline{\underline{\Pi}}$ is the Cauchy-Stress tensor for compressible flow

$$\begin{gathered}\underline{\underline{\Pi}} = \left\{\mu\left[\underline{\nabla}\underline{v}^T + (\underline{\nabla}\underline{v}^T)^T - \frac{2}{3}(\underline{\nabla}\cdot\underline{v})\underline{\underline{1}}\right] + \zeta(\underline{\nabla}\cdot\underline{v})\underline{\underline{1}}\right\} \\ \text{shear viscosity } \mu, \quad \text{bulk viscosity } \zeta\end{gathered} \tag{309}$$

where for incompressible flow one yields

$$\rho D_t\underline{v} = -\underline{\nabla}P + \mu\underline{\nabla}^2\underline{v} + \rho\underline{g} \tag{310}$$

Note: In an incompressible setting, the pressure P can be interpreted as a Lagrange multiplier which has to be chosen such that incompressibility really holds. Otherwise P is determined by a state equation, e.g. very basic $P(\rho) = k\left(\frac{\rho}{\rho_0} - 1\right), k > 0$ (variation of the ideal gas equation) or isothermal $P(\rho) = P_0 + c_0^2(\rho_0 - \rho)$, as previously discussed.

7.1.3 Energy equation

While me can forward the system only based on the Navier-Stokes equation and closure, let us write down the energy equation.

Let ϵ be the energy per volume so the energy per mass is $e = \frac{\epsilon}{\rho}$.

From basic thermodynamics, we can write for the internal energy U

$$\begin{aligned} dU = dQ + dW = dQ - PdV = TdS - PdV, \quad U = \epsilon V = eM \\ \text{volume } V = \frac{M}{\rho} \rightarrow dV = -\frac{M}{\rho^2} d\rho, \quad \text{total mass } M, \quad \text{entropy } S, \quad \text{pressure } P \end{aligned} \tag{311}$$

using this we find

$$\begin{aligned} \frac{de}{dt} = \partial_t e + (\underline{v} \cdot \underline{\nabla}) e = \frac{1}{M}\frac{dU}{dt} = \frac{1}{M} T \frac{dS}{dt} - \frac{1}{M} P \frac{dV}{dt} \\ = T\frac{ds}{dt} + \frac{P}{\rho^2}\frac{d\rho}{dt} \underbrace{=}_{\text{continuity eq.}} T\frac{ds}{dt} - \frac{P}{\rho}(\underline{\nabla} \cdot \underline{v}) \end{aligned} \tag{312}$$

7.2 A simple SPH fluid simulator*

Based on the Navier-Stokes equation in Lagrangian form we can construct a simple fluid simulator, here using semi-implicit aka symplectic Euler[12]. Pressure and viscosity forces are calculated separately. We still have to mind the CFL criterion (more on this later).

To code up our simulator we have to answer

- How do we construct the density from the SPH-particles positions $\underline{x}_i$?
- How do we calculate the gradients over fluid variables, so $\underline{\nabla} P$?

[12]The PySPH package for instance uses a second order predictor-corrector method.

```
for sph_particle_i in sph_particles:
    # reconstruct density ρ_i at x_i
for sph_particle_i in sph_particles:
    ### viscous-force calculation in case of a viscous fluid
    # / to make shocks resolvable using artificial viscosity
    # compute a_i^viscosity in the incomp. case = ν∇²v_i
    # v_i^* = v_i + Δt(a_i^viscosity + g), external accelerations g

    ### pressure force calculation
    # compute a_i^pressure = -(1/ρ_i)∇P

    ### forward the particles, here using symplectic Euler
    # v_i(t + Δt) = v_i^* + Δt · a_i^pressure
    # x_i(t + Δt) = x_i + Δt · v_i(t + Δt)
```

Code-Snippet 1: Simple SPH fluid simulator. We need two loops, as to calculate e.g. the pressure force on one SPH-particle, the densities at positions of other SPH-particles are necessary.

- How do we handle viscosity?

7.3 Smooth then discretize - smoothing kernels and their usage

Fluid quantities like the density are estimated though a kernel summation interpolant. Start by replacing a general fluid quantity $F(\underline{r})$ with a smoothed version by convoluting it with a smoothing kernel

$$\begin{aligned} &F(\underline{r}) \to F_S(\underline{r}) \equiv \langle F(\underline{r}) \rangle = \int F\left(\underline{r}'\right) W\left(\underline{r} - \underline{r}', h\right) d^3\underline{r}', \quad \text{smoothing width } h \\ &\text{kernel } W \text{ with } \int W\left(\underline{r}', h\right) d^3\underline{r}' = 1, \quad \langle F(\underline{r}) \rangle \underset{h \to 0}{\longrightarrow} F(\underline{r}), \text{ i.e. } W(\underline{r}, h) \underset{h \to 0}{\longrightarrow} \delta(\underline{r}) \end{aligned} \tag{313}$$

where the kernel has to be normed to not modify e.g. the total mass, and also differentiable (so that our fluid quantities are smooth). Typically, a spherical kernel is used

$$W(\underline{r}, h) = W(r, h) \tag{314}$$

which could be a Gaussian - but a Kernel with finite support, for instance a cubic spline, is better (more on that later).

7.3.1 Properties of the smoothing | approach for calculating derivatives of the smoothed fluid quantities

The smoothed version is 2nd order accurate with respect to the smoothing length (no first order correction as of the symmetry of the kernel)

$$\langle F(\underline{r}) \rangle = F(\underline{r}) + \mathcal{O}\left(h^2\right) \tag{315}$$

We can also find

$$\begin{aligned} \langle F(\underline{r}) + G(\underline{r}) \rangle &= \langle F(\underline{r}) \rangle + \langle G(\underline{r}) \rangle \\ \langle F(\underline{r}) \cdot G(\underline{r}) \rangle &= \langle F(\underline{r}) \rangle \cdot \langle G(\underline{r}) \rangle + \mathcal{O}\left(h^2\right) \\ \boxed{\frac{d}{dt} \langle F(\underline{r}) \rangle = \left\langle \frac{dF(\underline{r})}{dt} \right\rangle} & \\ \underline{\nabla} \langle F(\underline{r}) \rangle \underbrace{=}_{\text{Kernel with compact support}} \langle \underline{\nabla} F(\underline{r}) \rangle & \end{aligned} \tag{316}$$

where the main result that will allow us to make the fluid equation algebraic is

$$\boxed{\langle \underline{\nabla} F(\underline{r}) \rangle = \underline{\nabla} \langle F(\underline{r}) \rangle = \int F\left(\underline{r}'\right) \underline{\nabla} W\left(\left|\underline{r} - \underline{r}'\right|, h\right) d^3\underline{r}'} \tag{317}$$

so we weight $F(\underline{r}')$ using the gradient of the kernel which can be pre-computed.

7.3.2 Discrete formulation of the smoothing

We now introduce the SPH-particles at positions $\underline{r}_i$ where the fluid variable has value $F_i = F(\underline{r}_i)$. We assign a mass m_i to those particles. Together with the density $\rho_i = \rho(\underline{r}_i)$ we can write

$$\Delta r_i^3 \sim \frac{m_i}{\rho_i} \tag{318}$$

With this, assuming that those SPH-particles densely sample the space of interest, we can write the smoothed fluid quantity as

$$\boxed{F_s(\underline{r}) \equiv \langle F(\underline{r}) \rangle \simeq \sum_{j=1}^{N_i} \frac{m_j}{\rho_j} F_j W\left(\underline{r} - \underline{r}_j, h\right), \quad \text{number of neighbors } N_i} \tag{319}$$

Note: While this is similar to Monte-Carlo integration, the evaluation points are our SPH-particles which here turns out to be favorable over random sampling, as the distances between the particles tend to equilibrate due to pressure forces (making the interpolation smaller - still resulting noise is a problem of SPH).

$F_s(\underline{r})$ is defined everywhere and differentiable as the kernel is differentiable.

For the density we can write

$$\boxed{\rho_s(\underline{r}) = \sum_{j=1}^{N_i} m_j W(\underline{r} - \underline{r}_j, h)} \tag{320}$$

The smoothing length h should at least be larger than the particle distance.

7.3.3 Why a kernel with compact support is preferred?

Consider we are interested in the density ρ_i at $\underline{x}_i$. Note that the density at any point is based on the overlap of multiple smoothing kernels (see eq. 320).

Consider a Gaussian kernel

$$W_{\text{Gaussian}}(||\underline{r}_i - \underline{r}_j||, h) = \frac{1}{(\pi h^2)^{\frac{d}{2}}} \exp(-q^2), \quad q := \frac{||\underline{r}_i - \underline{r}_j||}{h}, \quad \text{dimension } d \tag{321}$$

then as of the infinite support, for the density ρ_i we would have to sum over all particles, and the density calculation at all SPH-particles $i = 1, \ldots, N$ would be $\mathcal{O}(N^2)$.

Now for a cubic spline Kernel

$$\begin{aligned} W(q) &= \sigma_3 \left[1 - \frac{3}{2}q^2\left(1 - \frac{q}{2}\right)\right], && \text{for } 0 \leq q \leq 1 \\ &= \frac{\sigma_3}{4}(2-q)^3, && \text{for } 1 < q \leq 2 \\ &= 0, && \text{for } q > 2 \end{aligned} \tag{322}$$

with normalization

$$d = 1 : \sigma_3 = \frac{2}{3h}, \quad d = 2 : \sigma_3 = \frac{10}{7\pi h^2}, \quad d = 3 : \sigma_3 = \frac{1}{\pi h^3} \tag{323}$$

the density calculation is only $\mathcal{O}(N_{ngb}N)$ with N_{ngb} being the average number of neighbors considered depending on the choice of h.

Note: The support size of SPH-particles is usually chosen to be $2h$ so that $W_{\text{Gaussian}}(||\underline{r}_i - \underline{r}'||, h) = 0$ for $||\underline{r}_i - \underline{r}'|| > 2h$, see figure 68.

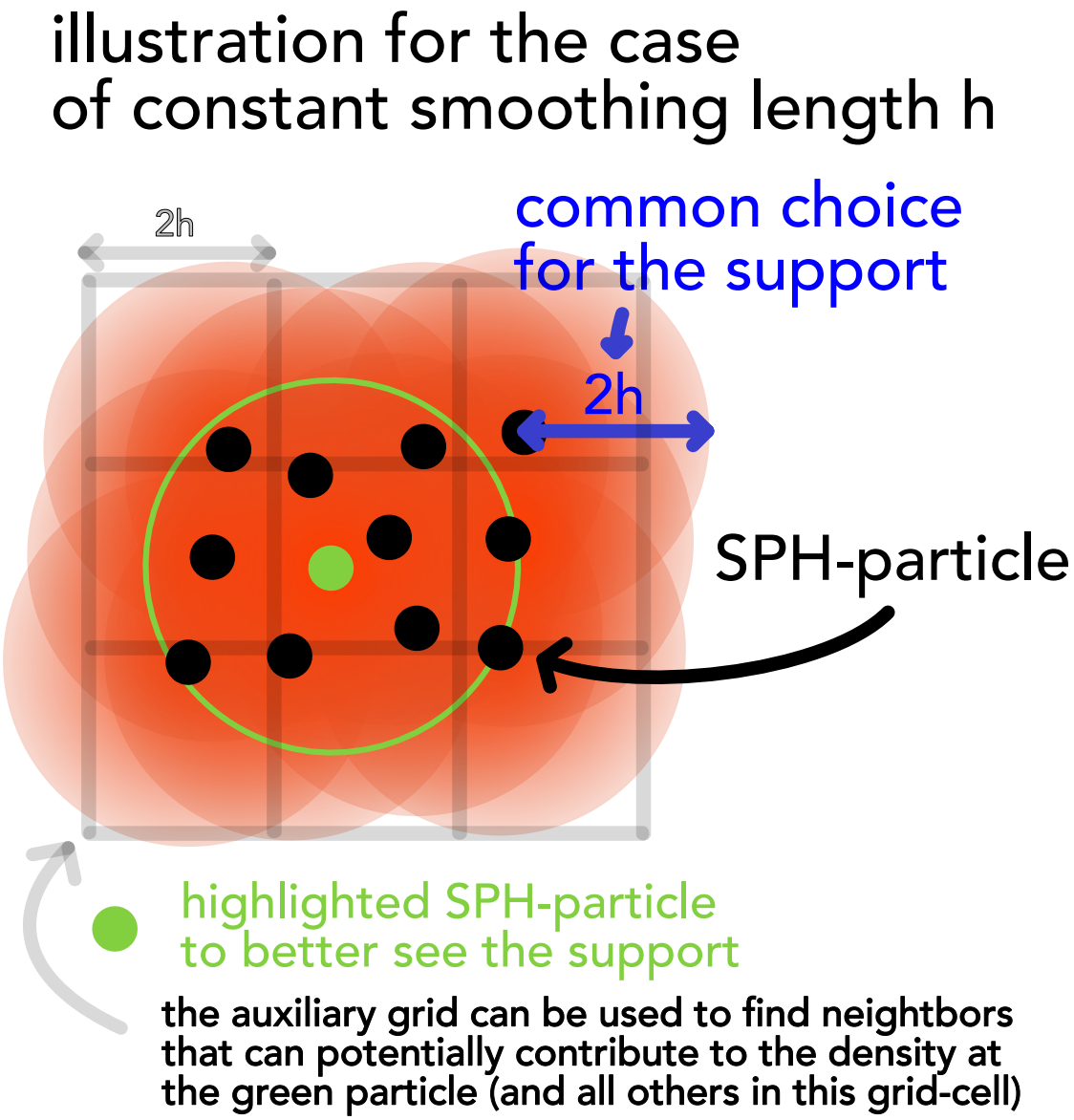

Figure 68: SPH illustration for fixed h.

7.3.4 How to make the smoothing length h variable in space to account for variations in the density? | sampling procedure in SPH - scatter and gather approach

Problem: Choosing a good overall smoothing length h is a problem in any algorithm using kernels (for instance also in Kernel Density Estimation). If h is chosen too large, we loose the details of the density distribution, if h is chosen to small, we get not a smooth density distribution but one with peaks at the positions of our SPH-particles. It makes more sense to use an adaptive smoothing length which is smaller in regions where SPH-particles are denser (to still resolve details there) and larger where they are more rarefied, so that in such regions the overall density would still make sense for a - in reality - continuous fluid, see figure 69

.

Idea: Use a variable smoothing length h.

There are two general approaches for introducing a variable smoothing length ρ_i into the calculation of our fluid quantities - the scatter and gather approach, as shown in table 13 and illustrated in figure 70.

Symmetry problem: Consider the effect of a variable smoothing length on how SPH-particles affect each other. In the schemes above this is not necessarily symmetric, leading to a force asymmetry and Newton's third law being broken (no conservation of total angular momentum).

We therefore have to symmetrize the equations of motion in $h_i = h(\underline{r}_i)$ and $h_j = h(\underline{r}_j)$. We make forces antisymmetric by substituting e.g.

$$h_{ij} = \frac{h_i + h_j}{2}, \quad \text{or geometric mean} \quad h_{ij} = \sqrt{h_i h_j} \tag{326}$$

for h_i and h_j in the force calculations. Therefore, a symmetric approach to the density is

$$\rho_s\left(\underline{r}_i\right) = \sum_{j=1}^{N_i} m_j W\left(r_{ij}, h_{ij}\right), r_{ij} = \left|\underline{r}_i - \underline{r}_j\right| \tag{327}$$

Note: As h is a function of $\underline{r}$ in the gather scheme, we must account for this in

$$\underline{\nabla} W\left(\left|\underline{r} - \underline{r}'\right|, h\right) = \underline{\nabla} W\left(\left|\underline{r} - \underline{r}'\right|, h\right)\big|_{h=const.} + (\underline{\nabla} h)\partial_h W\left(\left|\underline{r} - \underline{r}'\right|, h\right)\big|_{h=\text{ const.}} \tag{328}$$

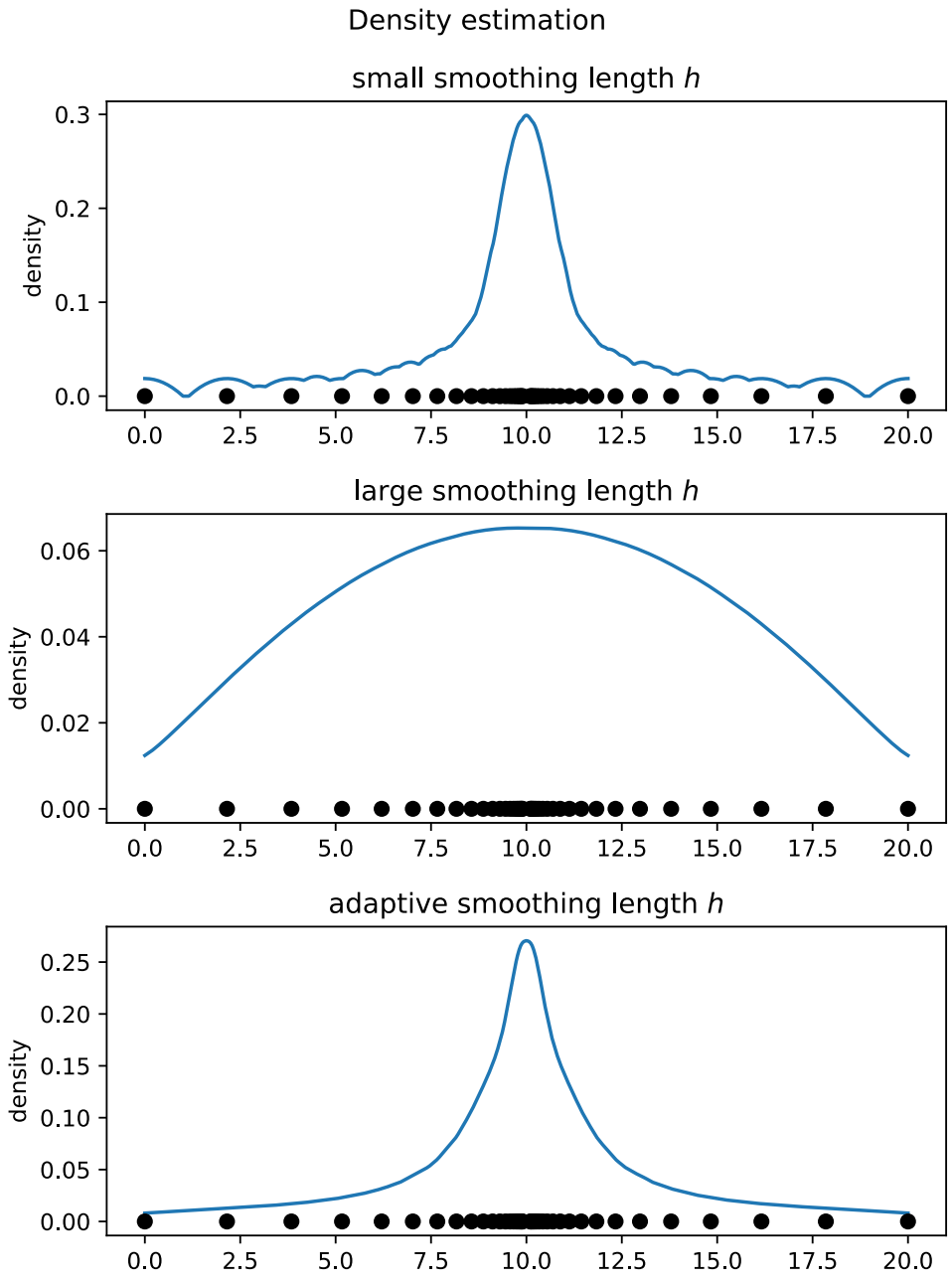

Figure 69: Density estimation

7.3.4.1 How to choose h_i?

We adjust h_i so that we always consider $50 \lesssim 50 \lesssim 500$ neighbors.

One choice is to choose h to keep N_{ngb} constant. Another is to scale h according to the density (higher for lower densities), e.g.

$$h_i = h_0 \left(\frac{\rho_0}{\rho_i}\right)^3, \quad \frac{dh}{dt} = -\frac{1}{3}\frac{h}{\rho}\frac{d\rho}{dt} \underbrace{=}_{\text{continuity eq.}} \frac{1}{3}h\underline{\nabla} \cdot \underline{v}, \quad \text{dimension } d \tag{329}$$

scatter	**gather**
each SPH-particle is assigned a smoothing length, the density at any point is calculated from the overlap of all surrounding density distributions	The observer at a position $\underline{r}$ has it's smoothing length h and assigns it to all SPH-particles in the relevant region. Assuming kernels with a compact support $2h$ this relevant region - starting from the observer - has radius $2h$.
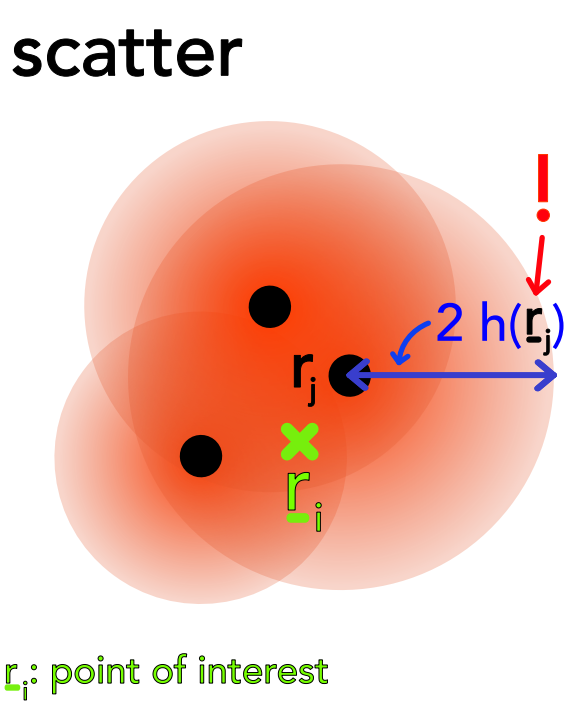	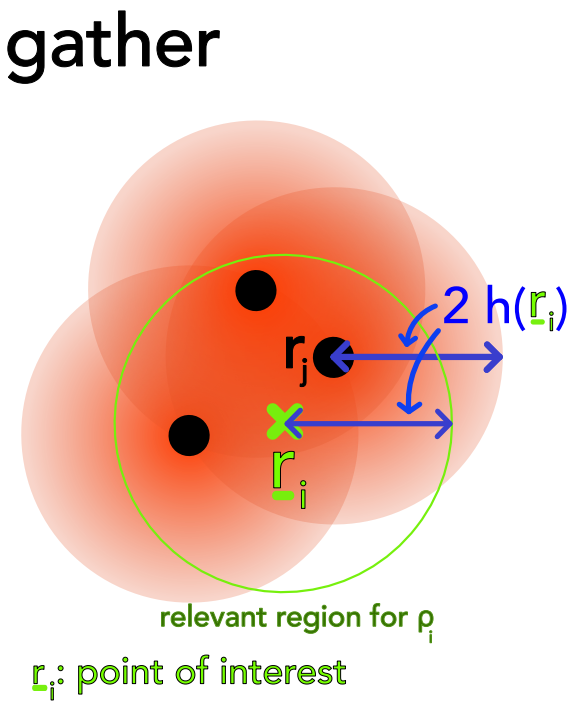
$\langle F(\underline{r})\rangle = \int_{N_i} F\left(\underline{r}'\right) W\left(\underline{r}-\underline{r}', h\left(\underline{r}'\right)\right) d^3\underline{r}'$ $\rho_s\left(\underline{r}_i\right) = \sum_{j=1}^{N_i} m_j W\left(r_{ij}, h_j\right), r_{ij} = \left\lvert \underline{r}_i - \underline{r}_j \right\rvert$ (324)	$\langle F(\underline{r})\rangle = \int_{N_i} F\left(\underline{r}'\right) W\left(\underline{r}-\underline{r}', h(\underline{r})\right) d^3\underline{r}'$ $\rho_s\left(\underline{r}_i\right) = \sum_{j=1}^{N_i} m_j W\left(r_{ij}, h_i\right), r_{ij} = \left\lvert \underline{r}_i - \underline{r}_j \right\rvert$ (325)
The total mass is conserved in the scatter approach, $\int \rho_s d^3\underline{r} = \sum m_i$	The total mass is not conserved in the gather approach, the error is only $\mathcal{O}(h^2)$ thoug.

Table 13: Scatter and gather approach for introducing a variable smoothing length h.

so that the mass ρh^3 is constant.

The neighbors can be found using a tree structure for partitioning space.

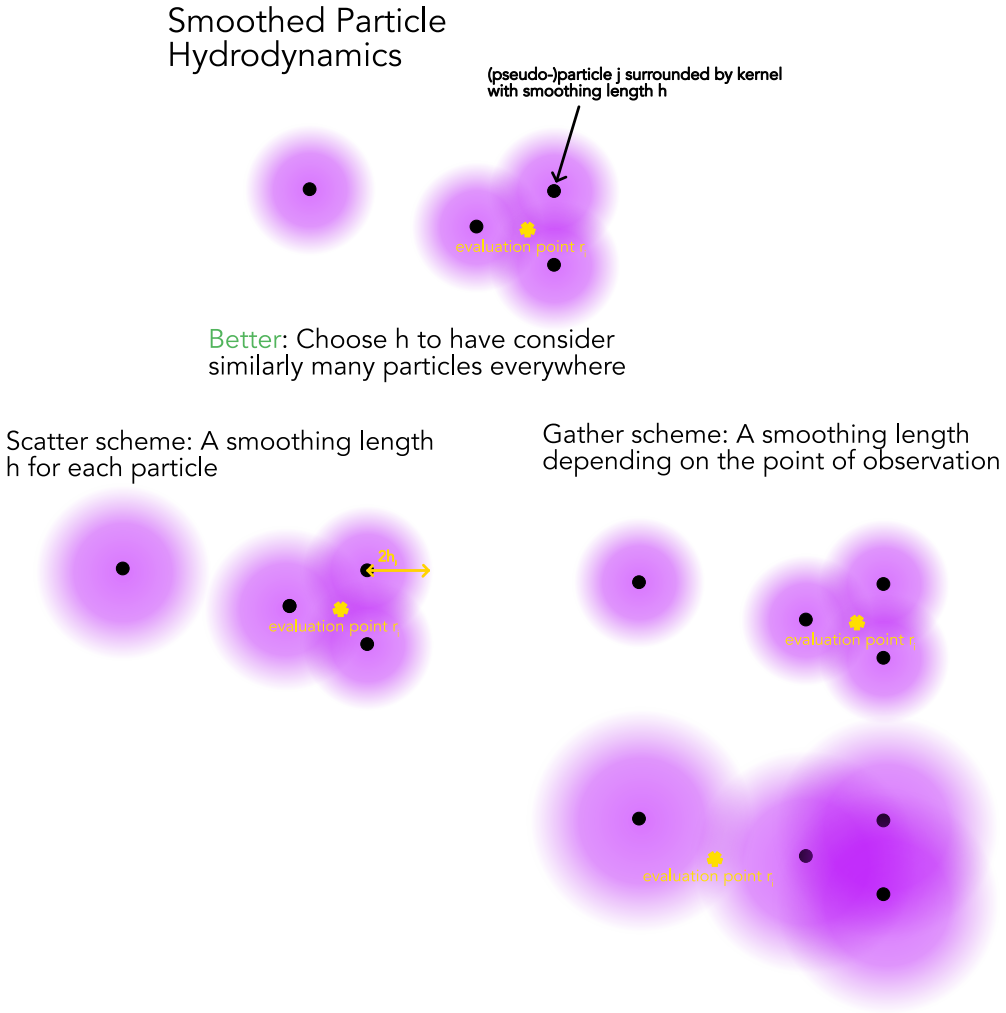

Figure 70: Scatter and gather approach for introducing a variable smoothing length h.

7.4 SPH continuity equation and equations of motion

We now know how to construct the densities ρ_i at the SPH-particles positions in one loop. Those densities are required for subsequent calculation of pressure forces etc. in a second loop.

7.4.1 SPH continuity equation

While better not used in forwarding the system, the SPH continuity equation can still be of interest.

Directly applying eq. 317 to the continuity equation in Lagrangian form, so $D_t\rho = -\rho\underline{\nabla}\cdot\underline{v}$, turns out to be extremely sensitive to the particle distribution, we can rewrite

$$\rho\underline{\nabla}\cdot\underline{v} = \underline{\nabla}\cdot(\rho\underline{v}) - \underline{v}\cdot\underline{\nabla}\rho \tag{330}$$

and applying eq. 317 and 319 we find for the i-th SPH-particle

$$\langle \underline{\nabla} \underline{v} \rangle_i = \frac{1}{\rho_i} \left[\left\langle \underline{\nabla}_i \cdot (\rho \underline{v})_i \right\rangle - \underline{v}_i \cdot \langle \underline{\nabla} \rho \rangle_i \right] = \frac{1}{\rho_i} \sum_{j=1}^{N_i} m_j \left(\underline{v}_j - \underline{v}_i \right) \underline{\nabla}_i W \left(r_{ij}, h_{ij} \right) \tag{331}$$

(which has the advantage that as it should be for all equal velocities $\underline{v}_i = \underline{v}_j$ we have $\langle \underline{\nabla} \underline{v} \rangle_i = 0$).

and thus the SPH continuity equation

$$\frac{d\rho_i}{dt} \simeq \sum_{j=1}^{N_i} m_j \underline{v}_{ij} \underline{\nabla}_i W \left(r_{ij}, h_{ij} \right), \quad \underline{v}_{ij} = \underline{v}_i - \underline{v}_j \tag{332}$$

7.4.2 Gradients in SPH

Note: There are multiple ways to obtain the SPH equations of motion. One is to find an expression for gradients and apply it to the Euler equations, another a variational approach, which directly guarantees certain conservation laws[a]

[a] There we start from the Lagrangian for inviscid (zero-viscosity) flow and then derive the Lagrangian equations of motion. The symmetries of the Lagrangian and absence of explicit time dependence directly give us energy conservation, momentum conservation from the translational invariance and momentum conservation from the rotational invariance.

As with the density, it is better not to directly apply eq. 317 but better to use the identities

$$\begin{aligned} \underline{\nabla} \cdot F(\underline{r}) &= \frac{1}{\rho} [\underline{\nabla} \cdot (\rho F(\underline{r})) - F(\underline{r}) \underline{\nabla} \cdot \rho] \\ \underline{\nabla} \cdot F(\underline{r}) &= \rho \left[\underline{\nabla} \cdot \left(\frac{F(\underline{r})}{\rho} \right) + \frac{F(\underline{r})}{\rho^2} \underline{\nabla} \cdot \rho \right] \end{aligned} \tag{333}$$

to obtain

$$\langle \underline{\nabla} \cdot F(\underline{r}) \rangle_i = \frac{1}{\rho_i} \sum_{j=1}^{N_i} m_j \left[F\left(\underline{r}_j \right) - F\left(\underline{r}_i \right) \right] \cdot \underline{\nabla}_i W_{ij}, \quad W_{ij} = W \left(r_{ij}, h_{ij} \right) \tag{334}$$

and the symmetric form

$$\langle \underline{\nabla} \cdot F(\underline{r}) \rangle_i = \rho_i \left[\sum_{j=1}^{N_i} m_j \left[\frac{F\left(\underline{r}_j \right)}{\rho_j^2} + \frac{F\left(\underline{r}_i \right)}{\rho_i^2} \right] \cdot \underline{\nabla}_i W_{ij} \right] \tag{335}$$

7.4.3 SPH Euler equation | The central ingredient to making our simple fluid simulator work

With the gradient-expression, we can tackle the Euler equation in convective (Lagrangian) from (Navier-Stokes without stress tensor / external forces), in other words we can find the **acceleration as of pressure** $\underline{a}_i^{\text{pressure}}$.

$$\underline{a}^{\text{pressure}} = -\frac{\underline{\nabla} P}{\rho} \tag{336}$$

so in the (anti)symmetric form

$$\boxed{\underline{a}_i^{\text{pressure}} = -\sum_{j=1}^{N_i} m_j \left[\frac{P_j}{\rho_j^2} + \frac{P_i}{\rho_i^2}\right] \cdot \underline{\nabla}_i W_{ij}} \tag{337}$$

This is the acceleration we need to get our simple fluid simulator working - P follows from the equation of state.

Note: Artificial viscosity will have to be added to allow for the treatment of shocks.

The equation is antisymmetric in i and j so momentum is conserved locally and globally (also follows from the variational method).

Other symmetrizations

$$\text{e.g. } \frac{1}{2}\left(\frac{P_i}{\rho_i^2} + \frac{P_j}{\rho_j^2}\right) \quad \leftrightarrow \quad \frac{\sqrt{P_i P_j}}{\rho_i \rho_j} \tag{338}$$

and additional correction factors are possible.

7.4.4 Including further accelerations

Further accelerations like self gravity can be calculated as usual

$$\underline{g}_i = -\underline{\nabla}\Phi_i = -G\sum_{j=1}^{N_i} m_j \frac{\underline{r}_{ij}}{r_{ij}^3} \tag{339}$$

7.5 Artificial Viscosity

The SPH equations formulated above keep the specific thermodynamic entropy A_i strictly constant.

The Euler equations, however, can produce true discontinuities in form of shock waves or contact discontinuities[13] where the specific entropy increases at the shock front - which our current SPH scheme will never display. We must introduce artificial viscosity for the necessary dissipation processes producing heat and entropy to be possible. The artificial viscosity dampening the motion of particles broadens the shock layer into a differentially resolvable form. Also, without artificial viscosity, particles would be able to interpenetrate. We want the viscosity to only be active at shocks and not disturb our ideal gas behavior.

7.5.1 Viscous Pressure

Based on the discretized estimate $\langle \underline{\nabla} \cdot \underline{v} \rangle_i$, viscosity can be added in form of the following pressure (von-Neumann-Richtmyer-Landshoff)

$$p_i^{AV} = \begin{cases} \underbrace{-\alpha_i^{AV} \rho_i c_i h_i (\underline{\nabla} \cdot \underline{v})_i}_{\substack{\text{combined shear and} \\ \text{bulk viscosity,} \\ \text{dampens post shock} \\ \text{osci.}}} + \underbrace{\beta_i^{AV} \rho_i h_i^2 (\underline{\nabla} \cdot \underline{v})_i^2}_{\substack{\text{Richtmyer} \\ \text{viscosity, prevent} \\ \text{interpenetration} \\ \text{in high Mach} \\ \text{number shocks}}} & \text{if } (\underline{\nabla} \cdot \underline{v})_i < 0, \\ 0 & \text{otherwise} \end{cases} \tag{340}$$

density ρ, sound speed c, smoothing length h, parameters α, β

7.5.2 Adding the artificial viscosity to the equation of motion

To our SPH Euler equation, we can add the viscous force as

$$\begin{aligned} \underline{a}_i^{\text{visc}} &= \left. \frac{d_{v_1}}{dt} \right|_{visc} = -\sum_{j=1}^{N_i} m_j \Pi_{ij} \cdot \underline{\nabla}_i \overline{W_{ij}} \\ \overline{W_{ij}} &= \frac{1}{2} W_{ij} \left(\frac{h_i + h_j}{2} \right), \quad \Pi_{ij} \text{ should be symmetric } \rightarrow \text{ antisymmetric force} \end{aligned} \tag{341}$$

where keeping the force antisymmetric retains conservation of linear and angular momentum.

[13] At the shock front the differential form of the Euler equation breaks down and the integral form leading to the Rankine-Hugoniot jump conditions has to be used.

For the viscous stress tensor we can model

$$\text{one possibility } \Pi_{ij} = \begin{cases} \left[-\alpha c_{ij}\mu_{ij} + \beta\mu_{ij}^2\right]/\rho_{ij} & \text{if } \underline{v}_{ij}\cdot\underline{r}_{ij} < 0 \\ 0 & \text{otherwise} \end{cases}, \quad \mu_{ij} = \frac{h_{ij}\underline{v}_{ij}\cdot\underline{r}_{ij}}{\left|\underline{r}_{ij}\right|^2 + \epsilon h_{ij}^2}$$
$$\text{mean sound speed } c_{ij} = \frac{c_i + c_j}{2}, \quad \text{singularity protection } \epsilon \simeq 0.01$$
$$\text{viscosity strength regulated by } \alpha \simeq 0.5 to 1, \beta \simeq 2\alpha \tag{342}$$

This form of a viscous force is a combination of a bulk and von-Neumann-Richtmyer viscosity and only acts if two particles (rapidly) approach [14] each other. It is Galilean invariant and vanishes for rigid body rotation.

The total momentum equation then is

$$\frac{d\underline{v}_i}{dt} = -\sum_{j=1}^{N_i} m_j \left(\frac{p_i}{\rho_i^2} + \frac{p_j}{\rho_j^2} + \Pi_{ij}\right) \underline{\nabla}_i W\left(r_{ij}, h_{ij}\right) - \underline{\nabla}\phi_i \tag{343}$$

In order to conserve total energy, work done against the viscous force has to show up as heat (discussed later).

7.5.3 Shear-Flow-Balsara correction

Problem: In the above we will also add high viscosity to shear flows (which we do not want), where particles also quickly approach each other (move adjacently with different velocities)

Idea: Such shear flows are marked by high vorticity $\underline{\omega} = \underline{\nabla} \times \underline{v}$, so for high vorticity we can crank down the artificial viscosity.

$$\tilde{\mu}_{ij} = \mu_{ij} \cdot \frac{f_i + f_j}{2}, \quad f_i = \tag{344}$$

7.5.4 Further viscosity switches

To reduce viscosity far away from shocks many other switches have been proposed, e.g. by making the viscosity strength parameters α variable in time and adopting $\beta = 2\alpha$.

[14] $\underline{v}_{ij}\cdot\underline{r}_{ij} < 0$, and μ_{ij} measure how strongly two particles approach each other.

Idea: We only want high $\Pi_i j$ when there is high compression, $\underline{\nabla} \cdot \underline{v}$ strongly negative, which we can use as a switch after which we let α_i decay exponentially.

7.6 SPH energy equation with artificial viscosity

The work done against the viscous force can be accounted in terms of energy or entropy.

Let us start with the hydrodynamic energy equation

$$\frac{d\epsilon}{dt} = \frac{\partial \epsilon}{\partial t} + \underline{v} \cdot \underline{\nabla} \epsilon = \frac{ds}{dt} - \frac{p}{\rho} \underline{\nabla} \cdot \underline{v} \tag{345}$$

from which for adiabatic systems with $\frac{ds}{dt} = 0$ and with eq. 334 we find

$$\frac{d\epsilon_i}{dt} = \frac{p_i}{\rho_i^2} \sum_{j=1}^{N_i} m_j \underline{v}_{ij} \cdot \underline{\nabla}_i W\left(r_{ij}, h_{ij}\right) \tag{346}$$

(where here we do not take the symmetric form as it can lead to unphysical solutions like negative internal energy).

To this we add a dissipation term due to artificial viscosity and incorporate heating and cooling sources into a function Γ_i to obtain

$$\boxed{\frac{d\epsilon_i}{dt} = \underbrace{\frac{p_i}{\rho_i^2} \sum_{j=1}^{N_i} m_j \underline{v}_{ij} \cdot \underline{\nabla}_i W_{ij}}_{\text{from hydrodynamic energy equation}} + \underbrace{\frac{1}{2} \sum_{j=1}^{N_i} m_j \Pi_{ij} \underline{v}_{ij} \cdot \underline{\nabla}_i W_{ij}}_{\text{dissipation from art. viscosity}} + \underbrace{\Gamma_i}_{\text{heating and cooling}}} \tag{347}$$

7.7 SPH Entropy equation

Alternatively to the energy equation, one can integrate an equation for the specific thermodynamic entropy A_i. The entropic function is defined by

$$P = A(s)\rho^\gamma, \quad \text{adiabatic index } \gamma \tag{348}$$

from which the internal energy follows as

$$\epsilon = \frac{P}{(\gamma - 1)\rho} = \frac{A(s)}{\gamma - 1} \rho^{\gamma - 1} \tag{349}$$

The SPH entropy equation can be derived as

$$\frac{\mathrm{d}A_i}{\mathrm{d}t} = -\frac{\gamma-1}{\rho_i}\Gamma_i + \frac{1}{2}\frac{\gamma-1}{\rho_i^{\gamma-1}}\sum_{\mathrm{J}=1}^{N_i} m_j \Pi_{ij} \underline{v}_{ij} \cdot \underline{\nabla}_i W\left(r_{ij}, h_{ij}\right) \tag{350}$$

From this using eq. 349 we can retrieve the internal energy and the temperature T_i (proportional to ϵ_i).

7.8 Maximum timestep - CFL criterion

A possible criterion is

$$\Delta t_i^{CFL} = 0.3\frac{h_i}{h\left|(\underline{\nabla}\cdot\underline{v})_i\right| + c_i + 1.2\left(\alpha_i c_i + \beta_i h_i \left|\min\left((\underline{\nabla}\cdot\underline{v})_i, 0\right)\right|\right)} \tag{351}$$

sound speed c_i, viscosity strength α_i, β_i

7.9 Notes on boundary modeling*

The two basic options are

- use fixed dummy particles (however those lead to the violation of the conservation of energy)
- use a fluid-solid force (e.g. inspired by the Lenard-Jones potential)

7.10 Reversibility in the context of viscosity-free, weakly-compressible SPH*

Note that a fluid rising up to a dam form again after a dam-break and anti-dissipative or *clumping-up* so anti-pressure behavior are very different. The advantage of our SPH particles representing a fluid so acting on e.g. pressure unlike normal particles, the main advantage of rediscretizing based on the fluid equations, is of course sustained.

The SPH equations (based on the Euler fluid equations) lead us to a numerically time-reversible scheme[15] for the evolution of the positions and velocities of our SPH-particles - we must take care though and

- use a reversible, symplectic method like leapfrog
- calculate the density from the current positions of the particles not the evolution equation avoiding accumulation of density errors and making our SPH evolution symplectic.

[15] Solving backwards in time while recovering the initial conditions.

- use fixed-point over floating-point arithmetic, to avoid floating point errors violating reversibility

Note: The SPH-particles (without added viscosity) obey reversible Hamiltonian dynamics.

Indeed, for the N particle distribution function $f_N(t, \underline{r}_1, \underline{p}_1, \ldots, \underline{r}_N, \underline{p}_N)$ the Liouville entropy

$$S^{\text{Liouville}}(f_N) = -\frac{k_B}{N!} \int d\underline{r}_1 \int d\underline{p}_1 \cdots \int d\underline{r}_N \int d\underline{p}_N f_N \ln\left(h^{3N} f_N\right) \tag{352}$$

remains - in theory and in the reversible simulation (Kincl and Pavelka, 2023) - constant.

However, the Boltzmann entropy - which is obtained by maximizing the Liouville entropy under the constraint of the one-particle distribution $f(t, \underline{r}, \underline{p})$[16]

$$S^{\text{Boltzmann}}(f) = -k_B \int d\underline{r} d\underline{p} f \left(\ln\left(h^2 f\right) - 1\right) \tag{353}$$

grows in the simulation of the dam break experiment in Kincl and Pavelka, 2023 (with velocity distribution becoming Maxwellian).

So forgetting the exact positions and momenta of our SPH particles, the one-particle density they describe increases in Boltzmann entropy, the 2nd law of thermodynamics emerges (statistically).

In the words from Kincl and Pavelka, 2023: »In summary, if we see all the positions and momenta in the SPH simulation, we can not see the second law of thermodynamics. Indeed, the simulation is reversible and the Liouville entropy remains constant. However, when we only focus on the one-particle distribution function, we can see the growth of Boltzmann entropy and thus irreversible behavior.«.

Note: Since we have a discrete (as of our discretization), deterministic, reversible system which can only existist in finitely many states, it is recurrent, thus will after long enough time come back to its initial state (unlikely though as of the high-dimensional phase space).

Note: The situation here is without any viscosity, so that if we invert the velocities and come back to our previous state (see figure 71) this is not anti-dissipation and does not happen when the system is dissipative (with viscosity). (?)

[16] Normalized to the number of particles.

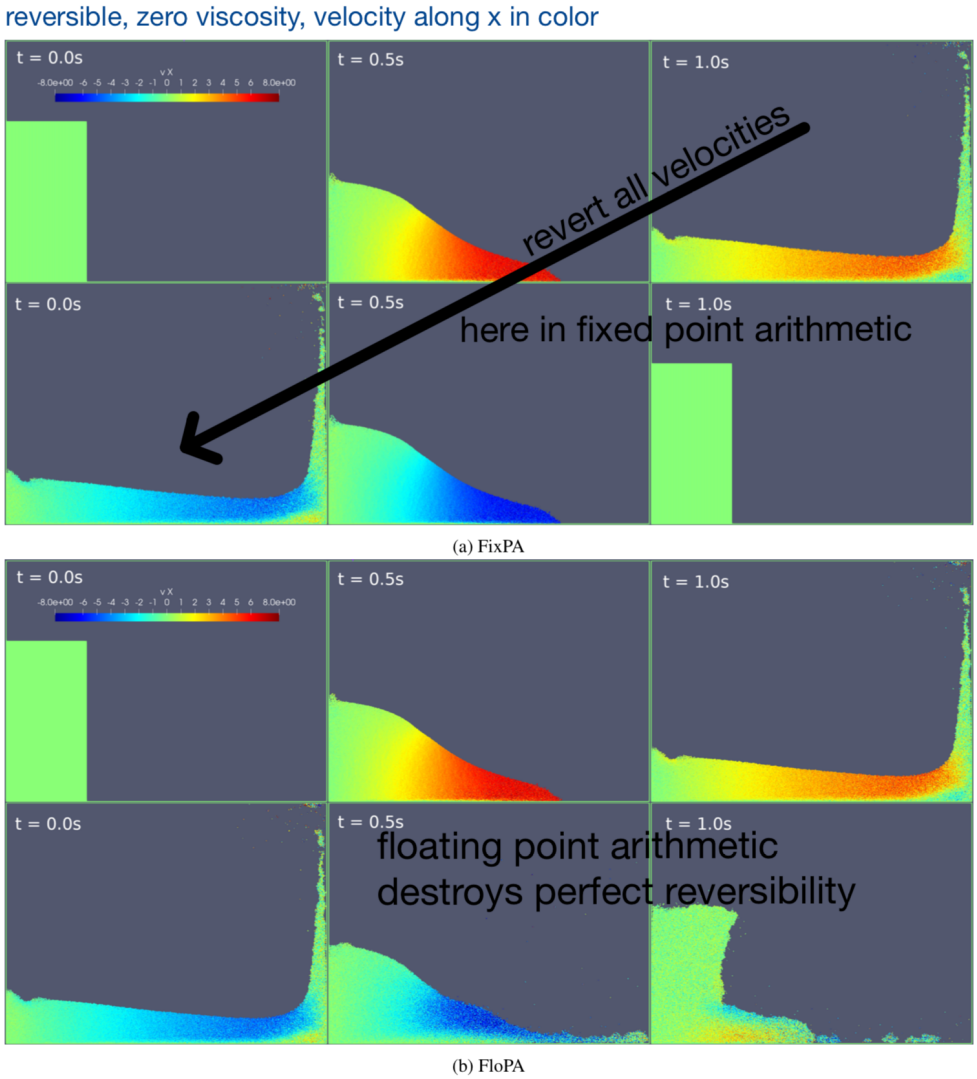

(a) FixPA

(b) FloPA

Figure 71: Reversible SPH simulation without viscosity at the example of a breaking dam. In floating-point arithmetic this reversible behavior is broken. Being in an initial state leading back to the *dam* is very unlikely so even slight deviations will make us not go back to the dam.

Note the different levels at play: The SPH-particles are artificial in that they describe the fluid not the fluid particles. So while the SPH-particles start out resting, there is still temperature and pressure. However, in the dam experiment (fig. 71) (and generally) the SPH particles themselves thermalize to a Boltzmann distribution (they start out in non-equilibrium), fitting to the equilibrium Boltzmann entropy (although we do not add any heat, Boltzmann entropy of the SPH-particles increases as we go from non-equilibrium to equilibrium). Note that this is not the same as the specific thermodynamic entropy of the fluid, as previously described.

7.11 Notes on the conservative formulation using Lagrange multipliers

Starting with the Lagrangian for inviscid, compressible flow

$$\mathcal{L} = \int \rho \left\{ \frac{1}{2} v^2 - u(\rho, s) \right\} d^3 r \tag{354}$$

the SPH equation with $s = \text{const.}$ follows from the Lagrange equation

$$\frac{d}{dt} \frac{\partial \mathcal{L}}{\partial \underline{v}} - \frac{\partial \mathcal{L}}{\partial \underline{r}} = 0 \tag{355}$$

(for variable smoothing length h under the constraint (Lagrange multiplier) $\rho_j h_j^3 = \text{const.}$) as

$$\frac{d\underline{v}_i}{dt} = -\sum_{j=1}^{N_i} m_j \left\{ \frac{1}{f_i} \frac{p_i}{\rho_i^2} \underline{\nabla}_i W(r_{ij}, h_i) + \frac{1}{f_j} \frac{p_j}{\rho_j^2} \underline{\nabla}_i W(r_{ij}, h_j) \right\}, \quad f_i = \left[1 + \frac{h_i}{3\rho_i} \frac{\partial \rho_i}{\partial h_i} \right] \tag{356}$$

From the symmetries of the Lagrangian it follows that energy, specific thermodynamic entropy, linear and angular momentum are conserved.

7.12 Further improvements

Ideas for improvement are

- it may be more physical to move particles with a smoothed flow velocity
- ...

7.13 Advantages and Disadvantages of SPH

Advantages and disadvantages of SPH are summarized in table 14.

Advantages	Disadvantages
• versatile and simple • automatically adaptive resolution, can cover large ranges in density and space • excellent conservation properties (energy, linear and angular momentum, not guarantueed in Eulerian codes) • inherent mass conservation • Galilean invariant and free from advection errors • can deal with complicated geometries as mesh-free • simple and transparent codes • very robust • as a particle scheme it is good for describing the transition from gaseous to stellar dynamical systems (e.g. formation of stellar clusters)	• limited accuracy in multi-D flow • low density regions are more poorly resolved • poorly handles shocks • noise as of discrete sums over limited neighbor set • jitter develops • fluid instabilities arcoss contact discontinuities are problematic such as Kelvin helmholtz instabilities • artificial viscosity limits the Reynolds number which can be reached • low convergence rate [17] • approximation of boundary conditions can be difficult • formation of voids • free surfaces can be problematic (density underestimated there) • magnetic fields are hard to handle (problems with stability and $\underline{\nabla} \cdot \underline{B} = 0$ requirement)

Table 14: Advantages and disadvantages of SPH.

8 Finite Element Methods

Finite element methods (FEM) are a class of methods for solving PDEs. Advantages include

- can work with flexible geometries
- handle geometrically intricate boundary conditions
- spatially adapt the resolution

Generally, numerical schemes need to represent a problem's solution by finitely many numbers, and then manipulate those numbers as true to the problem as possible. In finite volume methods we represent the solution as averages on cells which we update based on devised fluxes. In Smoothed Particle Hydrodynamics, we represent the fluid by a finite set of artificial *fluid particles* and update their positions and velocities according to the Lagrangian form of the fluid equations.

Idea of FEMs: In FEMs the solution domain is structured into finite elements with nodes on which base functions sit. The partial differential equation (or rather a weak form[a] of it) turns into equations for the (finitely many) weights of those basis functions.

[a]Weak here means, that the differential equation must not hold strictly locally, but for instance an integrated residual is to be zero, not the residual everywhere itself.

8.1 Finite element methods for linear PDEs

8.1.1 The solution is represented by weighted base functions on nodes within finite elements

The central ideas are

- Division of space: The space on which the solution sits is divided onto smaller regions called elements (e.g. segments in 1D, rectangles in 2D, cubes, octahedra, ... in 3D). Every element contains a certain number of points called nodes.
- Elementwise solution approximation: We element-wise approximate the solution with a set of linearly independent (not necessarily orthogonal) basis functions evaluated on nodes.

On an element we could for instance use a polynomial basis

$$\text{a line } \phi(x) = a_0 + a_1 x, \quad \text{or a parabula } \phi(x) = a_0 + a_1 x + a_2 x^2 \tag{357}$$

or Legendre polynomials.

Note: We need the same number of nodes as coefficients so that the values ϕ_i on the nodes fully specify our polynomial.

Better yet, we could use shape function N, so that our node values themselves are the coefficients we model.

So for n node values $\phi_1, \dots, \phi_n$ (called *expansion coefficients*), we can write the solution on the k-th element as

$$\phi^{(k)}(x) = \phi_1^{(k)} N_1^{(k)}(x) + \phi_2^{(k)} N_2^{(k)}(x) + \cdots + \phi_n^{(k)} N_n^{(k)}(x)$$
$$\text{shape functions } N_i^{(k)}, \text{ zero outside k-th element} \tag{358}$$

All elements use the same base function forms, but for each specific element the sum over its base functions is only non-zero in the respective element. We can therefore also write the total solution as

$$\phi(x) = \phi_1 N_1(x) + \phi_2 N_2(x) + \cdots + \phi_{\mathcal{N}} N_{\mathcal{N}}(x), \quad \text{in total } \mathcal{N} \text{ nodes} \tag{359}$$

Note: While we use 1D notation here, we can expand to $\phi(\underline{x}) = \sum_{i=1}^{n} \phi_i N_i(\underline{x})$. Time-dependency can be included as time-dependency of the weights aka expansion coefficients $\phi_i = \phi_i(t)$. But first we will consider constant coefficients, so a stationary (elliptic) problem.

Based on this the next step is turning the PDE into and algebraic equation for the expansion coefficients ϕ_i.

8.1.1.1 Example 1D linear reconstruction

A linear 1D example can be seen in figure 72.

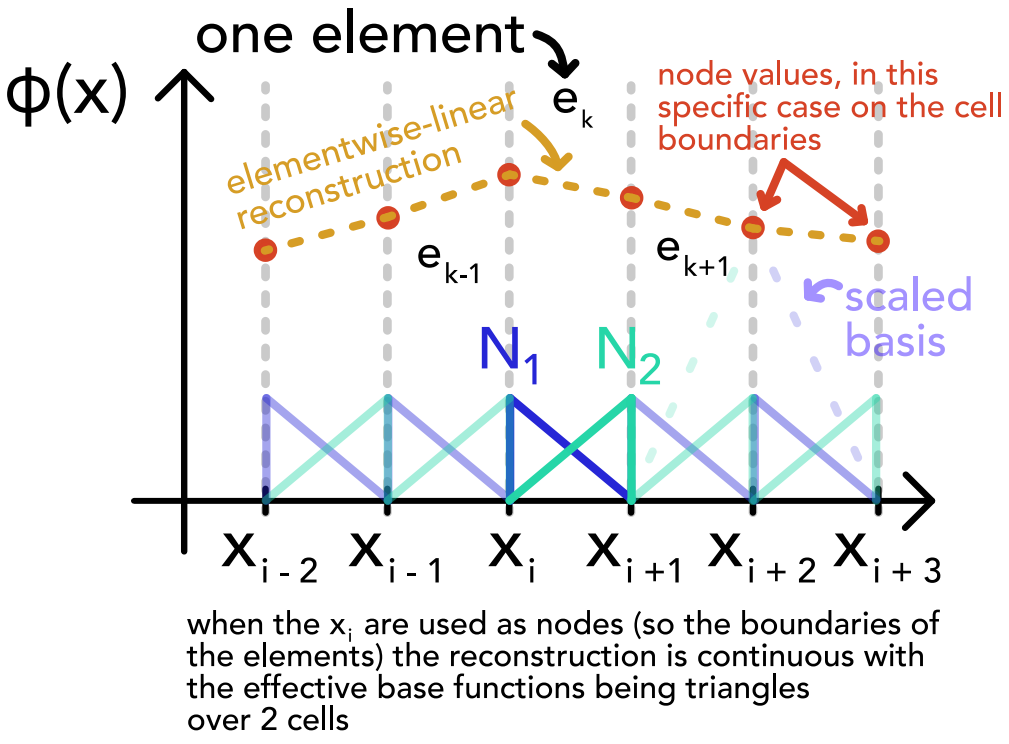

Figure 72: 1D linear reconstruction

8.1.2 From the PDE to an algebraic equation for the expansion coefficients $\phi_1, \ldots, \phi_n$

For now consider a stationary example (no time dependence of ϕ_j in one spatial dimension.)

In the following we find an algebraic expression (here even a system of linear equations) usually done for the expansion coefficients on one element. Afterwards the equations for all elements have to be assembled (to an overall linear system) in a further step. If the system has $\mathcal{N}$ total nodes, the final linear equation is described by an $\mathcal{N} \times \mathcal{N}$ system. See Lewis et al., 2004.

We might sometimes directly find such a system for all expansion coefficients and we will focus on that.

8.1.2.1 Inserting the finite element approximation into the PDE yields a residuum

Consider a linear PDE of the form

$$L\hat{\phi} + \hat{s} = 0, \quad \text{linear differential operator } \hat{L}, \text{ source term } \hat{s}, \text{ solution } \hat{\phi} \tag{360}$$

$\hat{L}$ being linear means $\hat{L}(a\phi + b\psi) = a\hat{L}\phi + b\hat{L}\psi$ for any functions ϕ, ψ and constants a, b.

We now plug in the finite element approximation $\phi(x)$ and source function $s(x)$

$$L\phi + s = R^{(k)}(x; \phi_1, \dots, \phi_n) = L\left(\sum_{j=1}^{n} \phi_j N_j(x)\right) + s \underbrace{=}_{L \text{ linear}} \sum_{j=1}^{n} \phi_j L N_j(x) + s \tag{361}$$

supscript k to indicate this is the residual over the k-th element

As only the shape functions depend on x, we only have to apply L to them. As of our approximation we have a generally non-zero residual.

8.1.2.2 Finding the expansion coefficients by minimizing the residual in some sense

We want to choose expansion coefficients minimizing the residual in some sense.

Ritz method: Here we require the integral over the residual to vanishes

$$\int_{\text{domain}} R\, dx = 0 \tag{362}$$

where here we consider the whole problem domain, to readily find the whole system of linear equations (but this might also be just an element). Therefore

$$R = R\left(x; \sum_{i=1}^{\mathcal{N}} \phi_i\right) \tag{363}$$

Weighted residual method Compared to the Ritz method weighting functions $w_i(x)$ are introduced

$$\int_{\text{domain}} w_i(x) R \, dx = 0, \quad i = 1, \ldots, \mathcal{N} \tag{364}$$

which leads to

- collocation method: Residuum is required to vanish at n points x_i inside the domain, $w_i = \delta(x - x_i)$
- least-square method: $w_i = \partial_{\phi_i} R \to \int_{\text{domain}} (\partial_{\phi_i} R) R \, dx = \frac{1}{2} \partial_{\phi_i} \int_{\text{domain}} R^2 \, dx = 0$
- Galerkin method: Choose basis functions themselves as weights, so $w_i(x) = N_i(x)$, so

$$\int_{\text{domain}} N_i(x) R \, dx = 0 \tag{365}$$

The general Galerkin principle is to multiple an equation by arbitrary test functions and describe the unknown field with the same set of basis functions.

8.1.2.3 A linear system for $\phi_1, \ldots, \phi_{\mathcal{N}}$ in the Galerkin scheme

Based on

$$\begin{aligned} \forall i \in 1, \ldots, \mathcal{N} : 0 = \int_{\text{domain}} N_i(x) R \left(\sum_j \phi_j N_j(x) \right) dx = \int_{\text{domain}} N_i(x) \cdot L \left(\sum_j \phi_j N_j(x) \right) + s dx \\ \underbrace{=}_{\text{L linear}} \sum_j \phi_j \underbrace{\int_{\text{domain}} N_i(x) L \left(N_j(x) \right) \, dx}_{A_{ij}} - \underbrace{\int_{\text{domain}} -N_i(x) s \, dx}_{b_i} \\ \to \sum_j \phi_j A_{ij} = b_i \end{aligned} \tag{366}$$

we can turn the PDE into a linear system for the expansion coefficients ϕ_i, compactly

$$\underline{\underline{A}} \underline{\phi} = \underline{b}, \quad \underline{\phi} = \begin{pmatrix} \phi_1 \\ \vdots \\ \phi_{\mathcal{N}} \end{pmatrix}, \quad \text{vector of source elements } \underline{b} \tag{367}$$

$\underline{\underline{A}}$ very sparse because of the localization of the expansion elements

FEMs are only good for linear PDEs (only if L is linear do we get a linear system for the coefficients) (sometimes non-linear PDEs can be linearized though)

Dynamical systems where the ϕ_i might change in time will follow shortly.

8.1.2.4 Example Application of Galerkin FEM

Consider the 1D Poisson equation (really an ODE)

$$\partial_x^2\phi(x) = 4\pi G\rho(x), \quad \text{van Neumann boundary conditions } \partial_x\phi|_{x_L} = \partial_x\phi|_{x_R} = 0 \tag{368}$$

Aim: From a given density distribution ρ we want to find the field ϕ.

We formulate the basis functions as triangular basis functions spanning two elements, as shown in figure 72. In this figure you can also see that one can formulate this in terms of basis functions only sitting on one element, which is more true to the previous introduction.

$$S_i(x) = \begin{cases} \frac{x-x_{i-1}}{\Delta x} & \text{for } x \in [x_{i-1}, x_i] \\ \frac{x_{i+1}-x}{\Delta x} & \text{for } x \in [x_i, x_{i+1}] \\ 0 & \text{otherwise.} \end{cases} \tag{369}$$

We have linear elements between $\mathcal{N}$ points, Δx apart.

The finite element approximation is

$$\phi = \sum \phi_i S_i(x) \tag{370}$$

we calculate the residual as

$$R = \partial_x^2\phi(x) - 4\pi G\rho(x) \tag{371}$$

so using the Galerkin weighting we get

$$\forall i = 1, ..., \mathcal{N} : \int_{x_L}^{x_R} S_i(x) \left(\partial_x^2\phi(x) - 4\pi G\rho(x)\right) dx = 0 \rightarrow \int_{x_L}^{x_R} S_i(x)\partial_x^2\phi(x)\, dx = \int_{x_L}^{x_R} S_i(x) 4\pi G\rho(x)\, dx \tag{372}$$

The LHS can be rewritten by integration over parts (mind $\partial_x\phi|_{x_L} = \partial_x\phi|_{x_R} = 0$)

$$\int_{x_L}^{x_R} S_i(x)\partial_x^2\phi(x)dx = -\int_{x_L}^{x_R} \partial_x S_i(x)\partial_x\phi(x)dx = -\int_{x_L}^{x_R} S_i(x)4\pi G\rho(x)dx = b_i \tag{373}$$

so the with the RHS

$$\int_{x_L}^{x_R} \partial_x S_i(x) \partial_x \sum \phi_j S_j(x) dx = \sum \phi_j \underbrace{\int_{x_L}^{x_R} \partial_x S_i(x) \partial_x S_j(x) dx}_{A_{ij}} = \sum \phi_j A_{ij} = b_i \tag{374}$$

we retrieve a linear equation with (use the definition of $S_i(x)$)

$$A_{ij} = \begin{cases} \frac{2}{\Delta x} \text{ for } i = j \\ -\frac{1}{\Delta x} \text{ for } i = j \pm 1 \\ 0 \text{ otherwise} \end{cases} \tag{375}$$

which would also follow from

$$\partial_x^2 \phi_i = \frac{\phi_{i+1} - 2\phi_i + \phi_{i-1}}{\Delta x^2} \tag{376}$$

8.2 Discontinuous Galerkin Method

Aim: We want to find the solution to a hyperbolic differential equation system. The solution is often characterized by discontinuities and shocks. Me might be interested in complex geometries, for which Finite Element Methods are very suitable.

Problem: Usual Finite Element Methods (FEMs) are piecewise polynomial and continuous - shocks are often smeared out.

Idea: Combine the advantages of Finite Element Methods and Finite Volume Schemes. Discontinuous Galerkin is a FEM - the problem domain is subdivided into a grid of a finite number of elements. We use a piecewise polynomial solution which can be discontinuous across cell interfaces, where we use the methods from finite volume to compute the intercell fluxes - so conservation laws are baked in.

Continuous and discontinuous Galerkin are illustrated in figure 73.

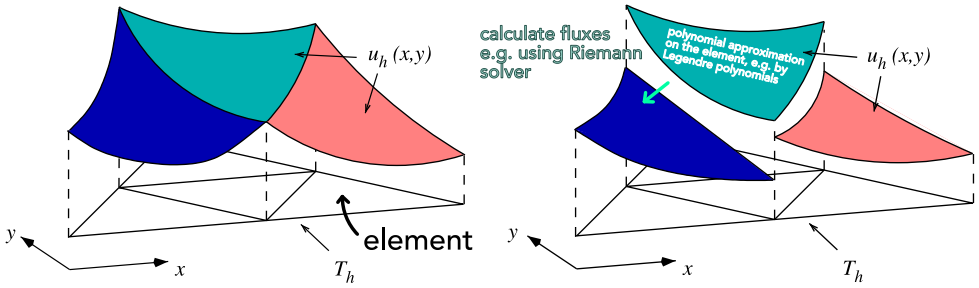

(A) Continuous Galerkin (B) Discontinuous Galerkin

Figure 73: Continuous and discontinuous Galerkin

8.2.1 Problem we want to tackle | Euler equations

Consider the 3D formulation of the Euler equations we know from dimensional splitting

$$\partial_t \underline{u}(\underline{x}) + \sum_{\alpha=1}^{3} \partial_{x_\alpha} \underline{f}_\alpha(\underline{u}) = 0, \quad \text{state vector } \underline{u} = \begin{pmatrix} \rho \\ \rho \underline{v} \\ \rho e \end{pmatrix} \tag{377}$$

$$\text{specific energy } e = \rho e_{th} + \frac{1}{2}\rho \underline{v}^2 \text{ with specific internal energy } e_{th}$$

with flux vectors

$$\underline{f}_1 = \begin{pmatrix} \rho v_1 \\ \rho v_1^2 + P \\ \rho v_1 v_2 \\ \rho v_1 v_3 \\ v_1(\rho e + P) \end{pmatrix}, \quad \underline{f}_2 = \begin{pmatrix} \rho v_2 \\ p v_1 v_2 \\ \rho v_2^2 + P \\ \rho v_2 v_3 \\ v_2(\rho e + P) \end{pmatrix}, \quad \underline{f}_2 = \begin{pmatrix} \rho v_3 \\ p v_1 v_3 \\ \rho v_2 v_3 \\ \rho v_3^2 + P \\ v_3(\rho e + P) \end{pmatrix} \tag{378}$$

$$\text{ideal gas closure } P = \rho e_{th}(\gamma - 1)$$

Aim: From a given initial state $\underline{u}(\underline{x}, t = 0) = u(\underline{x}, 0)$ we want to find the subsequent evolution of the fluid.

8.2.2 Steps in formulating the Dicontinuous Galerkin (DG) scheme

1. Subdivide the space into elements aka cells
2. Represent the fluid state on a cell using a polynomial basis (e.g. Legendre polynomials) with weights evolving in time; *nodal* vs *modal*
3. Find a general formula for the weights in the *modal* variant
4. Find the initial weights from specific *nodal* starting values in the *modal* scheme

5. Find an evolution equation for the weights

8.2.3 Subdivision and Representation | modal vs nodal

The fluid state is represented as a polynomial approximation (for the respective fluid variables) on the element (non overlapping elements with discontinuities in-between) - but how?

A typical DG cell is illustrated in figure 74.

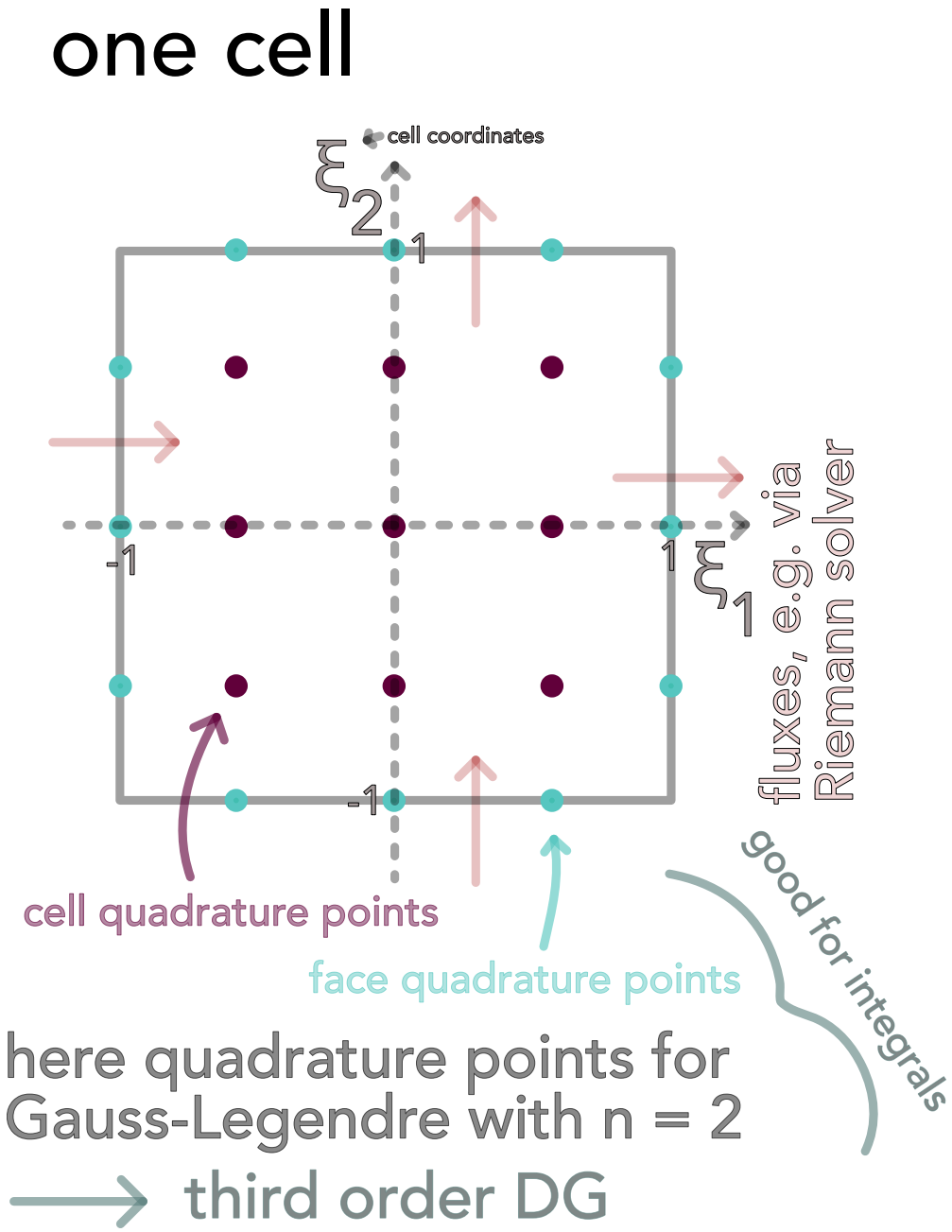

Figure 74: Typical DG cell

There are two possible representations of the solution

- **nodal**: We store and operate on fluid state vectors at chosen positions within the cell. In the Legrange interpolation with Lagrange polynomials of degree k, so $l_j(x) = \prod_{\substack{0 \leq m \leq k \\ m \neq j}} \frac{x - x_m}{x_j - x_m}$, for one fluid variable the node values are also the expansion coefficients, $u = \sum_{j=0}^{N(k)} u_j l_j(x)$. The positions of the nodes in the cell are chosen smartly regarding quadrature (integration) rules.
- **modal**: We store and operate on weights of usually orthogonal polynomials (usually Legendre). Integrals are still evaluated using quadrature rules. Initial weights have to be calculated based on nodal values.

We opt for **modal**.

The solution in the interior of cell K is given by a linear combination of $N(k)$ orthogonal and normalized basis functions $\phi_l^{(K)}$ (maximum degree of the basis functions is k).

$$\underline{u}^{(K)}(\underline{x}, t) = \sum_{l=1}^{N(k)} \underline{\omega}_l^{(K)}(t) \phi_l^{(K)}(\underline{x}) \tag{379}$$

where

- the space-time dependence of the fluid state was split into time dependent weights and space dependent basis functions
- the cell's state is completely given by the $N(k)$ weights

8.2.3.1 Example for an orthogonal polynomial basis: Legendre polynomials

We can combine Legendre polynomials to 3D base functions with degree up to k in the following manner

$$\begin{gathered} \left\{\phi_l(\underline{\xi})\right\}_{l=1}^{N(k)} = \left\{\tilde{P}_u(\xi_1)\,\tilde{P}_v(\xi_2)\,\tilde{P}_w(\xi_3) \mid u, v, w \in \mathbb{N}_0 \wedge u + v + w \leq k\right\} \\ \text{scaled Legendre polynomials } \tilde{P}_n(\xi) = \sqrt{2n+1} P_n(\xi) \\ \text{"special orthog. "} \int_{-1}^{1} P_i(\xi) P_j(\xi) d\xi = \begin{cases} 0 & \text{if } i \neq j \\ 2 & \text{if } i = j \end{cases} \end{gathered} \tag{380}$$

For a polynomial basis with maximum degree k we have

$$N(k) = \sum_{u=0}^{k} \sum_{v=0}^{k-u} \sum_{w=0}^{k-u-v} 1 \tag{381}$$

basis polynomials.

The first Legendre polynomials are

$$P_0(\xi) = 1, P_1(\xi) = \xi, P_2(\xi) = \frac{1}{2}\left(3\xi^2 - 1\right) \tag{382}$$

Note: The span of $P_0(x), P_1(x), \ldots, P_n(x)$ is the same as of $1, x, x^2, \ldots, x^n$. So

$$\forall \text{polynomial } P \text{ of degree } < n : \int_{-1}^{1} P(x)P_n(x)\,dx = 0 \tag{383}$$

8.2.4 Solving for the weights

Note: The main application of finding weights is finding the weights of the initial state. Going from weights to evaluations is easy.

Let's say we would know $\underline{u}^{(K)}(\underline{x}, t)$ - then we can determine the weights based on the orthogonality and normalization properties of the basis functions as

$$\underline{\omega}_j^K(t) = \frac{1}{|K|}\int_K \underline{u}^{(K)}\phi_j^{(K)}dV, \quad j = 1, \ldots, N(k)$$
$$\text{with } |K| \text{ volume of cell } K \tag{384}$$

We hereby choose $\phi_1^{(K)} = 1$ so that $\omega_1^{(K)}$ is the cell's average of the state vector $\underline{u}^{(K)}$ (constant term). $\phi_j^{(K)}, j \geq 2$ are higher order basis functions, with $w_j^{(K)}$ being the higher order moments of the state vector $\underline{u}^{(K)}$.

Scaled variable on cell: On a cube, we can define the basis functions in terms of a scaled variable $\underline{\xi}$.

$$\phi_l(\underline{\xi}) : [-1, 1]^3 \to \mathbb{R}, \quad \underline{\xi} = \frac{2}{\Delta x}\left(\underline{x} - \underline{x}^{(K)}\right)$$
$$\text{cell's center } \underline{x}^{(K)}, \text{ cell's sidelength } \Delta x \tag{385}$$

Idea: Let us approximate this integral by a quadrature rule.

First write the integral equation for the weights in the reference frame of a cubic cell with sidelength 2

$$\underline{\omega}_j^{(K)}(t) = \frac{1}{8}\int_{[-1,1]^3} \underline{u}^{(K)}(\underline{\xi}, t)\phi_j^{(K)}(\underline{\xi})d^3\underline{\xi}, \quad j = 1, \ldots, N(k) \tag{386}$$

We then apply Gauss-Legendre quadrature with $(k+1)^3$ quadrature points, so

$$\underline{\omega}_j^{(K)}(t) \approx \frac{1}{8} \sum_{q=1}^{(k+1)^3} \underline{u}^{(K)}\left(\underline{\xi}_q^{3D}, t\right) \phi_j^{(K)}\left(\xi_q^{3D}\right) w_q^{3D}, \quad j = 1, \ldots, N(k)$$

positions of quadrature nodes in cell's reference frame $\underline{\xi}_q^{3D}$, quadrature weights w_q^{3D} (387)

8.2.4.1 What even is Gauss-Legendre quadrature?*

It is intuitive that an integral can be approximated by the mean of evaluation points. However, it turns out, that one can exactly integrate polynomials of degree $2n-1$ with n smart evaluation points and weights. One such method is called Gauss-Legendre quadrature.

Claim: The approximation

$$\int_{-1}^{1} f(\xi) d\xi \approx \sum_{q=1}^{n} f\left(\xi_q^{1D}\right) w_q^{1D}$$
$$\text{roots } \xi_q^{1D} \text{ of } P_n(\xi), \text{ weights } w_q^{1D} = \frac{2}{\left(1 - \left(\xi_q^{1D}\right)^2\right)\left(P_n'\left(\xi_q^{1D}\right)\right)^2} \tag{388}$$

for $f : [-1, 1] \to \mathbb{R}$ is exact for polynomials of degree $2n-1$.

Proof: Let $f = P(x)$ have degree $\leq 2n-1$. Then we can write $P(x) = Q(x)P_{n+1}x + R(x)$ with $Q(x), R(x)$ polynomials of degree $\leq n$ ($P_{n+1}(x)$ is the $(n+1)$-th Legendre polynomial). Then

$$\begin{aligned}
\int_{-1}^{1} P(x)dx &= \underbrace{\int_{-1}^{1} Q(x)P_{n+1}(x)dx}_{=0 \text{ as } Q \text{ can be written in base } \{P_0,\ldots,P_n\} \perp P_{n+1}} + \int_{-1}^{1} R(x)dx \\
&= \int_{-1}^{1} R dx \\
&= \underbrace{\sum_{q=1}^{n} R\left(\xi_q^{1D}\right) w_q^{1D}}_{\text{exact as } R \text{ is a polynomial of degree} \leq n} \\
&= \sum_{q=1}^{n} \left(R\left(\xi_q^{1D}\right) + \underbrace{P_{n+1}(\xi_q^{1D}) \cdot Q(\xi_q^{1D})}_{=0, \text{as } \xi_q^{1D} \text{ roots of } P_{n+1}} \right) w_q^{1D} \qquad = \sum_{q=1}^{n} P(\xi_q^{1D}) w_q^{1D}
\end{aligned} \tag{389}$$

Formulation in higher dimensions: We generalize to $f : [-1, 1]^2 \to \mathbb{R}$ by

$$\int_{-1}^{1}\int_{-1}^{1} f(\xi_1, \xi_2)\, d\xi_1 d\xi_2 \approx \sum_{q=1}^{n}\sum_{r=1}^{n} f\left(\xi_q^{1D}, \xi_r^{1D}\right) w_q^{1D} w_r^{1D} = \sum_{q=1}^{n^2} f\left(\underline{\xi}_q^{2D}\right) w_q^{2D} \tag{390}$$

8.2.5 Finding initial weights - just apply the determination of weights to the initial state

The initial state $\underline{u}(\underline{x}, t = 0)$ is best represented by weights $\underline{\omega}_j^{(K)}(t = 0)$, such that

$$w_{l,i}^{(K)}(t = 0) = \underset{\underline{\omega}_{j,i}^{(K)}(t=0)}{\operatorname{argmin}} \int_K \left(u_i^{(K)}(\underline{x}, t = 0) - u_i(\underline{x}, t = 0)\right)^2 d^3\underline{x}, \quad i \text{ over state vector components} \tag{391}$$

which just leads us to the previous projection (eq. 384) and solution in eq. 387 at $t = 0$, where our initial state must be known on the quadrature nodes.

8.2.6 Evolution equation for the weights

We derive a DG scheme on cell K.

Weak form of the Euler equations: A weak formulation of the Euler equations for the polynomial approximation $\underline{u}^{(K)}$ on cell K is found by multiplying the Euler equations with the basis function $\phi_j^{(K)}$ and integrating over the cell K.

$$\int_K \left[\partial_t \underline{u}^{(K)} + \sum_{\alpha=1}^{3} \partial_{x_\alpha} f_\alpha\right] \phi_j^{(K)} dV = 0 \tag{392}$$

Integrating by parts and applying Gauss theorem, we get

$$\frac{d}{dt}\underbrace{\int_K \underline{u}^{(K)}\phi_j^K dV}_{\underline{w}_j^{(K)}\cdot|K|} + \sum_{\alpha=1}^{3}\underbrace{\int_{\partial K} f_\alpha n_\alpha \phi_j^K dS}_{\substack{\text{evaluate using Gauss-Quad, unknown flux across discont. via Riemann solver}}} - \sum_{\alpha=1}^{3}\underbrace{\int_K \underline{f}_\alpha \frac{\partial \phi_j^K}{\partial x_\alpha} dV}_{\substack{\text{evaluate via Gauss-Quad., interior flux known from state variable approx.}}} = 0 \tag{393}$$

$$\text{normal vector } \underline{n} = \begin{pmatrix} n_1 \\ n_2 \\ n_3 \end{pmatrix} \text{ on } \partial K$$

- we have found a system of coupled ODEs for the weights which can be solved for instance using RK schemes. Remember to transform to the cell coordinates $\left(d\xi^3 = \left(\frac{2}{\Delta x^{(K)}}\right)^2 dV\right)$ (from eq. 385).

8.2.7 Efficiency of DG and refinement schemes

Accuracy can be increased by

- p-refinement: higher order scheme (polynomials up to higher order degree in the basis set)
- h-refinement: finer grid with smaller spacing

In both cases, the number of weights increases. For isentropic vortex flow, one finds that p-refinement is much more efficient than h-refinement.

more on nodal vs modal, more details from script

References

Ardourel, Vincent (2017). »Irreversibility in the derivation of the Boltzmann equation«. In: *Foundations of physics* 47.4, pages 471–489.

Biamonte, Jacob et al. (2017). »Quantum machine learning«. In: *Nature* 549.7671, pages 195–202.

Bryant, Randal E and David Richard O'Hallaron (2011). *Computer systems: a programmer's perspective*. Prentice Hall.

Chou, C et al. (2007). »Numerical methods for stiff reaction-diffusion systems«. In: *DISCRETE AND CONTINUOUS DYNAMICAL SYSTEMS SERIES B* 7.3, page 515.

Courant, R., K. Friedrichs, and H. Lewy (Dec. 1928). »Über die partiellen Differenzengleichungen der mathematischen Physik«. In: *Mathematische Annalen* 100.1, pages 32–74. DOI: 10.1007/BF01448839. URL: https://doi.org/10.1007/BF01448839.

Graziani, F. et al. (2022). »Shock physics in warm dense matter: A quantum hydrodynamics perspective«. In: *Contributions to Plasma Physics* 62.2, e202100170. DOI: https://doi.org/10.1002/ctpp.202100170. URL: https://onlinelibrary.wiley.com/doi/abs/10.1002/ctpp.202100170.

Hairer, Ernst (June 2006). »Long-time energy conservation of numerical integrators«. In: *Lecture Notes Ser. FoCM Santander 2005* 331. DOI: 10.1017/CBO9780511721571.005.

Hairer, Ernst, Christian Lubich, and Gerhard Wanner (2003). »Geometric numerical integration illustrated by the Störmer–Verlet method«. In: *Acta Numerica* 12, pages 399–450. DOI: 10.1017/S0962492902000144.

Hairer, Ernst and Gerhard Wanner (1996). *Solving Ordinary Differential Equations II*. Springer Berlin Heidelberg. DOI: 10.1007/978-3-642-05221-7. URL: https://doi.org/10.1007/978-3-642-05221-7.

Hairer, Ernst, Gerhard Wanner, and Christian Lubich (2006). *Geometric Numerical Integration*. Springer-Verlag. DOI: 10.1007/3-540-30666-8. URL: https://doi.org/10.1007/3-540-30666-8.

Hairer, Ernst, Gerhard Wanner, and Syvert P. Nørsett (1993). *Solving Ordinary Differential Equations I*. Springer Berlin Heidelberg. DOI: 10.1007/978-3-540-78862-1. URL: https://doi.org/10.1007/978-3-540-78862-1.

Heiter, Pascal Frederik (2012). »On Numerical Methods for Stiff Ordinary Differential Equation Systems«. Master's thesis. Ulm University. URL: https://www.uni-ulm.de/fileadmin/website_uni_ulm/mawi.inst.070/abschlussarbeiten/masterthesis_pfh.pdf.

Higham, Nicholas J. (2002). *Accuracy and Stability of Numerical Algorithms*. Second. Society for Industrial and Applied Mathematics. DOI: 10.1137/1.9780898718027. URL: https://epubs.siam.org/doi/abs/10.1137/1.9780898718027.

Kincl, Ondřej and Michal Pavelka (Mar. 2023). »Globally time-reversible fluid simulations with smoothed particle hydrodynamics«. In: *Computer Physics Communications* 284, page 108593. DOI: 10.1016/j.cpc.2022.108593. URL: http://dx.doi.org/10.1016/j.cpc.2022.108593.

Lambert, J.D. (1991). *Numerical Methods for Ordinary Differential Systems: The Initial Value Problem*. Wiley. URL: https://books.google.de/books?id=P0vPnQEACAAJ.

Lefever, R. and G. Nicolis (1971). »Chemical instabilities and sustained oscillations«. In: *Journal of Theoretical Biology* 30.2, pages 267–284. DOI: https://doi.org/10.1016/0022-5193(71)90054-3. URL: https://www.sciencedirect.com/science/article/pii/0022519371900543.

Lewis, Roland W, Perumal Nithiarasu, and Kankanhalli N Seetharamu (2004). *Fundamentals of the finite element method for heat and fluid flow*. John Wiley & Sons.

Margolin, L. G. and N. M. Lloyd-Ronning (June 2023). »Artificial viscosity—then and now«. In: *Meccanica* 58.6, pages 1039–1052. DOI: 10.1007/s11012-022-01541-5. URL: https://doi.org/10.1007/s11012-022-01541-5.

Moser, Jürgen (1978). »Is the solar system stable?« In: *The Mathematical Intelligencer* 1.2, pages 65–71. DOI: 10.1007/BF03023062. URL: https://doi.org/10.1007/BF03023062.

Press, William H. et al. (2007). *Numerical Recipes 3rd Edition: The Art of Scientific Computing*. 3rd edition. USA: Cambridge University Press.

Rackauckas, Christopher and Qing Nie (2017). »Differentialequations.jl–a performant and feature-rich ecosystem for solving differential equations in julia«. In: *Journal of Open Research Software* 5.1, page 15.

Rackauckas, Christopher, Sciemon, et al. (Nov. 2022). *SciML/SciMLBook: v1.1*. Version v1.1. DOI: 10.5281/zenodo.7347643. URL: https://doi.org/10.5281/zenodo.7347643.

Rein, Hanno and David S. Spiegel (Nov. 2014). »ias15: a fast, adaptive, high-order integrator for gravitational dynamics, accurate to machine precision over a billion orbits«. In: *Monthly Notices of the Royal Astronomical Society* 446.2, pages 1424–1437. DOI: 10.1093/mnras/stu2164. URL: http://dx.doi.org/10.1093/mnras/stu2164.

Springel, Volker et al. (2023). *Lecture notes in Fundamentals of Simulation Methods*.

Ulmann, Bernd (May 2020). *Analog and Hybrid Computer Programming*. De Gruyter. DOI: 10.1515/9783110662207. URL: http://dx.doi.org/10.1515/9783110662207.